0	15.08.19	Issued for use	Team	AFJ	KH	
Rev.	Publish date	Description	Made by	Checked by	Project appro.	Client appro.

Client

Statens vegvesen

Tillatt for offentliggjøring.
Batymetridata er nedskalert til
50x50 m oppløsning.

Contractor

Norconsult ❖   DR. TECHN. OLAV OLSEN

Contract no.:

18/91094

Document name:

K12 – Summary report

Document no.:	Rev.:	Pages:
SBJ-33-C5-OON-22-RE-100	0	247

CONCEPT DEVELOPMENT FLOATING BRIDGE E39 BJØRNAFJORDEN

K12 – SUMMARY REPORT

REPORT

Project name:

CONCEPT DEVELOPMENT FLOATING BRIDGE E39
BJØRNAFJORDEN

Document name:

K12 – SUMMARY REPORT

Project number:	5187772/12777
Document number:	SBJ-33-C5-OON-22-RE-100
Date:	15.08.2019
Revision:	0
Number of pages:	247
Prepared by:	Project team
Controlled by:	Anette Fjeld
Approved by:	Kolbjørn Høyland

Table of Content

1   INTRODUCTION

1.1   Current report

This report gives a summary of the K12 floating bridge concept developed. Reference is made to the following reports and drawings made by the project team.

SBJ-32-C5-OON-22-RE-002	Concept selection and risk management	[1]
SBJ-32-C5-OON-22-RE-003	Analysis method	[2]
SBJ-32-C5-OON-22-RE-004	Verification and validation	[3]
SBJ-32-C5-OON-22-RE-005	Sensitivity studies	[4]
SBJ-32-C5-OON-22-RE-006	Parametric resonance	[5]
SBJ-32-C5-OON-22-RE-007	Aerodynamic optimization	[6]
SBJ-32-C5-OON-22-RE-008	Hydrodynamic optimization	[7]
SBJ-32-C5-OON-22-RE-009	Automated steel fabrication	[8]
SBJ-33-C5-OON-22-RE-011	K12 - Architectural design	[9]
SBJ-33-C5-OON-22-RE-012	K12 - Structural response analyses	[10]
SBJ-33-C5-OON-22-RE-013	K12 - Ship impact, Global assessment	[11]
SBJ-33-C5-OON-22-RE-014	K12 - Ship impact, Pontoons and columns	[12]
SBJ-33-C5-OON-22-RE-015	K12 - Ship impact, Bridge girder	[13]
SBJ-33-C5-OON-22-RE-016	K12 - Fatigue assessment	[14]
SBJ-33-C5-OON-22-RE-017	K12 - Design of bridge girder	[15]
SBJ-33-C5-OON-22-RE-018	K12 - Design of pontoons and columns	[16]
SBJ-33-C5-OON-22-RE-019	K12 - Design of cable stayed bridge	[17]
SBJ-33-C5-OON-22-RE-020	K12 - Design of abutments	[18]
SBJ-33-C5-OON-22-RE-021	K12 - Design of mooring and anchoring	[19]
SBJ-33-C5-OON-22-RE-022	K12 - Marine geotechnical design	[20]
SBJ-33-C5-OON-22-RE-023	K12 - Execution of construction	[21]

SBJ-33-C5-OON-05-DR-001	K12 - Road alignment - Plan and profile, profile no 35500 - 39250
SBJ-33-C5-OON-05-DR-002	K12 - Road alignment - Plan and profile, profile no 39250 - 43000
SBJ-33-C5-OON-05-DR-003	K12 - Road alignment - Plan and profile, profile no 43000 - 46750
SBJ-33-C5-OON-22-DR-001	K12 - General arrangement
SBJ-33-C5-OON-22-DR-101	K12 - Iso perspective 1
SBJ-33-C5-OON-22-DR-102	K12 - Iso perspective 2
SBJ-33-C5-OON-22-DR-103	K12 - Iso perspective 3
SBJ-33-C5-OON-22-DR-104	K12 - Iso perspective 4
SBJ-33-C5-OON-22-DR-105	K12 - Iso perspective 5
SBJ-33-C5-OON-22-DR-111	K12 - Floating bridge - Plan and elevation
SBJ-33-C5-OON-22-DR-121	K12 - Floating bridge - Pontoons and columns Type 1 - Structural arrangement
SBJ-33-C5-OON-22-DR-122	K12 - Floating bridge - Pontoons and columns Type 2 - Structural arrangement
SBJ-33-C5-OON-22-DR-123	K12 - Floating bridge - Pontoons and columns Type 2A - Structural arrangement
SBJ-33-C5-OON-22-DR-124	K12 - Floating bridge - Pontoons and columns Type 3 - Structural arrangement
SBJ-33-C5-OON-22-DR-125	K12 - Floating bridge - Pontoons and columns - Sections and details
SBJ-33-C5-OON-22-DR-131	K12 - Floating bridge - Anchors and mooring lines - Layout
SBJ-33-C5-OON-22-DR-132	K12 - Floating bridge - Anchors - Suction anchor plan, sections and details
SBJ-33-C5-OON-22-DR-133	K12 - Floating bridge - Anchors - Gravity anchor plan, sections and details
SBJ-33-C5-OON-22-DR-141	K12 - Floating bridge - Girder - Cross-sections 1
SBJ-33-C5-OON-22-DR-142	K12 - Floating bridge - Girder - Cross-sections 2
SBJ-33-C5-OON-22-DR-143	K12 - Floating bridge - Girder - Reinforced bridge girder ends
SBJ-33-C5-OON-22-DR-144	K12 - Floating bridge - Girder - Details part 1
SBJ-33-C5-OON-22-DR-145	K12 - Floating bridge - Girder - Column connection - Arrangement

SBJ-33-C5-OON-22-DR-146	K12 - Floating bridge - Girder - Column connection 2
SBJ-33-C5-OON-22-DR-147	K12 - Floating bridge - Girder - Wind guide and drainage
SBJ-33-C5-OON-22-DR-151	K12 - Cable-stayed bridge - Plan and elevation
SBJ-33-C5-OON-22-DR-152	K12 - Cable-stayed bridge - Tower - Plan and sections
SBJ-33-C5-OON-22-DR-153	K12 - Cable-stayed bridge - Tower - Cable attachment
SBJ-33-C5-OON-22-DR-154	K12 - Cable-stayed bridge - Bridge girder
SBJ-33-C5-OON-22-DR-155	K12 - Cable-stayed bridge - Bridge girder, cable attachment
SBJ-33-C5-OON-22-DR-156	K12 - Cable-stayed bridge - Reinforcement in critical sections
SBJ-33-C5-OON-22-DR-157	K12 - Cable-stayed bridge - Cable system - Arrangement and details
SBJ-33-C5-OON-22-DR-158	K12 - Cable-stayed bridge - Rock anchoring
SBJ-33-C5-OON-22-DR-159	K12 - Cable-stayed to floating bridge connection
SBJ-33-C5-OON-22-DR-160	K12 - Cable-stayed bridge - Isometric 3D-view
SBJ-33-C5-OON-22-DR-161	K12 - Cable-stayed bridge - Tower. Post-tensioning layout.
SBJ-33-C5-OON-22-DR-162	K12 - Cable-stayed bridge - Temperary connection of tower and girder
SBJ-33-C5-OON-22-DR-163	K12 - Cable-stayed bridge - Construction sequences
SBJ-33-C5-OON-22-DR-164	K12 - Cable-stayed bridge - Ballasting for instalment
SBJ-33-C5-OON-22-DR-171	K12 - Abutment Gulholmane - General arrangement
SBJ-33-C5-OON-22-DR-172	K12 - Abutment Gulholmane - Section and details I
SBJ-33-C5-OON-22-DR-173	K12 - Abutment Gulholmane - Section and details II
SBJ-33-C5-OON-22-DR-174	K12 - Abutment Gulholmane - Post-tensioning
SBJ-33-C5-OON-22-DR-175	K12 - Abutment Gulholmane - Connection to bridge girder end
SBJ-33-C5-OON-22-DR-176	K12 - Abutment South - General arrangement
SBJ-33-C5-OON-22-DR-177	K12 - Abutment South - Sections and details
SBJ-33-C5-OON-22-DR-181	K12 - Gulholmane approach bridge - General arrangement
SBJ-33-C5-OON-22-DR-191	K12 - Bjørnafjorden bridge - Membrane and pavement - Principle drawing
SBJ-33-C5-OON-22-DR-192	K12 - Bjørnafjorden bridge - Railings - Principle drawing
SBJ-33-C5-OON-22-DR-201	K12 - Fabrication - Bridge girder part 1
SBJ-33-C5-OON-22-DR-202	K12 - Fabrication - Bridge girder part 2
SBJ-33-C5-OON-22-DR-203	K12 - Fabrication - Bridge girder part 3
SBJ-33-C5-OON-22-DR-204	K12 - Fabrication - Bridge girder part 4
SBJ-33-C5-OON-22-DR-205	K12 - Fabrication - Bridge girder part 5
SBJ-33-C5-OON-24-DR-001	K12 - Tug moored at pontoon
SBJ-33-C5-OON-24-DR-002	K12 - Towing configuration 480 m section
SBJ-33-C5-OON-24-DR-003	K12 - Tow 480 m section - Vatlestraumen
SBJ-33-C5-OON-24-DR-004	K12 - General Arrangement Assembly Rig
SBJ-33-C5-OON-24-DR-005	K12 - General Arrangement High Assembly Rig
SBJ-33-C5-OON-24-DR-006	K12 - Bridge Moored Søreidvika
SBJ-33-C5-OON-24-DR-007	K12 - Assembly sequence Søreidvågen
SBJ-33-C5-OON-24-DR-008	K12 - Assembly sequence Søreidvågen
SBJ-33-C5-OON-24-DR-009	K12 - Assembly Section 1 & 2 Søreidvågen
SBJ-33-C5-OON-24-DR-010	K12 - Assembly 480 m sections
SBJ-33-C5-OON-24-DR-011	K12 - Assembly details, step #4
SBJ-33-C5-OON-24-DR-012	K12 - Towing configuration
SBJ-33-C5-OON-24-DR-013	K12 - Towing Hold Configuration, alt. A
SBJ-33-C5-OON-24-DR-014	K12 - Towing Hold Configuration, alt. A
SBJ-33-C5-OON-24-DR-015	K12 - Towing Søreidvåg to Bjørnafjorden
SBJ-33-C5-OON-24-DR-017	K12 - Assembly sequence Bjørnafjorden
SBJ-33-C5-OON-24-DR-018	K12 - North abutment installation, step #1
SBJ-33-C5-OON-24-DR-019	K12 - North abutment installation, step #2
SBJ-33-C5-OON-24-DR-020	K12 - Bridge Arriving at Bjørnafjorden
SBJ-33-C5-OON-24-DR-021	K12 - Floating Bridge at North Abutment
SBJ-33-C5-OON-24-DR-022	K12 - Connecting at high bridge end
SBJ-33-C5-OON-24-DR-023	K12 - Pre-installed anchors
SBJ-33-C5-OON-24-DR-024	K12 - AHTS connecting anchor lines
SBJ-33-C5-OON-24-DR-025	K12 - AHTS connecting anchor lines
SBJ-33-C5-OON-24-DR-026	K12 - Tensioner details
SBJ-33-C5-OON-24-DR-027	K12 - AHTS tensioning mooring lines
SBJ-33-C5-OON-24-DR-028	K12 - Mooring lines installed

The concept has been developed based on a design basis prepared by the Norwegian Public Roads administration, "Statens Vegvesen" (SVV)

SBJ-32-C4-SVV-90-BA-001	Design Basis Bjørnafjorden	[22]
SBJ-01-C4-SVV-01-BA-001	Design Basis MetOcean	[23]
SBJ-02-C4-SVV-02-RE-004	Design Basis Geotechnical design	[24]
SBJ-32-C4-SVV-26-BA-001	Design Basis Mooring and Anchor	[25]

1.2 Project context

Statens vegvesen (SVV) has been commissioned by the Norwegian Ministry of Transport and Communications to develop plans for a ferry free coastal highway E39 between Kristiansand and Trondheim. The 1100 km long coastal corridor comprise today 8 ferry connections, most of them wide and deep fjord crossings that will require massive investments and longer spanning structures than previously installed in Norway. Based on the choice of concept evaluation (KVU) E39 Aksdal Bergen, the Ministry of Transport and Communications has decided that E39 shall cross Bjørnafjorden between Reksteren and Os.

SVV is finalizing the work on a governmental regional plan with consequence assessment for E39 Stord-Os. This plan recommends a route from Stord to Os, including crossing solution for Bjørnafjorden, and shall be approved by the ministry of Local Government and Modernisation. In this fifth phase of the concept development, only floating bridge alternatives remain under consideration.
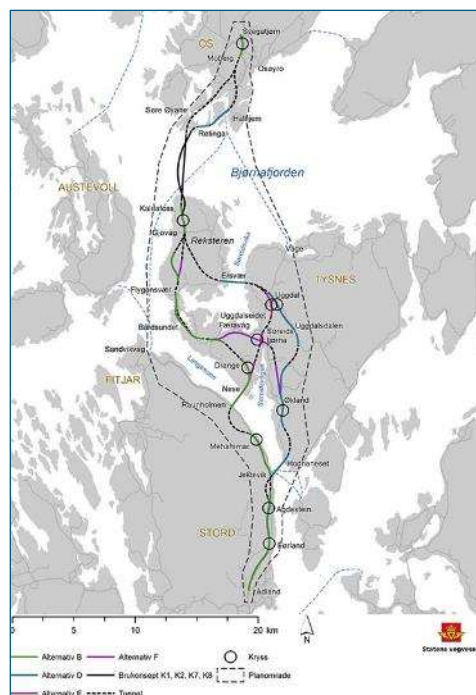
1.3 Project team

Norconsult AS and Dr.techn.Olav Olsen AS have a joint work collaboration for execution of this project. Norconsult is the largest multidiscipline consultant in Norway and is a leading player within engineering for transportation and communication. Dr.techn.Olav Olsen is an independent structural engineering and marine technology consultant firm, who has a specialty in design of large floating structures. The team has been strengthened with selected subcontractors who are all highly qualified within their respective areas of expertise:

- Prodtex AS is a consultancy company specializing in the development of modern production and design processes. Prodtex sits on a highly qualified staff who have experience from design and operation of automated factories, where robots are used to handle materials and to carry out welding processes.
- Pure Logic AS is a consultancy firm specializing in cost- and uncertainty analyses for prediction of design effects to optimize large-scale constructs, ensuring optimal feedback for a multidisciplinary project team.
- Institute for Energy Technology (IFE) is an independent nonprofit foundation with 600 employees dedicated to research on energy technologies. IFE has been working on high-performance computing software based on the Finite-Element-Method for the industry, wind, wind loads and aero-elasticity for more than 40 years.
- Buksér og Berging AS (BB) provides turn-key solutions, quality vessels and maritime personnel for the marine operations market. BB is currently operating

30 vessels for harbour assistance, project work and offshore support from headquarter at Lysaker, Norway.

- Miko Marine AS is a Norwegian registered company, established in 1996. The company specializes in products and services for oil pollution prevention and in-water repair of ship and floating rigs, and is further offering marine operation services for transport, handling and installation of heavy construction elements in the marine environment.
- Heyerdahl Arkitekter AS has in the last 20 years been providing architect services to major national infrastructural projects, both for roads and rails. The company shares has been sold to Norconsult, and the companies will be merged by 2020.
- Haug og Blom-Bakke AS is a structural engineering consultancy firm, who has extensive experience in bridge design.
- FORCE Technology AS is engineering company supplying assistance within many fields and has in this project phase provided services within corrosion protection by use of coating technology and inspection/maintenance/monitoring.
- Swerim is a newly founded Metals and Mining research institute. It originates from Swerea-KIMAB and Swerea-MEFOS and the metals research institute IM founded in 1921. Core competences are within manufacturing of and with metals, including application technologies for infrastructure, vehicles / transport, and the manufacturing industry.

In order to strengthen our expertise further on risk and uncertainties management in execution of large construction projects Kåre Dybwad has been seconded to the team as a consultant.

1.4   Project scope

The objective of this project phase was to develop 4 nominated floating bridge concepts, document all 4 concepts sufficiently for ranking, and recommend the best suited alternative. The characteristics of the 4 concepts were as follows:

- K11: End-anchored floating bridge. In previous phase named K7.
- K12: End-anchored floating bridge with mooring system for increase robustness and redundancy.
- K13: Straight side-anchored bridge with expansion joint. In previous phase named K8.
- K14: Side-anchored bridge without expansion joint.

In order to make the correct recommendation all available documentation from previous phases were thoroughly examined. Design and construction premises as well as selection criteria were carefully considered and discussed with the Client. This formed basis for the documentation of work performed and the conclusions presented. Key tasks were:

- Global analyses including sensitivity studies and validation of results
- Prediction of aerodynamic loads
- Prediction of hydrodynamic loads
- Ship impact analyses, investigation of local and global effects
- Fatigue analyses
- Design of structural elements
- Marine geotechnical evaluations
- Steel fabrication
- Bridge assembly and installation
- Architectural design
- Risk assessment

2 CONCEPT DESCRIPTION AND SELECTION

2.1 Concept selection

Based on the work performed, the given design basis, available background data and defined evaluation criteria, the project team has selected K12, the moored arch, as the preferred strait crossing concept for Bjørnafjorden and focus of further concept optimization.

The four concepts have been evaluated with respect to cost, robustness, sustainability, aesthetics and an engineering judgement ranking performed by the conceptual expert team. In the engineering judgement process, the decisive factors were robustness, life expectancy and complexity of the main load carrying structures. The highlights of each evaluation are provided on a general level in this chapter, and concept specific in chapter **Error! Reference source not found.**. A summary of the combined evaluation can be seen in **Error! Reference source not found.**.

All concepts have acceptable utilization with respect to safety and functionality and has been matured to an adequate level. The concepts are therefore deemed comparable and suitable for a conclusive recommendation.

> *Table 2-1: The resulting concept ranking and individual score per category for each concept. The score expresses the equivalent cost in MNOK. A lower value is better.*

Concept	K11	K12	K13	K14	
Concept cost	13 521	**13 424**	13 694	13 605	(p85 concept cost)
Robustness	2 450	**2 270**	2 992	2 813	(p85 cost of consequence)
Sustainability	667	**641**	682	678	(p85 cost of Co2-equivalents)
Aesthetics	-500	**-500**	-300	-500	Weighted value of monumental building
Summed impact	16 138	**15 835**	17 068	16 596	[MNOK]
Difference in impact	- 930	**- 1 233**	0	- 472	[MNOK]
Engineering Judgment	2	**1**	4	3	Nominated Ranking
Compiled Ranking	**2**	**①**	**4**	**3**	Final Ranking

A summary of the engineering judgement evaluation is shown on the following page.

	K11	**K12**
Pros:	- Known technology, built before (in a smaller scale) - Simple system, easy to calculate response from loads, ductile behavior - Known eigenperiods which are difficult to move - Larger capacity for unknown overloading due to stronger bridge girder - Installation of complete assembled floating bridge, less work in Bjørnafjorden - Less maintenance, few "wearing parts"	- Redundant system with double horizontal load-carrying system. - Largest potential for- and flexibility in designing a robust solution. - Mooring reduces the response and increases design life compared to K11. Possible to increase design life further with small amount of additional steel. - Fibre rope mooring gives favorable interaction with bridge girder. - Linear behavior of mooring without risk of successive mooring line failure for known load cases - Installation of complete assembled floating bridge, less work in Bjørnafjorden, simple mooring hook-up - Few and manageable anchor locations - No joints and bearings
Cons:	- Lack of redundancy - Uncertain wind load as turbulence spectra are normally not applied to structures with long eigenperiods - Large, concentrated forces at landfalls - Requires larger clearance between tower legs	- Mooring needs replacement within design life. Complexity and costs related to this operation not sufficiently reflected. - Challenging soil conditions, risk of underwater slides - Limited experience with taut mooring on these water depths
Rank:	**2**	**1**
Reason:	Most simple	Most robust

	K13	**K14**
Pros:	- Redundancy in mooring - Fibre rope mooring gives favorable interaction with bridge girder. - Linear behavior of mooring without risk of successive mooring line failure for known load cases. - Simplest production. - Potential for moving landfall north onto the bank outside Gulholmane and obtaining a shorter bridge.	- Redundancy in mooring - Fibre rope mooring gives favorable interaction with bridge girder. - Linear behavior of mooring without risk of successive mooring line failure for known load cases. - No joints and bearings
Cons:	- Mooring, part of main load-carrying system, needs replacement within design life. Complexity and costs related not sufficiently reflected. - Challenging soil conditions, risk of underwater slides - Many and some unfavorable anchor positions. - Limited experience with taut mooring on these water depths - Great number of work operations performed on the fjord. - Monotonic driving experience - Maintenance of joints and bearings - Noise from joints	- Mooring, part of main load-carrying system, needs replacement within design life. Complexity and costs related not sufficiently reflected. - Challenging soil conditions, risk of underwater slides - Some unfavorable anchor positions. - Limited experience with taut mooring on these water depths - Great number of work operations performed on the fjord.
Rank:	**4**	**3**

2.2   Alignment

K12 is the moored arch alternative, and the developed concept has two mooring groups, with four moored pontoons in each group. The cable-stayed bridge in the south has the tower placed on Svarvhelleholmen and provides the navigation channel with 45 m sailing height. The cable-stayed bridge is straight, while the floating bridge has a radius of 5000 m and lands on Gulholmane
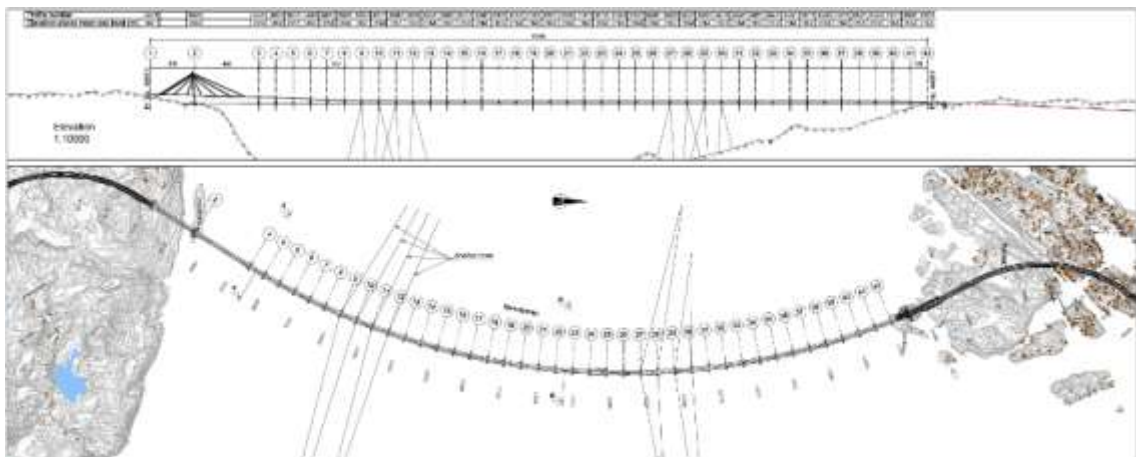
>   *Figure 2-1: Plan and elevation*

>   *Figure 2-2: Bridge model inserted into 3D panorama. Viewed from east.*

> *Figure 2-3: Bridge model inserted into 3D panorama. Viewed from north-west.*

2.3   Key figures

> *Table 2-2: Key conceptual figures*

Geometry - arch	R = 5 000 m
Length	5 440 m
Cable stayed bridge main span – pylon to first pontoon	450 m
No. of pontoons	39
Pontoon spacing	120 m
No of expansion joints	0
No of bearings	0
First 5 horisontal eigenperiods	56, 49, 32, 21, 16 s
No. Of Mooring groups	2
Mooring position Approx.	0,33L 0,67L
Horisontal mooring stiffness – anchor group	800 kN/m
Bridge girder steel	79 905 ton
Pontoon steel	38 174 ton
Column steel	8 481 ton
Girder cross section - typical	1,72 m^2
Girder I_z - typical	132 m^4
Girder I_y - typical	3,2 m^4

3   GLOBAL RESPONSE ANALYSES

3.1   Analysis setup

3.1.1   General input

The global analyses have been performed by use of three different software programs. The time domain dynamic analyses are performed in 3DFloat [26], frequency domain dynamic analyses are performed in DynNO/ABAQUS (see appendix D), and ship impact analyses are performed in ABAQUS, while the static analyses are performed in Sofistik [27].

All models apply the same geometry, mesh (except the ship impact model) and boundary conditions.

Element type is Euler-Bernoulli Beam, and the bridge girder is represented by 6 elements between pontoons.

In the global analyses considered for the concept selection the mooring system is represented by a single cable element giving it a linear behavior. Global dynamic analyses with a finer mesh shows that this representation is sufficiently accurate. See [4].
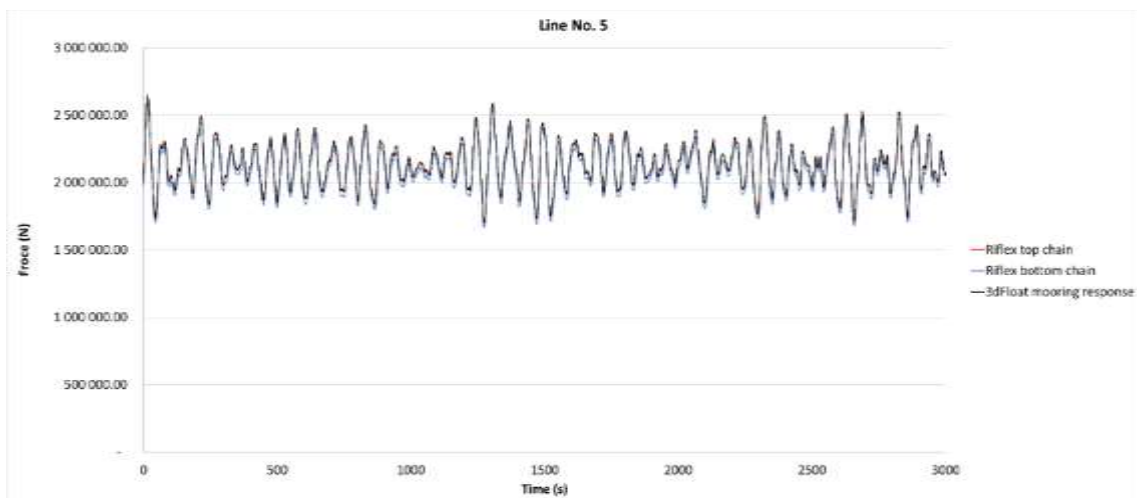
> *Figure 3-1 Example of response comparison 3DFloat – Simo Riflex for line 5*

3.1.2   Dynamic setup time domain analyses

The time step used is 0.1s. Benchmark of global analyses [3] verifies that 0.1s is a converged time step as it produces similar response as the frequency domain solver.

The analyses are divided into three phases:
— In the first phase (pre-phase) the model is introduced to a lot of damping so that the initial motion is stopped. This gives us a zero (reference) point in time from which the environmental response can be traced. The duration of the pre-phase is 500s.
— The next phase is the ramping phase. Here the environmental states are ramped up, so that the bridge starts to move as it should during a storm. The duration of the ramping phase is 1500s.

— The last phase is the analysis phase from where the response is measured. This phase lasts for 3600s.

3dfloat applies a co-rotated coordinate system that considers nonlinearities such as geometric stiffness, drag from different angles of incident, and aero- and hydrodynamic viscous damping. Other effects are frequency dependent potential damping, force and added mass, and second order drift forces.

Modal analysis show that the chosen mesh length is capturing the modal shapes with regards to heave, sway and axial behavior for the first 100 modes. With regards to high frequency torsional behavior, a somewhat finer mesh would have been preferable, but since high frequency torsional response is not the most vital global response for this phase, the mesh is deemed good enough.

A Rayleigh damping has been applied on the structure. The ratio is set to 0.5% for two frequencies. The angular frequencies chosen are 0.0785 rad/s and 2.094 rad/s. This gives us the structural damping presented in Figure 3-2.
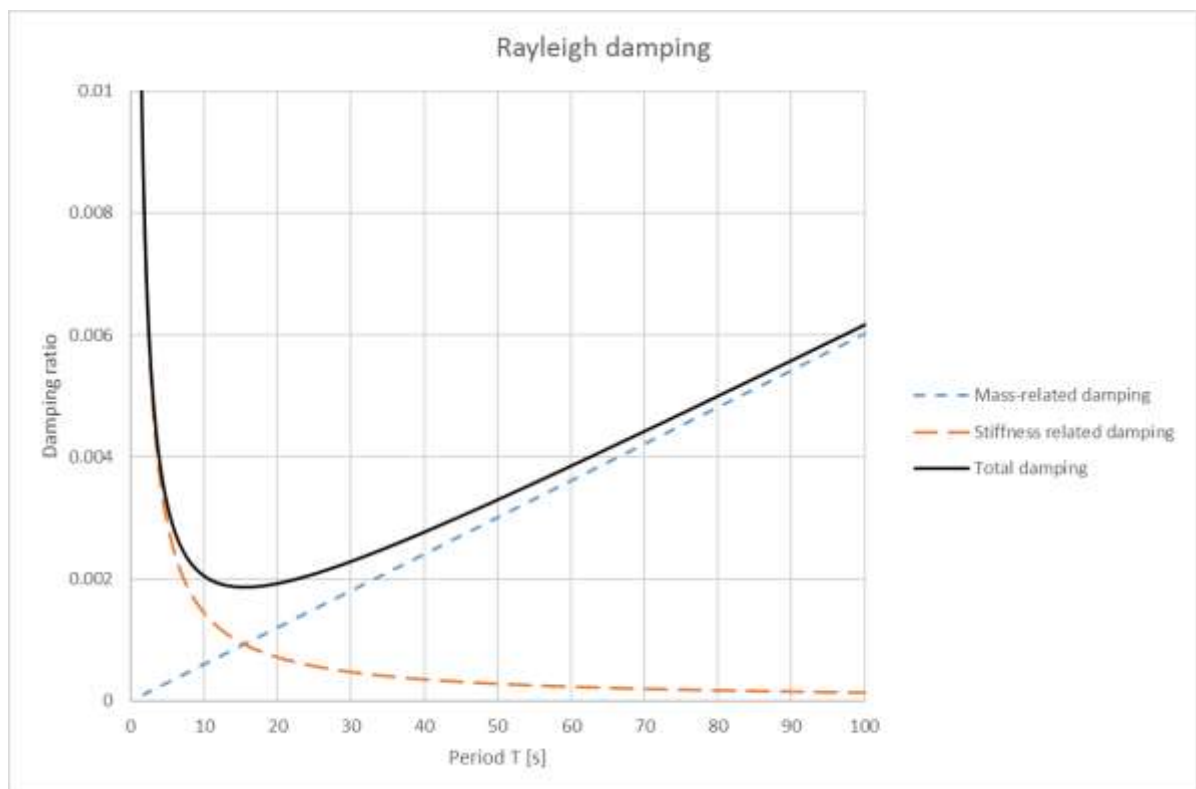
> *Figure 3-2: Chosen Rayleigh damping*

3.1.3 Dynamic setup frequency domain analyses

The frequency domain analyses are performed in DynNO/ABAQUS. DynNO is a program developed by Norconsult that calculate response from dynamic stochastic loads, such as wind and waves, in the frequency domain. DynNO uses the input from a modal analysis in ABAQUS and calculates the multimodal response in modal coordinates.

The program can describe stochastic loads with spatial variations, and both aerodynamic and hydrodynamic effects. The aerodynamic motion induced forces can be described using the quasi-steady theory or the more complete description with aerodynamic derivatives. Hydrodynamic loads from linear potential theory such as potential damping and added mass can be included with input from Wamit. Viscous damping effects can be included through an iterative calculation using stochastic linearization through the Borgman model [28].

The ABAQUS models are generated based on the information database in the GreenBox system. An identical element mesh to the 3Dfloat and Sofistik models is used. The element formulation B31 is used, which is a linear 3D Timoshenko beam element.
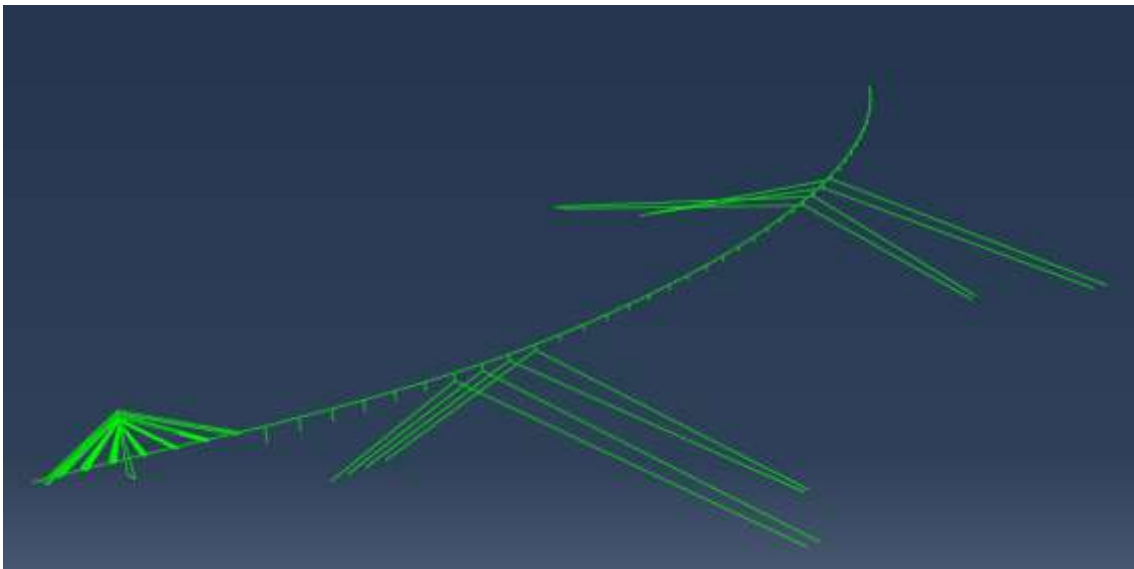
> *Figure 3-3 ABAQUS model of K12-model20*

To get a straight bridge after dead load is introduced, pontoon buoyancy forces are applied and the elements of the cable stayed bridge are subjected to temperature strains to counteract the strains from the dead loads. The buoyancy forces and the temperature strains are calculated by an iterative approach.

During the iterations the pontoon points are modeled with vertical boundary conditions. These are removed and replaced with vertical forces according to the reaction forces representing the buoyancy forces for the pontoons. In all iterations the change of element lengths according to the target geometry is calculated for all elements in the cable stayed bridge part. The cables are subjected to temperature contractions to counteract the tensile strains from the dead loading, whereas the girder and the tower is subjected to temperature expansion. After the iterations the loaded bridge obtains its initial geometry.

The iteration steps are performed with nonlinear geometry definitions activated. After the permanently loaded configuration is obtained an eigenvalue solution step is performed including geometric stiffness effects.

The ABAQUS model is used for flutter investigations, so it is important to model the rotational inertia relatively good.

3.1.4   Dynamic setup for ship impact analysis

The dynamic analyses used for global evaluation of ship impacts are performed in Abaqus. The model is generated based on the information database in the GreenBox system. When implemented in Abaqus CAE a few modifications are done to the geometry and the model is re-meshed. The model is described in detail in the "Ship impact, global assessment" report [11].

3.1.5   Static setup

All static analyses are performed by use of Sofistik [29]. The static response is based on a non-linear analysis of the permanent loads that takes large deformation and the p-delta frame effect in to consideration. The geometric stiffness influence of the permanent loads from the bridge girder and the pontoon towers are thus accounted for in this pre-analysis. The remaining static analyses are linear analyses that takes the updated stiffness from the pre-analysis as a basis for the new analyses.

3.1.6   Ship impact global FE-model

The ship impact analyses have been performed using Abaqus [30]. For the ship impact analyses, the implicit solver is used. The FE-model geometry consists of wires only, which means the only applicable elements are beam and truss elements. Except for the cables the elements are of the type B31 which are 2-node 3-dimensional beam elements with a linear geometric order (uses linear shape functions for the approximations between integration point and the element ends). The cable elements are of the type B31H. B31H are the same elements as B31 but with two additional variables related to the axial force and transverse shear force.

The element size of the cables is set to a large number such that one cable is one element only, which improves the computational behavior. This means the geometric stiffness of the cable is neglected, but as the cables are tensioned the representation of the overall behavior is quite good. This is the same way as the cables are represented in the global design models in 3D-float and also the global verification model from Abaqus. For the rest of the model the global element size is approximately 10 m, meaning all the structural elements are parted into calculation elements of approximately 10 m.

The pontoons are not included physically in the model, but their hydrostatic characteristics are represented. These are implemented using connector elements (see Appendix A.2) with elastic behavior and damping. The connectors are applied at water level and describe a linear stiffness for vertical motions and for rotations about horizontal axis (longitudinal and transverse). The pontoon structural masses are applied in the buoyancy center and includes rotational inertias.

Viscous damping on the pontoons is included in the horizontal degrees of freedom (U1, U2), as a function of the horizontal velocity. The drag factors are based on CFD-analysis, see the hydrodynamic optimization report [7]:
-    0.3 in the longitudinal direction
-    0.6 in the transverse direction

Added mass is applied in the same point as the water plane stiffness. Added mass is conservatively set to infinite frequency values. The added mass is specified for all six degrees of freedom.

3.1.7 Ship impact analyses

The ship impact analysis is performed on a stabilized model with gravity, tensioning of cables and pontoon buoyancy applied. There is a static step in the beginning of the analysis to obtain this stabilized model, before the implicit dynamic ship impact steps in the time domain.

The dynamic response from the impact energy depend on ship stiffness and stiffness and mass of the structure. To ensure a ductile design the analysis considers the differences in stiffness. This is done by transferring the energy through the following steps:
1. Ship bow-pontoon/deckhouse-girder impact. Represented by a force-indentation curve, based on local analysis.
2. Bridge structure. Represented by global FE-model.

For the pontoon side impacts (90 deg, girder longitudinal direction) there has also been performed local analysis giving moment-rotation-curves for bending and torsion in columns, as the section forces for some impacts are larger than the elastic capacities.

By combining the stiffness and mass in different parts of the system in one model, we obtain a realistic energy distribution. For the connection between ship and pontoon this can be illustrated with the graph in Figure 3-4. The graph shows that the mobilized resistance is equal in the two systems, and that this balance, together with the force-indentation relations, give the corresponding deformations and energy absorption in each part of the system.
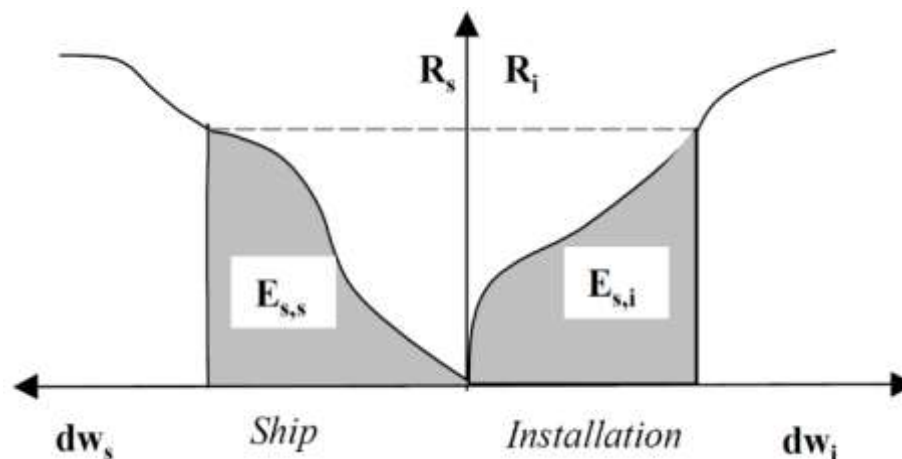
> *Figure 3-4 Force equilibrium based on force-indention curves.*

Figure 3-5 shows an overview of the workflow used for the ship impact analysis. The figures and graphs inside are for illustration purpose only.
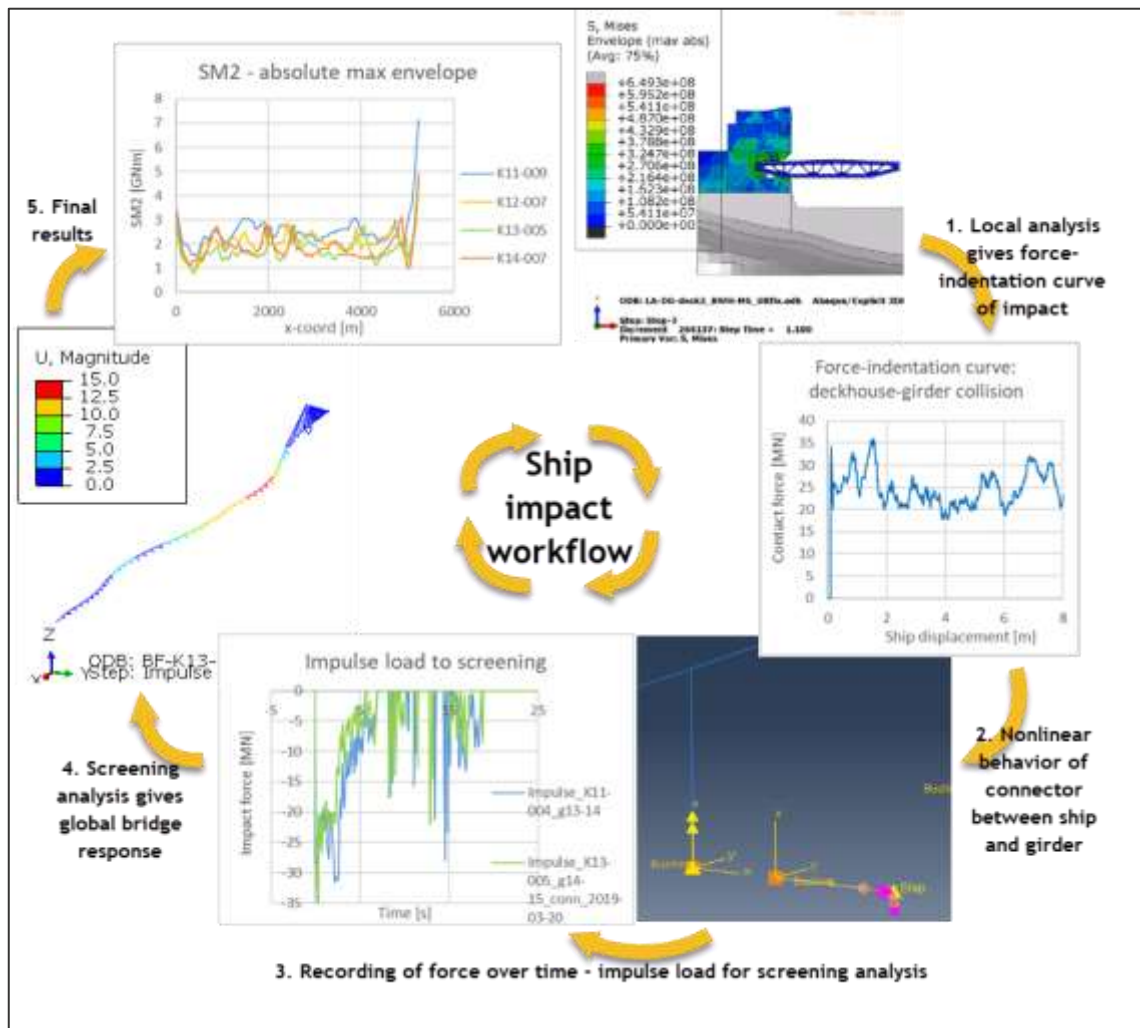
> *Figure 3-5 Ship impact workflow. Step 1: Local analyses as in report [12] and [13].*
> *Step 2: Global analyses with spring-mass-system. Step 3-4: Screening analyses.*
> *Step 5: Post-processing of results and evaluations.*

Ship impact on pontoons

The ship impact analysis is set up using a point mass describing the ship and a connector element. The connector element represents the force-indentation between the ship and the pontoon. The "ship" is set up with an initial speed in the impact direction and allowed to move in the horizontal plane only. Between the ship and the pontoon there is a connector element representing the deformation of the ship bow and the pontoon wall as given from the local analysis. The connector element has an inelastic behavior in the impact direction. The elastic part of the compression behavior is set to a large number, as the results from the local analysis includes both linear and plastic deformations. The pontoon deformation connector is elastic in the transverse direction and for separation of ship and pontoon, both with low stiffnesses. The transverse stiffness is set to 1000 times the tensional stiffness, to see if the ship changes direction due to deformations in the column and pontoon. There is no connection for vertical motions, allowing the pontoon center point to move independently of the ship in the vertical direction.

During the impact event and response, the ship is restricted from vertical and rotational movement, and is moving in the horizontal plane only. The kinetic energy in of the ship mass is transferred to the connector system until the ship is stopped and sent back by the strain energy accumulated in the bridge during the impact. The connector elements have a very low spring stiffness for separation of the ship and pontoon, allowing the ship to "float away". The ship impact setup is shown in Figure 3-6.

Note that the distances in Figure 3-6 are only for visual representation and that the true force-indentation characteristics are given as properties in the connector elements, see Table 3-1.

> *Table 3-1 Ship-pontoon connector properties*

Degree of freedom	Property	Stiffness
U1- - axial compression, elastic part	Elastic, stiff	10 GN/m
U1- - axial compression, plastic part	Plastic	From force-indentation curve
U1+ - axial tension/elongation	Elastic, soft	0.1 N/m
U2 +/- - transverse motion	Linear elastic	100 N/m
U3 – vertical motion	None	-
UR1/UR2/UR3 – rotational DOFs	None	-
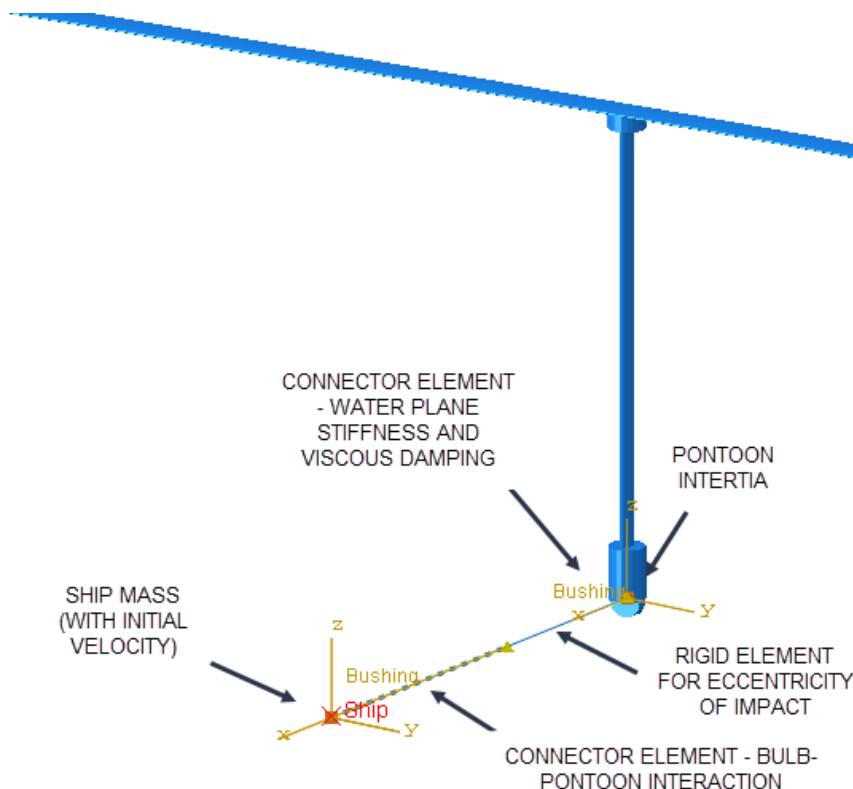
> *Figure 3-6: Ship impact setup for a head-on (0-deg) ship impact on pontoon in axis 3 (for an older model version). Note that the length of the connector is only for visual representation.*

The mass of the ship is placed in the reference point "Ship", while the inertia-properties of the pontoon placed in the buoyancy center. The rigid element has a length equal to the distance from pontoon center to the transition between straight and curved pontoon wall. As all the pontoons are 58 m long, this is 58/2 m minus half of the pontoon width – respectively 23 m, 21.75 m and 20.25 m for the 12 m, 14.5 m and 17.5 m wide pontoons. As the center of the impact from the container ship (center bulb) is approximately at the buoyancy center of the pontoon (2,5 m below water plane), the rigid element is horizontal.

Ship impact on bridge girder
Impact directly on the bridge girder is modelled with a single connector that takes deckhouse and girder deformation into account.
1. The ship is modelled as a point mass with mass and velocity consistent with the impact energy.
2. Deckhouse-girder indentation is modelled with a connector element using force-indentation curve from local analysis.

Figure 3-7 shows graphically how the point mass, the connector element and the bridge girder are connected. The figure show both the model rendered displaying beam element profiles (above) and wire frame model to show relevant element connections (below).
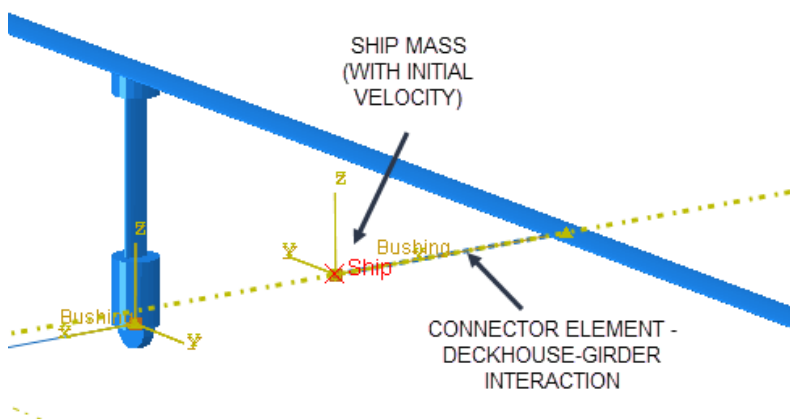
> *Figure 3-7: Ship impact setup for impact on bridge girder. Note that the length of the connector is only for visual representation. Above with beam profile rendering, below without.*

3.1.8   Fatigue analyses

The general workflow for calculating fatigue life is shown below:

1. Creation of relevant FE analysis models:
    a. Global analysis models of the bridge to calculate section forces from the different fatigue load cases; environmental loads, tidal loads and traffic loads.
    b. Local FE models and hand calculations for calculation of stress transfer factors (see ch. 3.4.1) from unit loads at specific points, see Figure 3-9.
2. Establish fatigue specific parameters, i.e. detail categories, design fatigue factors and stress concentration factors, see Table 10-1.
3. Create script that calculates fatigue life for specific points for the entire length of the bridge girder based on the abovementioned points:
    a. Calculation of local stress ranges from global loads based on stress transfer factors from unit load model.

b. Rainflow count of the stress data for all load cases
c. Damage/fatigue life calculation for load types separately
d. Combination of stresses from environmental, tidal and traffic loads according to design basis and DNV-GL Fatigue methodology to calculate combined damage/fatigue life.

This procedure has been used to calculate fatigue life at midspan between all axes and at each axis, see Figure 3-8, for the entire bridge length. Points checked on the girder are shown in Figure 3-9. Stresses calculated for these extremal points are conservatively used for both outer plates as well as trapezoidal stiffeners. The same is done for top and bottom of columns, see Figure 3-10 and Figure 3-11.
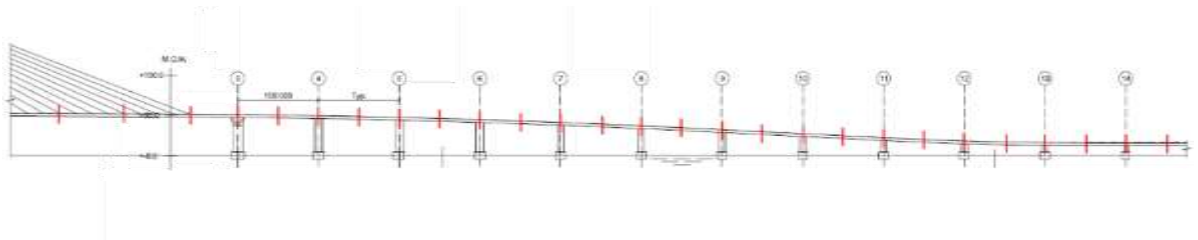
> *Figure 3-8: Areas checked for fatigue damage along the entire length of the bridge*
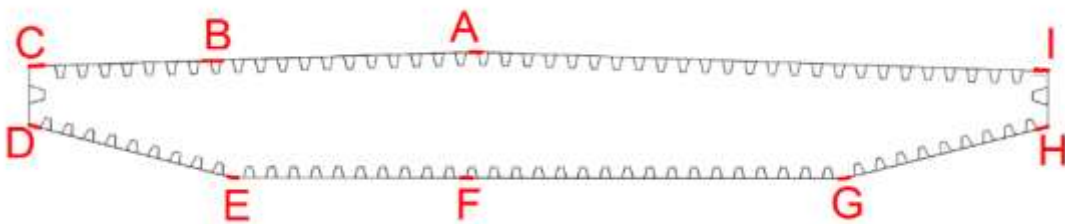
> *Figure 3-9: Points that have been checked for fatigue damage at all midspans and axes.*
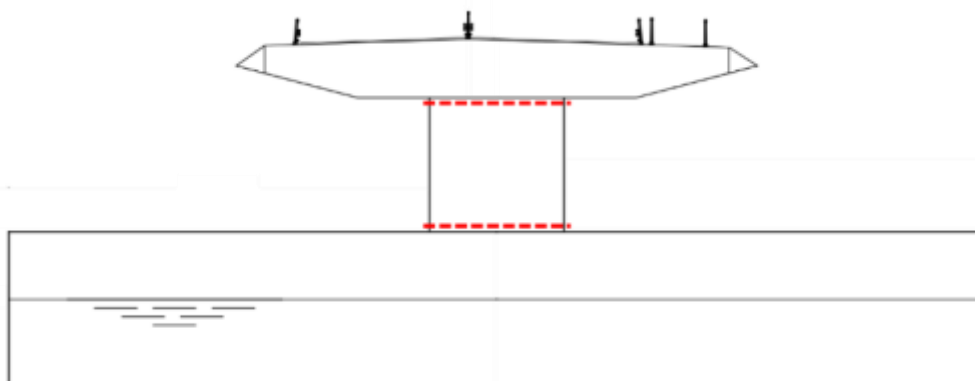
> *Figure 3-10: Cross-sections checked at all columns, ref. point A and C shown below*
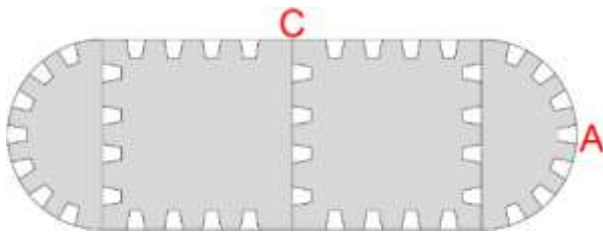
> *Figure 3-11: Points checked for strong and weak axis bending (A and C respectively)*

Fatigue calculations from dynamic environmental loads such as wind and wave loading are computationally demanding since a large number of environmental loads need to be simulated. This make frequency domain calculations attractive for such calculations as it is computationally effective compared with time domain analyses. The system is expected to behave quite linear for the load cases dominating the fatigue life, so frequency domain calculations are deemed applicable.
A challenge arises when estimating damage from frequency domain calculations when the response is multimodal and/or wide banded, as it is for the Bjørnafjord floating bridge. Several methods for estimating fatigue damage from response spectral densities are presented in the literature, but they all come with significant simplifications. The established preferred method to calculate fatigue damage from dynamic environmental loads is the Rainflow cycle counting method. This method is based on stress time series from the dynamic response.

The dynamic response calculations are performed with DynNO. From these analyses corresponding section force time series can be simulated by Cholesky decomposition of the complex response spectral density matrix. In this way the Rainflow cycle counting method can be used for fatigue damage calculations for frequency domain analyses as well.
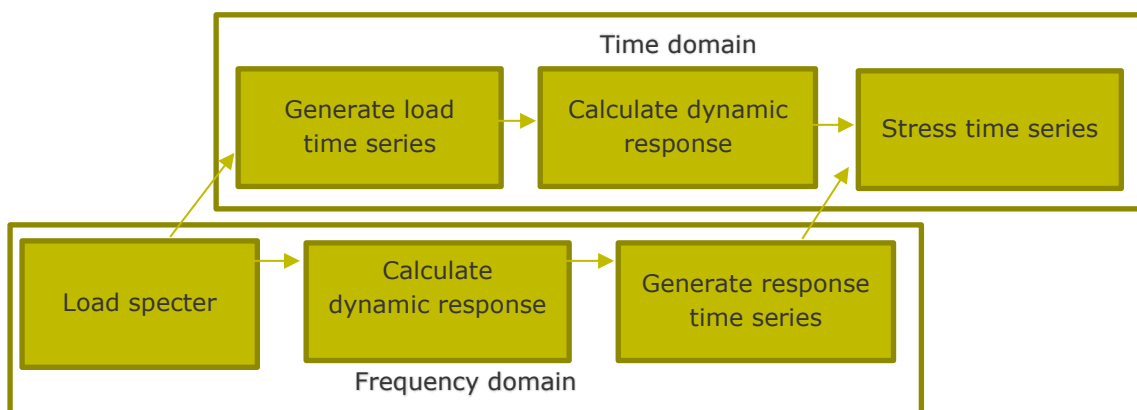
> *Figure 3-12: Fatigue calculation overview*

Point B on the bridge girder is checked for local wheel stresses in combination with global loads. All other points are checked for global loads only. This is because point B is governing for local traffic due to significant stresses from both weak and strong axis moments from environmental loads in addition to being located at the outermost edge of the slow lane directly under lorry wheels.

3.2 Response estimation

3.2.1 Stress calculation

The stresses are calculated according to the expressions below, and the chosen stress points are seen in Figure 3-13.

Normal stress at point

$$\sigma_x = \pm \frac{N_x}{A_x} \pm \frac{M_y}{W_y} \pm \frac{M_z}{W_z}$$

Shear stress at point

$$\tau_x = \frac{M_x}{W_x}$$

Von Mises stress at point

$$\sigma_{VM} = \sqrt{\sigma_x^3 + 3\tau_x}$$

The shear stress for horizontal shear force is not included
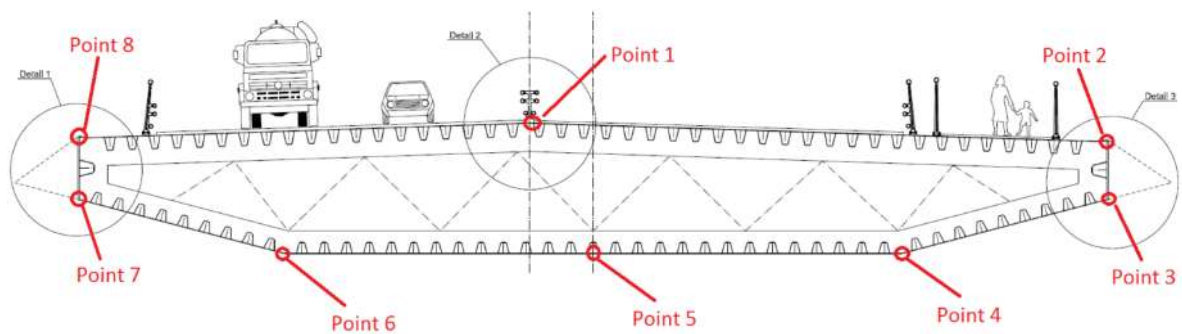
> *Figure 3-13 Stress points in cross section*

3.2.2 Monitoring of the global analyses

The response of the structure is monitored in time-series. The different responses that are documented are shown in the table below

> *Table 3-2 Monitored responses*

	Forces	Moments	Displ.	Accel.	Stresses	Wave height
Main girder	X	X	X (6 dof)	X (6 dof)	X	
Pontoons			X (6 dof)	X (6 dof)		X
Pontoon edge			X (6 dof)	X (6 dof)		X
Pontoon columns	X	X				
Cable stayed tower	X	X				
Cables	X				X	
Mooring lines	X					

The forces, moments, acceleration, displacements and wave heights are given directly by the simulation program. The stresses are traced by use of stress gauges placed around in the cross section as displayed in Figure 3-13. Time series for each stress gauge is found by combining the time series from moments and forces as described in sec. 3.2.1 For each time step the stress is calculated for each of the eight points in the cross section. Doing this it becomes unnecessary to evaluate the simultaneity of the different stress contributions. The associated moments and forces contributing to the stress at each stress gauge are retained so that they later can be used in a cross-section design check. The freeboard can be calculated based on timeseries of displacements and time series of wave height.

3.2.3   Time series vehicles

During each coupled analysis cars are sent from one side of the bridge to the other with a speed of 70km/h.

The time series of the car takes the following into consideration:

1. The road position on the main girder.
    a.   The cars are located a distance y from the center of the girder.
2. The static position of the bridge as the car moves along it (Accelerations due to driving in a vertical or horizontal curve)
3. The dynamic position of the bridge as the car moves along it (Accelerations due to the dynamic behavior of the bridge)

3.2.4   Extreme values

In order to extract the 100 year response from the 100 year sea states, long term analyses have shown that the 90 percentile value of the short-term extreme response distribution is a good approximation. In order to get the 90 percentile value from the time series the following method has been applied.

The mean of the maximum of the different storm simulations gives us the 0.5 percentile response. In order to get the 0.9 percentile response, we have applied an extreme value distribution fitting approach applying the Gumbel-distribution using the maximum likelihood method. When using this approach one can easily extract the wanted percentile response.

Due to heavy simulation time a simplification has been made regarding the 1 year extreme response values. One year response is taken as 0.7 times the 100 year response.

$$R_{1year} = 0.7 * R_{100year}$$

This is a somewhat crude estimation, but the reasoning for the chosen factor is described in the Analysis method report [2]

3.2.5   Evaluation of number of seeds

The error estimation was performed on the final end-anchored bridge model in the phase 3 of the Bjørnafjorden project with the results seen below.
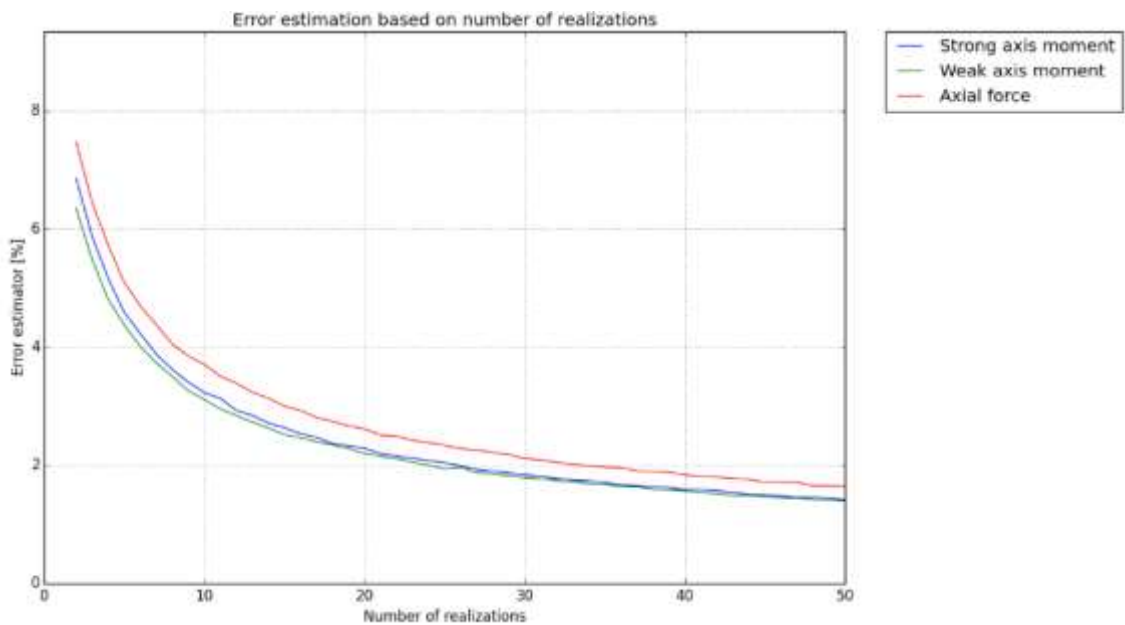
> *Figure 3-14 Standard deviation of error estimation based on number of realizations (Method presented by DNV)*
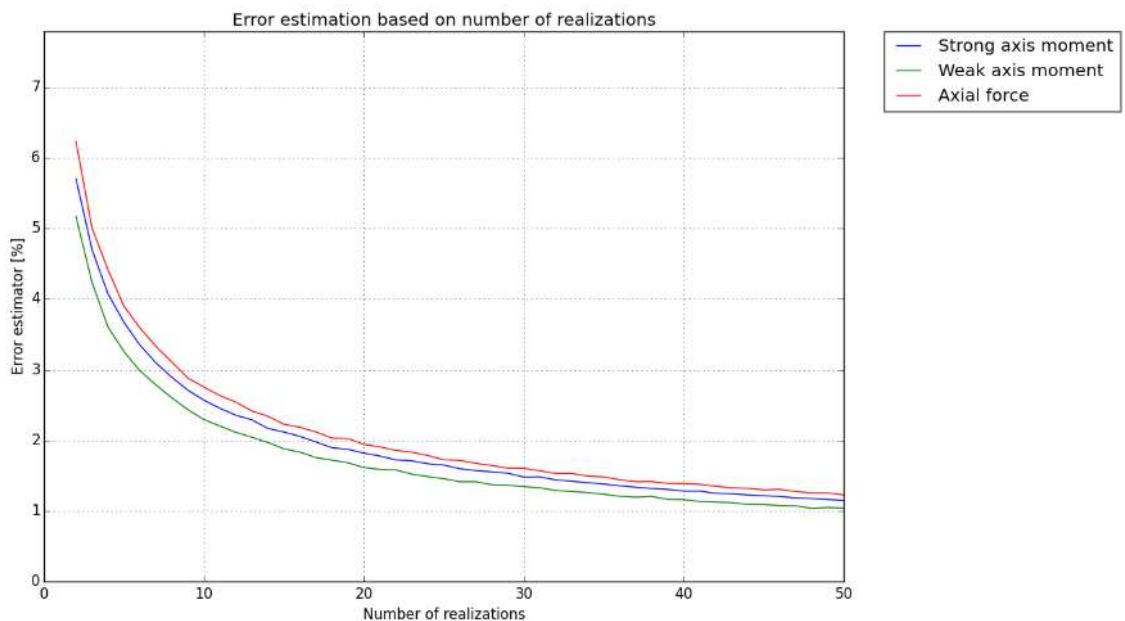
> *Figure 3-15 Standard deviation of error estimation based on number of realizations (Factor-method)*

As seen in Figure 3-14 the error is largest for axial force and smallest for weak axis moment. The estimated error is below 4% for all response categories when applying more than 10 realizations, and below 3% when running more than 20 realizations. Comparing the factor method in Figure 3-15 with the applied DNV-method in Figure 3-14, one can see that the convergence of the factor method with regards to realizations is somewhat faster.

The dynamic contribution to the limit state response can be up to about 50% of the total contribution to the limit state stress. By running 10 or more realizations (uncertainty of 2% in stresses) residual uncertainty is far below other uncertainties within the project and thus considered satisfying for the global analyses in this phase.

3.3   Validation of instability phenomena

The new developments of 3DFloat include methods and implementations to take into account variations of turbulent wind and irregular wave conditions across the fjord, tailored to provide the environmental conditions required by the MetOcean Design Basis.

The instability phenomena examined include coupled flutter, torsional flutter, galloping, vortex shedding, static divergence and wake-induced and rain-wind induced instability. The bridge deck is not sensitive to torsional flutter, galloping or static divergence.

The stay cables are not sensitive to rain-wind induced vibrations or wake galloping. It is unclear whether dry galloping could be a problem. If more elaborate methods indicate problems, damping devices or cross-sties can be used on the outer-most cables.

Simplified calculations show that the bridge deck is not sensitive to excessive vortex-induced vibrations during operation, but wind tunnel tests are needed to rule out this phenomenon. Stay cables are not sensitive to excessive vortex shedding vibrations during operation.

The close spacing between sea surface and girder raise concern about vertical turbulence created by the waves affecting the airloads on the girder. An analytical model for interaction between girder and wave surface has been developed and applied to the low part of the bridges. The interaction is modest for the 1-year ULS conditions but should be taken into account for lift and pitching moment for 100-year ULS conditions. This can be included in coupled simulations by modification of the wind spectrums.

A workshop on instability phenomena identified a possible wave-wind-structure instability that should be examined in the next phase of the project.

Finally, a two-phase CFD simulation of waves, wind, girder and columns gives a qualitative demonstration that girder/column/sea surface interactions can be computed with CFD.

The analyses and calculations performed are described in the validation report [3]

Special attention and great effort have been devoted to potential issues with parametric resonance. Two approaches are used to substantiate that parametric excitation will not be a design driver for any of the considered floating bridge concepts. The first approach is defined by NTNU as a criterion that indicate that significant effects from parametric resonance on design values can be deemed unlikely. The other approach, a conservative design approach, utilizing the nature of the quadratic hydrodynamic viscous damping from pontoon motions, indicate that some considered swell cases that does not pass the above-mentioned criterion are not able to set up design driving stresses even for a conservative situation. This is documented in the report "Parametric resonance" [5].

3.4   Sensitivity and parameter studies

A separate report, Sensitivity studies [4] has been issued to document the multiple sensitivity and parameter studies performed in order to recommend the current K12 floating bridge concept. The report covers the following topics;

- – Wind spectrum uncertainty
- – Influence of swell waves on total response
- – Evaluation of abnormal environmental conditions
- – Horizontal curvature of bridge
- – Evaluation of anchor stiffness
- – Number of anchor groups
- – Evaluation of critical wind direction
- – Study of the effect of connection between the bridge girder and the cable stayed bridge tower
- – Evaluation of anchor loss
- – Pushover analysis
- – Evaluation of skew wind force due to traffic
- – Evaluation of directional grid for governing load cases
- – Sensitivity of wave spread
- – Discretization of mooring lines
- – Evaluation of critical wind directions

4 AERODYNAMICS

The wind loads are important design drivers for the conceptual designs. Details affecting drag, such as rails, water drainage system, maintenance system rails and the shape of the columns have been investigated.

The starting point for the bridge girder is profile K7-1 resembling the Langenuen/Julsundet girders, described in the wind tunnel test report [31]. Review of the test data, literature studies, extensive validation of the CFD tool and further optimization with CFD support the choice of this girder. The CFD optimization studies suggest that a drag reduction up to 10% can be achieved by modification of the nose fairings. This reserve is not utilized; the measured static coefficients of [31] are used for the load calculations in this phase.

The following sections provides a summary of the airfoil data used in the models Abaqus/DynNO and 3DFloat in this phase of the project. More details on the analyses performed can be found in the report "Wind loads and aerodynamic optimization" [6].

4.1 Static load coefficients without the presence of sea surface boundary

Static load coefficients used in combinations, where environmental loads are dominant:

Wind direction	C_D	C_L	C_M	$dC_L / d\alpha$	$dC_M / d\alpha$
West	0.699 (-1.5⁰)	-0.447 (-1.5⁰)	-0.040 (-1.5⁰)	3.607	1.077
East	0.671 (-1.4⁰)	-0.575 (-1.4⁰)	-0.076 (-1.4⁰)	3.563	1.230

Static load coefficients used in combinations with both environmental loads and traffic:

Wind direction	C_D	C_L	C_M	$dC_L / d\alpha$	$dC_M / d\alpha$
West	1.090 (+1.5⁰)	-0.382 (-1.5⁰)	-0.095 (-1.5⁰)	2.273	0.842
East	1.134 (+1.5⁰)	-0.295 (-1.5⁰)	-0.092 (-1.5⁰)	1.347	0.482

Static loads coefficients obtained without use of free-surface boundary should be used for the bridge deck on the high bridge.

4.2 Static load coefficients with the presence of sea surface boundary

Static load coefficients used in combinations, where environmental loads are dominant:

Wind direction	C_D	C_L	C_M	$dC_L / d\alpha$	$dC_M / d\alpha$
West	0.826 (-1.5⁰)	-0.515 (-1.5⁰)	-0.043 (-1.5⁰) 0.016 (+1.5⁰)	3.613	1.229
East	0.866 (-1.5⁰)	-0.521 (-1.5⁰)	-0.037 (-1.5⁰) 0.021 (+1.5⁰)	3.825	1.217

Static load coefficients used in combinations with both environmental loads and traffic:

Wind direction	C_D	C_L	C_M	$dC_L / d\alpha$	$dC_M / d\alpha$
West	1.194 (+1.6^0)	-0.389 (-1.5^0)	-0.082 (-1.5^0)	1.915	0.802
East	1.406 (+1.5^0)	-0.282 (-1.6^0)	-0.071 (-1.6^0)	1.064	0.597

Static loads coefficients obtained with the presence of sea surface boundary should be used for the bridge deck on the low bridge.

4.3   Airfoil tables used in 3DFloat

Figure 4-1 shows test data for K7-1 with rails, no traffic, and the presence of a sea surface boundary from [31]. The lift and moment coefficients are normalized with the girder width, the drag with girder HEIGHT. The figures also include the data we had available in the previous phase of the project for the Langenuen/Julsundet girder. The geometries are similar. The differences can be used to appreciate the considerable uncertainties in the wind loads on the girders. "Upstream" means the pedestrian lane is on the upwind side of the girder.
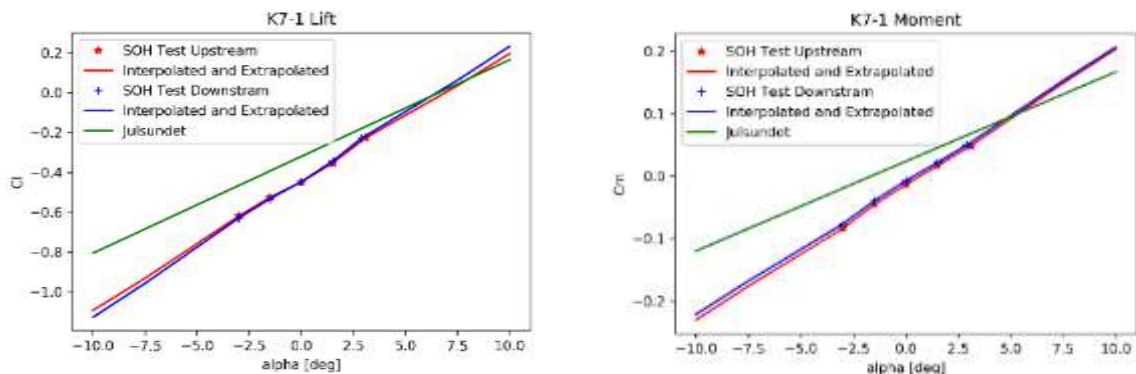
> *Figure 4-1: Lift and moment coefficients, reference length girder width*
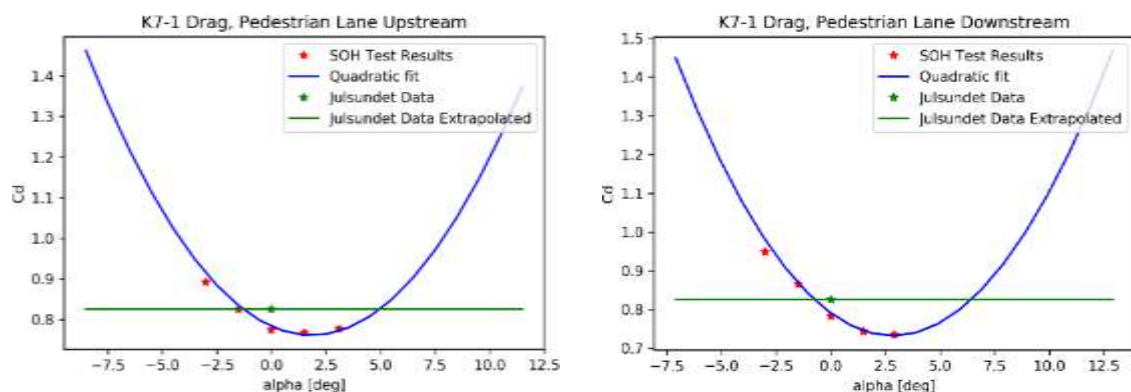
> *Figure 4-2: Drag coefficients, reference length girder height.*

The lift and moment curves are extrapolated to +-10 deg AoA. The drag curves are extrapolated to a region +-10 deg around AoA for minimum drag, with a quadratic function

from thin-airfoil theory. The coefficients in the function were fitted with an optimization procedure minimizing the sum of square errors between the fitted curve and data points.

For generality and robustness, 3DFloat airfoil data are given through +-180 deg AoA. By combining the pedestrian upstream- and downstream data, flat-plate data for +-90 deg and symmetry considerations, the inputs shown in Figure 4-3 are generated for a girder with the pedestrian lane upstream at zero AoA (element z axis pointing up and y axis pointing downstream).
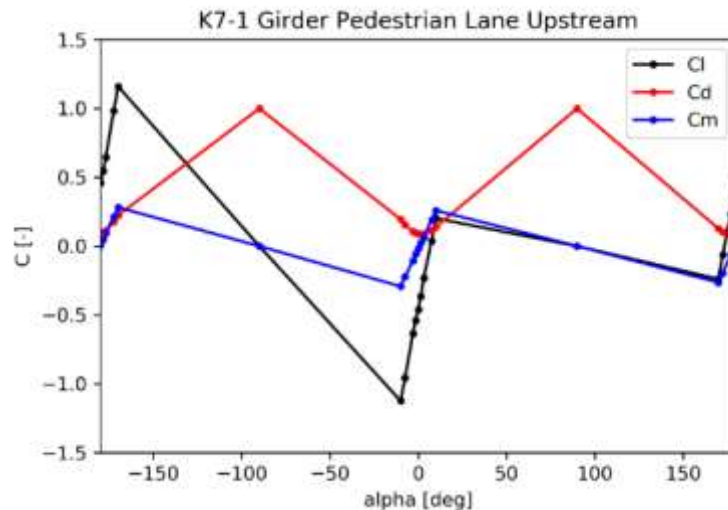
> Figure 4-3: Summary of Airfoil Coefficients.
> *The pedestrian lane is upstream for zero AoA, downstream for 180 deg AoA.*

4.4   Canoe-shaped pontoon

Drag coefficient of the canoe-shaped cross-section can be defined with a use Eurocode [32] assuming perfectly rounded rectangle.

> *Table 4-1: Drag of canoe-shaped pontoon*

V [m/s]	L [m]	B [m]	R [m]	$c_{f,0}$	Ψ_R	λ	Ψ_λ	C_D	Force [kN/m]
10	58	12	6	1,023	0,5	70	0,921	0,471	0,346
20	58	12	6	1,023	0,5	70	0,921	0,471	1,386
30	58	12	6	1,023	0,5	70	0,921	0,471	3,117

λ – effective slenderness, Ψ_λ – end-effect factor

4.5   Bridge cables

Bridge cables have circular cross-section and therefore procedure provided by Eurocode can be used to determine their drag coefficient. In should be noted that in reality inclined cables will be seen by the wind as of elliptical shape. Although this fact is neglected herein as we

consider only static drag force, it should be taken into account when assessing wind-induced instabilities of the stay cables.

Drag coefficients depend on the cable diameter, surface roughness, cable length and the wind speed. In addition, depending on the Reynolds number, the cable can be classified in the subcritical or supercritical flow range, which has a huge impact on the drag coefficient.. The effect of roughness is investigated by assuming roughness to be equal 0.2 mm or 2.0 mm. The lengths of the cables are in the range between 467 m (longest cable) and 125 m (shortest cable). Due to small Reynolds numbers, cable transmission from sub to supercritical region occurs at high wind speeds (V>30 m/s), therefore the drag coefficient at lower velocities can be assumed to be 1.2. Drag coefficient for cables is given in Table 4-2.

> *Table 4-2: Drag coefficient for circular cross-section.*

V [m/s]	d [m]	l [m]	roughness [mm]	supercritical region?	Re	λ	Ψλ	CD	Force [kN/m]
25	0,1	467	2	no	1,67E+05	3269	1,21	1,20	0,05
25	0,1	467	0,2	no	1,67E+05	3269	1,21	1,20	0,05
25	0,1	125	2	no	1,67E+05	875	1,11	1,20	0,05
25	0,1	125	0,2	no	1,67E+05	875	1,11	1,20	0,05
35	0,1	467	2	yes	2,33E+05	3269	1,21	1,20	0,09
35	0,1	467	0,2	yes	2,33E+05	3269	1,21	0,96	0,07
35	0,1	125	2	yes	2,33E+05	875	1,11	1,15	0,09
35	0,1	125	0,2	yes	2,33E+05	875	1,11	0,88	0,07

λ – effective slenderness, Ψλ – end-effect factor

4.6   Bridge columns

Several column cross-sections have been investigated, including rectangular cross-sections. Also, in this case the Eurocode can be used to estimate the drag coefficient. Because strong winds are the most interesting, we assume that the wind direction is perpendicular to the main axis of the bridge, meaning that wind blows along the longer side of the column. Herein we consider several lengths of the column sides that gives an area of roughly 60m^2. According to Eurocode the drag coefficient is dependent on the rounding radius r, but not on the wind speed. Several values of r have been therefore considered in the Table 4-3.

> *Table 4-3. Drag coefficient for rounded rectangles*

V [m/s]	d [m]	b [m]	r [m]	$c_{f,0}$	ΨR	λ	Ψλ	C_D	Force [kN/m]
30	14	4	0	1,253	1,000	70	0,921	1,154	2,545
30	14	4	0,2	1,253	0,875	70	0,921	1,010	2,227
30	14	4	0,5	1,253	0,688	70	0,921	0,794	1,750
30	14	4	1	1,253	0,500	70	0,921	0,577	1,273

30	12	5	0	1,522	1,000	70	0,921	1,402	3,863
30	12	5	0,2	1,522	0,900	70	0,921	1,261	3,477
30	12	5	0,5	1,522	0,750	70	0,921	1,051	2,897
30	12	5	1	1,522	0,500	70	0,921	0,701	1,932
30	16	3	0	0,991	1,000	70	0,921	0,913	1,509
30	16	3	0,2	0,991	0,833	70	0,921	0,760	1,258
30	16	3	0,5	0,991	0,583	70	0,921	0,532	0,880
30	16	3	1	0,991	0,500	70	0,921	0,456	0,755

λ – effective slenderness, $\Psi\lambda$ – end-effect factor, Ψ_R – reduction factor for rounded corners

For the circular alternative:

V [m/s]	d [m]	l [m]	roughness [mm]	supercritical region?	Re	λ	Ψ_λ	CD	Force [kN/m]
30	8,5	10	1	yes	1,70E+07	70	0,92	0,78	3,73

For elliptic alternative:

V [m/s]	b [m]	d [m]	Re	Flow type	C_D	Force [kN/m]
10	6	13	1,20E+07	Turbulent	0,20	0,66
20	4	18	8,00E+06	Turbulent	0,14	0,30

4.7   Bridge tower

Wind actions are crucial for the design of a bridge tower that supports the cable stayed-bridge. Static aerodynamic loads as well as the vortex shedding phenomenon in the wake of the tower should be assessed individually. In order to verify design wind loads applied on the tower, CFD studies and in the later phase wind tunnel tests are recommended.

5   HYDRODYNAMICS

The hydrodynamic work presented in [7] is concentrated on providing sufficiently conservative but also cost optimal hydrodynamic input for the global analysis and concept development with focus on pontoon geometry. The work has been focused on the following activities:

1- Overview of theoretical approaches versus model test investigation provided by SVV
2- Exploring higher-order panel modelling in WAMIT to reduce numerical uncertainty
3- Pontoon geometrical variations – base cases and parametric variation
4- Viscous effects and possible modelling of appendices devices to reduce parametric resonance
5- Hydrodynamic interaction between pontoons including both potential theory and CFD analyses
6- Wave current interaction
7- Higher order hydrodynamic loads
8- Wind and wave conditions for temporary phase

The work performed for providing input to the global bridge design is presented here, while further details regarding method investigation can be found in the report "Hydrodynamic optimization" [7].

5.1   Acceptance criteria for hydrodynamic activities

From a global point of view, the pontoons must satisfy the following minimum requirements:

- Displacement: Sufficient buoyancy to carry the bridge.
- Vertical hydrostatic stiffness: Sufficient waterplane area to withstand vertical traffic loads.
- Rotational hydrostatic stiffness: Sufficient metacentric height to withstand moments due to eccentric traffic loads and static wind loads.
- Ballast: Sufficient design ballast to account for uncertainty in weights.

5.2   Static motion limitations

Static motion limitations of the bridge with traffic and static wind as load scenarios are taken from [22] and presented in Table 5-1.

> *Table 5-1 Static motion limitations*

Motion limitation	Load scenario	Maximum motion
Vertical deformation from traffic loads	0.7xtraffic	$u_y \leq 1.5m$
Rotation about bridge axis from eccentric traffic loading	0.7xtraffic	$\theta_x \leq 1.0$ deg
Rotation about bridge axis from static wind load	1-year static wind	$\theta_x \leq 0.5$ deg

5.3   Pontoons used in global bridge design

This section presents the geometric and hydrodynamic properties for the pontoons used in the global bridge design for K12 Model 30. Hydrodynamic properties are found by the hydrodynamic software WAMIT [33], and are found by analyses of a single pontoon.

5.3.1   Pontoon geometry

The geometry for the K12 Model 30 pontoon types are presented in Table 5-2. Figure 5-1 shows the distributions of the pontoon types along the bridge girder.
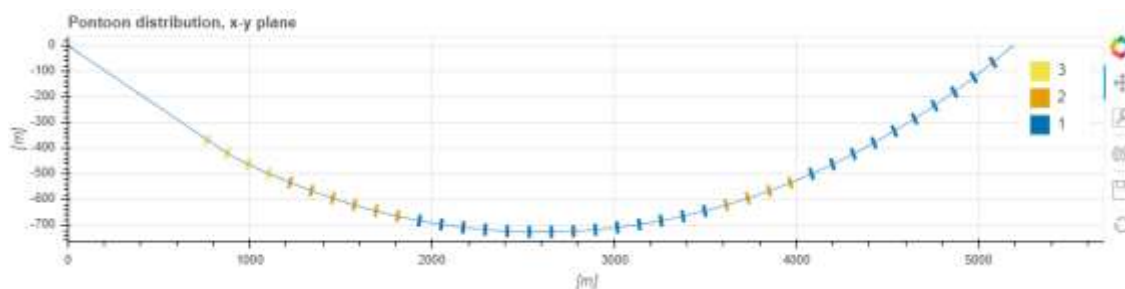

> *Figure 5-1: Pontoon distribution*

> *Table 5-2: Structural properties for pontoon types*

Pontoon type	3 – WAMIT57	2 – WAMIT58	1 – WAMIT59
Length [m]	58	58	58
Width [m]	12	14	17
Draft [m]	5	5	5
Waterplane area [m2]	665	796	924
Displaced volume [m3]	3325	3979	4619
Structural mass [kg]	9.83e5	1.55e6	1.78e6
Mass of displaced volume [kg]	3.41e6	4.08e6	4.73e6
Vertical center of gravity [m]	-0.83	-1.02	-1.16
Vertical center of buoyancy [m]	-2.50	-2.50	-2.50

5.3.2   Hydrodynamic added mass

Added mass for the pontoon types used in the global bridge design is presented in Figure 5-2 to Figure 5-7.
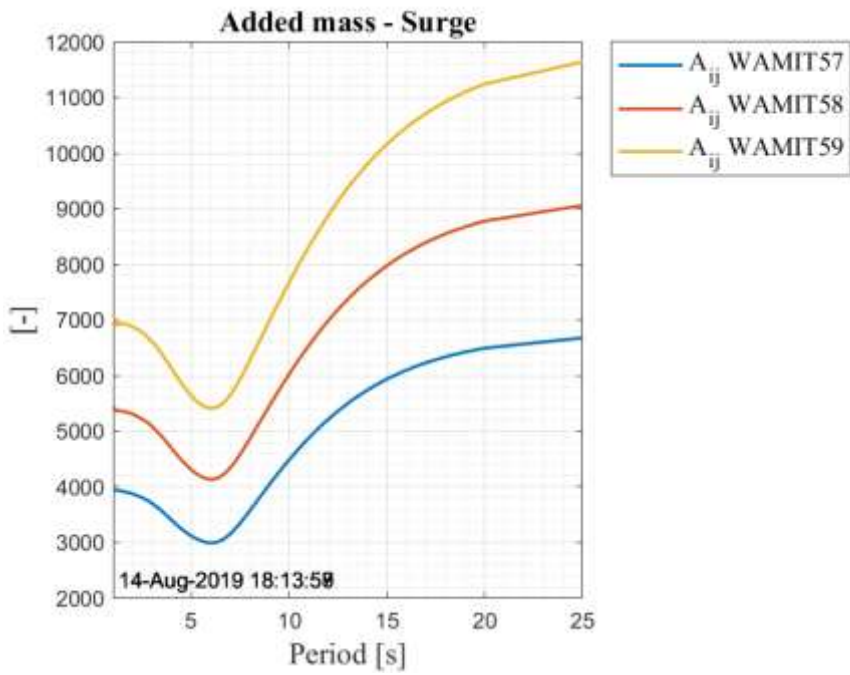
>   *Figure 5-2: Non-dimensional added mass surge*
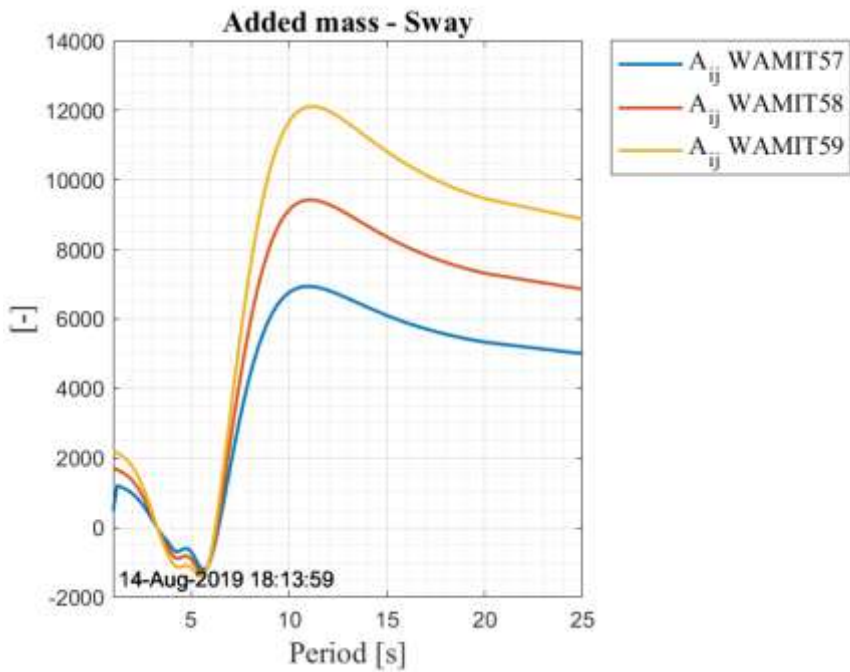
>   *Figure 5-3: Non-dimensional added mass sway*

> *Figure 5-4: Non-dimensional added mass heave*
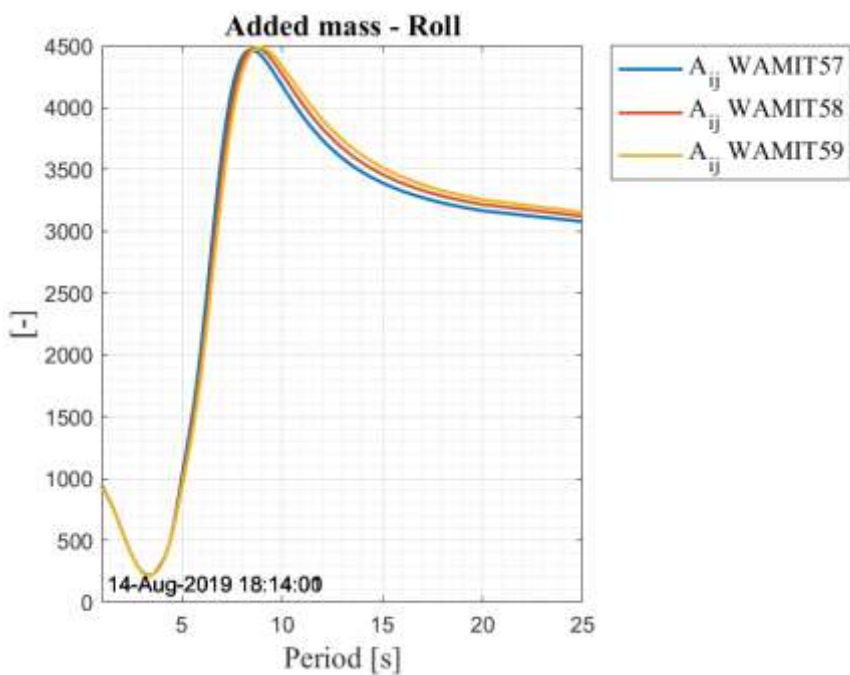
> *Figure 5-5: Non-dimensional added mass roll*
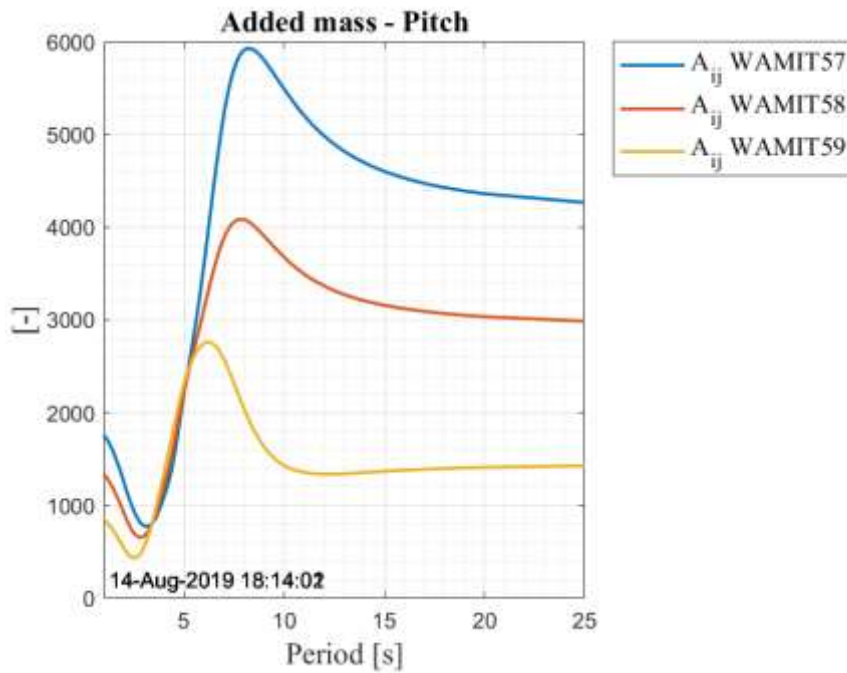
> *Figure 5-6: Non-dimensional added mass pitch*
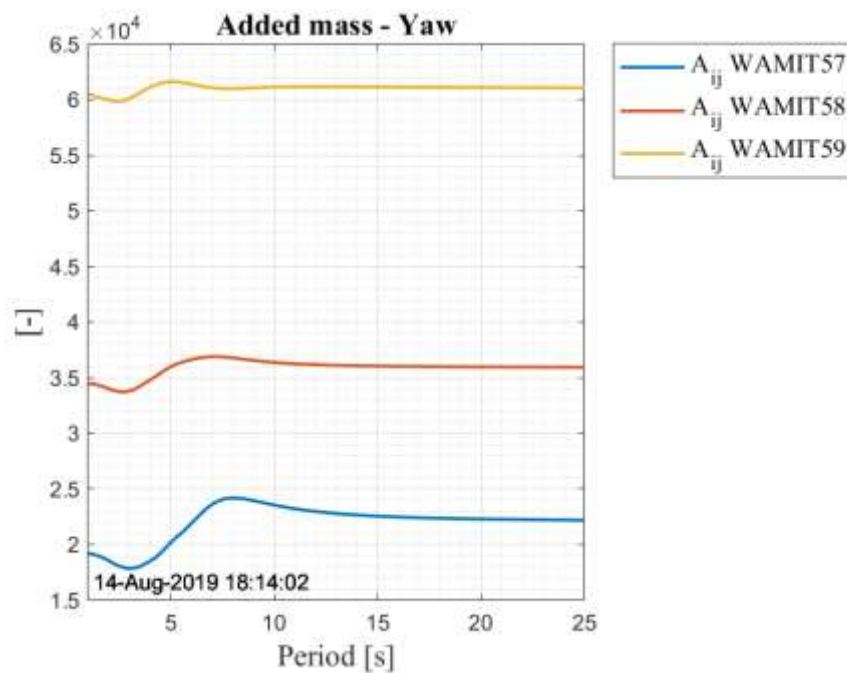
> *Figure 5-7: Non-dimensional added mass yaw*

5.3.3   Hydrodynamic potential damping

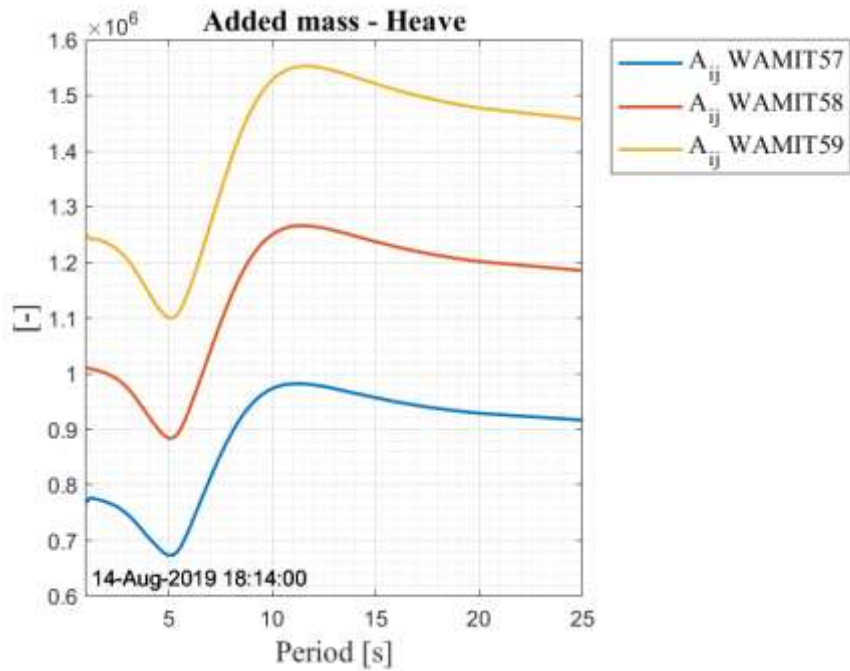Potential damping for the pontoon types used in the global bridge design presented in Figure 5-8 to Figure 5-13.
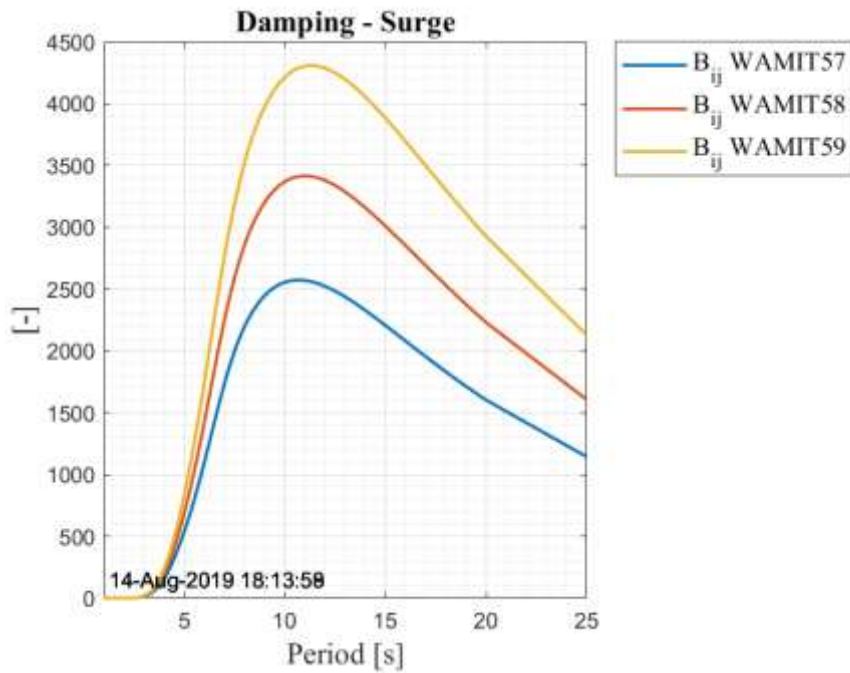
> *Figure 5-8: Non-dimensional potential damping surge*
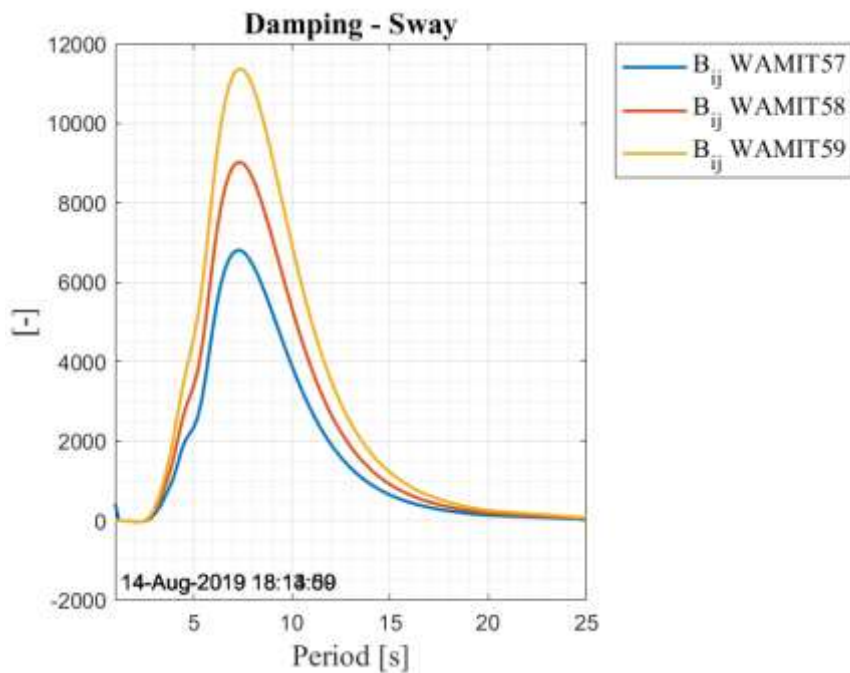
> *Figure 5-9: Non-dimensional potential damping sway*
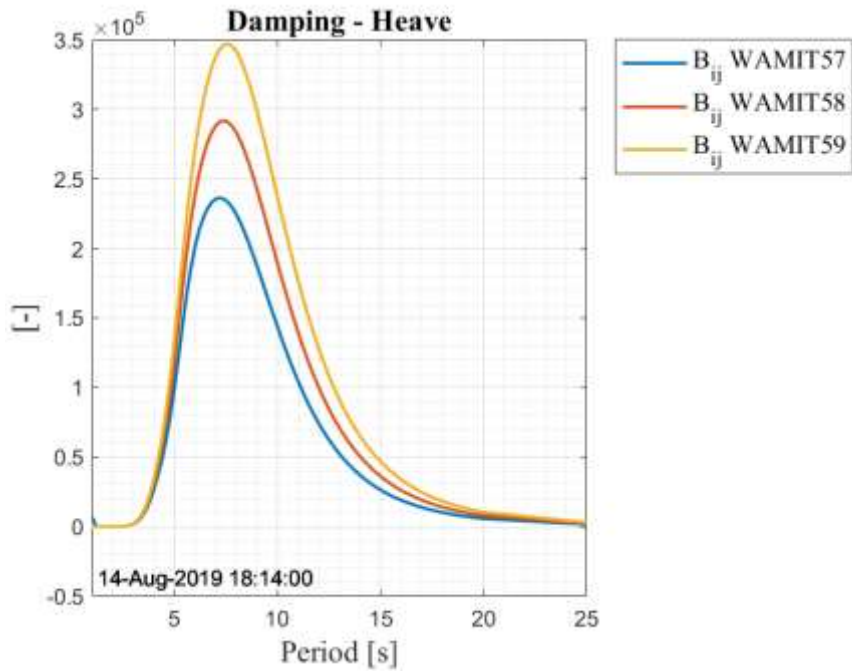
> *Figure 5-10: Non-dimensional potential damping heave*
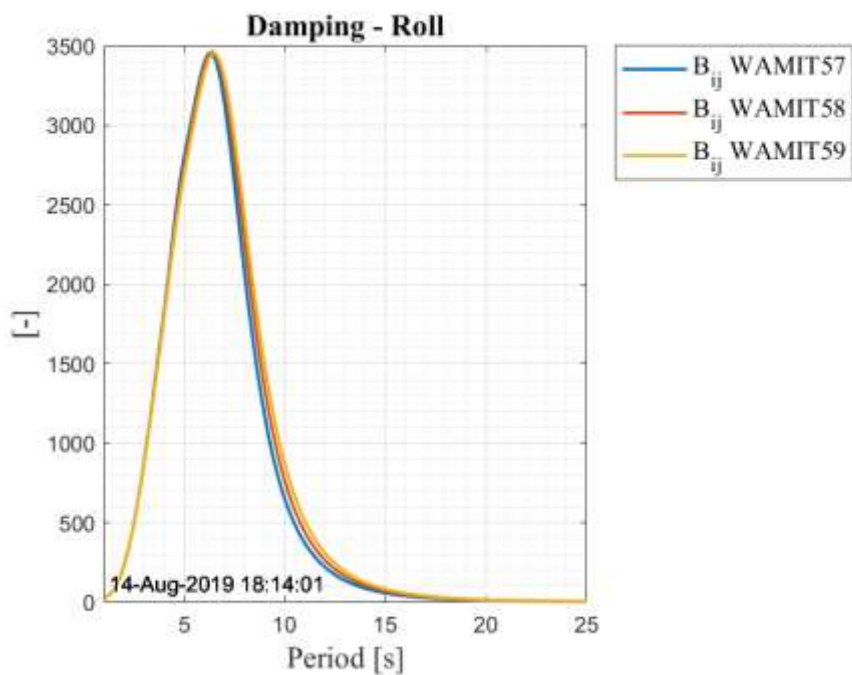
> *Figure 5-11: Non-dimensional potential damping roll*
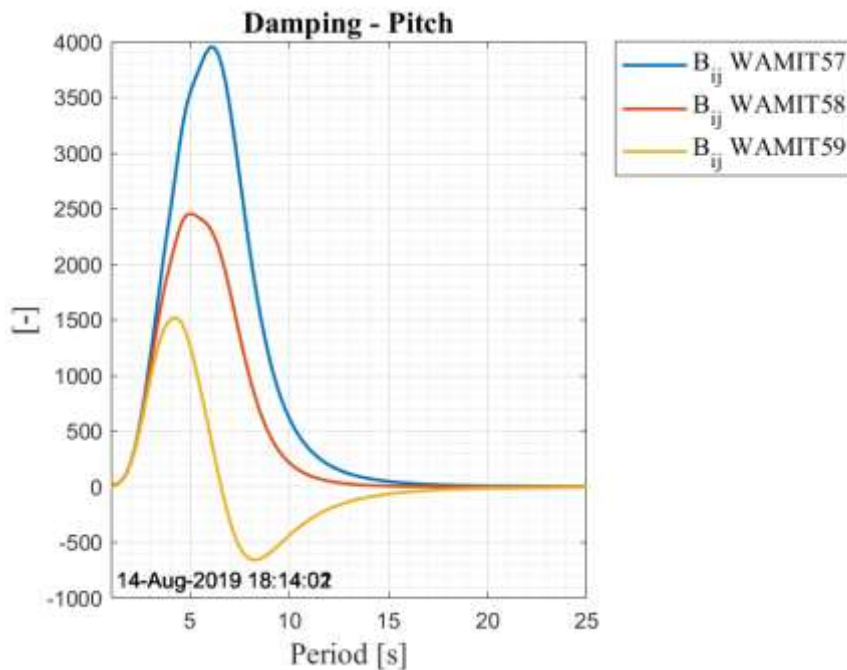
> *Figure 5-12: Non-dimensional potential damping pitch*
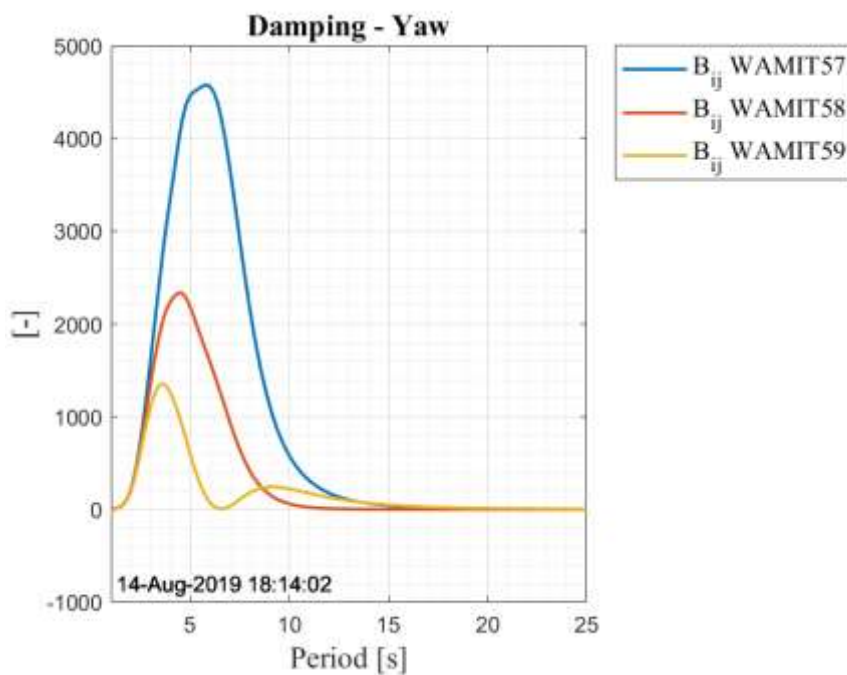
> *Figure 5-13: Non-dimensional potential damping yaw*

5.3.4 Hydrodynamic excitation force

Hydrodynamic excitation force from 0-, 45- and 90 degrees wave heading are presented in Figure 5-14 to Figure 5-25. 0 degrees wave heading is defined as waves propagating along the pontoon length, and 90 degrees along the pontoon width.
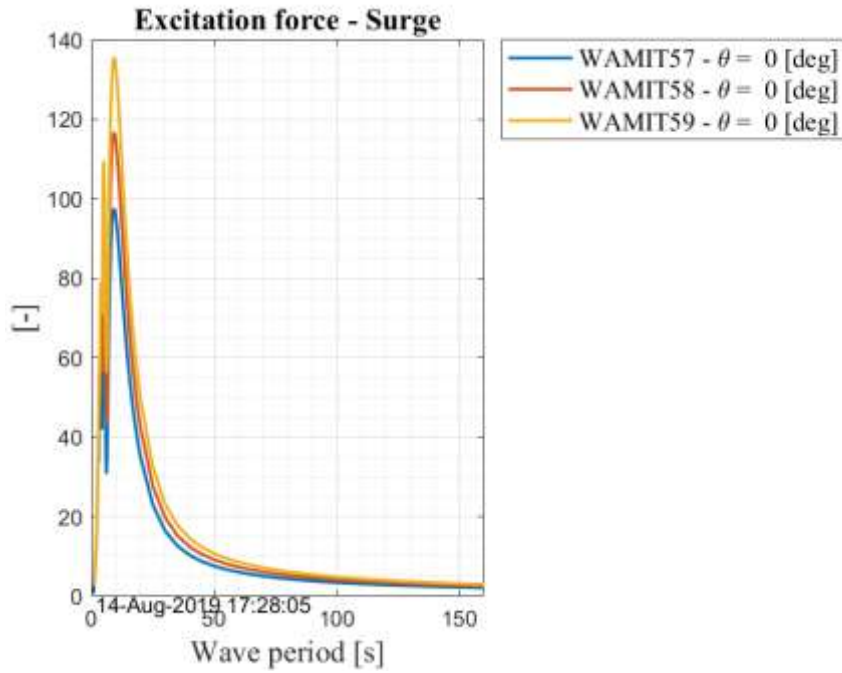
> *Figure 5-14: Non-dimensional excitation force surge, 0 degrees wave heading.*
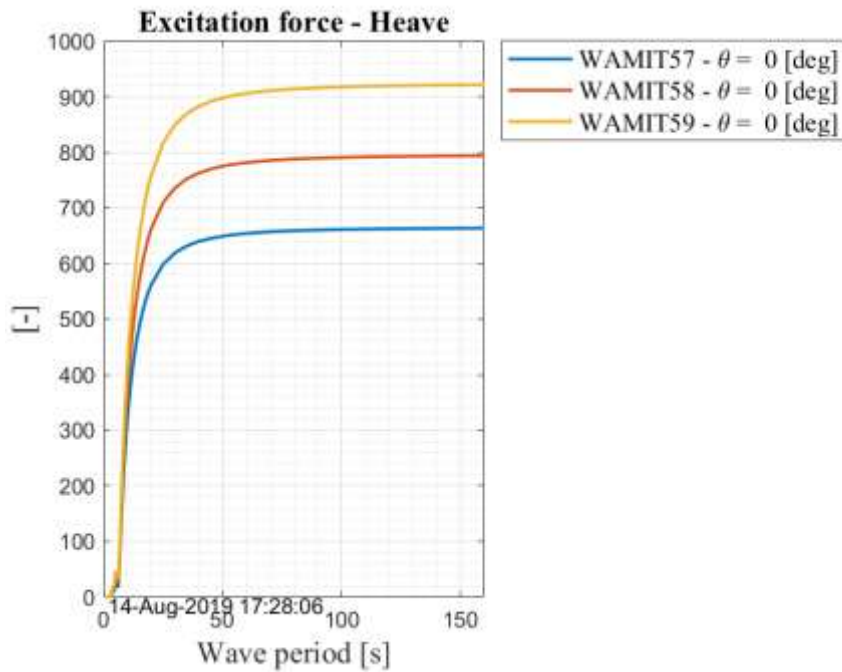
> *Figure 5-15: Non-dimensional excitation force heave, 0 degrees wave heading*
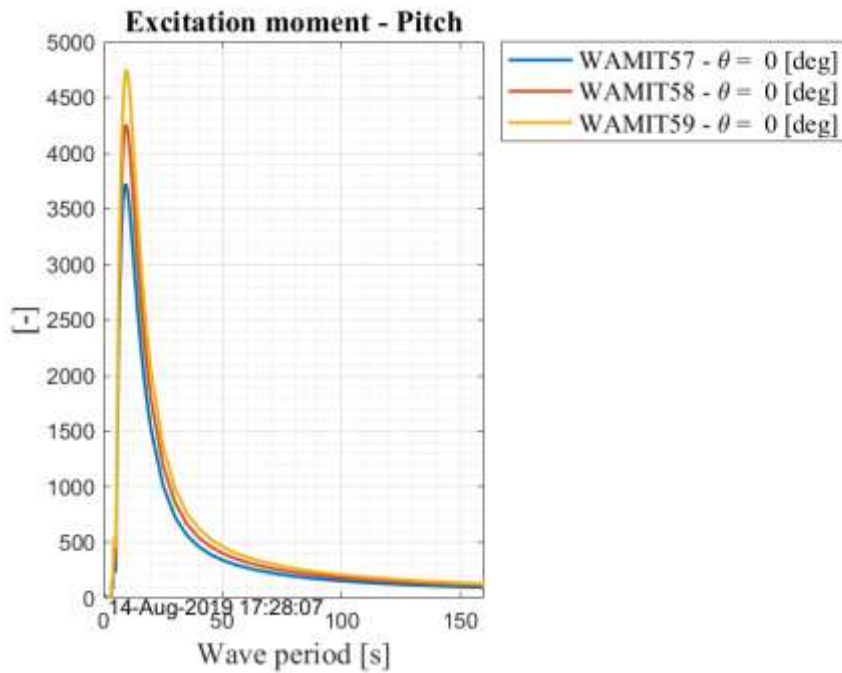
> *Figure 5-16: Non-dimensional excitation moment, 0 degrees wave heading*
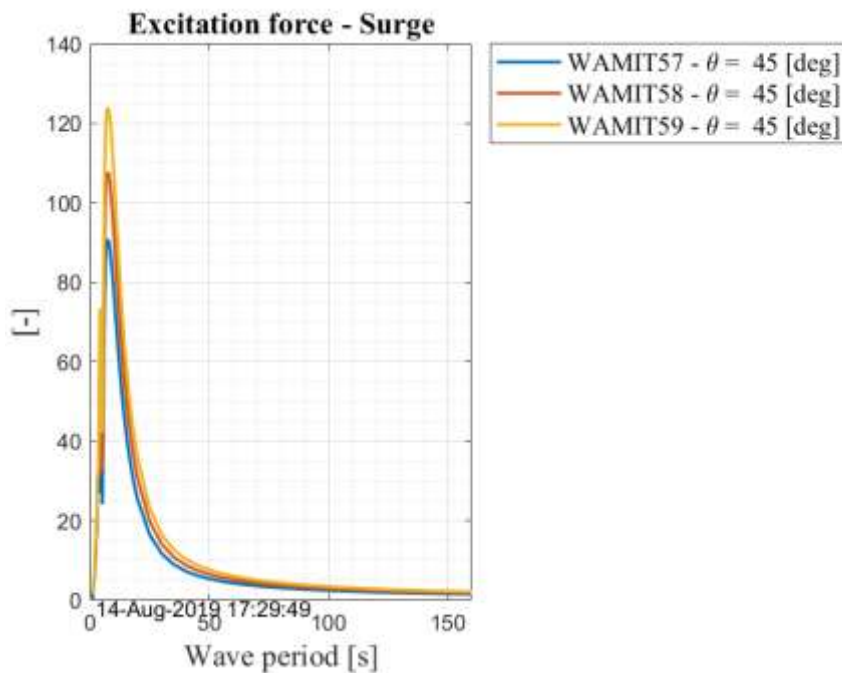
> *Figure 5-17: Non-dimensional excitation force surge, 45 degrees wave heading*
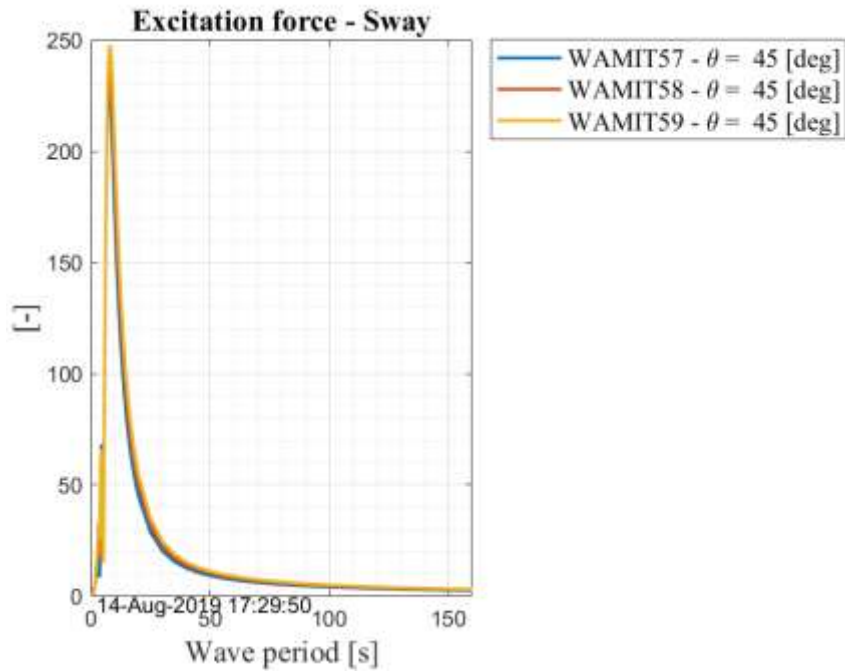
> *Figure 5-18: Non-dimensional excitation force sway, 45 degrees wave heading*
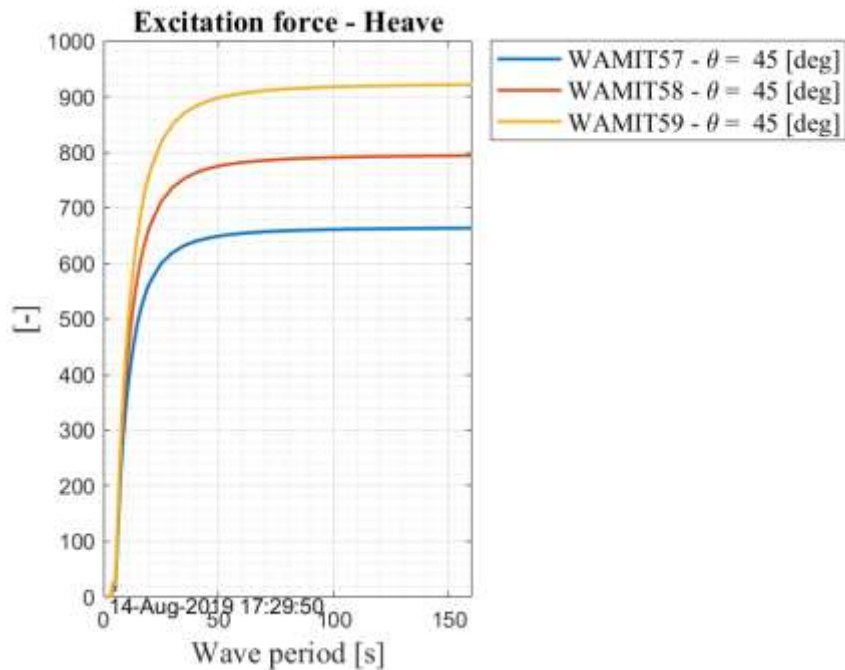
> *Figure 5-19: Non-dimensional excitation force heave, 45 degrees wave heading*
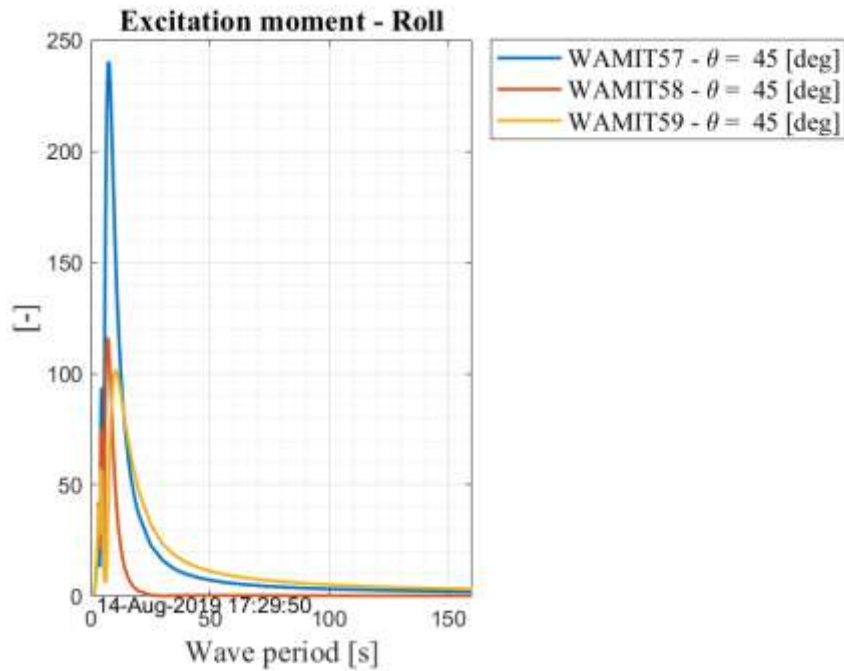
> *Figure 5-20: Non-dimensional excitation force roll, 45 degrees wave heading*
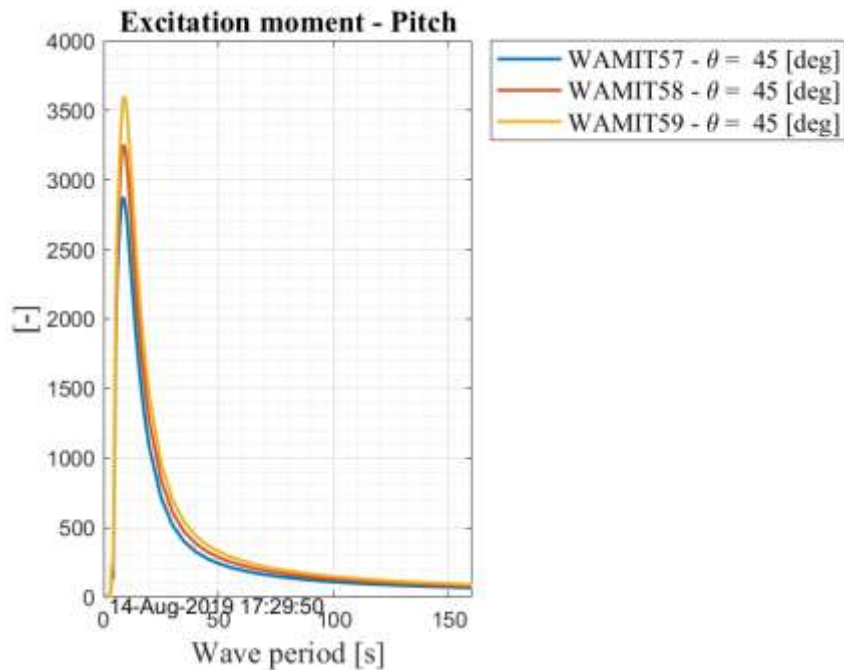
> *Figure 5-21: Non-dimensional excitation force pitch, 45 degrees wave heading*
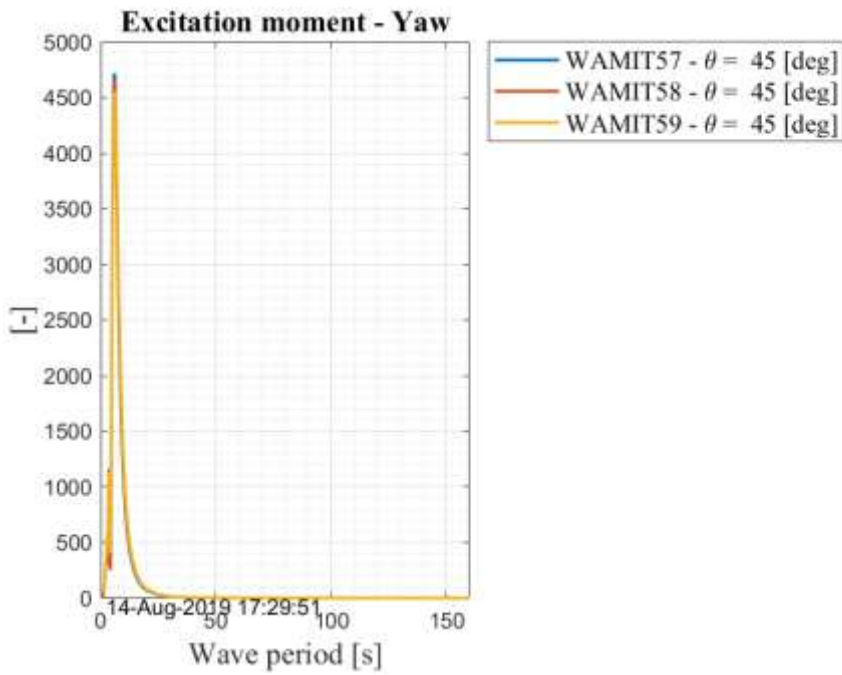
> *Figure 5-22: Non-dimensional excitation force yaw, 45 degrees wave heading*
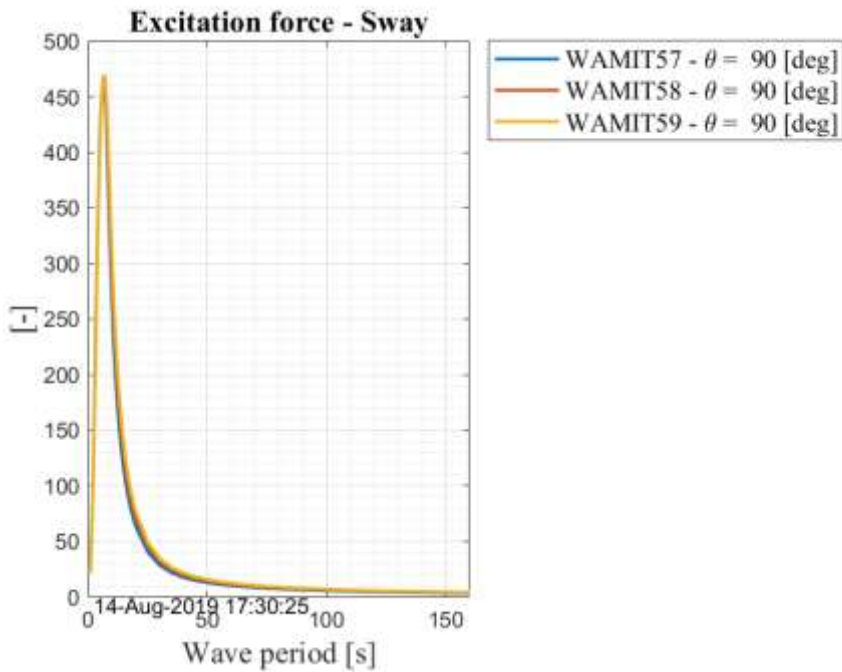
> *Figure 5-23: Non-dimensional excitation force sway, 90 degrees wave heading*
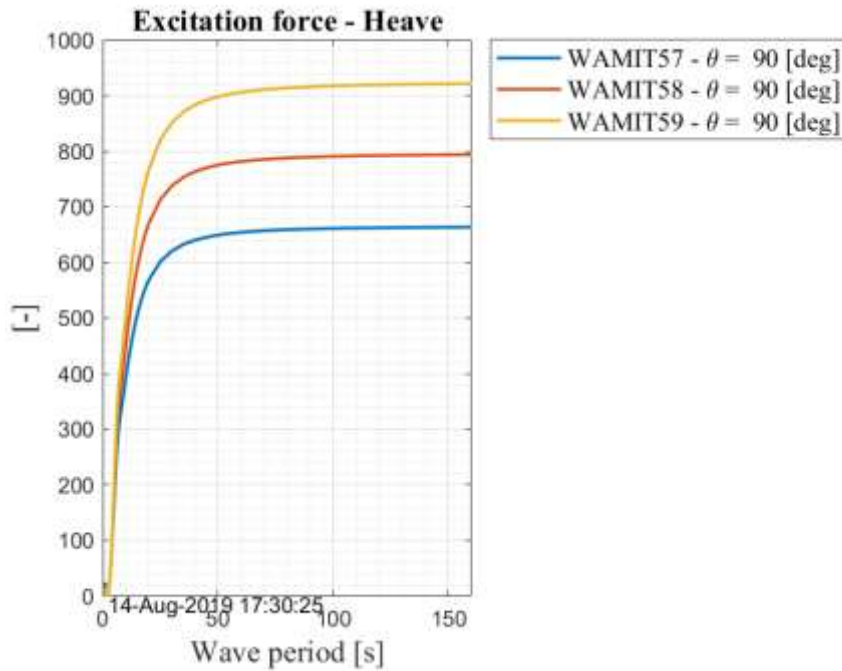
> *Figure 5-24: Non-dimensional excitation force heave, 90 degrees wave heading*
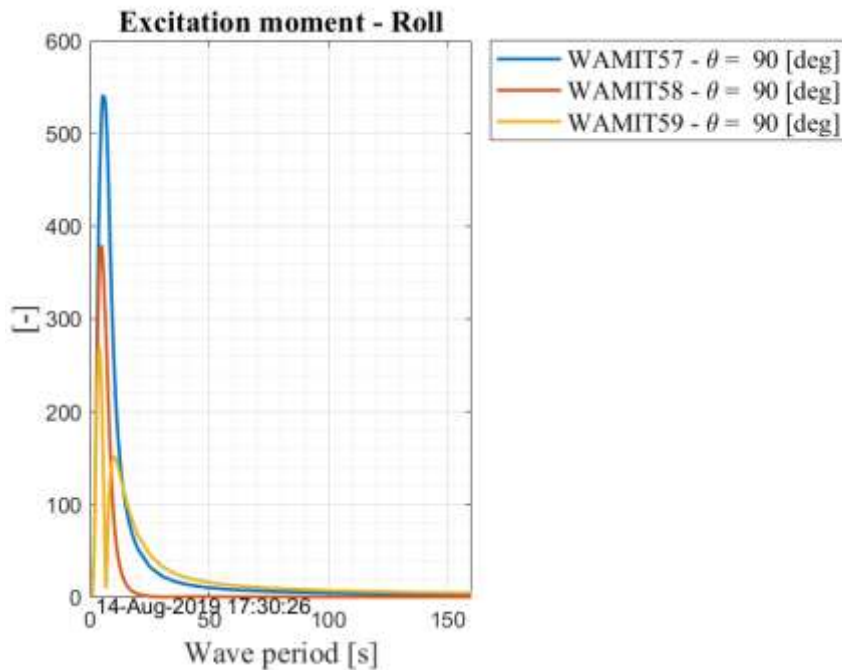
> *Figure 5-25: Non-dimensional excitation moment roll, 90 degrees wave heading*

5.3.5   Second order mean drift force

Second order mean drift force is found by use of momentum integration, and results from 0-, 45- and 90-degrees wave heading is presented in Figure 5-26 to Figure 5-30.
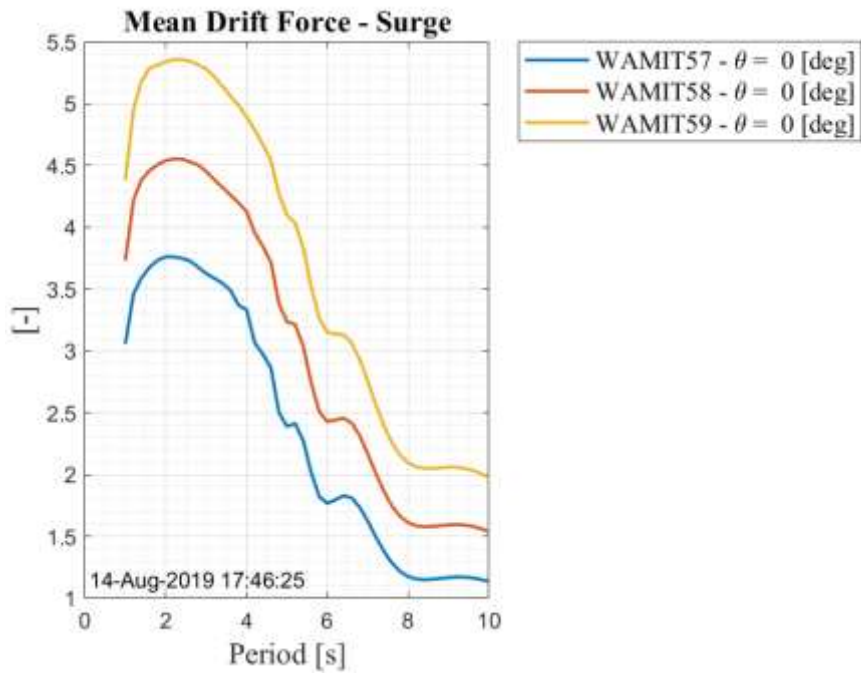
> Figure 5-26: Non-dimensional surge drift force from momentum integration, 0 degrees

> wave heading
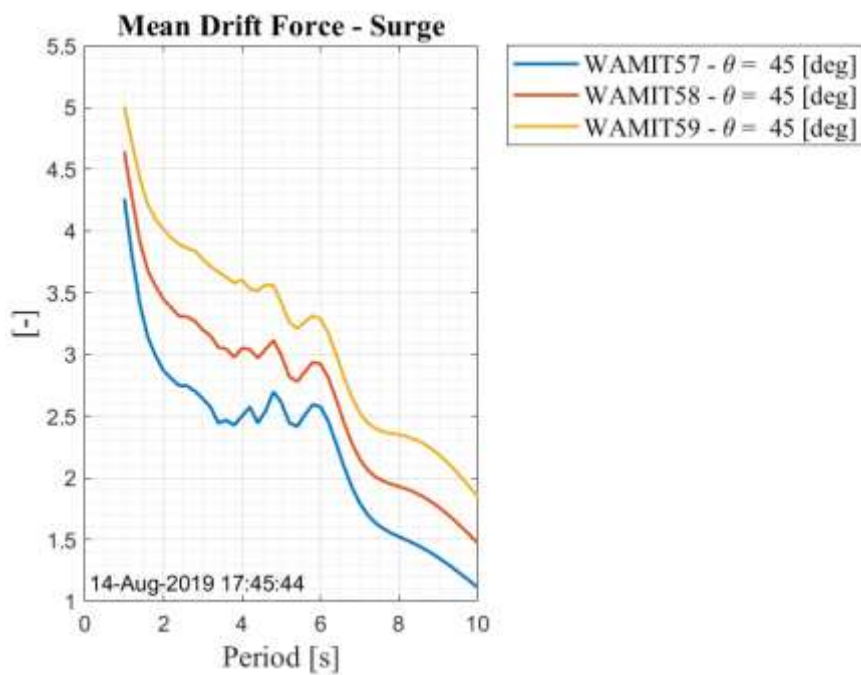
> Figure 5-27: Non-dimensional surge drift force from momentum integration, 45 degrees wave heading
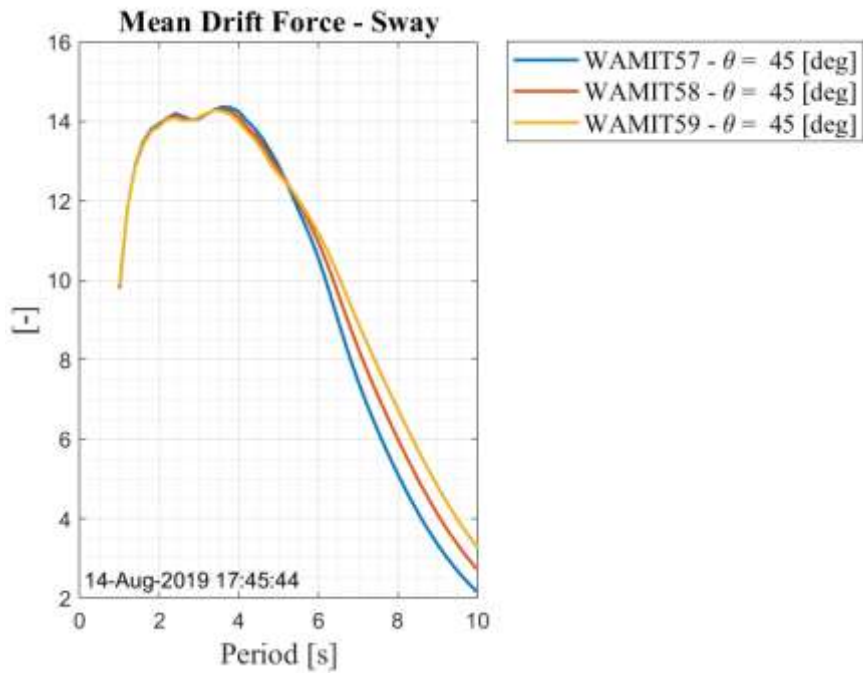
> *Figure 5-28: Non-dimensional sway drift force from momentum integration, 45 degrees wave heading*
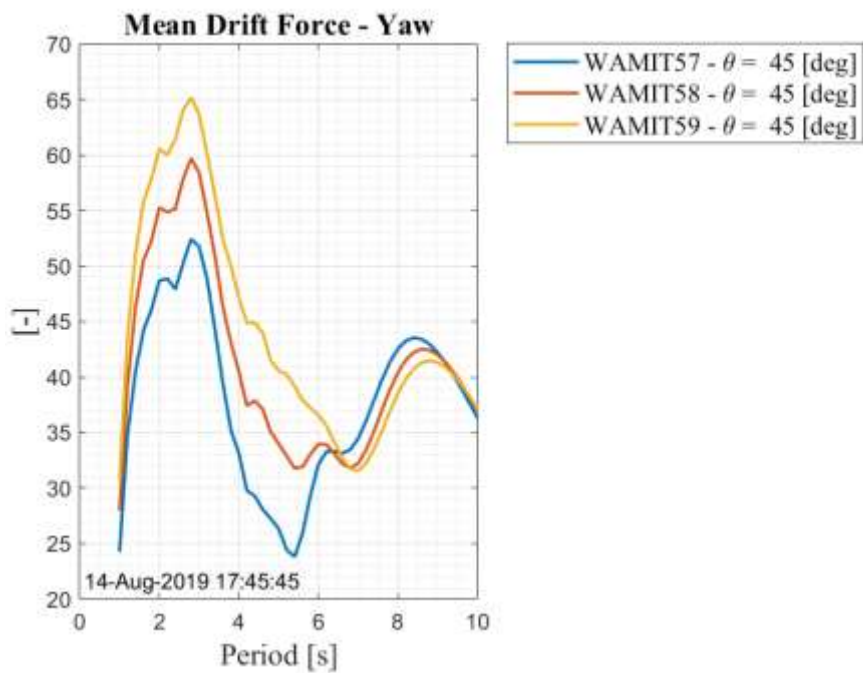
> *Figure 5-29: Non-dimensional yaw drift force from momentum integration, 45 degrees wave heading*
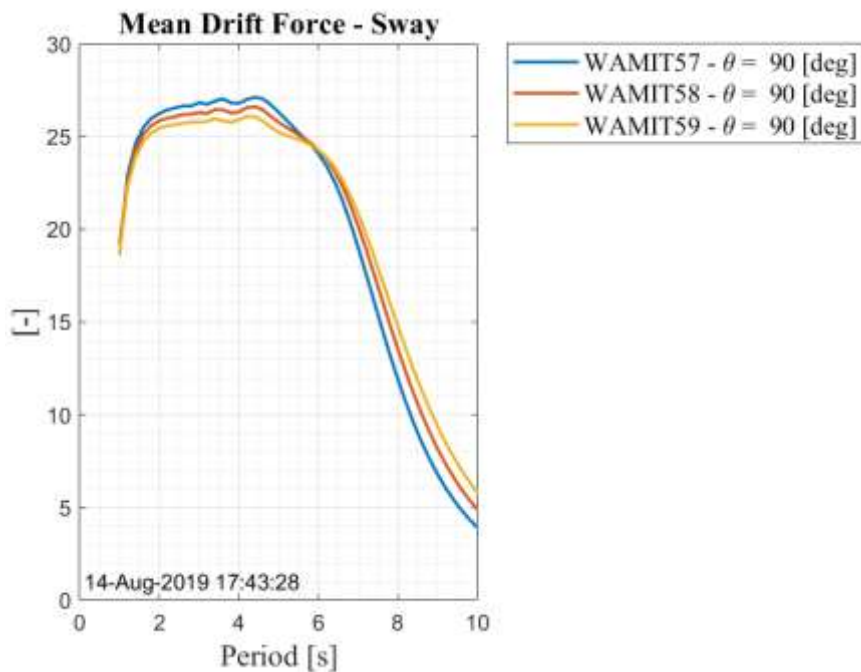
> *Figure 5-30: Non-dimensional sway drift force from momentum integration, 90 degrees wave heading*

5.3.6   Hydrodynamic viscous loads

Hydrodynamic viscous drag and lift coefficients are obtained from CFD analyses. This is considered the best source of viscous coefficients currently available. The viscous load coefficients depend highly on the flow regime. The steady-state coefficients, i.e. the force and moment coefficients in uniform flow due to current or forward speed, are used in analyses. The drag coefficient Cds and lift coefficient Cls are presented in Figure 5-31. Analyses are performed for a pontoon with L=58m, D=5m and B=12m. The force in the current direction is given by:

$$F_{drag} = \frac{1}{2}\rho C_d A_{ref} V|V|$$

Where A_{ref} = 50m^2 is the frontal area of the pontoon and is used for all angles of attack. The force normal to the current direction is:

$$F_{lift} = \frac{1}{2}\rho C_l A_{ref} V|V|$$
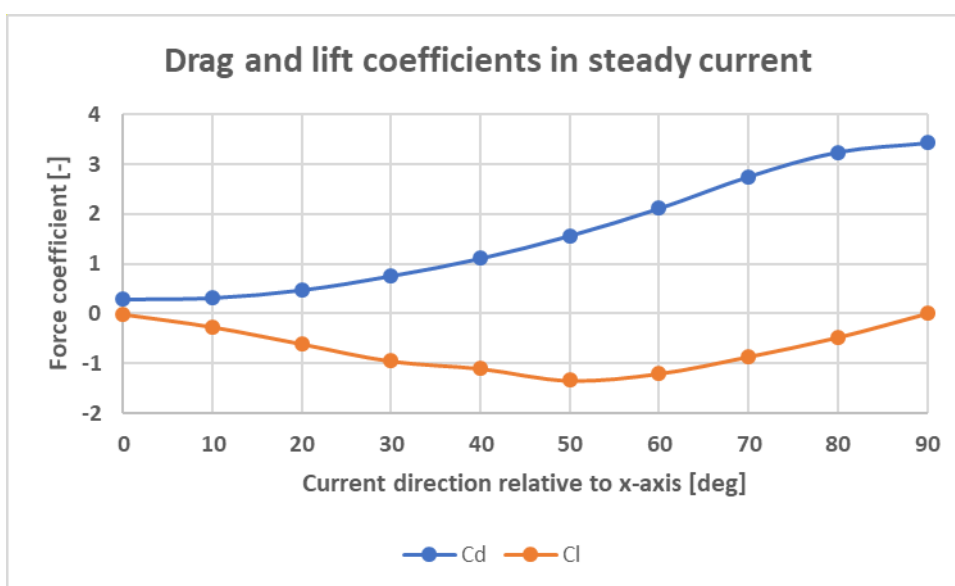
> *Figure 5-31: Drag and lift coefficients versus angle of attack for steady current, estimated with CFD analyses. C_d and C_l are normalized towards the frontal area of the pontoons (50m^2).*

Table 5-3 provides the corresponding drag coefficient in surge and sway direction, normalized towards the respective reference area.

> *Table 5-3: Drag coefficient in surge and sway from CFD analyses*

Direction	Reference area	Cds
Surge (transverse bridge axis)	50 m^2	0.3
Sway (longitudinal bridge axis)	290 m^2	0.6

5.4　Pontoon interaction

A study comparing results for single- and multibody analyses in WAMIT [33], revealed that interaction effects are significant for both added mass, damping, 1st order excitation and mean drift force. A large increase in oscillations is observed for multibody analyses, and forces/moments perpendicular to incoming wave direction arise for multibody analyses, see Figure 5-32 to Figure 5-33. This is due to the standing wave field between the pontoons. The wave lengths are short compared to the long pontoons, such that the pontoons are perceived as vertical walls, giving reflection of a considerable amount of the waves and initiation of a standing wave field.

Figure 5-32 illustrated the increased frequency and amplitude of oscillations typical for interaction effects for added mass and damping. Similarly, the frequency and amplitude of oscillations increased for the excitation forces in multibody analyses, and interaction effects, gives rise to excitation forces perpendicular to incoming wave direction as shown in Figure 5-33. The same effects occur for mean drift force.
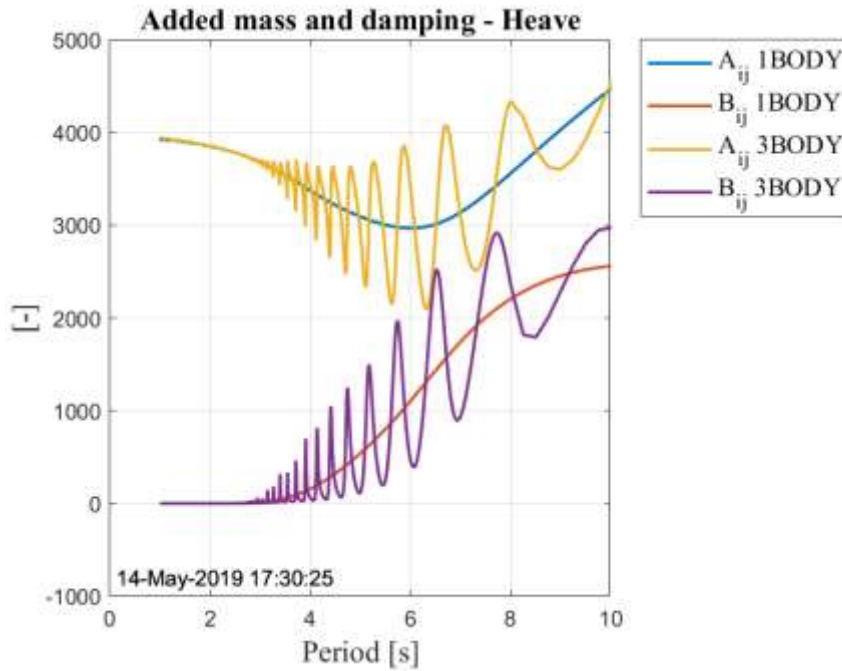
> *Figure 5-32: Added mass and damping in heave for single- and multibody analyses.*
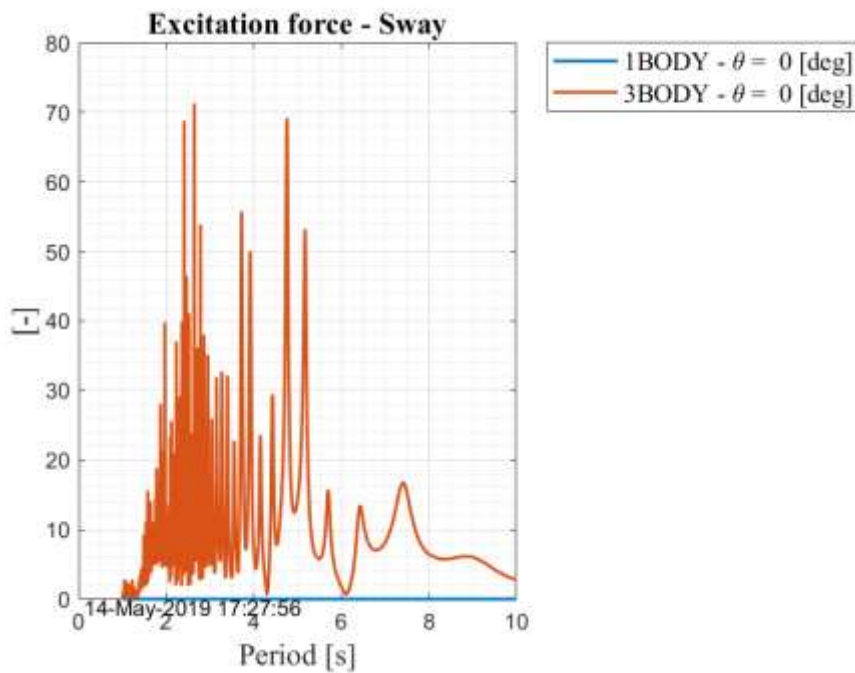
> *Figure 5-33: Excitation force in sway for wave heading 0 degrees for single- and multibody analyses.*

A study performed with increased center distance revealed that the interaction effect is not significantly affected by the center distance between the pontoon. This is due to a standing wave field.

5.5   Wind wave analyses along floating bridge towing route

Wind wave analyses are performed for 12 selected points along the towing route from Eikelandsfjorden to the bridge location. The points are shown in Figure 5-34 and the extreme values of significant wave height with 1-year return period and corresponding wave direction in Table 5-4. Table 5-5 shows design towing wave height and periods for points along the bridge for design wind speed 15 m/s for different directions.
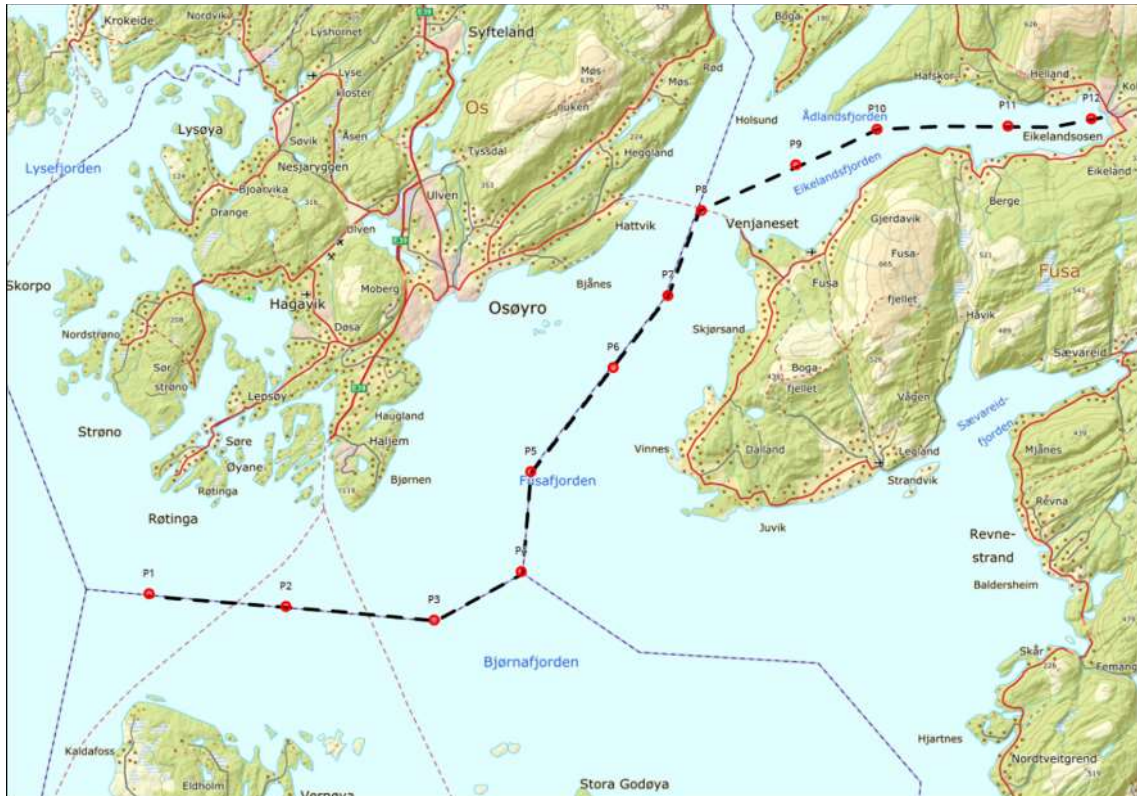
> *Figure 5-34: Towing route and points used for wind wave analysis*

> *Table 5-4: Extreme values of significant wave height along towing route with 1-year return period and their corresponding wave direction*

Towing point	Wave direction (deg)	Significant wave height (m)
P1	90	1.7
P2	90, 270	1.6
P3	270	1.7
P4	270	1.7
P5	240	1.4
P6	180	1.4
P7	180, 210	1.4
P8	210	1.4
P9	240	1.3
P10	1.2	4.0

P11	1.0	3.5
P12	1.0	3.5

> *Table 5-5: Design towing load along towing route from Eikelandsfjorden for points shown in Figure 5-34, design wind speed: 15 m/s*

	Wind Speed (m/s)	0		30		60		90		120		150		180		210		240		270		300		330	
		Hs	Tp	Hs	Tp	Hs	Tp	Hs	Tp	Hs	Tp	Hs	Tp	Hs	Tp	Hs	Tp	Hs	Tp	Hs	Tp	Hs	Tp	Hs	Tp
P1	15	0.67	2.97	0.62	2.76	1	3.99	1.27	4.4	0.96	3.82	0.64	2.78	0.75	3.29	0.83	3.37	0.72	2.89	0.76	3.06	0.91	3.61	0.94	3.77
P2	15	0.55	2.57	0.86	3.72	1.14	4.07	1.23	4.21	1.05	3.78	0.95	3.47	0.94	3.45	0.95	3.49	0.89	3.34	0.94	3.5	0.94	3.72	0.66	3.09
P3	15	0.89	3.5	1.07	3.87	1.03	3.73	1.12	3.95	0.97	3.67	0.75	3.02	0.89	3.31	0.9	3.28	0.85	3.34	1.02	3.76	0.88	3.45	0.72	2.92
P4	15	0.89	3.43	0.94	3.59	0.87	3.41	1.04	3.79	1.02	3.71	0.84	3.23	0.8	3.16	0.88	3.38	0.98	3.65	1	3.79	0.75	3.09	0.76	3.05
P5	15	0.74	3.07	0.89	3.51	0.76	3.12	0.8	3.34	1.06	3.86	1	3.63	0.96	3.54	1.01	3.68	0.96	3.72	0.69	3.08	0.6	2.56	0.64	2.72
P6	15	0.67	2.97	0.81	3.33	0.65	2.82	0.52	2.35	0.55	2.58	0.86	3.52	1.07	3.82	1.11	3.96	0.92	3.63	0.64	2.84	0.47	2.23	0.51	2.33
P7	15	0.68	2.94	0.77	3.22	0.54	2.67	0.45	2.11	0.46	2.14	0.59	2.93	1.02	3.96	1.18	4.17	0.89	3.65	0.57	2.69	0.46	2.15	0.48	2.28
P8	15	0.61	2.74	0.8	3.19	0.75	3.04	0.57	2.55	0.46	2.2	0.59	2.75	0.98	3.91	1.17	4.23	0.8	3.62	0.45	2.25	0.41	1.98	0.46	2.2
P9	15	0.51	2.35	0.59	2.55	0.62	2.74	0.49	2.43	0.42	2.02	0.4	1.97	0.46	2.52	0.85	4.04	0.91	3.9	0.62	2.73	0.54	2.4	0.49	2.26
P10	15	0.32	1.69	0.35	1.82	0.47	2.29	0.52	2.49	0.37	2.02	0.32	1.68	0.41	2.17	0.68	3.13	0.83	3.42	0.58	2.92	0.34	1.89	0.3	1.6
P11	15	0.26	1.49	0.26	1.48	0.35	1.92	0.44	2.18	0.36	1.96	0.28	1.56	0.27	1.52	0.34	1.98	0.59	2.98	0.65	2.97	0.44	2.21	0.34	1.8
P12	15	0.26	1.49	0	0	0	0	0	0	0	0	0	0	0.27	1.52	0.34	1.98	0.59	2.98	0.65	2.97	0.44	2.21	0.34	1.8

6 LOADS

6.1 Static loads

6.1.1 Permanent loads

The permanent loads include the selfweight of the girder, buoyancy of the pontoons and the pretension loads of the cable stays. These loads are balanced in order to minimize the bending moments of the bridge girder and tower.

The steel weight of the girder is calculated in [15] and summarized in sec. 11.5. In addition to the steel weight, permanent equipment such as railings and asphalt are included in the self-weight of the girder, as shown in Table 6-1.

> *Table 6-1 Additional permanent weight included in bridge girder self-weight*

Additional permanent weight	Unit load	Equivalent line load
Asphalt, driving lanes	2.0 kN/m^2	4000 kg/m
Asphalt, pedestrian lanes	1.5 kN/m^2	600 kg/m
Permanent equipment	-	500 kg/m
Total:		5100 kg/m

6.1.2 Traffic loads

The design traffic load is according to the Eurocode traffic load system (LM1) from Eurocode 1991-2:2003+NA:2010, N400 and *«Forskrift for trafikklast på bruer, ferjekaier og andre bærende konstruksjoner i det offentlige vegnettet»*, ref. [22]. A summary of the traffic models is shown in Table 6-2.

> *Table 6-2 LM1 traffic load specification*

Lane	Width	Distributed area load	Axle load	Horizontal traffic load	α-factors
Lane 1	3 m	α_{q1} * 9.0 kN/m^2	α_{Q1} * 2x300 kN	900 kN	α_{q1}=0.6, α_{Q1}=1.0
Lane 2	3 m	α_{q2} * 2.5 kN/m^2	α_{Q2} * 2x200 kN	0 kN	α_{q2}=1.0, α_{Q2}=1.0
Lane 3	3 m	α_{q3} * 2.5 kN/m^2	α_{Q3} * 2x100 kN	0 kN	α_{q3}=1.0, α_{Q3}=1.0
Pedestrian Lane	3 m	α_{fk} * 2.5 kN/m^2	0	0 kN	α_{fk}=1.0
Remaining area	14 m	α_{qr} * 2.5 kN/m^2	0	0 kN	α_{qr}=1.0
Total:	23 m + 3 m	73.7 kN/m	1200 kN	900 kN	

Lane positions for LM1 application is described in [10].

6.1.3 Temperature loads

> *Table 6-3 Maximum and minimum air temperature for given return periods.*

Return period	Minimum temperature °C	Maximum temperature °C
1 year	-7	25
10 year	-12	29
50 year	-15	32
100 year	-17	33

For 100-year return period, temperature giving zero strain in the structure is assumed to be +8°C, with temperature variations of +/-25°C applied to the whole model (except structures below water surface).

6.1.4 Current loads

The extreme values of hourly sea currents (m/s) for four different locations at the planned bridge crossing is described in design basis along with relative factors for sectoral extreme speeds (every 45°) for return periods of 10, 50 and 100 years. Linear interpolation is used between the locations to calculate the current speeds at the pontoon locations (and assumed constant from end locations towards north and south shore).

The current forces acting on the pontoons are calculated according to the formulae given below:

$$F_{current} = \frac{1}{2} * \rho_{water} * U(x)^2 * \sum (C_d * A_p)$$

Where

ρ_{water} is the density of water, equal to 1025 kg/m^3

$U(x)$ is the current speed at pontoon X

$\sum (C_d * A_p)$ is the total projected drag area of the pontoon, which depends on the pontoon size, shape and orientation (the angle to the current)

The applied current loads applied to the pontoon nodes, for sector W for a 100-year return period, are shown in the below figure.
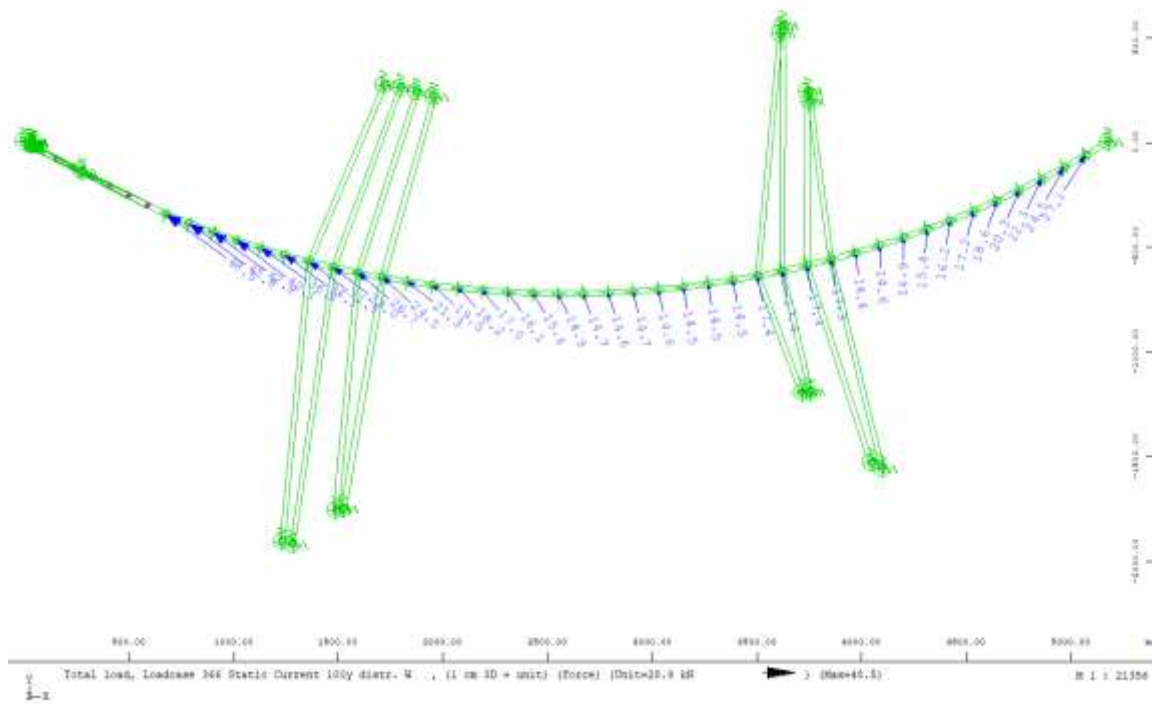
> *Figure 6-1 Static current loads 100-year (in kN), sector W.*

6.1.5   Static wind

Static wind cases mentioned here are not applied together with coupled analyses as the coupled analyses already have static wind contributions, but are used in some sensitivity studies and included here for completeness.

The design basis along with N400 and NS-EN 1991-1-4:2005+NA provide input for the wind loading.

The formulae for calculating the wind profile for 1h mean is available in design basis, and gives the following mean wind speeds at height 10 meters:

> *Table 6-4 1h and 10min mean wind speeds for given return periods at z=10m*

Return period (years)	Wind speed 1h mean (m/s)	Wind speed 10min mean (m/s)
1	21.4	22.9
10	25.8	27.6
50	28.5	30.5
100	29.6	31.7
10000	35.9	38.4

Reduction factors applies for sectors and are used to find the sectoral extremes. The factors are applied to the wind speeds. The directional reduction factors are found in design basis.

For strong winds the mean wind can be assumed to have the following distributions along the bridge axis (note that V means mean wind speed):

1) Constant
2) Linearly varying from 0.6 x V at one end to V on the other
3) Linearly varying from 0.8 x V at one end to V in the middle to 0.8 x V on the other end.

The wind load is applied as linearly varying line loads applied to each beam in the global element model, calculated from local wind speed where location along the bridge span, height above the sea level, drag area and rotation of the element relative to the wind direction and wind speed distribution are accounted for.

Typical wind load application is shown in the figures below:
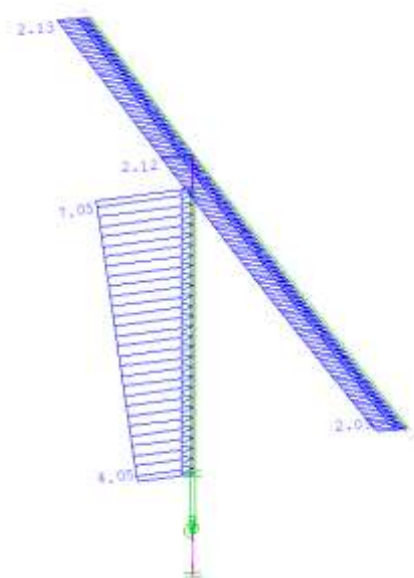
> *Figure 6-2 Typical wind load applied to bridge girder and pontoon tower (in this particular case, 100y constant wind sector 90 deg / wind from east, pontoon tower no. 8 from south)*
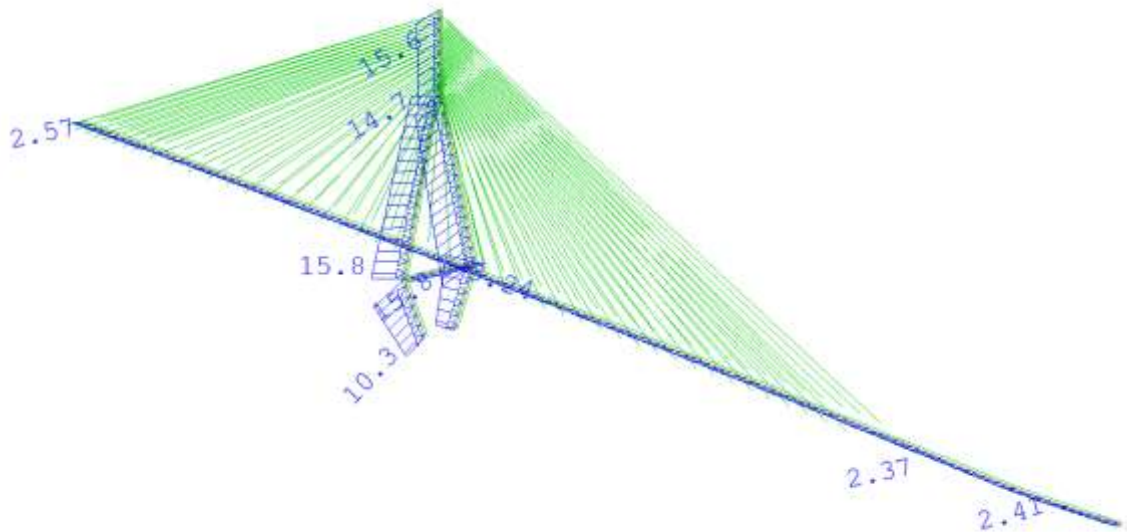
> *Figure 6-3 Typical wind load applied to bridge girder and land tower (in this particular case, 100y constant wind sector 90 deg / wind from east)*

Typical wind distribution response (bridge strong axis moment, Mz):
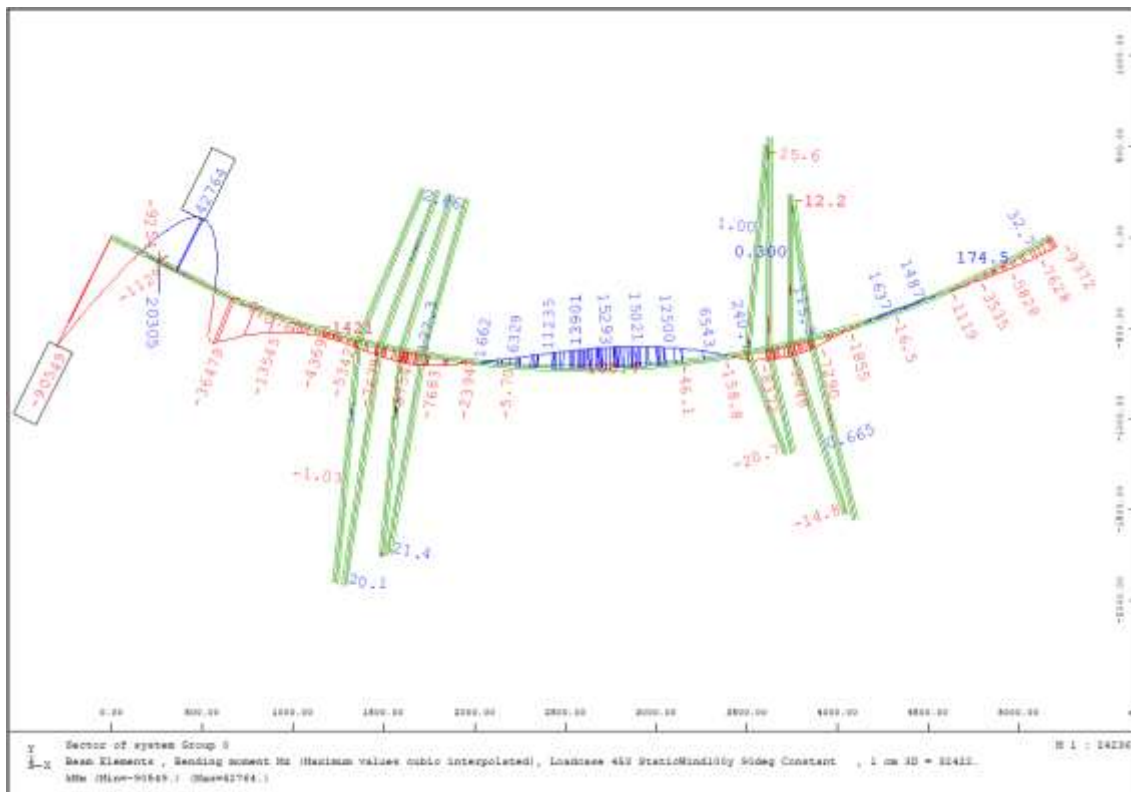
> *Figure 6-4 Typical wind response for constant wind speed along bridge, for wind from directly east*
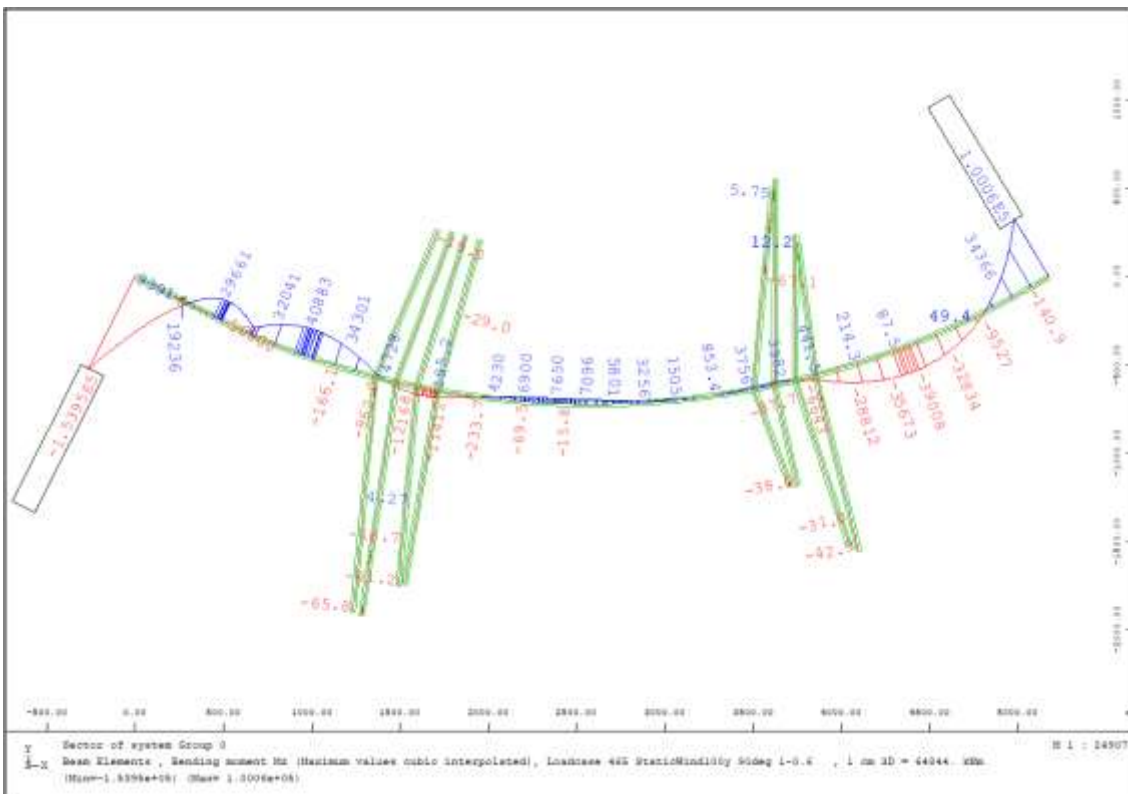
> *Figure 6-5 Typical wind response for linearly varying wind speed from 100% at south, to 60% at north end of bridge, for wind from directly east*
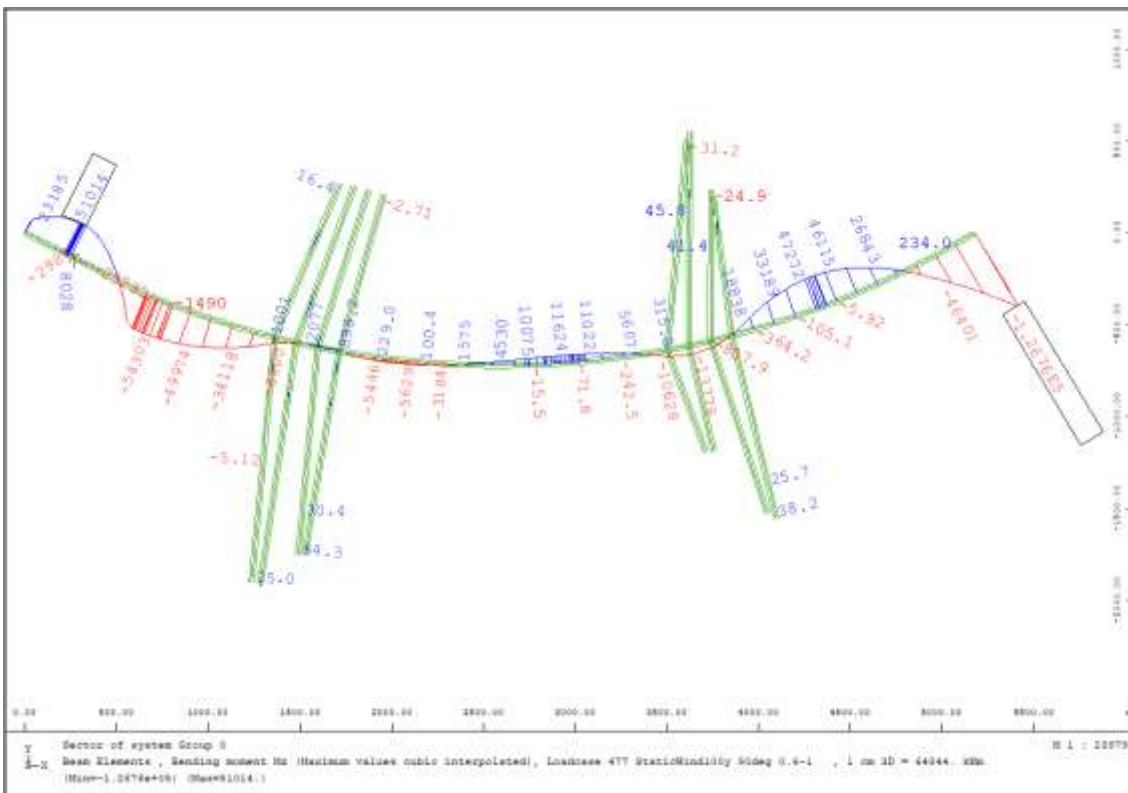
> *Figure 6-6 Typical wind response for linearly varying wind speed from 60% at south, to 100% at north end of bridge, for wind from directly east*
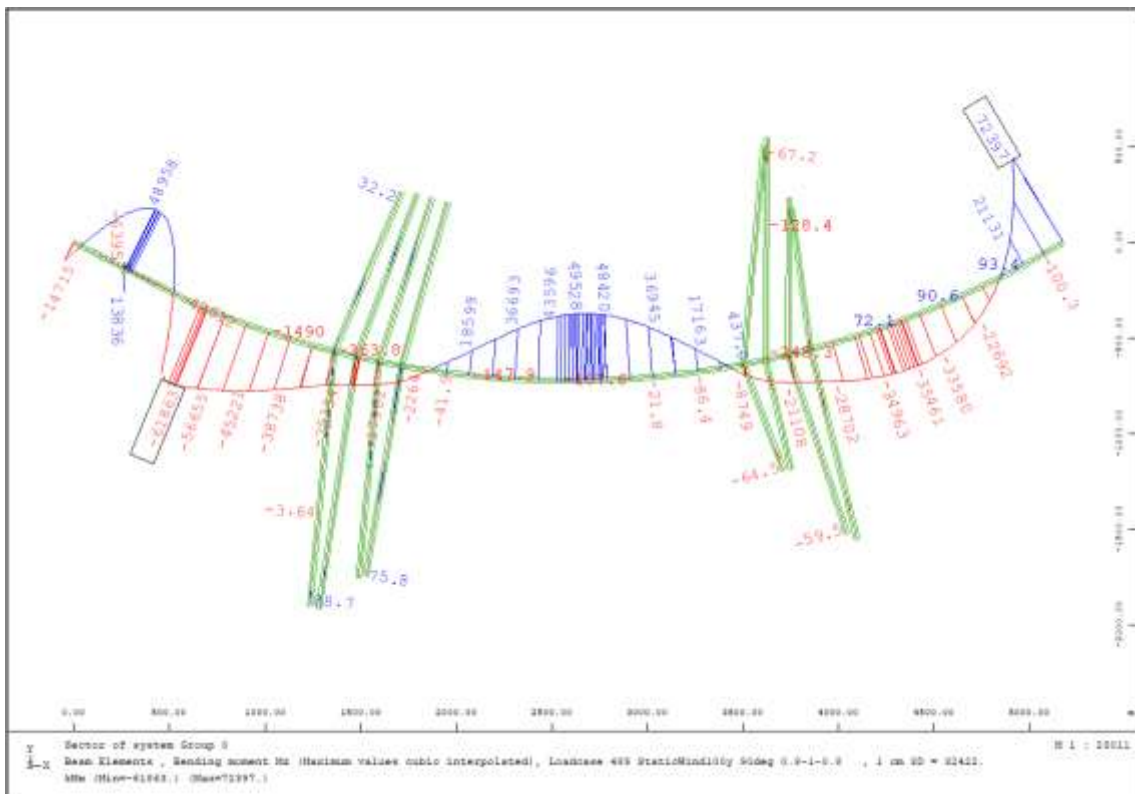
> *Figure 6-7 Typical wind response for linearly varying wind speed from 80% at south, to 100% at center of bridge, to 80% at north end of bridge, for wind from directly east*

6.1.6   Tidal loads

> *Table 6-5 Tidal amplitudes*

Tidal amplitudes	Value [m]
Lowest Astronomical Tide	0
Mean Low Water	0.39
Mean Sea Level	0.77
Mean high water	1.15
Highest Astronomical Tide	1.53

> *Table 6-6 Water level related to return periods relative to LAT.*

Return periods (years)	Highest water level (m)	Lowest water level (m)	Storm surge (m)
1	1.81	-0.20	+/- 0.235
10	1.97	-0.30	+/- 0.37
100	2.10	-0.50	+/- 0.535
10000	2.50	-0.65	+/- 0.81

Calculation of storm surge (100y) and combined factor:

Total tide	= (2.1-(-0.5))/2	= 1.3 m
Astronomical tide	= 1.53-0.765	= 0.765 m
Storm surge tide	= 1.3-0.765	= 0.535 m

According to design basis [22] the astronomical component is independent of the environmental conditions, whereas the surge component is governed by the atmospheric conditions. Since the confidence on the two components vary, that is, astronomical tide values are lot more predictable than the surge components are, appropriate safety factors can be applied separately on each component during further design.

A load factor for astronomical tide is not explicitly given in this design basis. However, in design basis for phase 3 of the Bjørnafjorden it was suggested that it should have a load factor of 1.1. Thus, this has been applied in this phase as well.

Load factor astronomical tide = 1.1
Load factor storm surge part of tide = 1.6

Combined load factor 100 year conditions = 1.6*0.535 /1.3+1.1*0.765/1.3= 1.31

Tidal variations are applied as loads and applied to each pontoon as follow:

$$F_{pontoon,i,100y} = +/- \rho_{water} * g * A_{pontoon,i,WL} * \Delta_{Tidal,100y}$$

Tidal variations are applied as loads on each pontoon and summarized in Table 6-7 for each pontoon type.

> *Table 6-7 Tidal loads*

Pontoon type	Area of pontoon at WL (m²)	Tidal load (kN)
1	559	+/- 7301
2	665	+/- 8694
3	770	+/- 10064
4	873	+/- 11413

6.1.7 Marine fouling

Marine fouling is calculated in accordance with Håndbok N400 [34]. The forces applied to the static model at the pontoon is summarized in Table 6-8 for each of the pontoon types.

> *Table 6-8 Pontoon loads from marine fouling. example from K12.*

Pontoon type	Area subjected to marine fouling	Submerged weight	Permanent loading from marine fouling
Pontoon 1	1259 m²	468 N/m²	589 kN
Pontoon 2	1378 m²	468 N/m²	645 kN
Pontoon 3	1496 m²	468 N/m²	700 kN
Pontoon 4	1611 m²	468 N/m²	754 kN

6.1.8   Water density

The effect of variation in water density is deemed negligible.

6.2   Coupled loads

The coupled loads consist of static wind loads, turbulent wind loads and wave loads. The governing sea states concerning K12 are presented.

Among wave loads we need to consider that we have both waves from weather systems far away (Swell waves) and locally generated waves (Wind generated waves). In the global analyses performed for the final documentation both are included.

Figure 6-8 shows the wind generated sea direction and wind direction for the applied sea states. The swell is coming from 250 degrees for those sea-states where that is included.
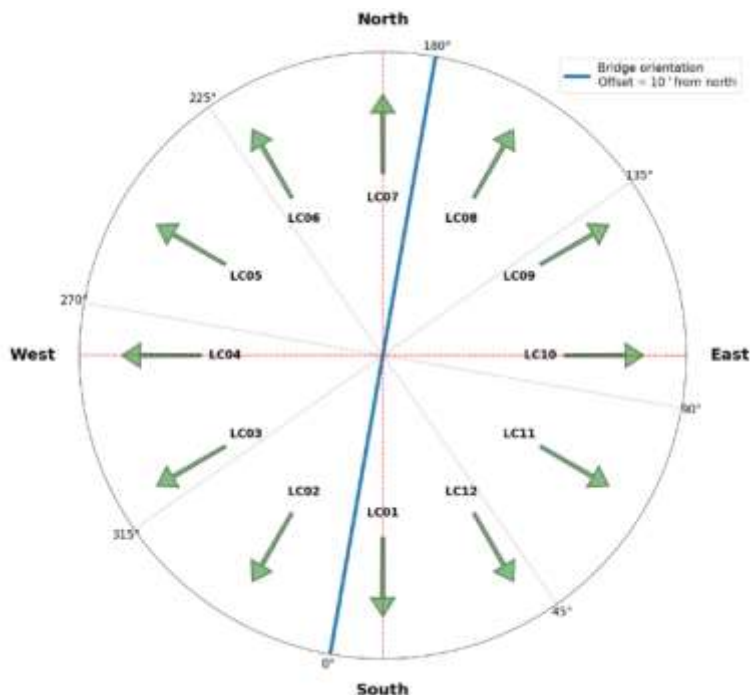
> *Figure 6-8 Sea state directions relative to both bridge direction and cardinal coordinate system.*

More information with regards to the wave conditions and wind conditions are given in Table 6-9, Table 6-10 and Table 6-11, respectively. The wind generated waves are represented by spatially inhomogeneous sea-conditions where both Tp and Hs vary along the bridge. The variations for the different sea states are shown in report SBJ-33-C5-OON-RE-012 Structural response analyses [10], Appendix C - K12 Coupled analysis.

6.2.1 Wind generated wave conditions with a 100 year return period

The Hs-values are increased by 4% due to global warming, which design basis states tabulated values shall be increased by

> *Table 6-9 Wave conditions, return period 100 year*

	Hs	Tp	Gamma	Wave Direction (from)	Spread, s
LC01	0.83	4.00	2.30	190	11
LC02	0.728	4.2	2.30	160	11
LC03	0.936	4.1	2.30	130	11
LC04	2.184	5.5	2.30	100	11
LC05	1.456	4.6	2.30	70	11
LC06	1.248	4	2.30	40	11
LC07	1.248	3.9	2.30	10	11
LC08	1.456	4.6	2.30	340	11
LC09	1.456	4	2.30	310	11
LC10	1.872	4.5	2.30	280	11
LC11	2.08	5.2	2.30	250	11
LC12	1.248	4.6	2.30	220	11

*s=2n+1

6.2.2 Swell wave conditions with a 100 year return period

> *Table 6-10 Wave conditions swell*

	Hs	Tp	Gamma	Wave Direction (from)	Spread, s
LC01	0.34	16.0	5.0	250	31
LC02	-	-	-	-	-
LC03	-	-	-	-	-
LC04	-	-	-	-	-
LC05	-	-	-	-	-
LC06	-	-	-	-	-

LC07	0.34	16.0	5.0	250	31
LC08	0.34	16.0	5.0	250	31
LC09	0.34	16.0	5.0	250	31
LC10	0.34	16.0	5.0	250	31
LC11	0.34	16.0	5.0	250	31
LC12	0.34	16.0	5.0	250	31

*s=2n+1

6.2.3 Wind conditions with a 100 year return period

The wind speed-values are increased by 4% due to global warming (Compared to values in design basis)

> *Table 6-11 Wind conditions*

Load case	Wind Spectrum	Wind speed at ref height	Turbulence intensity	Ref wind height	Wind Profile	Wind Exp	z,0	Wind Dir (from)
[-]	[-]	[m/s]	[-]	[m]	[-]	[.]	[m]	[Deg]
LC01	Kaimal	21.55	14%	10	Power Law	0.13	0.01	190
LC02	Kaimal	21.55	14%	10	Power Law	0.13	0.01	160
LC03	Kaimal	21.55	14%	10	Power Law	0.13	0.01	130
LC04	Kaimal	26.17	14%	10	Power Law	0.13	0.01	100
LC05	Kaimal	26.17	14%	10	Power Law	0.13	0.01	70
LC06	Kaimal	26.17	23.5%	10	Power Law	0.13	0.01	40
LC07	Kaimal	26.17	23.5%	10	Power Law	0.13	0.01	10
LC08	Kaimal	26.17	23.5%	10	Power Law	0.13	0.01	340
LC09	Kaimal	27.71	14%	10	Power Law	0.13	0.01	310
LC10	Kaimal	30.78	14%	10	Power Law	0.13	0.01	280
LC11	Kaimal	30.78	14%	10	Power Law	0.13	0.01	250
LC12	Kaimal	30.78	14%	10	Power Law	0.13	0.01	220

6.3 Accidental load cases

6.3.1 Ship impact

Ship impacts are defined as accidental load conditions related to a recurrence period of 10 000 years. The Norwegian Public Roads Administration (NPRA) has in handbook N400 [34] set this as the limit where less likely events are disregarded.
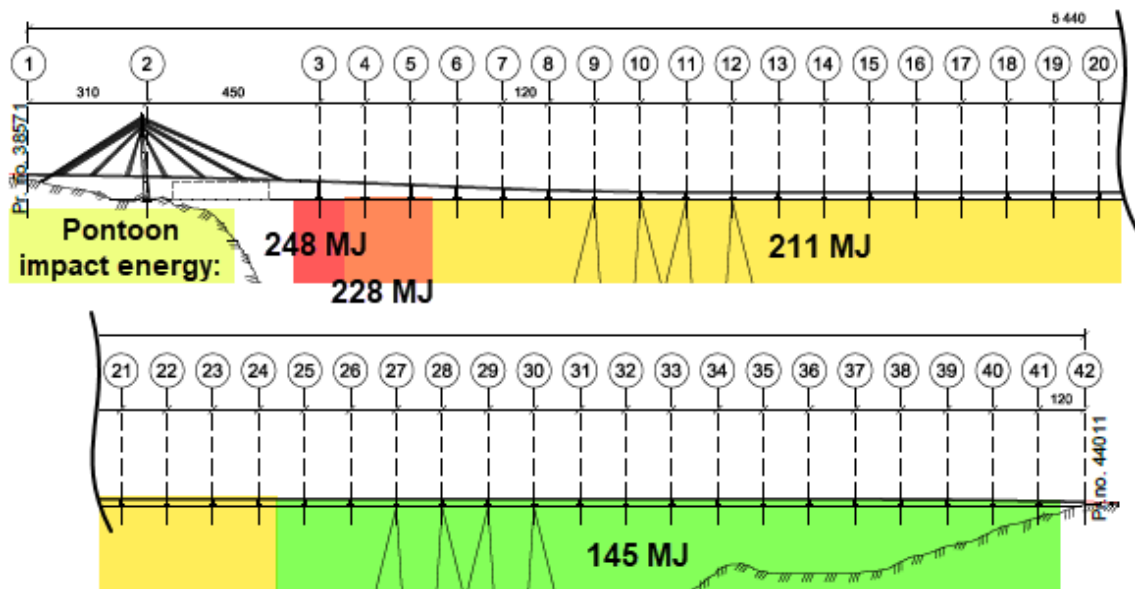
> *Figure 6-9: Numbering of axis referring to pontoons and distribution of pontoon impact energy. From drawing SBJ-33-C5-OON-22-DR-001.*

Impact scenarios are based on the specified cases in the Design basis [22]:
- Bow collisions with bridge pontoons (centric and eccentric), all possible impact angles
- Deckhouse collision with bridge girder
- Sideway collisions (against the pontoons longitudinal walls)
- Submarine impact
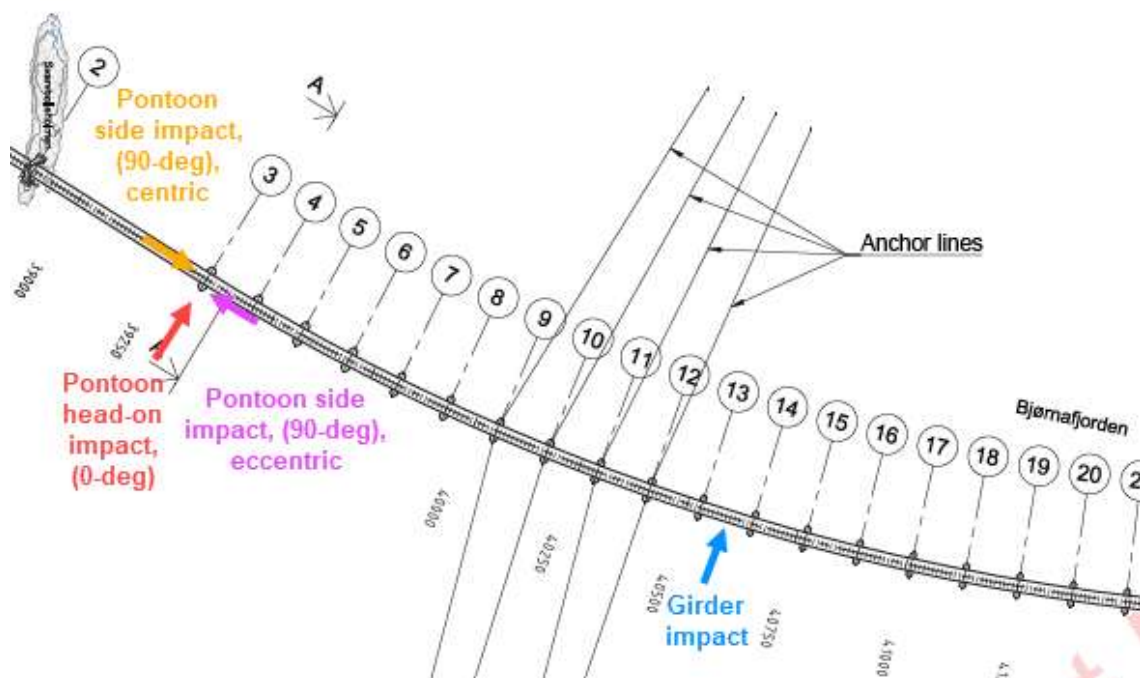
> *Figure 6-10: Ship impact illustration. Examples of the main impacts studied*

7 LOAD COMBINATIONS

7.1 Combination overview

In Table 7-1 below, the limit states and design criteria checks applied in this study are presented. The different load combination numbers define different combination rules, each with different load factors for different load contributions. For a more thorough description of the limit states and design criteria, see Chapter 7.2 through Chapter 7.7 and the design basis [22].

> *Table 7-1 Summary of combinations*

Comb. number	Combination type	Description
21	SLS load combinations	Traffic load dominating
22	SLS load combinations	1 year conditions with traffic
23	SLS load combinations	100 year conditions without traffic
24	SLS load combinations	Infrequent
25	SLS load combinations	Quasi-permanent
31	ULS load combinations	ULS 6.10a, 1 year conditions with traffic
32	ULS load combinations	ULS 6.10a, 100 year conditions without traffic
33	ULS load combinations	ULS 6.10b, 1 year conditions with traffic
34	ULS load combinations	ULS 6.10b, 100 year conditions without traffic
35	ULS load combination	DNV Mooring consequence class 1
36	ULS load combination	DNV Mooring consequence class 2
41	Static motion limitation	0.7x traffic
42	Static motion limitation	1-year static wind

7.2 Ultimate limit state

According to Design Basis [22], chapter 7.3.2, the bridge characteristic response in ULS shall be defined based on an environmental event with return period of 100 years, in which the bridge is assumed closed for traffic. Additionally, characteristic response from environmental and traffic loading shall be evaluated with an environmental event with a return period of 1 year. The events are evaluated with respect to load combination principles of EQU and STR. Load combination factors applied are according to Design Basis and presented in Table 7-2 to Table 7-5.

7.2.1   Ultimate limit state – EQU

In load combination set 31, the worst load combination according to Table 7-2 are conservatively combined with LF for environmental loads as dominating load (1,6) with 1-year RP.

> *Table 7-2: ULS-EQU load combination factors COMB 31, $\gamma \times \psi_0$*

Load		Dominating load			
		G	L	T	C
Self-weight	G	**1.0/0.9**	1.0/0.9	1.0/0.9	1.0/0.9
Traffic	L	0.95	**1.35**	0.95	0.95
Temperature	T	0.84	0.84	**1.2**	0.84
Other loads	C	1.05	1.05	1.05	**1.5**
Environmental*	E	1.6	1.6	1.6	1.6

> *Table 7-3: ULS-EQU load combination factors COMB 32, $\gamma \times \psi_0$*

Load		Dominating load
		E
Self-weight	G	1.0/0.9
Temperature	T	0.84
Environmental, 100 year, without traffic	E	**1.6**
Other loads	C	1.05

7.2.2   Ultimate limit state – STR

In load combination set 33, the worst load combination according to Table 7-4 are conservatively combined with LF for environmental loads as dominating load (1,6) with 1-year RP.

> *Table 7-4: ULS-STR load combination factors COMB 33, $\gamma \times \psi_0$*

Load		Dominating load			
		G	L	T	C
Self-weight	G	**1.35/1.0**	1.2/1.0	1.2/1.0	1.2/1.0
Traffic	L	0.95	**1.35**	0.95	0.95
Temperature	T	0.84	0.84	**1.2**	0.84
Other loads	C	1.05	1.05	1.05	**1.5**
Environmental*	E	1.6	1.6	1.6	1.6

> *Table 7-5: ULS-STR load combination factors COMB 34, $\gamma \times \psi_0$*

Load		Dominating load
		E
Self-weight	G	1.2/1.0
Temperature	T	0.84
Environmental, 100 year, without traffic	E	**1.6**
Other loads	C	1.05

7.2.3   Ultimate limit state – GEO

ULS load factors for geotechnical design are given by DNVGL OS C101 [35] Chapter 2 Section 10 and presented in Table 7-6.

> *Table 7-6: ULS-GEO load coefficients for consequence class 1 (COMB 35) and 2 (COMB 36)*

Load factor	ULS CC1	ULS CC2
γ_{mean}	1.1	1.4
γ_{dyn}	1.5	2.1

7.2.4   Ultimate limit state – FAT

ULS-FAT is evaluated according to the procedure established by DNVGL as described in [22], Chapter 7.3.2.

7.3   Accidental limit state

The accidental limit stat load combinations are described in [22], with load factors as shown in Table 7-7. The limit states described comprises two stages; the purpose of stage A is to control the magnitude of local damage for the bridge subjected to an accidental load, and stage B is to check the behavior of the bridge in a damaged condition. Load combination factors are presented in Table 7-7 and Table 7-8 and taken from Design Basis [22].

7.3.1   ALS Standard

> *Table 7-7: ALS load combination factors, ψ_2, stage A*

Load combinations	Stage A			
	Earthquake	Abnormal environmental loads	Fire and explosion	Ship impact
Self-weight	1.0	1.0	1.0	1.0

Traffic	0.5	0	0.5	0.5
Accidental loads				
Earthquake	1.0	0	0	0
Environmental loads, 10.000 year	0	1.0	0	0
Ship impact	0	0	0	1.0
Fire and explosion	0	0	1.0	0

> *Table 7-8: ALS load combination factors, ψ_2, stage B*

Load combinations	Stage B (damaged condition)		
	Pontoon filled with water	Lost mooring cable	Lost cable stay
Self-weight	1.0	1.0	1.0
Environmental loads, 100 year	1.0	1.0	1.0
Accidental loads			
Pontoon filled with water	1.0	0	0
Lost mooring cable	0	1.0	0
Lost stay cable	0	0	1.0

7.3.2   ALS – GEO

ALS load factors for geotechnical design are given by DNVGL OS C101 [35] Chapter 2 Section 10 and presented in Table 7-9.

> *Table 7-9: ALS-GEO load coefficients for consequence class 1 and 2*

Load factor	ALS CC1	ALS CC2
γ_{mean}	1	1.1
γ_{dyn}	1	1.25

7.4   Serviceability limit state

7.4.1   SLS characteristic

According to design basis chapter 7.3.1 [22] the characteristic SLS should be used to determine bearing displacements. Table 7-10 and Table 7-11 shows combinations and combination factors applied, based on Design Basis [22].

> *Table 7-10 Combination factors SLS [22] COMB21, ψ_0*

Load		Dominating load			
		G	L	T	C
Self-weight	G	**1.0**	1.0	1.0	1.0
Traffic	L	0.7	**1.0**	0.7	0.95
Temperature	T	0.7	0.7	**1.0**	0.84
Environmental, 1 year, with traffic	E_{1yr}	0.7	0.7	0.7	1.12
Other loads	C	0.7	0.7	0.7	**1.0**

> *Table 7-11 Combination factors SLS [9] COMB22 (Environmental 1 year with traffic) and COMB23 (Environmental 100 year without traffic) , ψ_0*

Load		COMB22,E_{1yr}	COMB22,E_{100yr}
Self-weight	G	1.0	1.0
Traffic	L	0.7	-
Temperature	T	0.7	0.7
Environmental	E	**1.0**	**1.0**
Other loads	C	0.7	0.7

7.4.2   SLS in-frequent

The in-frequent load combination shall be used for evaluation of minimum vertical navigation clearance, as stated in Design Basis [22], Chapter 7.3.1.

> *Table 7-12 Load combinations and factors in-frequent SLS [22], ψ_0*

Load		Dominating load			
		L	T	E_{50yr}	C
Self-weight	G	1.0	1.0	1.0	1.0
Traffic	L	**0.8**	0.7	0.7	0.7
Temperature	T	0.6	**0.8**	0.6	0.6
Environmental, 50 year, with traffic	E_{50yr}	0.6	0.6	**0.8**	0.6
Other loads	C	0.6	0.6	0.6	**0.8**

Table 7-12 shows an example of combinations to be evaluated, as presented in Design Basis.

7.4.3 SLS quasi-permanent

Combination factors for the quasi-permanent SLS condition are given in design basis [22] and presented in Table 7-13, with $\psi_2 = 0$ for variable loads.

> *Table 7-13: Combination factors for quasi-permanent SLS condition*

Load		Dominating load			
		L	T	E$_{50yr}$	C
Self-weight	G	1.0	1.0	1.0	1.0
Traffic	L	**0.2/0.5**	0.2/0.5	0.2/0.5	0.2/0.5
Temperature	T	0/0.5	**0/0.5**	0/0.5	0/0.5
Environmental, 50 year, with traffic	E$_{50yr}$	0/0.5	0/0.5	**0/0.5**	0/0.5
Other loads	C	0/0.5	0/0.5	0/0.5	**0/0.5**

7.5 Fatigue limit state

See SBJ-33-C5-OON-22-RE-016 Fatigue Assessment [14].

7.6 Static deflection, motion and comfort criteria

Bridge acceleration limitations shall be established based on driver comfort and are described in Design Basis Chapter 9.3 [22].

In Design Basis chapter 9.2 static deflection and motion criteria for the bridge is described, see Table 7-14 below.

> *Table 7-14 Static deflection and motion criteria taken from Design Basis [22]*

Motion limitation	Load scenario	Maximum motion
Vertical deformation from traffic loads	0.7xtraffic	uy≤1.5m
Rotation about bridge axis from eccentric traffic loading	0.7xtraffic	θx≤1.0 deg
Rotation about bridge axis from static wind load	1-year static wind	θx≤0.5 deg

7.7   Freeboard/Stability criteria

In design basis chapter 9.1 the freeboard and stability criteria that should be maintained are described.

1. For structural parts that do not follow the tide, the freeboard should be maintained for the highest water level for a tide with a 100 year return period.
2. The stability of the bridge shall be evaluated with respect to ULS-EQU. For the 1-year condition, the change of mass and aerodynamic coefficients of the bridge girder due to presence of traffic shall be accounted for.

Also, according to N400 freeboard should be maintained during environmental conditions with a return period of 100 years.

Sensitivity studies of the robustness of the structure when freeboard is temporarily lost shall be conducted.

8   STRUCTURAL RESPONSE

The response can currently be found on the web olavolsen.interactive.no [36] for K12 – Model 27. Most relevant responses of the bridge girder are also presented in the structural response analyses report [10], and selected results are summarized in this chapter

8.1   Coordinate systems

Displacements and accelerations are presented according to the global coordinate system given in Figure 8-1.
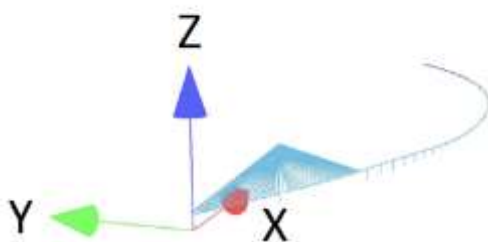
>   *Figure 8-1 Global coordinate system*

Forces and moments are presented according to the local coordinate systems presented in Figure 8-2.

8.2   ULS stress response

The most utilized stress points in the top deck (P1 and P7) are governed by the 100 year environmental condition with no traffic included, see *ULS 6.10b – 100 year conditions without traffic in Chapter* 7.2.2

The most utilized stress point in the bottom plate (P3 and P5) are governed by the dominant traffic condition, see *ULS 6.10b – 1 year environmental with traffic in Chapter* 7.2.2

From global analyses max and min stresses in each stress point is given, along with the combination of FX, FY, FZ, MX, MY and MZ which gives the max/min stress. Stresses from the global response analyses to recalculate stresses with design cross section properties. Both ULS comb 33 with traffic and ULS comb 34 without traffic (100 years RTP) are recalculated.
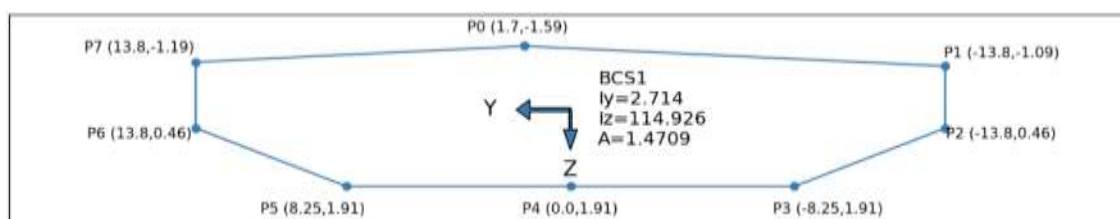
>   *Figure 8-2 Stress points*

8.3   Vertical deformation from 0.7 x traffic loads

Figure 8-3 and Figure 8-4 shows the deformation from two different sets of reduction factors, one for traffic with a larger influence length (>1000m), while the other is for influence lengths below 200m.
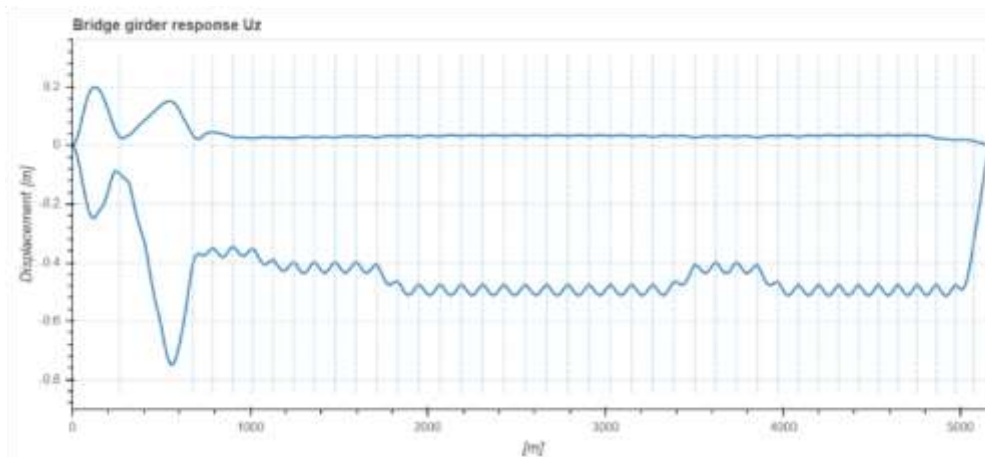

>   *Figure 8-3 Vertical displacement- with reduction factors corresponding to an influence length >1000 m*
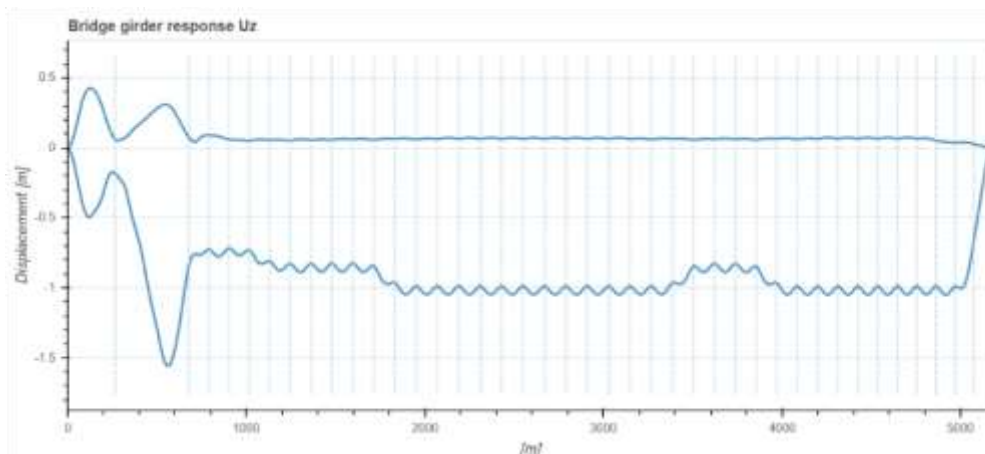
>   *Figure 8-4 Vertical displacement – with no reduction factors (corresponding to influence length <200m), not valid for the cable stayed bridge.*

The vertical deformation for the cable stayed bridge is somewhere in between the two presented cases. It is difficult to say exactly what it is but most likely it is below the deformation requirement of 1.5m.

The floating bridge has influence lengths below 200m in vertical direction, but the deformation is still within the requirement.

8.4   Rotation about bridge axis from eccentric traffic loading

The maximum rotations of the bridge girder from eccentric traffic loading is 19.2mrad and 23.2mrad for 0.7 x ULS traffic load factored for influence lengths 1000m and 200m respectively.

Maximum rotation about bridge axis = (23mrad/1000) * (180/pi) = 1.3 deg

Most likely the torsional rotation should be controlled by influence lengths close to 1000m due to the long torsional modes.

The maximum rotation for this case is about 1.1 degrees which is slightly above the requirement of 1.0 degrees. This can easily be accounted for in the next phase by increasing the length of the pontoon by a meter or two.

8.5   Rotation about bridge axis from static wind load

As seen from Figure 8-5 the rotation from mean wind never exceeds 0.15 degrees, which is far below the requirement in design basis of 0.5 degrees. The load conditions applied are similar to the governing sea states with a return period 100 years but adjusted for the 1 year conditions.
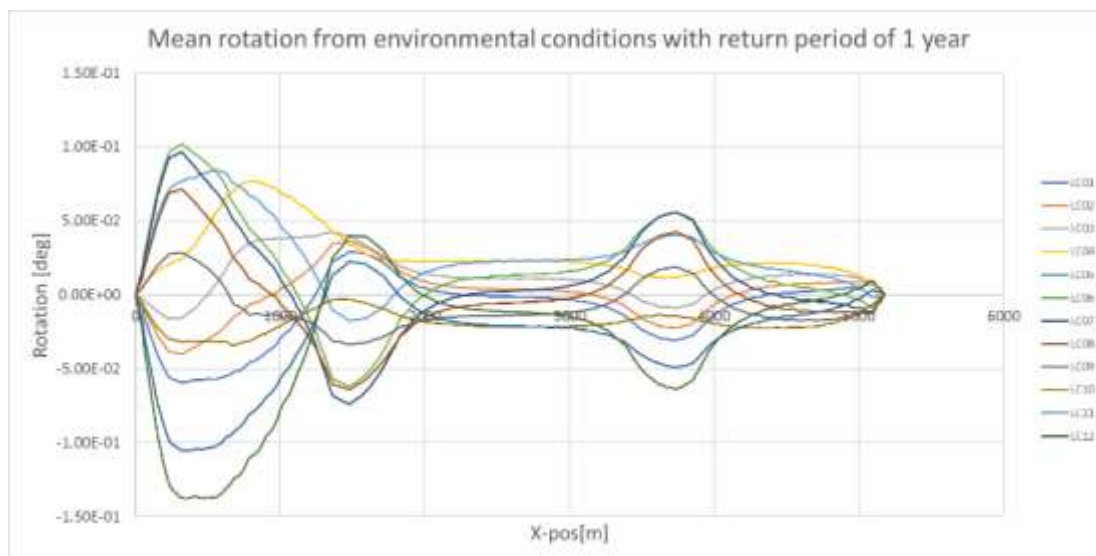
> *Figure 8-5 Mean rotation from environmental conditions (Mean wind)*

8.6   Check of free board

The pontoon free board is checked with regards to displacement from center of pontoon, displacement at pontoon end due to rotation of the pontoon, tides and wave elevation.

Maximum loss of draft in 100 year conditions is about 0.8 meters for the center of the pontoons, and the maximum rotation of the pontoon is about 2.37 degrees. The rotation and displacement of the pontoon comes from excitations of different modes, i.e. they are uncorrelated.

The pontoons affected by tide has a relative tidal displacement (RP=100 years) of about 0.4 meters closest to the landfall in north, but relatively small displacement from the environmental conditions and can be disregarded. The remaining pontoons follows the tide.

The pontoon in axis 38 (4700m in global X position) is the pontoon that based on the plot will have the smallest freeboard.

The maximum wave elevation is about 2.5m.

How correlated the wave elevation is with the elevation at the pontoon edges is difficult to say for certain but most likely they are not very correlated. If there is any correlation this should be positive. (Pontoon elevation follows wave elevation). Thus, it will be conservative to assume that they are uncorrelated.

The freeboard criteria are satisfied, and the minimum freeboard is calculated to be about 1.14m. Detailed results are show in the **structural response report** [10].

8.7   Comfort requirement

The OVTV values is well within the limit of $0.315m/s^2$ for 1-year environment condition. The mean OVTV value is around $0.146m/s^2$ and the maximum response found was $0.177m/s^2$.

Note that acceleration from wind is larger than the acceleration from bridge motion.

The results are shown in detail in the structural response report [10].

8.8   Global stability

A global stability evaluation has been performed as a part of the structural response analyses [10].

The global stability is very good, the metacentric height GM (distance from COG to meta center of the structure) is above 17 m for all intact situations. By taking one pontoon out of the equation (basically increasing the load span from 120m to 180m) one still maintains a good stability with a metacentric height above 7m.

8.8.1   ULS-EQU stability

The stability of the bridge is evaluated with respect to ULS-EQU. For the 1-year condition, the change of mass and aerodynamic coefficients of the bridge girder due to the presence of traffic is accounted for.

The largest rotation found from the environmental analyses with a return period of 100 years is 2.3 degrees. The bridge must tilt beyond 8 degrees to lose water plane area, so the bridge is stabile with regards to the requirements.

Assuming a tilt from ULS traffic of 1 degree (design basis requirement), this increases the drag factor with 7% for wind with 0 degrees incident, see Figure 8-6. The moment factor increases from 0.013 to 0.045 for wind with 0 degrees incident angle which is not enough to introduce any significant further rotation of the girder. The airflow through the traffic increase the drag factor by 40%. Introducing 1 year environmental conditions reduces the wind load with a factor of 0.52 (26m/s)^2/(36m/s^2) as well as considerably lower rotations from waves.

Adjustments in mass for local reinforcements in detail design is most likely not enough to cause considerably changes in the eigen modes of the structure.

The rotation from a ULS scenario including traffic is most probably smaller (0.52*1.4*1.07=0.78) than the case with traffic, and far away from losing the waterplane area and the global stability.
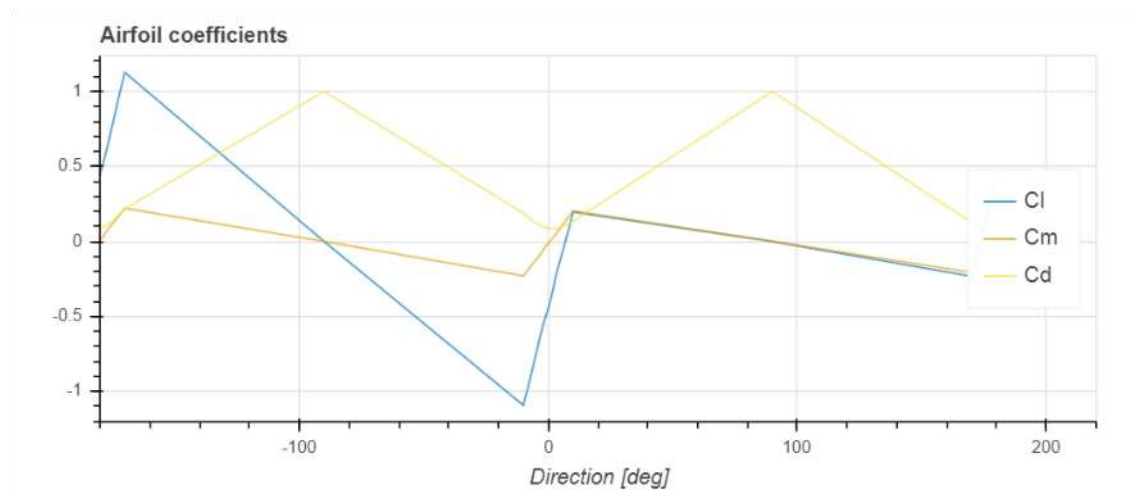
> *Figure 8-6 Drag factor with respect to bridge girder width*

8.8.2 Loss of freeboard

According to design basis sensitivity studies of the robustness of the structure when freeboard is temporarily lost shall be conducted. For the current design we are not very close to losing the freeboard. However, if we were close, a standard procedure for investigating this issue would be to examine the restoring moment for various tilt angles (GZ-curve). The area below this curve should be larger than the area below the corresponding wind heel moment for similar angles until the construction loses its stability.

Restoring moment area > Safety factor (1.3 in DNV-standards) * *Windheel moment area (0 deg ->instability deg)*

A further investigation finding the GZ-curve and compare it to the wind heel curve have not been done. However, the high GM factor indicates that the initial restoring moment will be very large. This can be looked further in to in the next phase but is most likely not an issue.

8.9   Accelerations from coupled analysis

8.9.1   Max/min response

8.9.2 Mean response

Bridge girder acceleration x

Bridge girder acceleration y

Bridge girder acceleration z
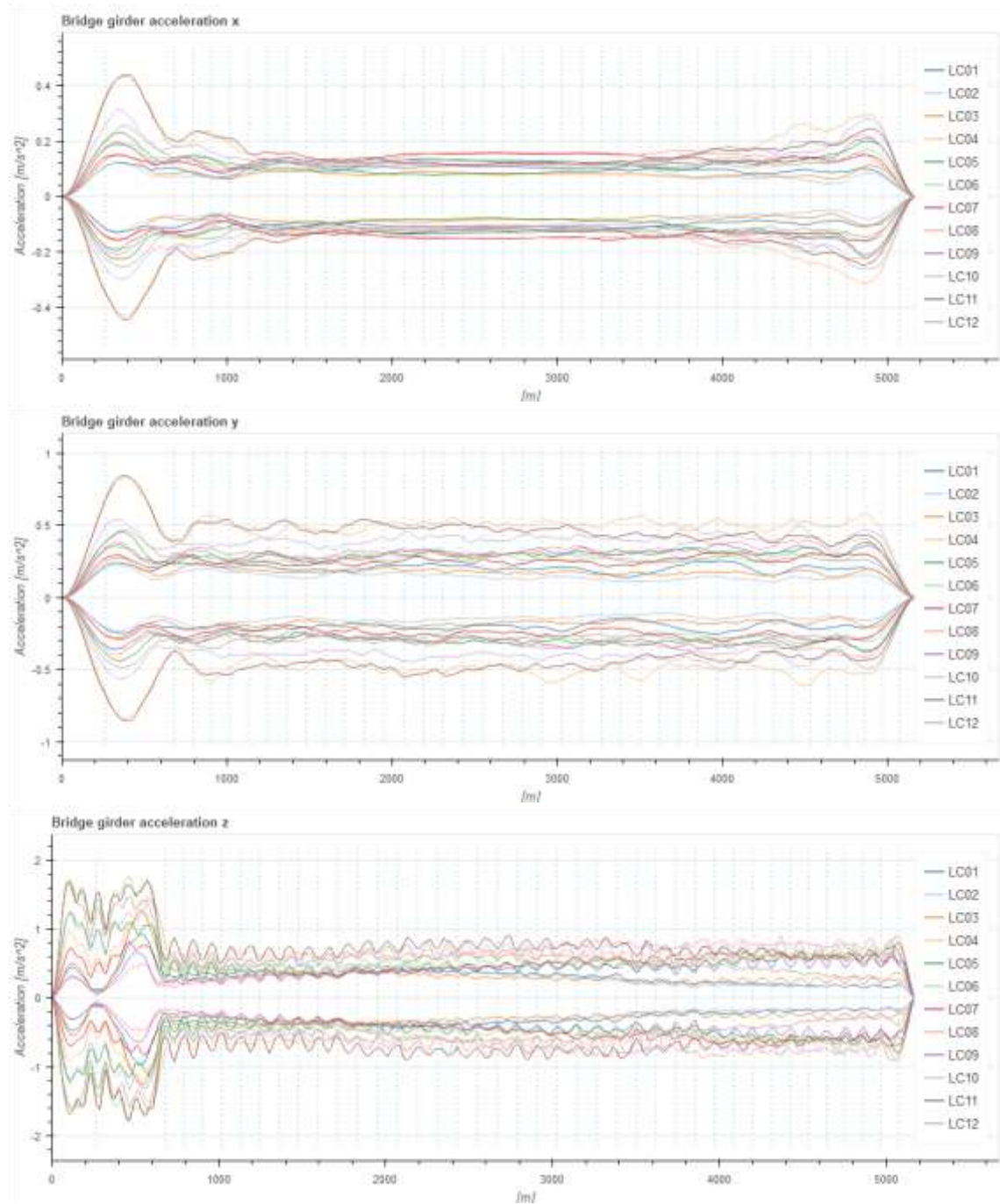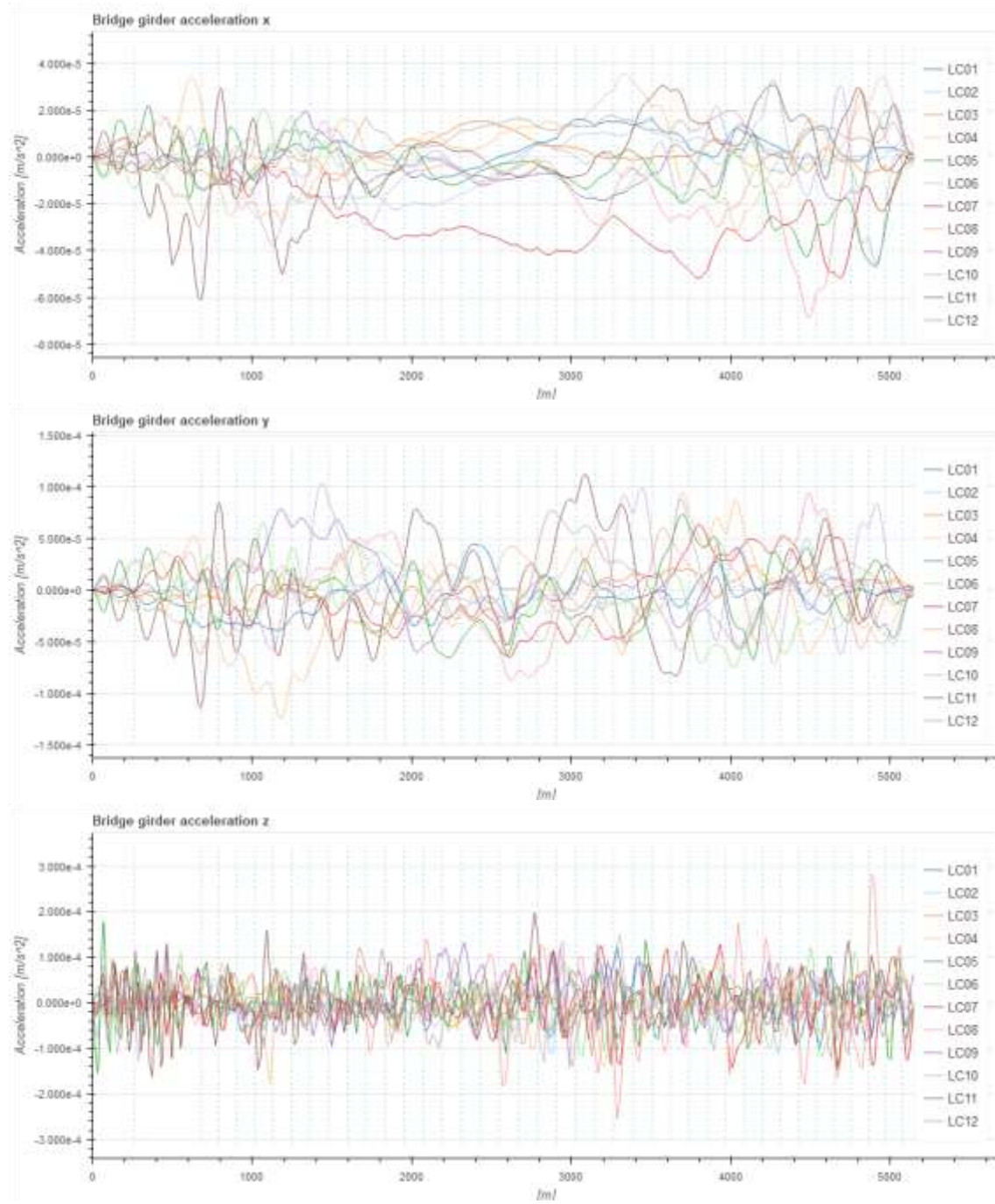
8.10   Displacements from coupled analysis

8.10.1   Max/min response
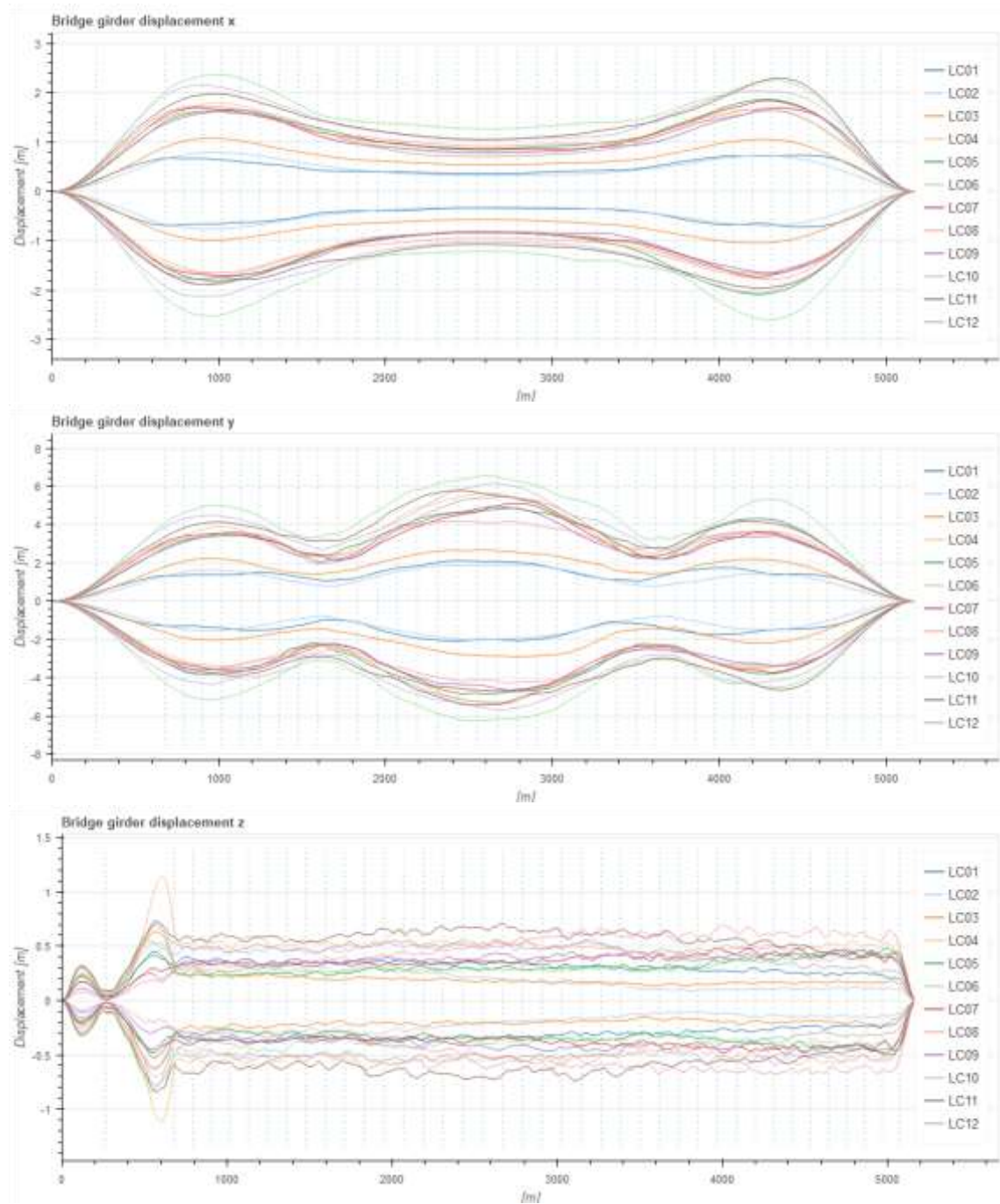
8.10.2 Mean response
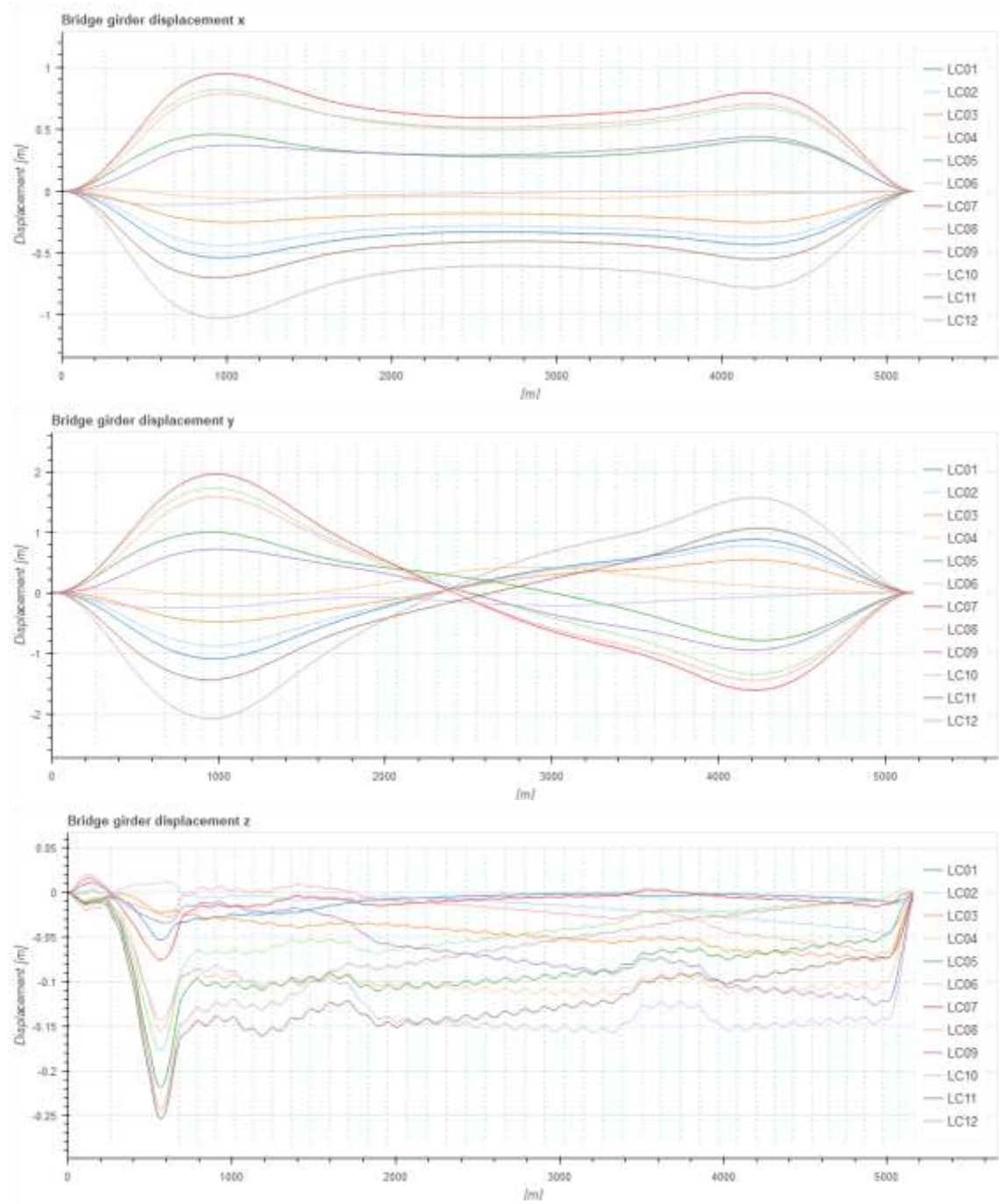
8.11   Forces from coupled analysis

8.11.1   Max/min response

8.11.2 Mean response

Bridge girder force x

Bridge girder force y

Bridge girder force z
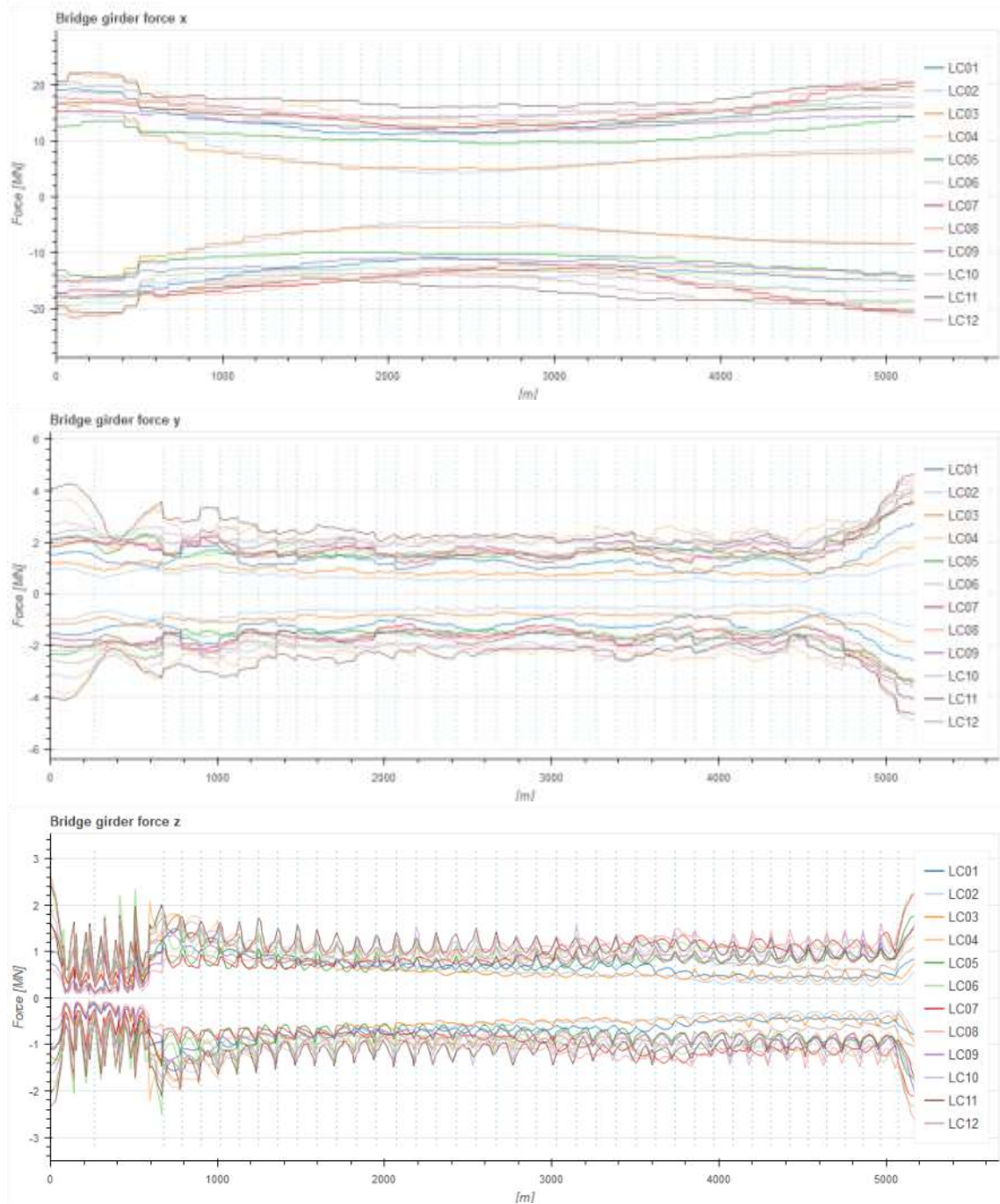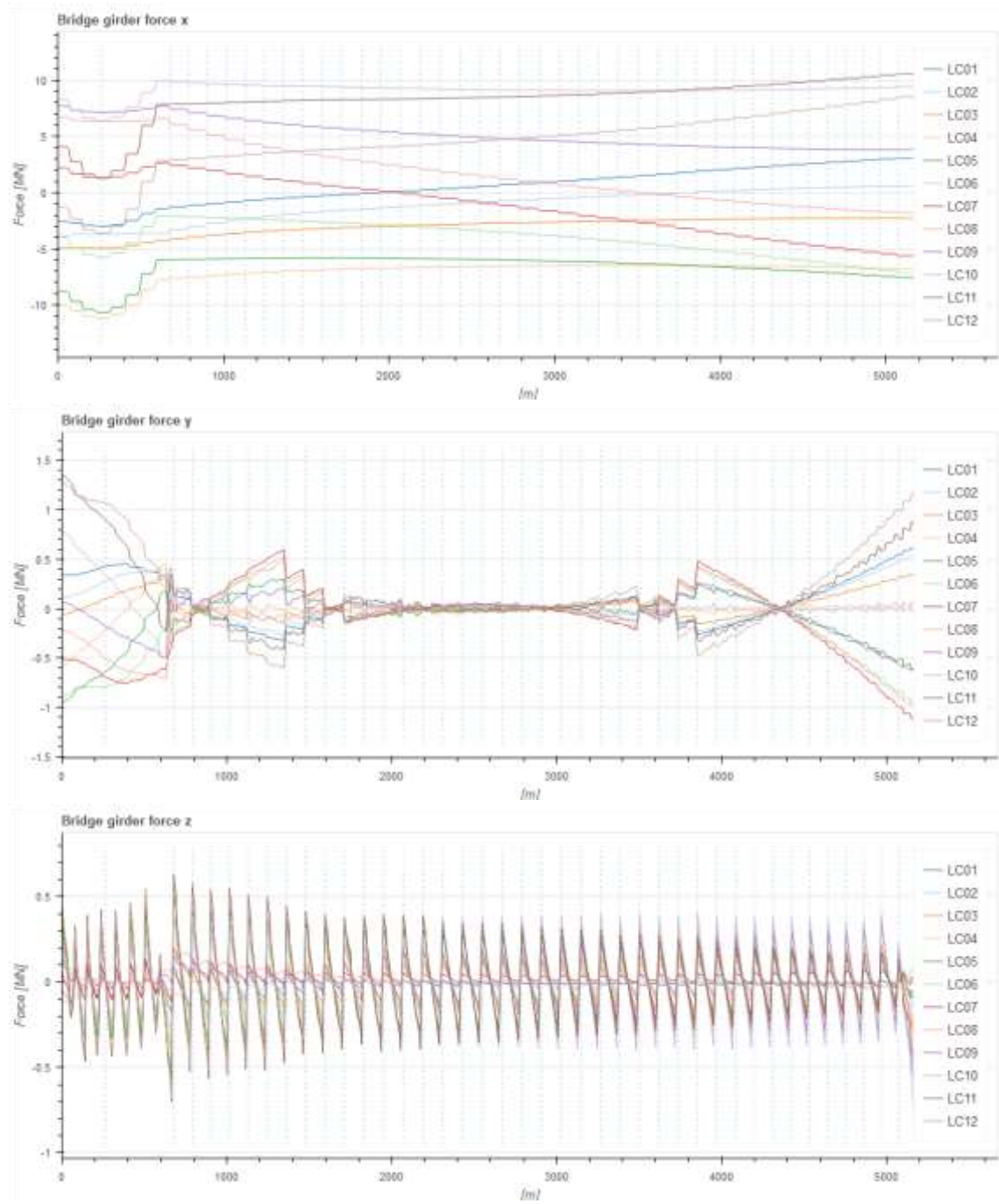
8.12 Moments from coupled analysis

8.12.1 Max/min response

Bridge girder moment x

Bridge girder moment y

Bridge girder moment z
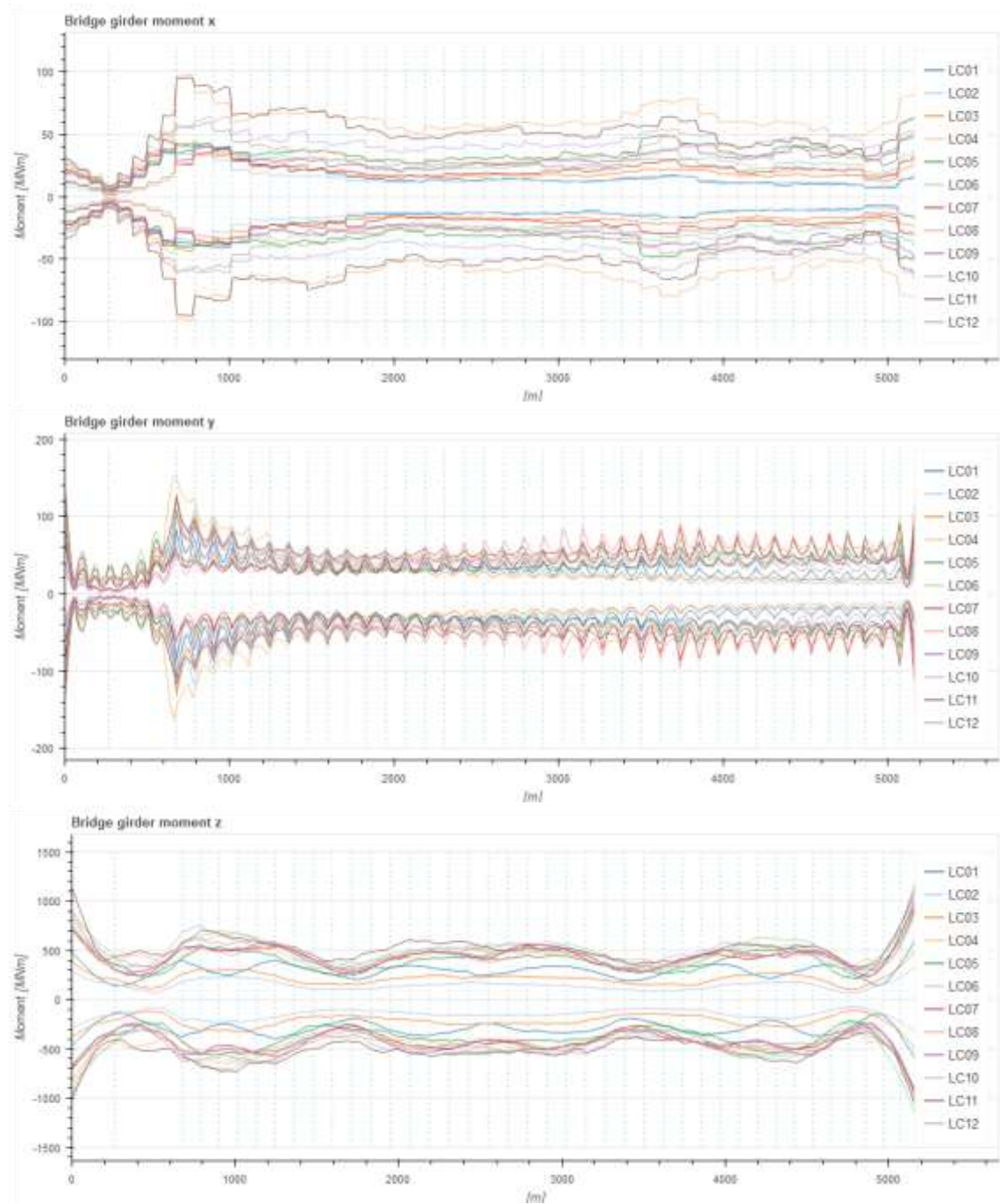
8.12.2 Mean response
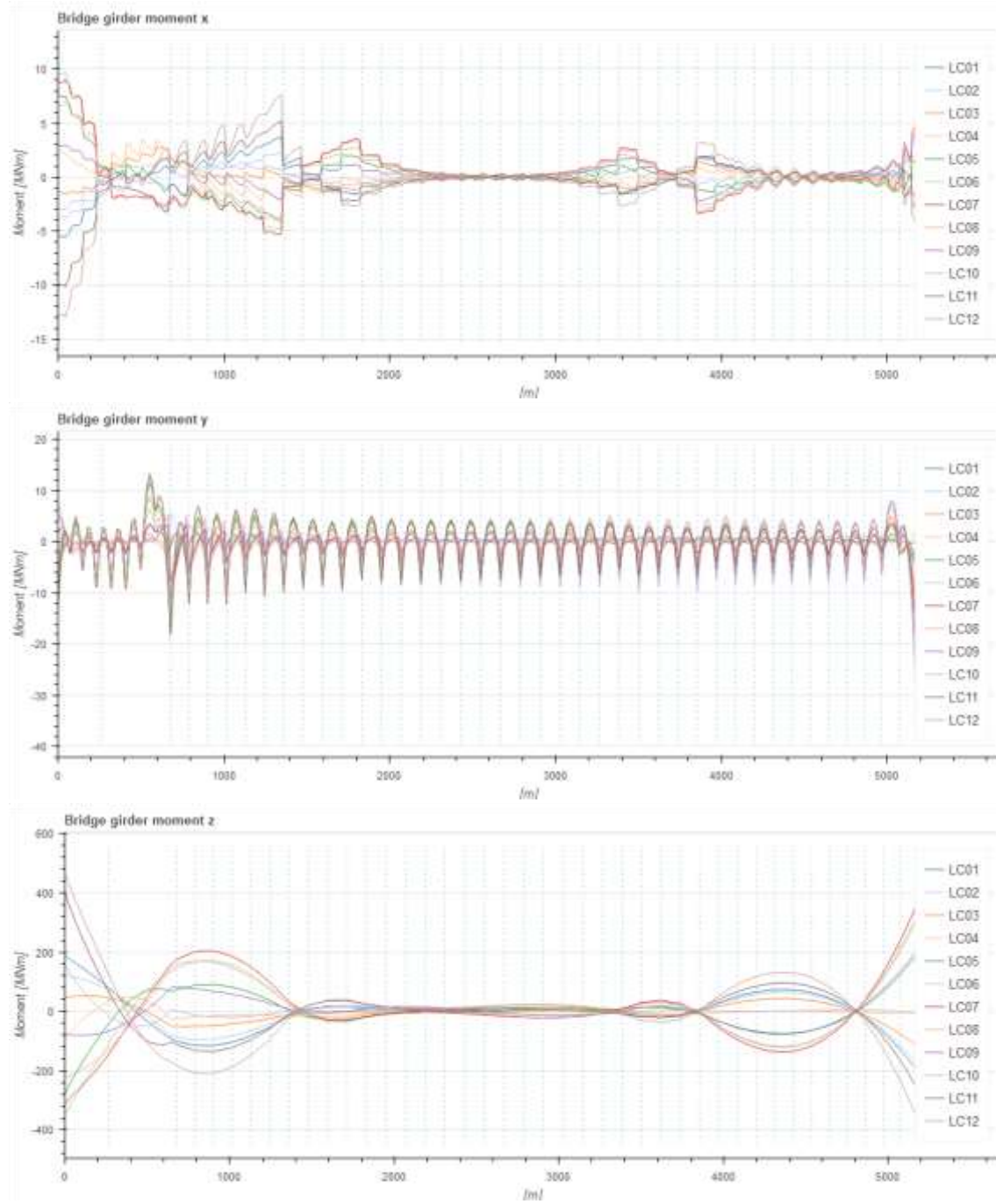
9 ALS RESPONSE

9.1 Extreme environmental response – RP=10000y

Global analyses for environmental conditions with a return period of 10000 years show that the response about weak axis and typical weak axis stress points (P3 and P5) supersedes the load factor of 1.6 (closer to 1.7) compared to the response from environmental conditions with a return period of 100 years. With regards to strong axis and typical strong axis stress points (P1 and P7) the response does not supersede the 1.6 factor (closer to 1.5).

For further details, see [4].

9.2 Loss of two anchor lines on same side of anchor group.

As one can see from Figure 9-1 and Figure 9-2 below, the loss of anchor has close to no impact on the environmental response, but makes some difference on the permanent load condition. However, the sum of the effects is small compared to the change in load factor between the two limit states. Thus, the anchor line loss situation is not governing with regards to the design of bridge girder.
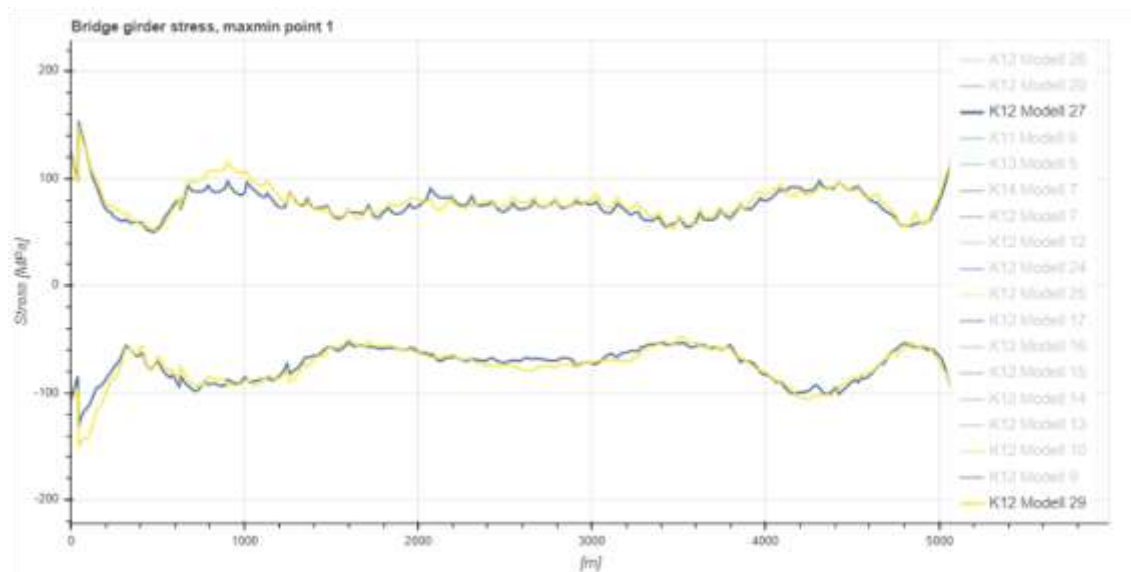
> *Figure 9-1 Comparison of stress response in point P1 – Anchor line loss (model 29) vs Anchor intact (model 27)- Environmental response*
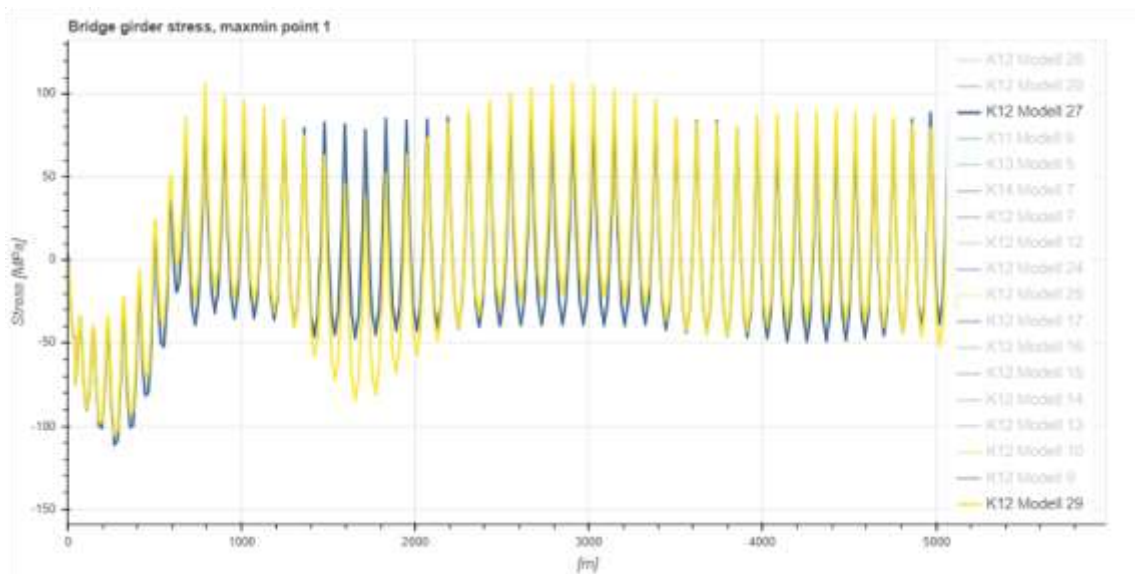
> *Figure 9-2 Comparison of stress response in point P1 – Anchor line loss (model 29) vs Anchor intact (model 27)- Environmental response*

The local effects with regards to this accidental state are handled in SBJ-33-C5-OON-22-RE-021-B- K12 - Design of mooring and anchoring [19].

9.3 Loss of stay-cable

The loss of a single stay-cable does not have a significant effect on the global bridge response during service after the loss, as long as the effect is treated right in the local design of the stay-cables. However, the transient effect right after the loss may give increased loads to the neighboring cables. This ALS situation is handled in SBJ-33-C5-OON-22-RE-019 Design of cable stayed bridge [17].

9.4 Ship impact

9.4.1 Screening of impact scenarios

There has been performed screening analysis of girder impacts to investigate the global behavior of the bridge. The screening analysis consists of 22 impacts on 11 locations. Impact from both west and east are considered. The chosen cases are assumed to be representative for all girder impacts, as they include critical points along the girder such as high bridge close to navigation channel, both anchor groups, center of span between anchor groups/abutments and critical points for the fixation of north end.

The response presented in this chapter is the response that is regarded as relevant for the global design:

- Bridge girder strong axis bending moment
- Maximum displacement of anchor point (K12-K14) – gives maximum elongation of anchor line
- Horizontal displacement of bridge girder at bridge tower, orthogonal to bridge girder.

Important assumptions for the screening analysis:

- Traffic loads are neglected, as the intended purpose was concept screening
- For screening analysis, there has only been considered impacts to the bridge girder, as this is the impact with most energy and will transfer the most energy to global girder motions.

The connector analysis gets the ship impact force from a mass-spring system that requires a force equilibrium between the ship and pontoon at each step. This is a quite fast analysis in pure calculation time, but it is time demanding to do the modelling in Abaqus CAE. This is the reason for doing the screening analysis with impulse loads, which is easier to mass produce by programming.
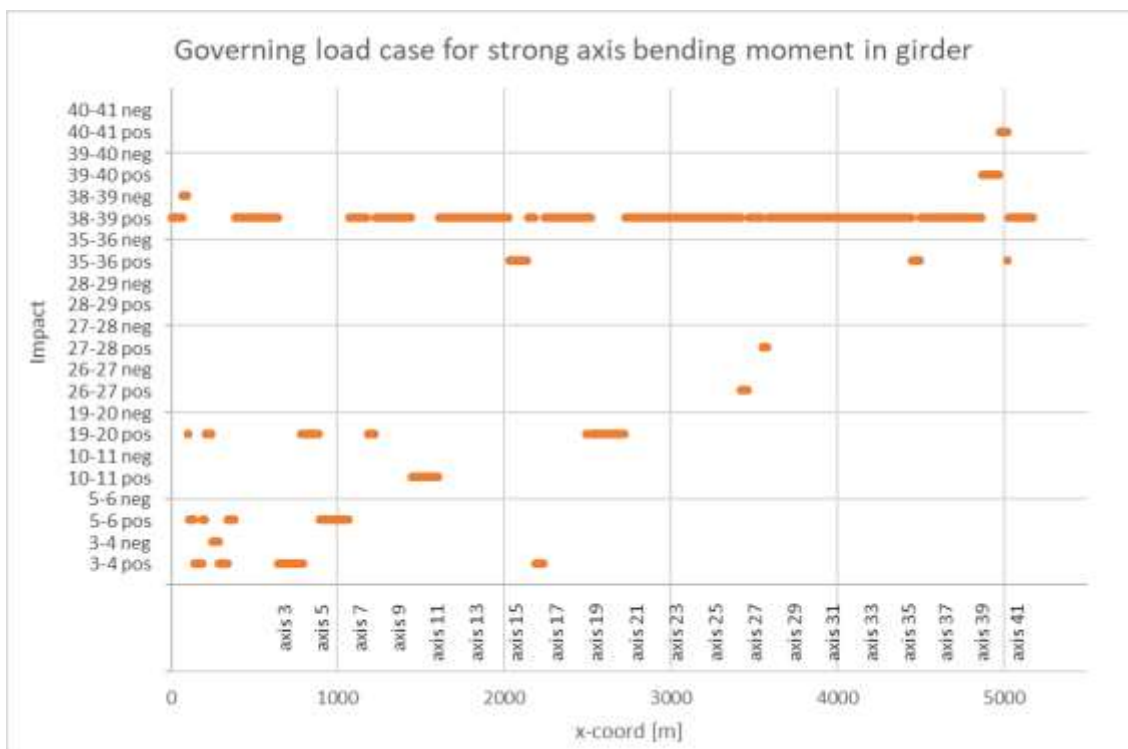
> *Figure 9-3 Governing impacts along girder for strong axis bending moment in girder, based on screening impulse analysis.*

Relevant input to design calculations from the screening analysis are the strong axis bending moments, the horizontal displacement of the girder at the land tower and the elongation of the anchor lines due to ship impact.

The highlighted results are shown in Table 9-1.

> *Table 9-1 Bridge girder responses from screening analysis*

Measure parameter	Maximum response
Strong axis bending moment in south end	3,74 GNm
Strong axis bending moment in "span", between abutments	2,95 GNm
Strong axis bending moment in north end	6,60 GNm
Maximum displacement anchor line and position anchor line	13,25 m – pontoon axis 30
Maximum horizontal displacement of girder at bridge tower, orthogonal to girder.	3,85 m – impact between axis 38-39

9.4.2 Local analysis of impact on pontoons and columns

Bow-pontoon collision is studied for a container bow and an ice-strengthened bow. The impact directions are either head-on the pontoon or 90-degree at the transition between straight and curved pontoon wall. Impact with the ice-strengthened bow is also performed 90 degree between bulkheads and frames too obtain a softer behavior. In the local collision analyses, the pontoon is fixed against movements at the boundary of the modelled pontoon.

The pontoon in axis 3 is the basis for all impact simulations documented, since this pontoon is subjected to the largest impact energy. The final pontoon width has become slightly larger (17 m) than the pontoon geometry utilized in this report (16 m), but this is considered to have negligible influence on the results.

Input from local collision response to global collision assessment are the force-displacement curves. The force-displacement curve gives the relationship between the contact force and the indentation between ship deckhouse and bridge girder. These curves are put into the global finite element model of the bridge structure by a non-linear connector element representing the ship and pontoon.

When global assessment has been conducted, several response parameters are revealed for further local damage evaluation. This includes as the most important the amount of energy that is dissipated locally and the indentation between bow and pontoon.

Bow-pontoon collision characteristics
In the local simulations performed, the pontoon dissipates most of the energy while the ship bow is less damaged. The distribution of energy dissipation between the pontoon and the ship bow is in the area 85/15 [%]. This means that the displacement of the connector element obtained from the global assessment can almost be transferred directly as the indentation in the pontoon.

Figure 9-4 shows the force-displacement curves for the different ship bows and directions investigated. Table 9-2 evaluates the maximum and mean contact force for the period up to 4 m ship displacement from these curves.

> *Table 9-2: Maximum and mean contact force [MN] impact bow-pontoon 0-4 m ship displacement*

Load case	Max. contact force [MN] 0-4 m	Mean contact force [MN] 0-4 m
Container, head-on	34	27
Container, 90-degree	27	21
Ice-strengthened, head-on	19	11
Ice-strengthened, 90-degree	22	13
Ice-strengthened, 90-degree between bulkheads/frames	23	7
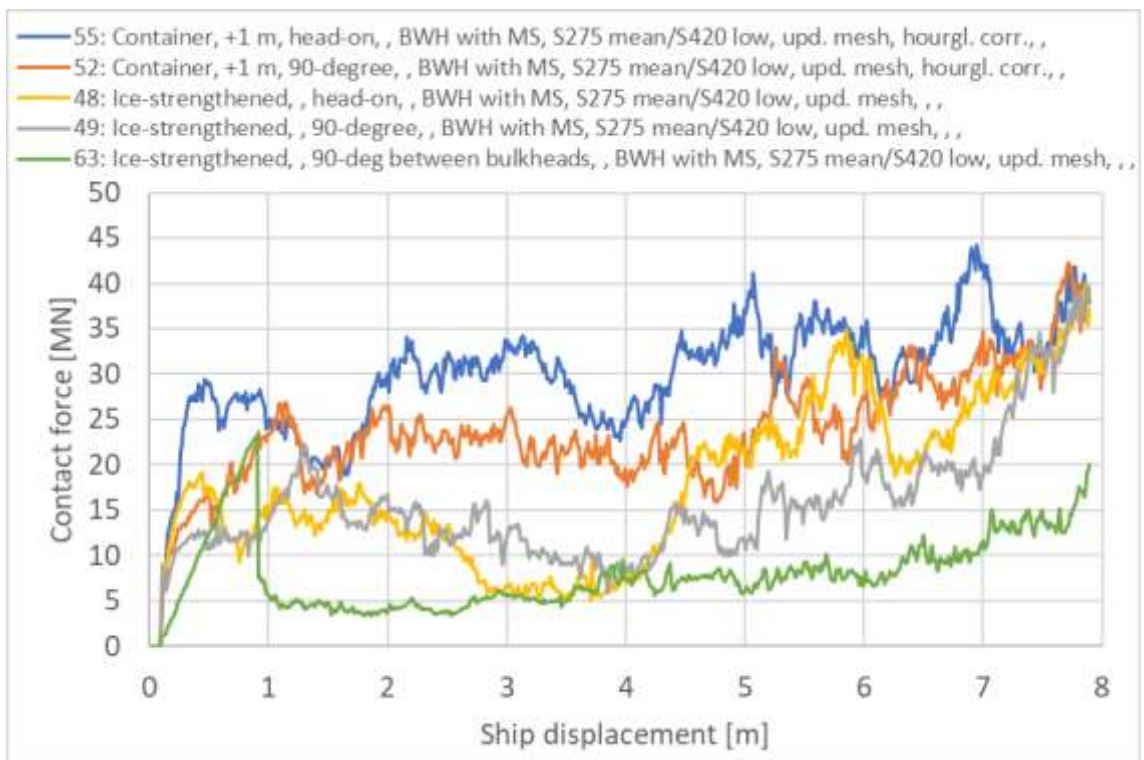
> *Figure 9-4: Contact force [MN] impact bow-pontoon*

Force reduction options
Different impact force reduction options have been tested. The damage of the pontoon is regardless severe for a slender design, which is preferred for other load cases and limit states. However, a reduced force level for pontoon collision is beneficial for the bridge girder and column.

The reduction of the force level is limited for the modifications investigated: 2 mm reduction to plate thickness, reduced stiffener height from 320 mm to 240 mm and 0.5 m corrugated bulkhead. The type of ship that hits the pontoon and the direction of the impact is of greater importance but cannot be controlled.

Sensitivity of ship impact response
The ship impact simulations performed are sensitive to several parameters. In addition to type of ship bow and direction and location of impact, sensitivity is studied for material parameters including superduplex steel, material damage models, mesh size, element type, impact height and ship velocity.

The simulation of bow-pontoon collision is sensitive to change in material parameters of the pontoon and less sensitive to change in material parameters of the ship bow. The reason is that the pontoon is more damaged in collision with the ship bow. However, only conventional types of ship bows have been studied. An inverted bow for example may reveal other impact characteristic.

9.4.3   Investigated impact scenarios

Bow collision with pontoon is handled in the local impact report, SBJ-33-C5-OON-22-RE-015-K12 - Ship impact, Pontoons and columns, [12]. The local analysis gives a force-indentation curve used for further evaluations and as input to the global analysis.

For ship-pontoon impact evaluations three pontoons have been chosen for detailed studies:
1) Axis 3 – large pontoon with the tallest column
2) Axis 12 – anchored pontoon (medium size) with quite large impact energy
3) Axis 20 – small pontoon at the center of the bridge

The three pontoons have been evaluated for three different impacts:
a) Head on impact – impact at pontoon end, orthogonal to bridge girder
b) 90-degree centric impact – impact at pontoon center, impact direction alongside bridge girder
c) 90-degree eccentric impact – impact eccentric on pontoon (at transition between straight long side and curved end), impact direction alongside bridge girder

9.4.4   Plastic hinge in column for 90-degree pontoon impact

The bridge design is sensitive to the strength of the column, especially the connection between the column and the girder. For the 90-degree pontoon impact on the high bridge, a shear force in the bottom of the column of 30-35 MN leads to bending moments in the column top of 13-1500 MNm. As the weak axis elastic capacity of the "normal" bridge girder is about 650 MNm, the 90-degree ship-impact will lead to local plastic deformations in the girder if the column is not made weaker. For the repair of the bridge, it is easier to change a column than replace a part of the girder. Therefore, the column needs to be designed weaker than the girder. This is solved by reinforcing the girder locally and to design the column to

withstand the given ship impact, but not more. In this way, the ship impact damage is limited to the column top in addition to the pontoon.

The 90-degree pontoon impacts lead to high section forces in the columns, both in bending and torsion. The tall columns are both highly utilized for bending and torsion, while the short columns are highly utilized for torsion. There has been performed FE-analysis of this detail to ensure a good design of this connection. These analyses are governing for the design of the column top and girder reinforcement above columns.

The tall columns need to be accurately designed: The column weak axis bending resistance must be lower than the girder weak axis bending resistance to make sure there is limited damage in the girder at the impact. At the same time, it must be strong and ductile enough to withstand the impact and the following post impact state. To make sure the girder behaves elastic, there is placed a voute on the top of the high bridge columns to avoid stress concentrations in the girder. This ensures a plastic hinge in the columns, below the voute.
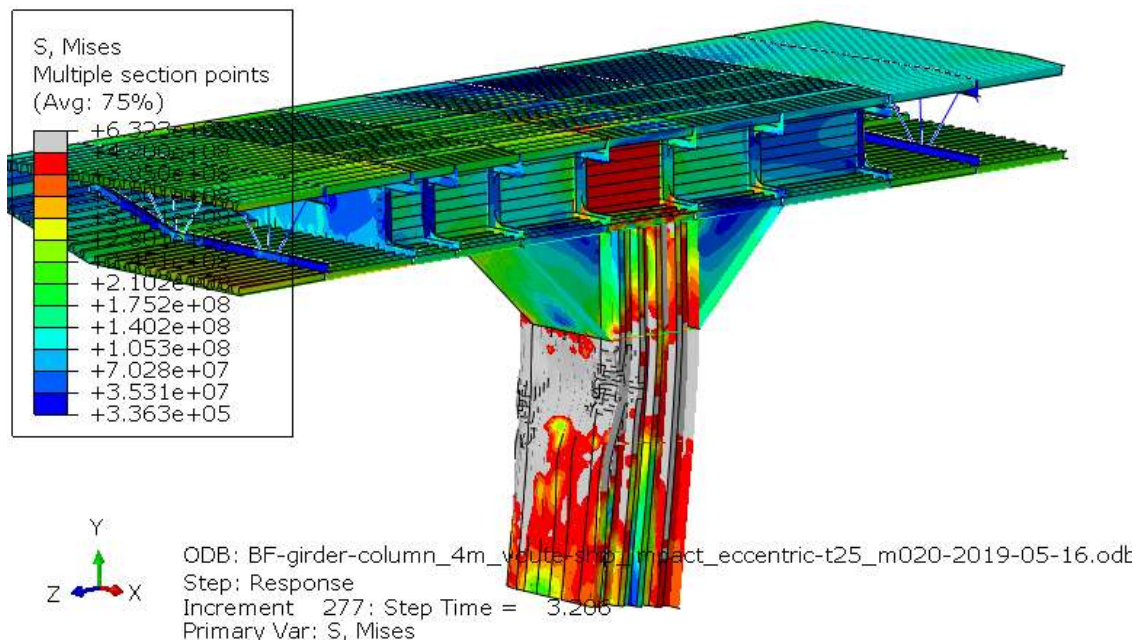
> *Figure 9-5 Plastic hinge in tall column (axis 3), local model. Local reinforcement of girder and a voute in the column top makes sure most plastic deformations takes place in the column. SeeAppendix F for details.*

For the low bridge columns, the situation is a bit different as the shorter column leads to a lower bending moment at the top of the column, and the bridge girder weak axis capacity is no longer governing for the design of the bending resistance of the column. As the column is stiffer both for weak axis bending and torsion, the damage will mainly happen between the ship and the pontoon, and the shear force and torsion in the short columns will be higher than for the high bridge long columns. Hence, the short columns need to be stronger than the high columns, especially for torsion moments.
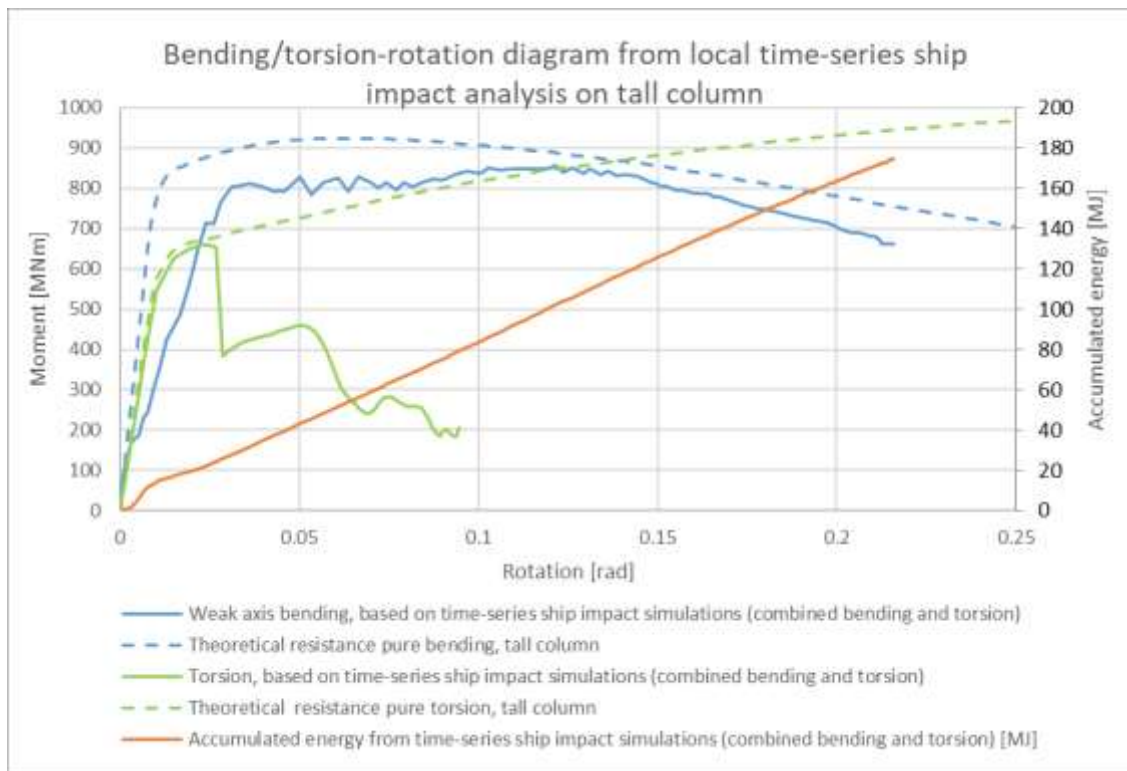
> *Figure 9-6 Bending/torsion-rotation diagrams from the column plastic hinge evaluations.*

9.4.5 Results from ship impacts on pontoons

Ship impacts on pontoons are governing for the column design, especially the tall columns. They are also governing for the design of the girder stiffeners and bulkheads above columns.

The ship impact characteristics are given by the design basis. The loads are presented in Table 9-3.

> *Table 9-3 Ship impact characteristics pontoon impacts axis 3, 12 and 20.*

| Impact characterstic	Axis 3	Axis 12	Axis 20
Ship mass (incl. 5 % added mass) [tonne]	15 293	13 922	13 922
Ship initial velocity [m/s]	5,7	5,5	5,5
Ship initial kinetic energy [MJ]	248	228	228

The main results from the ship-pontoon impacts are presented in Table 9-4. The three force-displacement curves from local analyses are used as input. This means the same force-indentation curve is used for both 0-deg and 90-deg ice bow impacts, which probably underestimates the contact force (and overestimates the indentation) in the 0-deg ice bow impact.

> *Table 9-4 Main results from impacts on pontoons axis 3, 12 and 20.*

Parameter	Impact ship and direction	Pontoon axis 3	Pontoon axis 12	Pontoon axis 20
Maximum indentation between ship and pontoon [m]	0-deg, container	2,0	2,5	2,3
	0-deg, ice bow	8,0	9,5	9,0
	90-deg centric, container	3,5	-	8,0
	90-deg centric, ice bow	8,5	-	13
	90-deg eccentric, container	2,8	7,0	7,5
Maximum force between ship and pontoon [MN]	0-deg, container	32	33	33
	0-deg, ice bow	21	30	30
	90-deg centric, container	25	-	40
	90-deg centric, ice bow	28	-	33
	90-deg eccentric, container	25	33	40
Plastic dissipation (energy) between ship and pontoon [MJ]	0-deg, container	50	65	60
	0-deg, ice bow	70	95	85
	90-deg centric, container	70	-	185
	90-deg centric, ice bow	90	-	200
	90-deg eccentric, container	55	170	180
Plastic dissipation (energy) in column top plastic hinge [MJ]	0-deg, container	-	-	-
	0-deg, ice bow	-	-	-
	90-deg centric, container	170	-	-
	90-deg centric, ice bow	150	-	-
	90-deg eccentric, container	185	10	-
Maximum elongation of anchor line [m]	0-deg, container	11	8	7
	0-deg, ice bow	11	7,5	6,5

Noticeable results from the ship pontoon impacts are listed below:
- In the centric 90-degree impact on axis 3 with the tall column, 240 of 248 MJ, or 97 % of the initial kinetic energy is dissipated locally in the pontoon and column. Most in the column – which means this is a very critical detail for the bridge design. The plastic displacement of the pontoon center due to weak axis rotation in the column top is 10 m. This gives an extra second order moment from the buoyancy load in the post-impact state.
- Maximum indentation between ship and pontoon is 8,5 m or more on all three pontoon types, which means that water ingress in (maximum) 4 pontoon compartments must be expected for all pontoon types.
- The maximum elongation of anchor line is as expected (due to less energy) less than for the girder impact.
- The maximum indentation is a 90-degree centric impact on the small pontoon in axis 20. The total indentation is 13 m, which means the bulb could penetrate all the way through the pontoon which has a width of 12 m. See force-indentation curve in Figure 9-7 and damage in ship and pontoon on Figure 9-8.
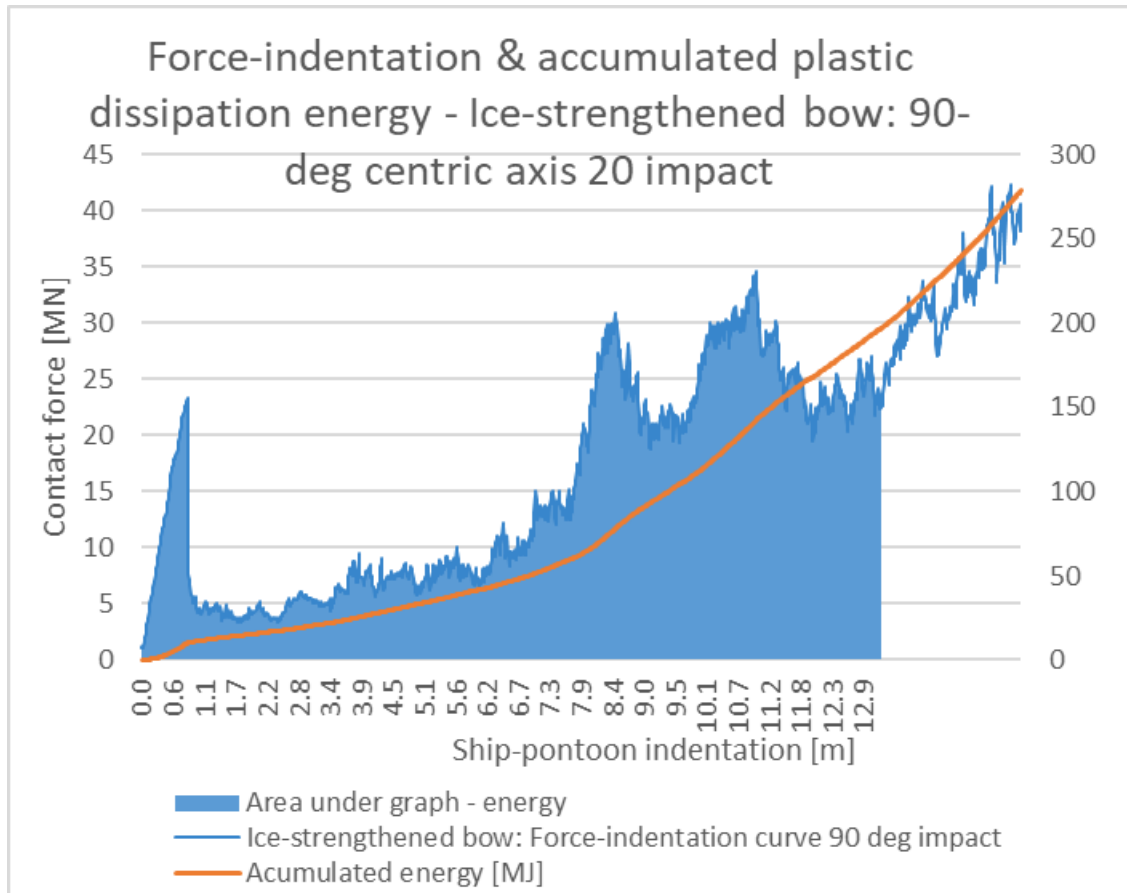
Figure 9-7 Force-indentation curve for pontoon impact with ice strengthened bulb. Total indentation is 13 m and the dissipated plastic energy is 200 MJ.
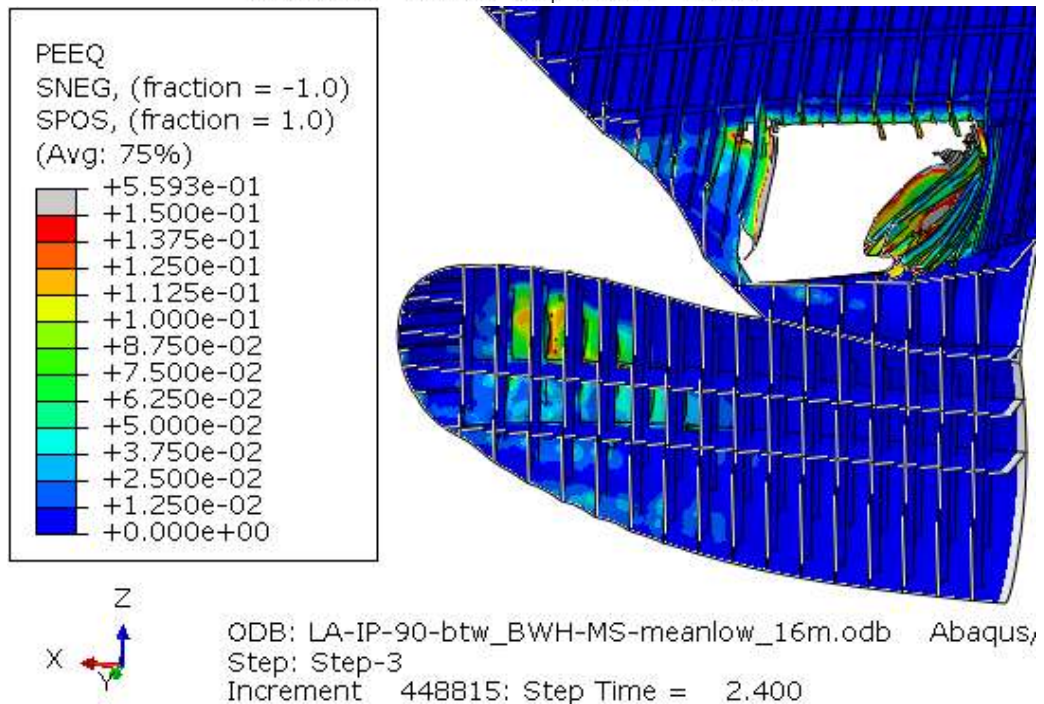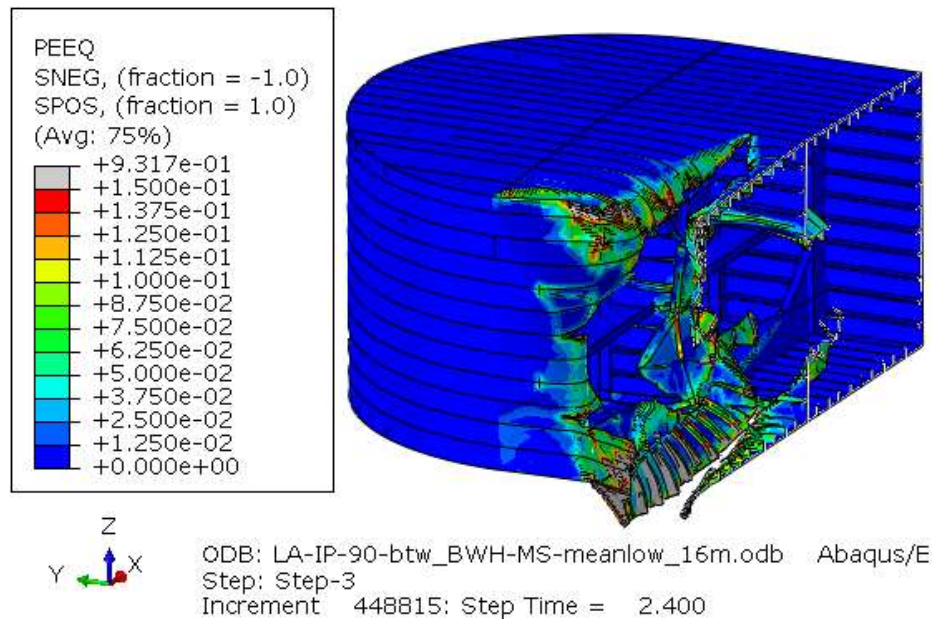
> *Figure 9-8 Damaged ship and pontoon at 13 m indentation between ship and pontoon. Taken from local analysis as described in local analysis report [12]. This pontoon is 16 m wide, while the axis 20 pontoon with the 13 m indentation is 12 m wide. This impact could penetrate the entire pontoon.*

9.4.6   Ship impact on bridge girder

Deckhouse-girder collision is studied for the girder at three impact heights on the deckhouse: At deck 2, inclined at deck 4 and between deck 2 and 3. In the local collision

analyses, the bridge girder is fixed against movements at the boundaries of the modelled girder.

When global assessment has been conducted, several response parameters are revealed for further local damage evaluation. This includes as the most important the amount of energy that is dissipated locally and the indentation between ship deckhouse and bridge girder. All girder impacts have been placed midspan between the axis. This is the total indentation of the impact in meters, and the amount of energy transferred to local damage as plastic dissipation in the connector between girder and ship. The total amount of energy in the girder impact is 385 MJ. The remaining energy is mainly transferred into elastic strain and kinetic energy in the bridge. For evaluation of the damage and distribution of indentation and energy between the deckhouse and girder, see report on Ship impact, Bridge girder [13].

> *Table 9-5 Maximum indentation between deckhouse and girder along bridge*

Impact between axis	Description	Indentation [m]	Plastic dissipation energy [MJ]
5-6	Ramp, near cable bridge	5,9	178
10-11	Center of first anchor group	5,6	157
19-20	Center of bridge	5,3	160
26-27	Right outside second anchor group	5,4	164
39-40	Towards north, gives large bending moment in northern abutment	8,0	241
41-north end	Close to abutment north, stiffest impact	12,9	383

Deckhouse-girder collision characteristics
In the local simulations performed, the deckhouse dissipates most of the energy while the girder is less damaged. The distribution of energy dissipation between the deckhouse and the girder is in the area 85/15 [%]. This distribution causes the compression of the bridge girder to stabilize at approximately 0.8 m. The displacement of the connector element obtained from the global assessment is therefore close to the indentation in the deckhouse alone.

Figure 9-9 shows the force-displacement curves for the different locations investigated. Table 9-6 evaluates the maximum and mean contact force for the period up to 8 m ship displacement from these curves.

> *Table 9-6: Maximum and mean contact force [MN] impact deckhouse-girder 0-8 m ship displacement*

Location	Max. contact force [MN] 0-8 m	Mean contact force [MN] 0-8 m
At deck 2	44	30
Inclined at deck 4	38	27
Between deck 2 and 3	35	20
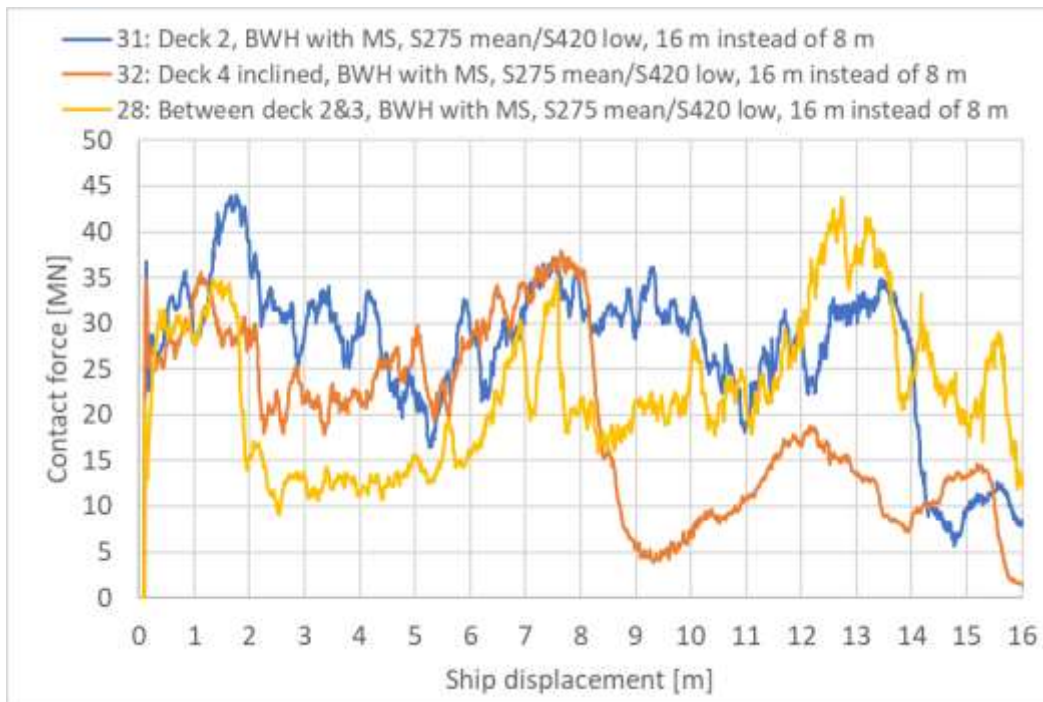
> *Figure 9-9: Contact force [MN] impact deckhouse-girder*

Figure 9-10 show the deckhouse and bridge girder damage for load case A, bridge girder at deck 2, at 8 m ship displacement. The deckhouse is subjected to severe damage for all impact locations, while damage to the bridge girder is limited. Deformations are not scaled.
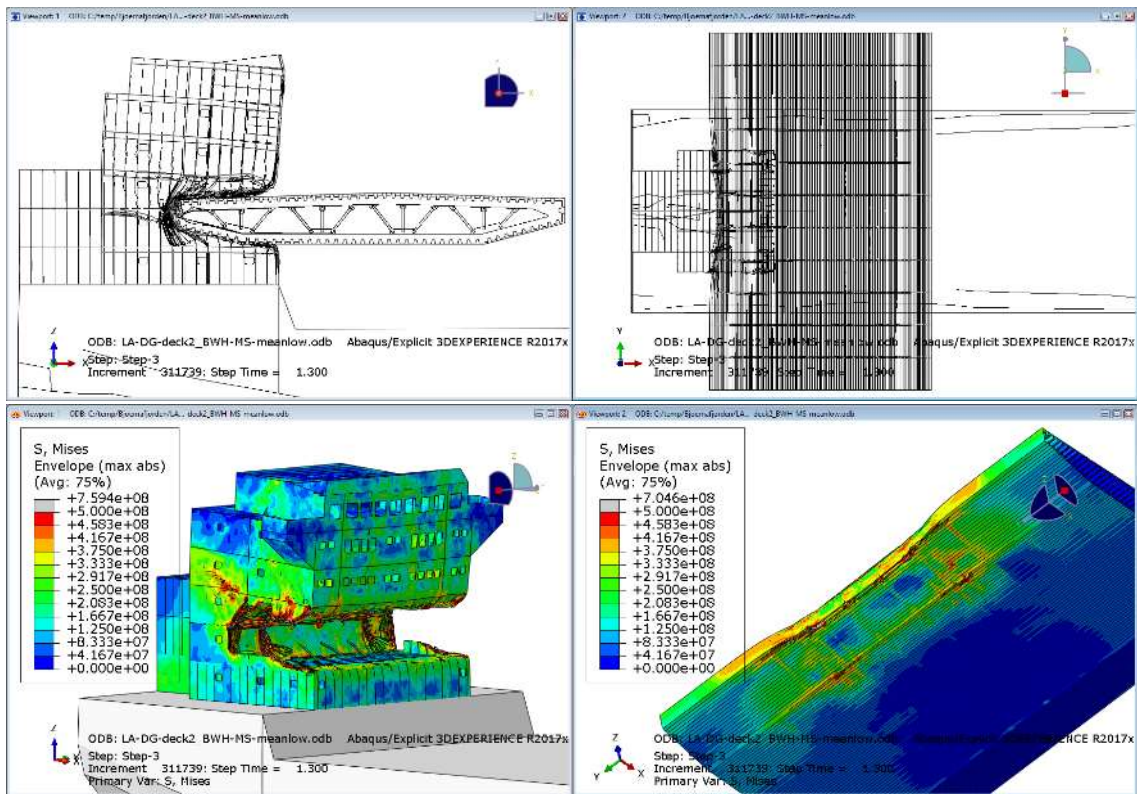
> *Figure 9-10 von Mises stress [MPa] load case A: Bridge girder at deck 2*

Sensitivity of ship impact response
The ship impact simulations performed are sensitive to several parameters. In addition to location of impact, sensitivity is studied for material parameters, material damage models, element type, mass scaling and reinforced bridge girder.

The simulation of deckhouse-girder collision is less sensitive to change in material parameters of the bridge girder and sensitive to change in material parameters of the deckhouse. The reason is because the deckhouse is the weaker structure in collision with the bridge girder.

Residual capacity of bridge girder
Residual capacity of the bridge girder is evaluated with push-over analyses of the intact and damaged bridge girder with either pure moment about strong axis or pure moment about weak axis. Stresses and deformations from the ship impact analysis are preserved for the residual evaluation. The residual capacities shown in Table 9-7 is the apex of the resulting load-rotation curves. A simple evaluation of the section forces shows that the damaged bridge girder has enough capacity for the 100-year environmental loading.
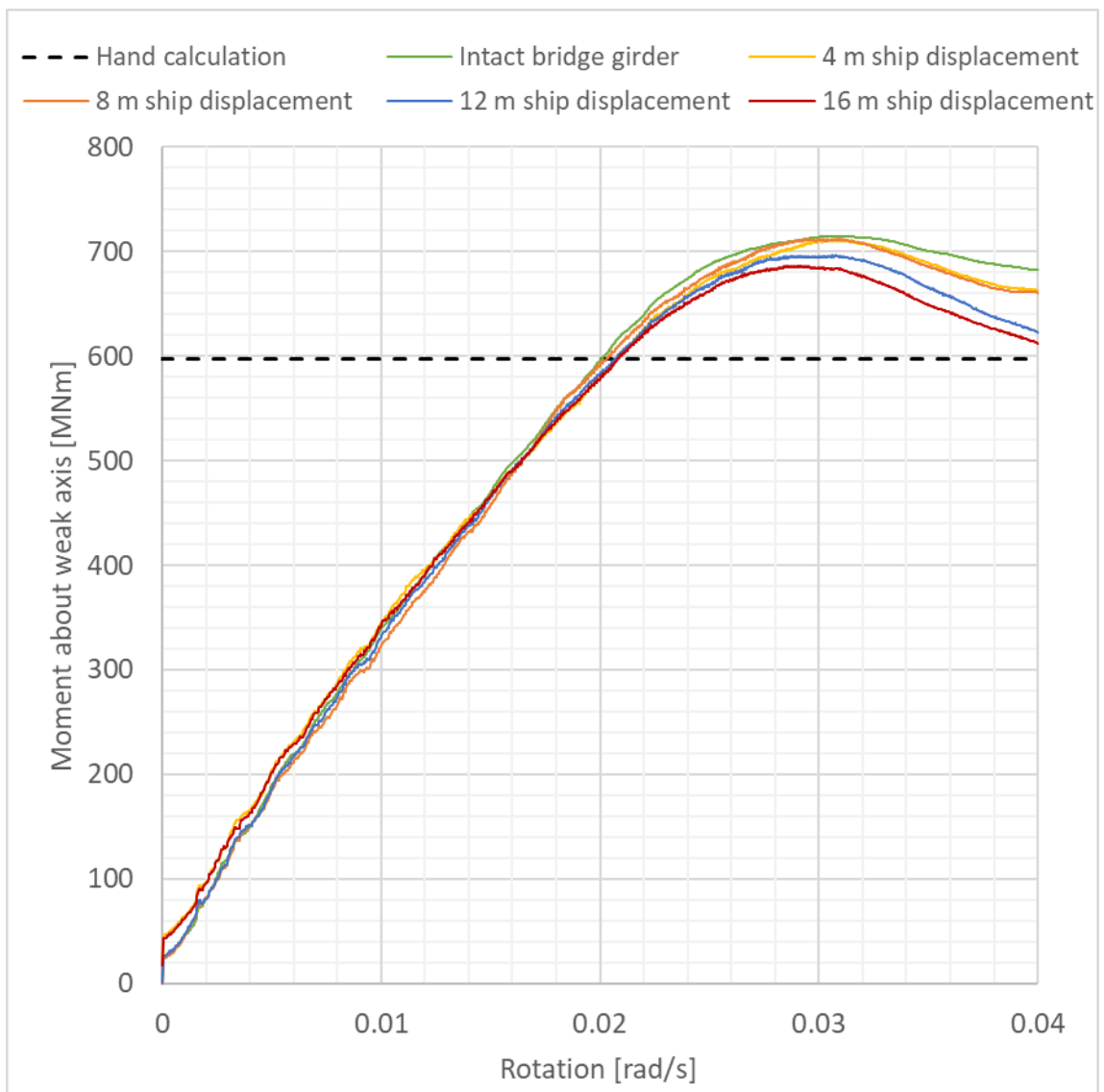
> *Figure 9-11 Load-rotation curve for moment about weak axis*

> *Table 9-7: Residual capacity of bridge girder after ship impact*

	Moment about strong axis	Moment about weak axis
Intact bridge girder	100 %	100 %
4 m ship displacement	92.3 %	99.6 %
8 m ship displacement	88.2 %	99.6 %
12 m ship displacement	87.4 %	97.4 %
16 m ship displacement	84.7 %	96.0 %

9.4.7 Post impact capacity

According to design basis the bridge must withstand a 100-years storm post impact in an accidental limit state. Post impact capacity has been evaluated and found acceptable for five main types of ship impact damage:

1) Local damage in bridge girder
2) Local damage in pontoon, leading to water filling of pontoon compartments
3) Local damage in tall columns due to pontoon impact
4) Local damage of column due to direct hit from a ship bow
5) Loss of anchor lines

See ship impact reports for details [11] [12] [13].

10 FATIGUE DESIGN LIFE

This chapter provides a summary of FLS calculations and results. Details on method and results can be found in fatigue assessment report [14]

10.1 Overview of design parameters

> *Table 10-1: Overview of fatigue design parameters trapezoidal stiffeners and outer skin*

Point	Detail type	Detail category**	DFF	Girder section	Plate thickness	SCF
A C I	Trapez. stiffener top	F	2,5	BCS1	8 mm	1,0*
D E F G H	Trapez. stiffener bottom	F	2,5	BCS1	8 mm	1,0*
A C I	Trapez. stiffener top	F	2,5	BCS2	12 mm	1,0*
D E F G H	Trapez. stiffener bottom	F	2,5	BCS2	12 mm	1,0*
A C D E F G H I	Trapez. stiffener top and bottom	F	2,5	P1-P5, HF6 (north and south end)	Varying	1,0*
B	Modified trapez. Stiffener top	F	2,5	All	Varying	1,0*
A C I	Top deck plate	D	2,5	BCS1	14 mm	1,13
D E F G H	Bottom plate	D	2,5	BCS1	12 mm	1,2
A C I	Top deck plate	D	2,5	BCS2	14 mm	1,13
D E F G H	Bottom plate	D	2,5	BCS2	12 mm	1,2
A C D E F G H I	Outer plates top/bottom	D	2,5	P1-P5, HF6 (north and south end)	Varying	1,5
Column A	Trapez. stiffener	F	2,5	Column		1,5
Column C	Trapez. stiffener	F	2,5	Column		1,5
Column A	Outer plates	D	2,5	Column		2,0
Column C	Outer plates	D	2,5	Column		2,0

* *detail category chosen from Eurocode* [37] *includes SCF for stiffener welds within normal tolerance levels.*
** S-N curves in air is used for all considered points.

10.2 Unit load analyses

Stresses for points shown in Figure 3-9 are calculated according to chapter 3.
Figure 10-1 show stresses from unit moment about weak axis. There is observed small variations in the stresses due to the stiffeners. Stresses are extrapolated from each point A-I by extracting S11 stresses (parallel to bridge length) from a set of elements in each point. This is in turn used to calculate stresses for other cross sections used. Stress transfer factors for cross-section 1 (BCS1), including SCFs from analysis model, are shown in Table 10-2, and the rest of the cross-sections are shown in the fatigue assessment report [14].
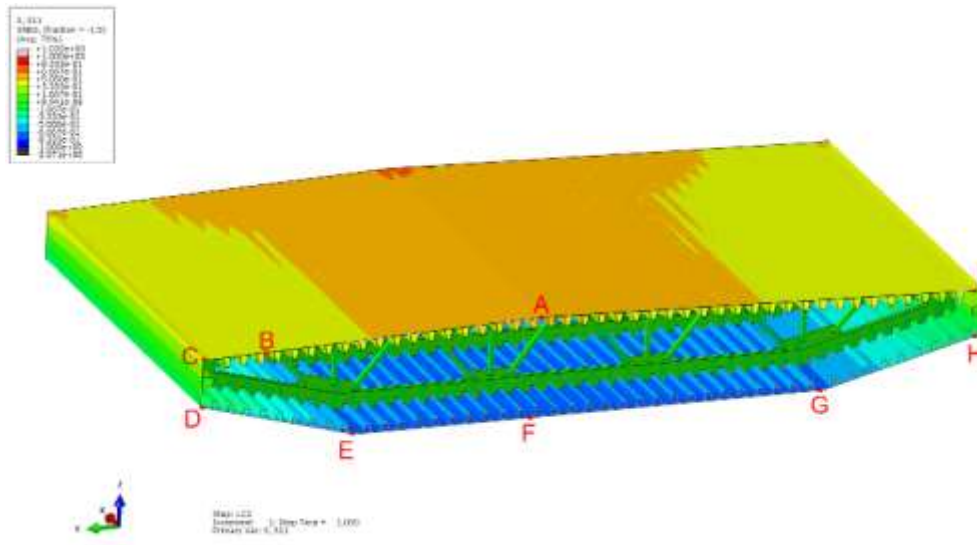
> Figure 10-1: S11 stresses (along bridge length) from unit moment about weak axis (1 Nm)

> Table 10-2: Stress transfer factors for cross-section BCS1

Point	Unit(Nxx) [MPa/N]	Unit(Myy) [MPa/Nm]	Unit(Mzz) [MPa/Nm]
A	0,680	-0,586	0,014
B	0,680	-0,480	0,083
C	0,680	-0,438	0,123
D	0,680	0,196	0,126
E	0,680	0,704	0,077
F	0,680	0,722	0,02
G	0,680	0,704	-0,074
H	0,680	0,172	-0,125
I	0,680	-0,402	-0,126

10.3 Fatigue calculations from local traffic

See Table 10-3 below for max. stress ranges as well as calculated corresponding damage for rest of stress ranges. This is for the point with the largest stress variations where stiffeners are welded together, hotspot 3, as shown on Figure 10-2.
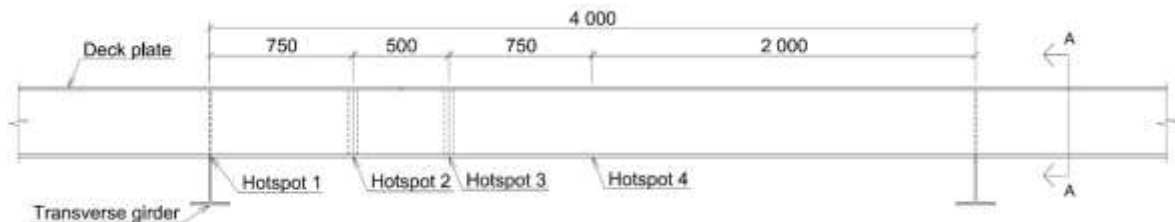
> *Figure 10-2: Considered areas for local traffic load*

Furthermore, the partial damage from the rest of the stress ranges is calculated as:
Partial damage = (Sum yearly damage all lorries all stress ranges) - (Sum yearly damage max stress ranges)
This partial damage is added to the damage calculated from the combination formula as an initial damage.
The data in the table is valid for the welded box stiffener shown in Figure 10-3.
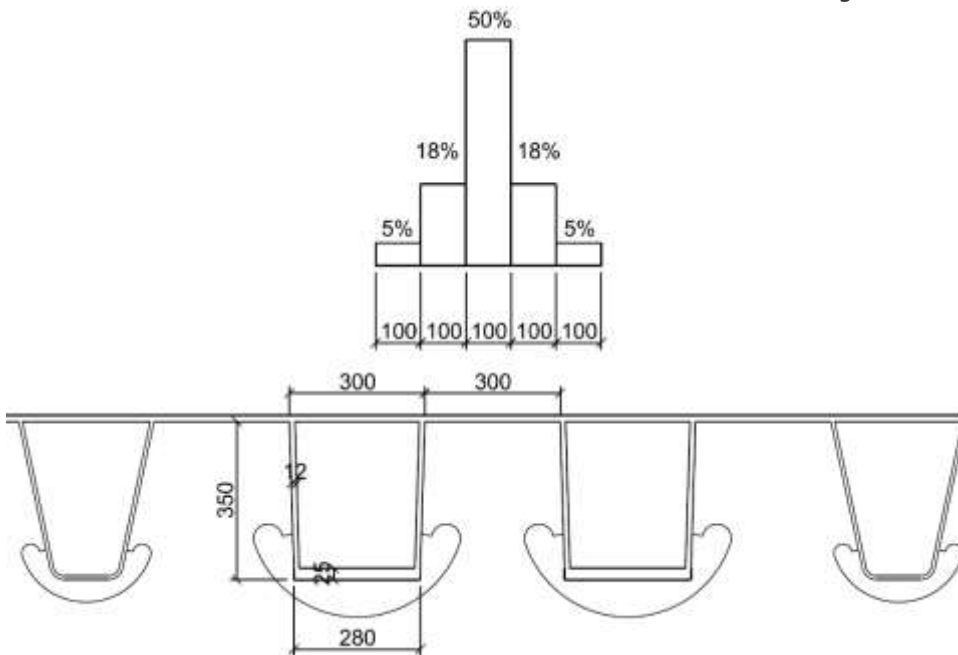
> *Figure 10-3: Principle sketch of welded box stiffener geometry* to be used under each wheel lane (2 per wheel) under both slow lanes, with traffic distribution shown.*

*The cope holes shown have not been detailed accordingly at this stage.

> *Table 10-3: Input to combination formula for the chosen welded box stiffener*

Lorry #	Max. stress range (MPa)	Cycles /year	Corresponding yearly damage

Lorry 1	7,659	50000	0,000001069
Lorry 2	10,472	12500	0,000001277
Lorry 3	11,079	125000	0,000016920
Lorry 4	9,781	37500	0,000002722
Lorry 5	7,144	25000	0,000000377
	Sum yearly damage max stress ranges		0,000022365
	Fatigue life (years) local traffic only		10150 yrs
	Sum yearly damage all lorries all stress ranges		0,00003941
	Partial damage from rest of stress ranges		0,000017043

Fatigue life for the stiffener, point B, is shown in Figure 10-5.

10.4   Global analyses bridge girder

10.4.1   Bridge girder outer skin

Calculated outer skin fatigue life at point A-F from the combination formula in DNVGL Fatigue Design Methodology [38] Comment: Fatigue life is greater than 100 years all over the bridge. In the lower part, fatigue damage is generally governing in the field, except for at the area closest to the stay cable bridge where bending moments from the tallest columns yield greater fatigue damage than in the field.
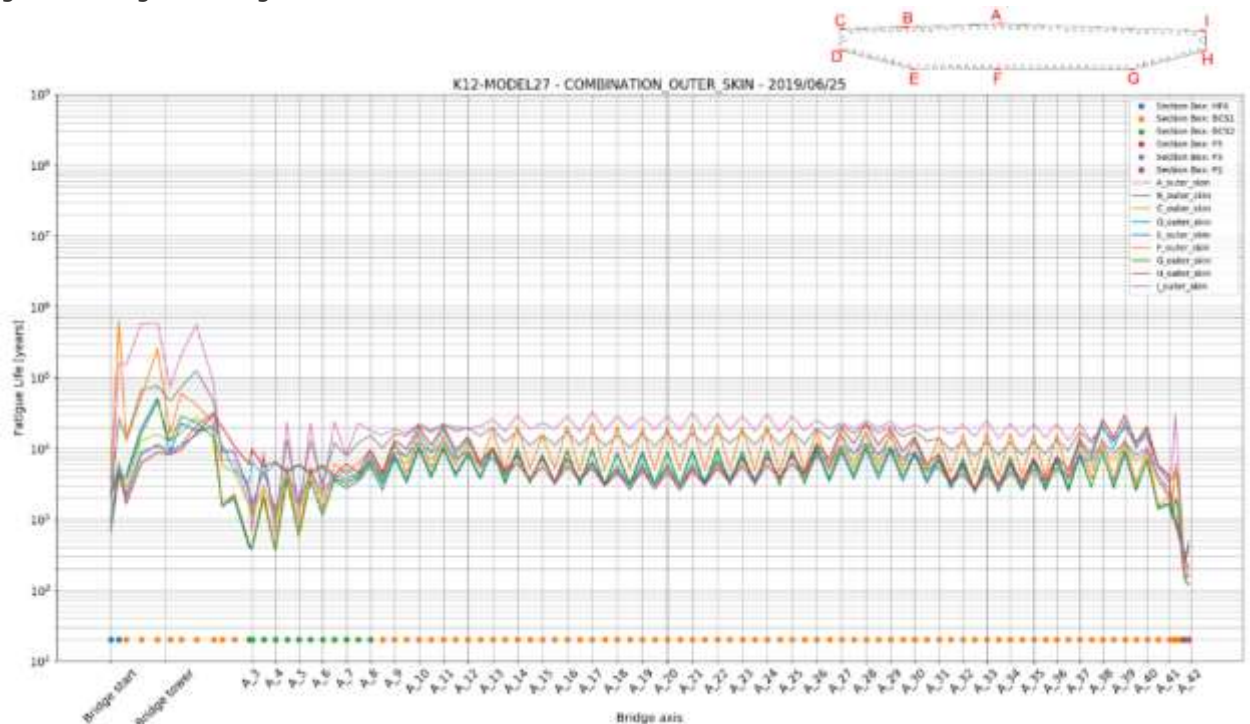
> *Figure 10-4: Outer skin fatigue life plot by use of the combination formula*

10.4.2   Bridge girder trapezoidal stiffener – combination formula local and global loads

Calculated stiffener fatigue life at point A-F from the combination formula.

Comment: Fatigue life is greater than 100 years all over the bridge including point B, where local traffic damage is included.
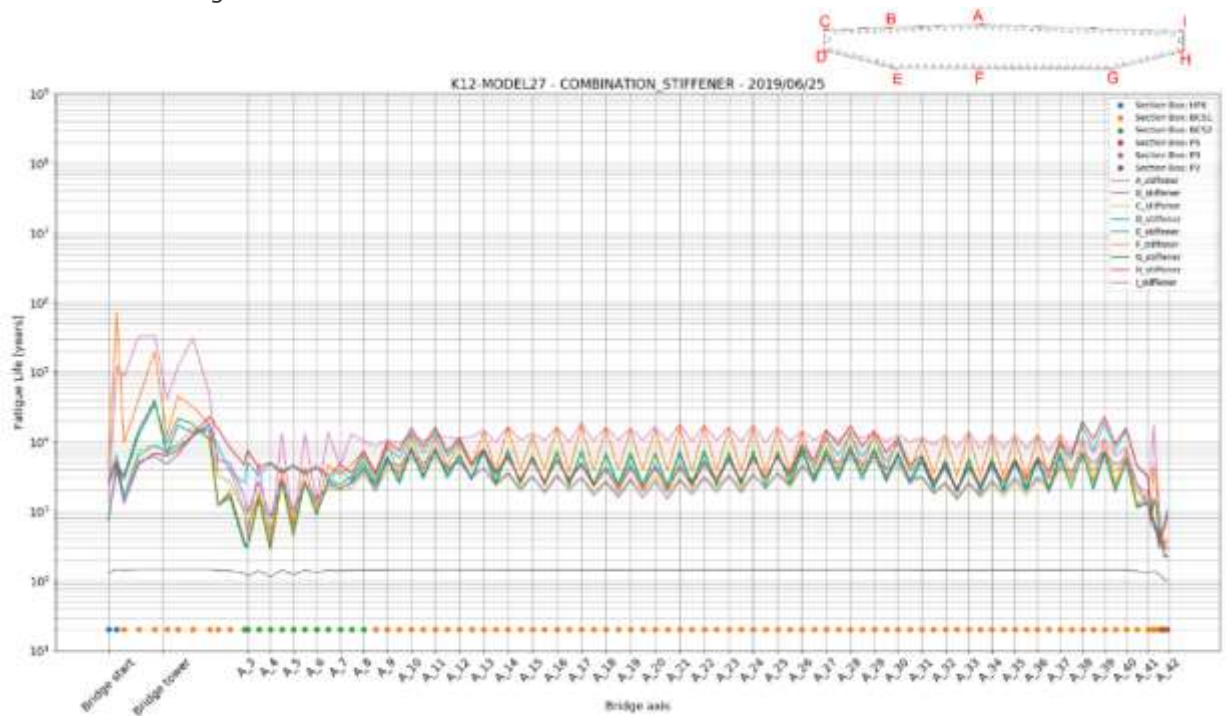
> *Figure 10-5: Trapez. stiffener fatigue life plot by use of the combination formula*

10.5   Analyses columns

Plots of fatigue life of columns based on detail category D for outer skin and F for trapezoidal stiffeners, SCF 2,0 and 1,5 respectively (butt welds). Fatigue life is shown below.
Calculated column fatigue life at point A and C from the combination formula. Comment: Fatigue life is greater than 100 years from axis A_6 (south end) to axis A_41(north-end).
The top part of the column, at weak axis point A need further detailing.
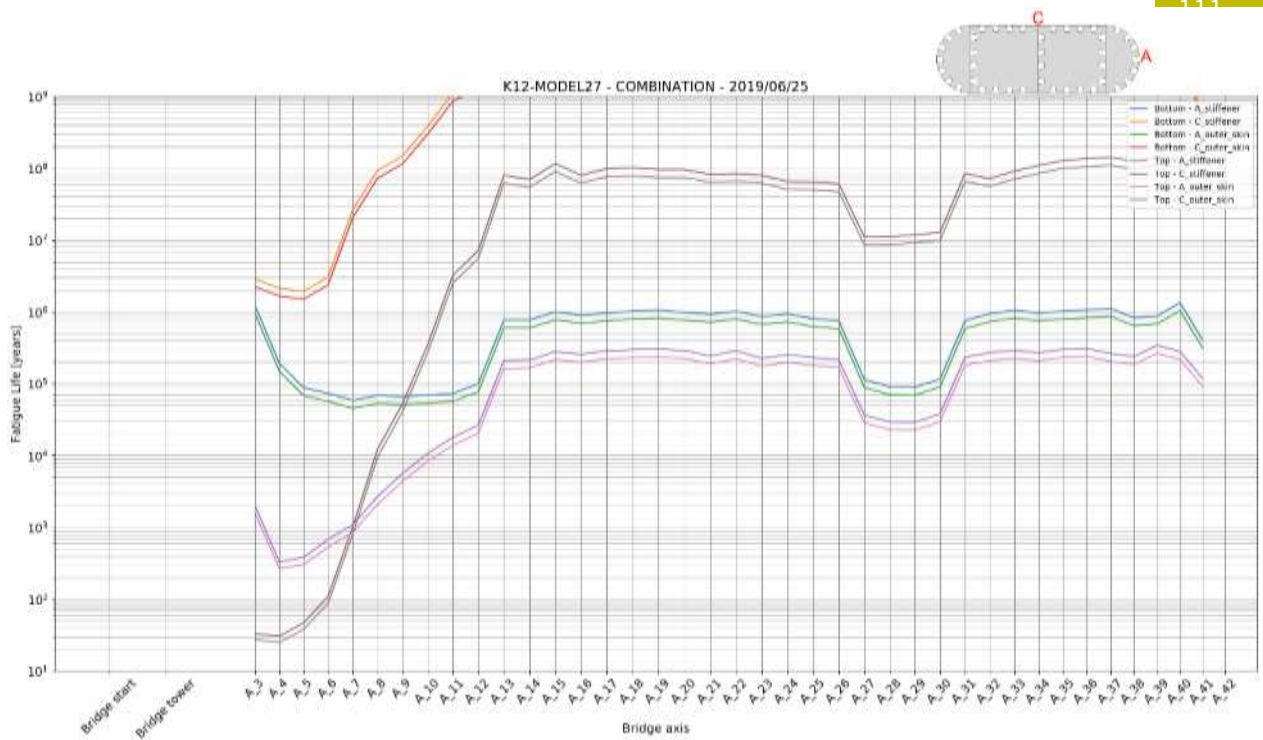
> *Figure 10-6: Column fatigue life plot by use of the combination formula*

10.6   Temporary phases

The installation phases have been analysed and were shown to give less stresses in the bridge than a normal operating condition. Ref. SBJ-33-C5-OON-22-RE-023 App. 02 and SBJ-33-C5-OON-22-RE-023-B K12. The reason for not focusing on this is;

* There is no traffic on the bridge
* The environmental loading is less severe
* There are more side anchors than for the in-place condition (appr. every 500m)

As long as the fatigue life is over 100 years + duration of installation, it is concluded that the fatigue life for installation phases is not problematic.
It should be noted that fatigue design for temporary phases (including transportation) must be revisited at a later point.

11 BRIDGE GIRDER

11.1 Cross-sections

11.1.1 General

The cross section of the bridge girder is constructed as a steel box girder with stiffened plate panels welded together to form a box. There are transverse girders with 4 meters spacing. The shape of the box girder is shown in the figure below with outer dimensions.
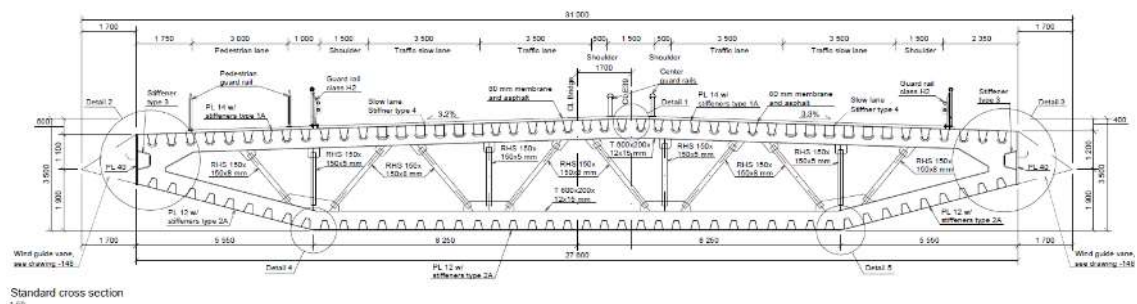
> Figure 11-1: Bridge standard cross-section standard cross section in low part of floating bridge and cable stayed bridge

The outer dimensions of the box girder are kept constant throughout the length of the bridge. In order to handle the varying section forces along the bridge, the thickness of the stiffeners is varied along the bridge. There are two main types of cross-sections, the standard cross section in low part of floating bridge and cable stayed bridge, and the reinforced cross section in high part of floating bridge

In next phase of the project, further optimization of cross sections should be performed. In this phase, a study of various stiffeners is reported and it may be possible to reduce steel amount in mid spans of the girder with use of smaller stiffeners.

Transverse girders/frames spaced with distance 4,0 m along the bridge, except in bridge ends. They are constructed as truss structures. The geometry of the cross frames is shown in the figure below.
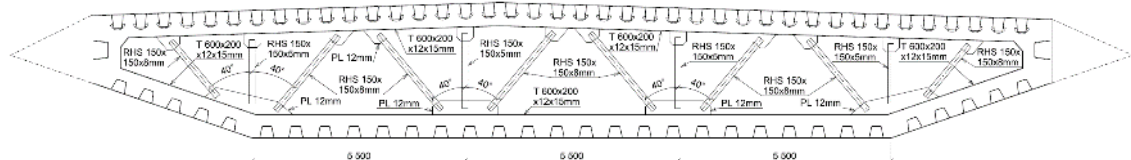
> Figure 11-2: Transverse girders in section 1 and 2

The transverse girders consist of a T-section beam (T 600x200x12x15 mm) welded to the plates and stiffeners around the cross section and a truss structure of RHS 150x150x8 mm as diagonal struts and RHS 150x150x5 mm as vertical struts.

At column/girder connections there are heavy reinforcements with additional longitudinal bulkheads and reinforced transverse bulkheads.

The last 56 meters of the girder are heavily reinforced in both ends towards abutment connections. There are additional longitudinal bulkheads and transverse girders/bulkheads with spacing 2 meters. The cross section at the ends allows for full yielding with plastic hinges according to NS-EN 1993-1-1 sec. 5.6. This introduces a large robustness to the concept versus overloading.

See drawings SBJ-33-C5-OON-22-DR-141 to -147 for cross-section arrangement and dimensions.

The steel grade used in the bridge girder is steel grade S420N/NL.

11.1.2 Properties used in global analyses

The cross-section properties used in the global static and dynamic analyses are summarized in the table below. The properties in the below table are calculated based on the gross cross section without reductions for shear lag effects and plate buckling, and without reinforcements at the column-girder connections.

	Section 1	Section 2	P1	P2	P3	P4	P5	P6
Position x from south	51 – 710 and 1375 - 5384	710 - 1375	5384 - 5395	5395 - 5405	5405 - 5415	5415 - 5425	5425 - 5435	5435 – 5440 and 0 - 51
A	$1,47$ m^2	$1,74$ m^2	$1,59$ m^2	$1,82$ m^2	$2,05$ m^2	$2,29$ m^2	$2,52$ m^2	$2,634$ m^2
COG	$1,91$ m	$1,91$ m	$1,88$ m	$1,82$ m	$1,77$ m	$1,71$ m	$1,65$ m	$1,62$ m
I_y	$2,71$ m^4	$3,20$ m^4	$2,95$ m^4	$3,41$ m^4	$3,88$ m^4	$4,35$ m^4	$4,81$ m^4	$5,049$ m^4
I_z	$114,9$ m^4	$132,0$ m^4	$121,5$ m^4	$134,8$ m^4	$148,0$ m^4	$161,2$ m^4	$174,5$ m^4	$181,1$ m^4

Stresses reported from the global analyses are calculated based on these properties. It will later be shown that these stresses give results to safe side. However, some of these stresses are above design stresses, and consequently, an updated design check based on actual cross sections is executed.

In next chapter, cross section properties based on the actual design are calculated.

11.1.3 Design cross section properties

Design cross sections are based on the actual design:

- Reinforcements at column supports, as shown on drawings are included in section properties
- Reinforcements at abutment supports, as shown on drawings are included in section properties
- Shear lag effects are conservatively accounted for

Design cross sections are used to re-calculate stresses at column supports and mid spans along the bridge.

> *Table 11-1: Cross section properties mid span*

	Design		Analyses	
	Type 1	Type 2	Type 1	Type 2
A	1,47	1,74	1,47	1,74
NA	1,85	1,81	1,91	1,91
I_y	2,52	3,06	2,71	3,2
I_z	114,91	132,00	114,9	132
W_{yo}	1,362	1,688	1,419	1,675
W_{yu}	1,527	1,814	1,704	2,013

> *Table 11-2: Cross section properties at columns*

	Design		Analyses	
	Type 1	Type 2	Type 1	Type 2
A	2,25	2,52	1,47	1,74
NA	1,68	1,69	1,91	1,91
I_y	3,59	4,16	2,71	3,2
I_z	136,20	153,28	114,9	132
W_{yo}	2,132	2,469	1,419	1,675
W_{yu}	1,975	2,295	1,704	2,013

> *Table 11-3: Cross section properties at bridge ends*

Pos x	0		8		16	
	Design	Analyses	Design	Analyses	Design	Analyses
A	4,49	2,634	3,51	2,52	2,77	2,29
NA	1,60	1,62	1,61	1,65	1,71	1,71
I_y	8,95	5,049	6,58	4,81	5,23	4,35
I_z	329,4	181,1	254,5	174,5	218,5	161,2
W_{yu}	5,580	3,117	4,077	2,915	3,057	2,544
W_{yo}	3,897	2,214	3,488	2,600	2,918	2,430

Pos x	32		48	
	Design	Analyses	Design	Analyses
A	2,11	2,05	2,03	1,47
NA	1,78	1,77	1,78	1,91
I_y	4,22	3,88	3,32	2,71
I_z	158,2	148	142,4	114,9
W_{yu}	2,365	2,192	1,863	1,419
W_{yo}	2,460	2,243	1,932	1,704

11.2   ULS cross-section capacity check

11.2.1   Method

The cross-section resistance is calculated according to NS-EN 1993-1-5 and NS-EN 1993-1-1 with the following procedure:

1. Calculation of shear resistance according to EN 1993-1-1, section 6.2.6
2. Interaction between shear and bending are neglected when utilization in shear is less than 50% according to EN 1993-1-1, section 6.2.8
3. Tension stress in all members are calculated. Capacity is limited to yield-stress
4. Compression stress in plates are calculated. Since local buckling will not occur, capacity is limited to yield-stress. Stresses are calculated in outermost fiber.
5. Compression stress in stiffeners is calculated and stiffener buckling is checked. Stresses are calculated in COG of the stiffener.
   - Column type buckling behavior will be dominant for all stiffened plates
   - The buckling load resistance gives the maximum allowable compression stress in COG of the stiffener/plate column.

11.2.2   Plate buckling due to direct stress

Plate buckling resistance is checked according to NS-EN 1993-1-5 sec. 4.5. Column behavior buckling is governing.

Maximum allowable compression stresses are calculated for stiffener type 1A, 2A, 1B, 2B and 3 in ordinary cross section 1 and 2. The stresses are in the centroid of the effective column. Dimensioning compression stress for plates with trapezoidal longitudinal stiffeners is:

| Bridge deck and web: | ULS | 342 MPa | Bottom plates: | ULS | 330 MPa |
| | ALS | 376 MPa | | ALS | 363 MPa |

The stresses should be calculated in centroid of Plate/stiffener column

Maximum compression stresses are calculated for T-stiffener used at the end of the bridge at the abutments. The stresses are in the centroid of the effective column. Note that spacing between transverse beams are 2 meters in this area. This ensures that buckling will not occur even at yield stress. Dimensioning compression stress for plates with T-longitudinal stiffeners is:

| Bridge deck and web: | ULS | 382 MPa | Bottom plates: | ULS | 382 MPa |
| | ALS | 420 MPa | | ALS | 420 MPa |

11.2.3   Stress calculations in bridge girder

From global analyses max and min stresses in each stress point are given, along with the combination of FX, FY, FZ, MX, MY and MZ which gives the max/min stress. It's therefor easy to recalculate stresses with design cross section properties. Both ULS comb 33 with traffic and ULS comb 34 without traffic (100 years RTP) are recalculated.

Stress control is executed in 7 points in plates, and 7 points in stiffeners along the cross section as shown in the figure below:
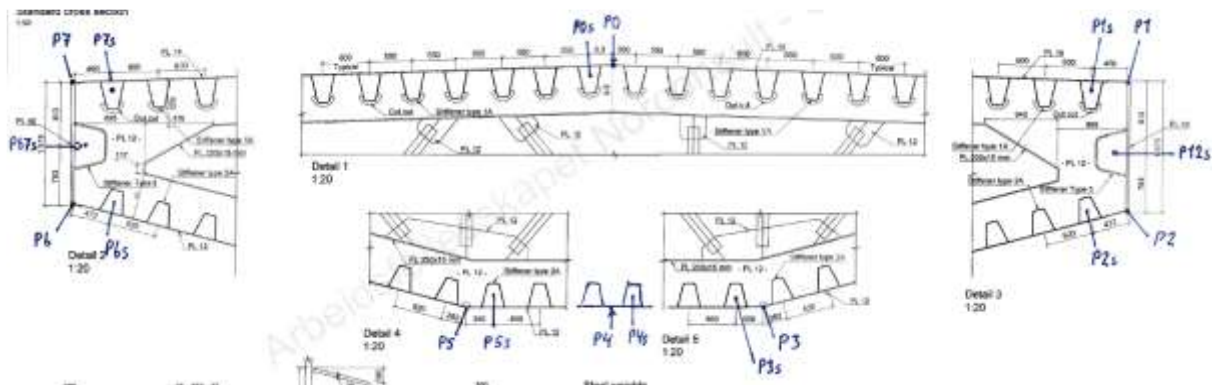
> *Figure 11-3*   *Points for stress calculations*

Section modulus Wy and Wz tabulated for cross sections along the bridge in each stress point can be found in report design of bridge girder [15].

At bridge ends, no stress control in stiffeners is required since the transverse cross girder distance is 2,0 meters and the stiffeners may be utilized to full yield.

11.2.4 Stresses ULS 33 1-year return period with traffic

Results for plate side points 1 – 7 are presented in the following figures:
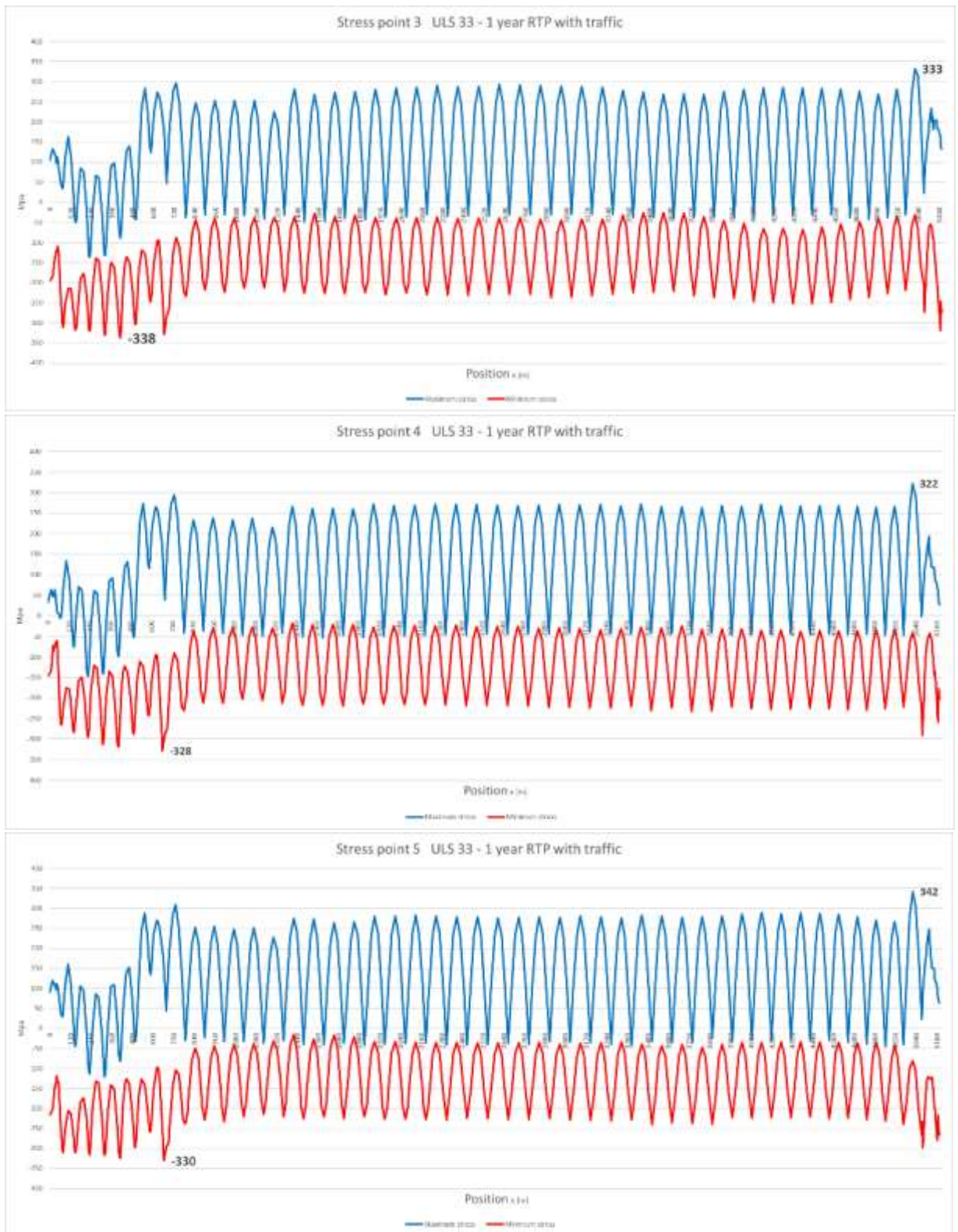
Stress point 3   ULS 33 - 1 year RTP with traffic

Stress point 4   ULS 33 - 1 year RTP with traffic

Stress point 5   ULS 33 - 1 year RTP with traffic

From the figures, we observe that maximum and minimum normal stresses are:

σ_{max} = 342 MPa   Stress point 5 x-pos 5021   End span between axis 41 and 42
σ_{min} = -338 MPa   Stress point 3 x-pos 410   In cable stayed bridge

All stresses in plates < σ_d =382 MPa   OK

According to 11.2.2 max compression stress in stiffener at point 3 is -330 MPa. We need to do a stress control in the stiffener. This is presented in the following figure:

Stress point 3 Stiffener_ ULS 33 - 1 year RTP with traffic

From the figure, we see that maximum compression is -326 MPa < -330 MPa OK

11.2.5 Stresses ULS 34 100-year return period

Results for plate side points 1 – 7 are presented in the following figures:
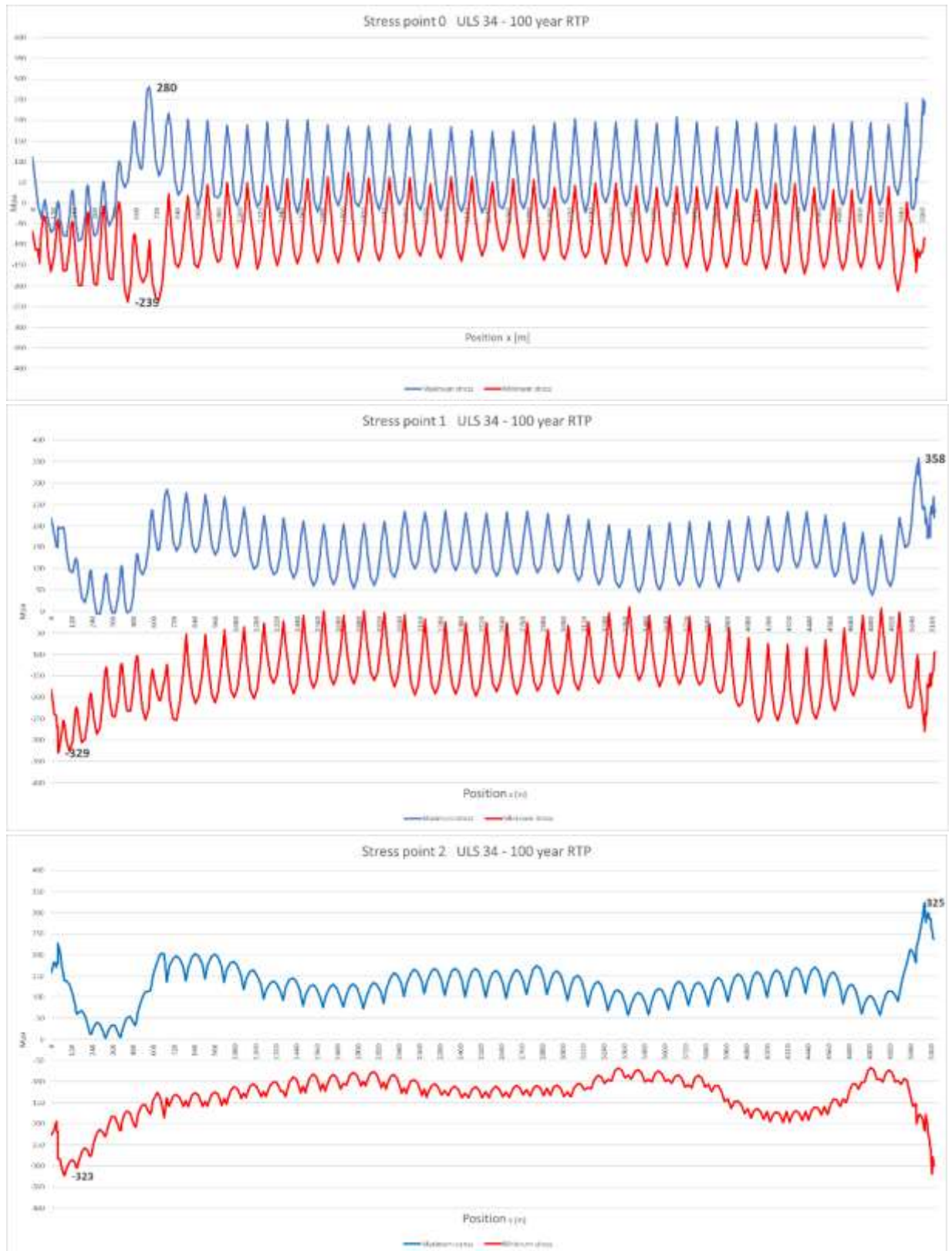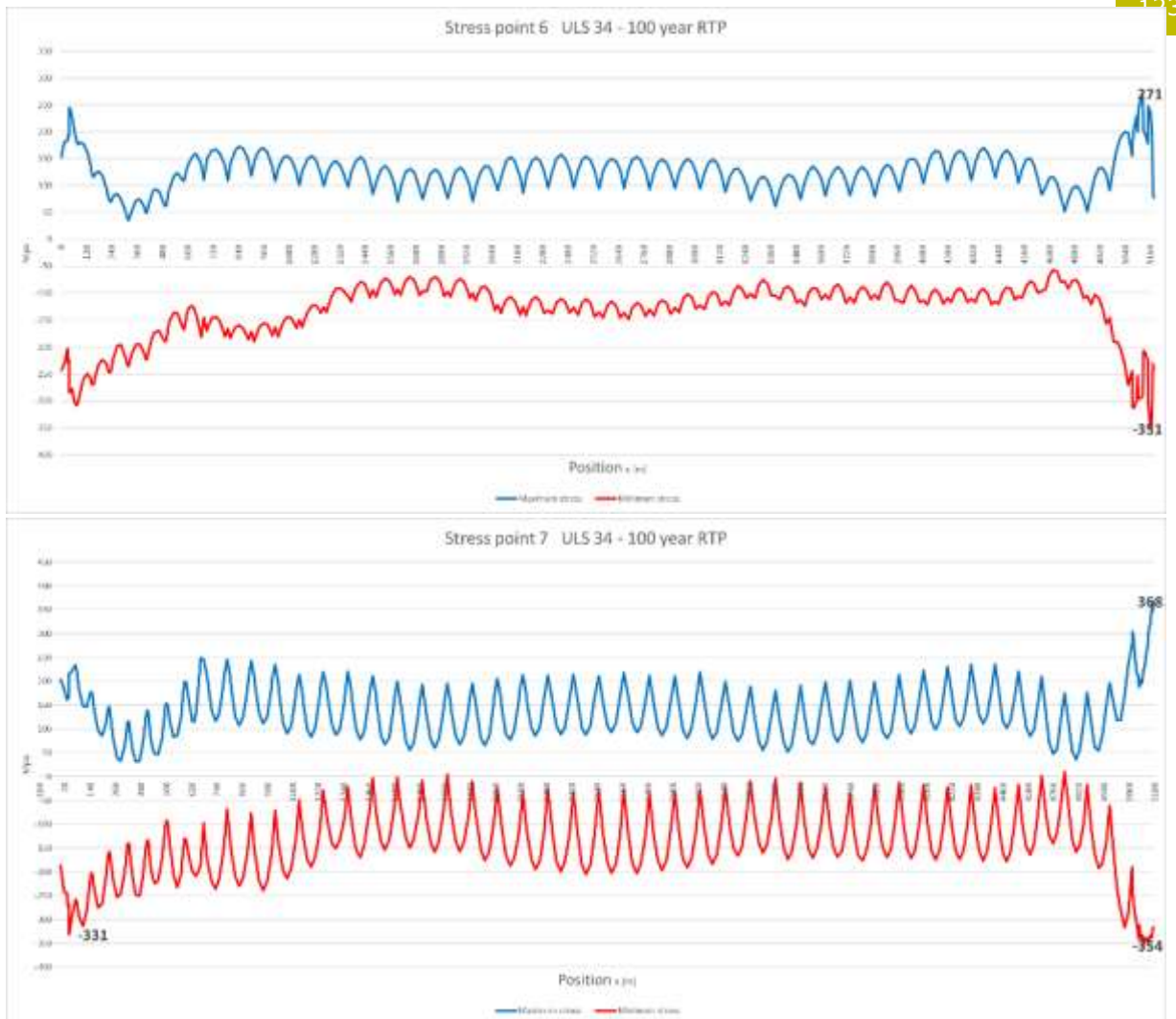
Stress point 3   ULS 34 - 100 year RTP

Stress point 4   ULS 34 - 100 year RTP

Stress point 5   ULS 34 - 100 year RTP

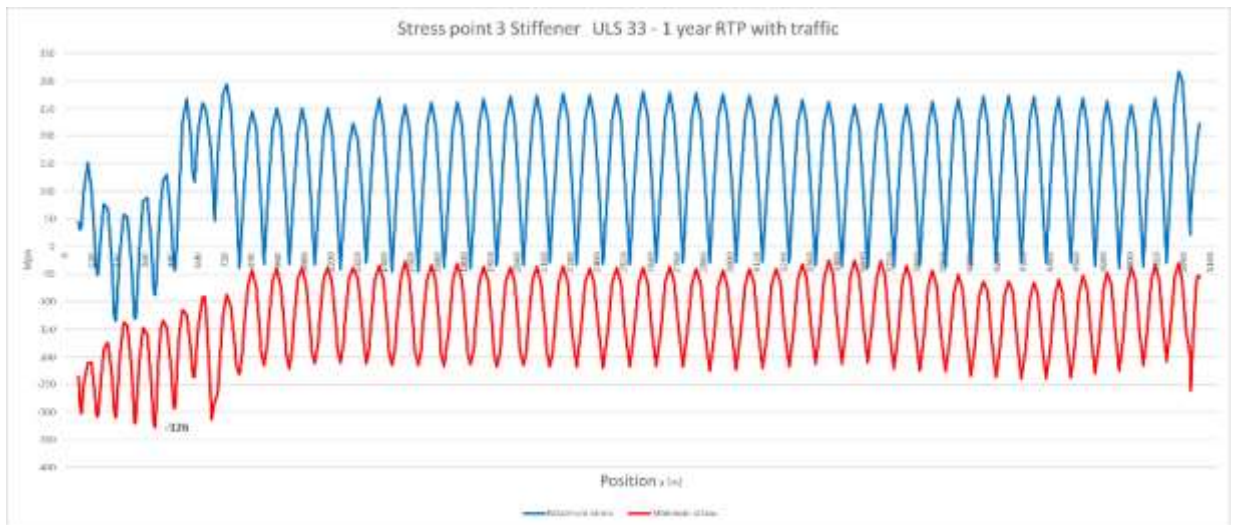Stress point 6   ULS 34 - 100 year RTP

Stress point 7   ULS 34 - 100 year RTP

From the figures, we observe that maximum and minimum normal stresses are:

σ_{max} = 368 MPa   Stress point 7   x-pos 5176   Reinforced end span
σ_{min} = -370 MPa   Stress point 5   x-pos 5163   Reinforced end span

All stresses in plates < σ_d =382 MPa   OK
Compression stress -370 MPa is OK in reinforced end span

We also observe that maximum compression stress in ordinary cross sections are:
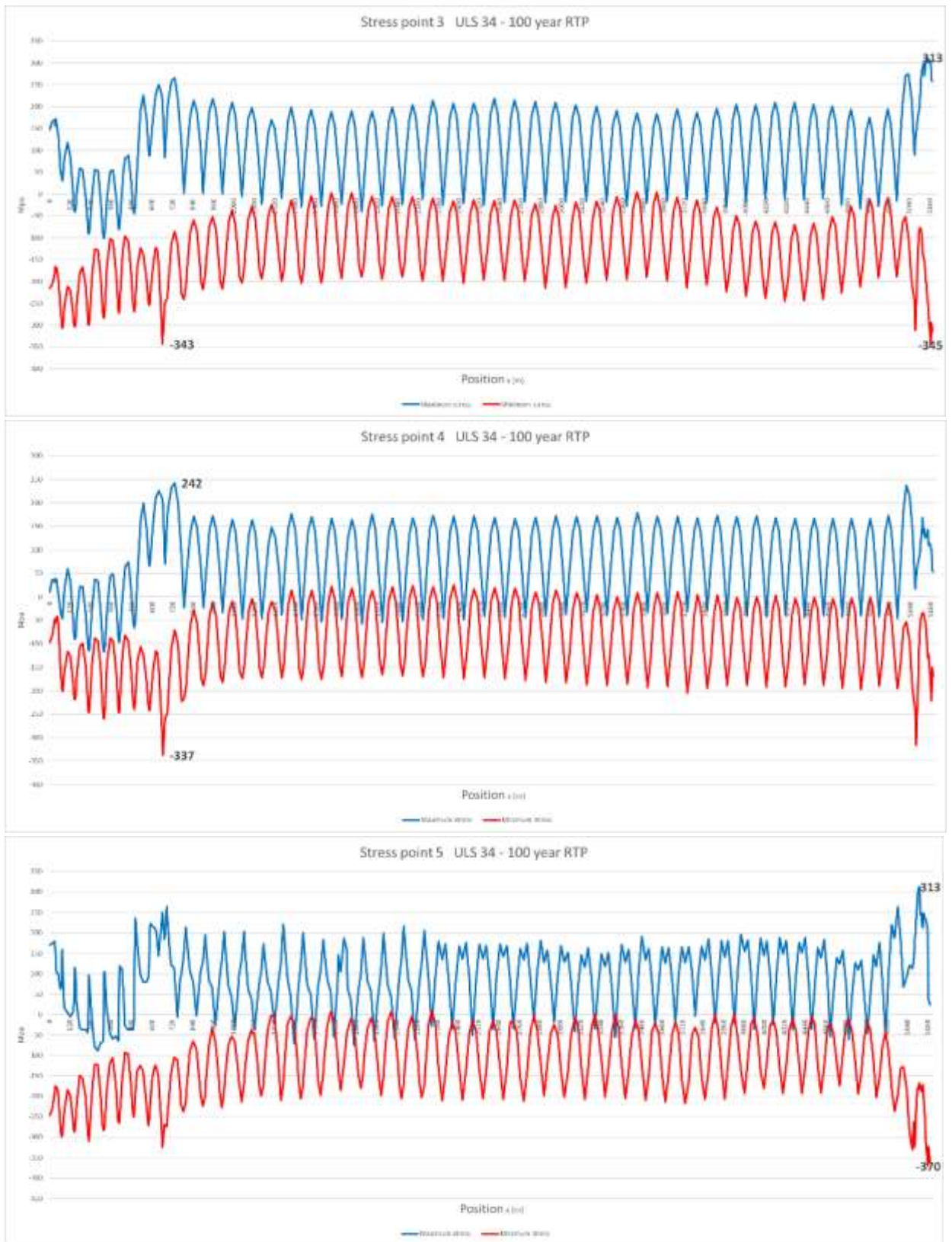
σ_{min} = -343 MPa   Stress point 3   x-pos 664   Closes to axis 3

According to 11.2.2 max compression stress in stiffener at point 3 is -342 MPa. However, the stress in stiffener is lower than 343 MPa and stiffener check is OK.

11.2.6   ULS check – conclusion

ULS check shows that the girder has capacity to resist ultimate limit state load actions. If we compare to stress calculations from global analyses, we will see that design stresses are lower at column supports due to reinforcements even if shear lag effects are included. In mid span, design stresses are higher due to shear lag effects.

11.2.7   Transverse girders

Purpose of transverse girder:
- Support stiffeners. Calculated according to NS-EN 1993-1-5, section 9.2,1
- Transfer support loads from stiffeners to the web plates in the steel girder

Two different load cases are considered:
1. Compression in deck and tension in bottom plates
   Applied weight, traffic and lateral load downwards on deck
2. Compression in bottom plates and tension in deck plates
   Applied weight at deck and lateral load downwards at bottom plate

The transverse girder is analyzed in FEM-Design. Model is shown below with the different loads applied. Girder is pin joint supported at the outermost parts of the model.
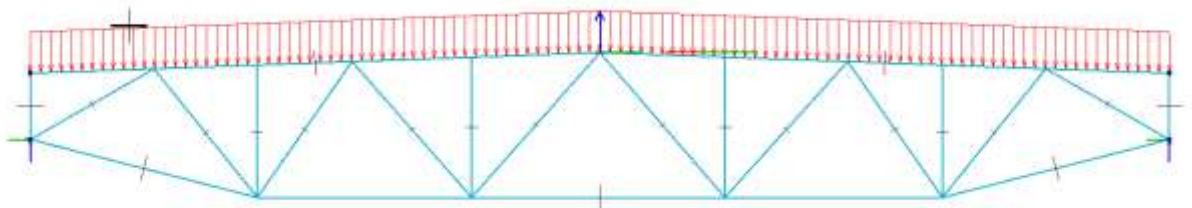
Weight and lateral load from stiffeners at deck
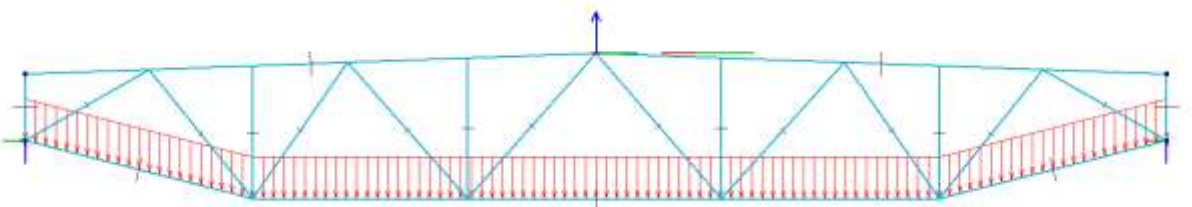
Lateral load from stiffeners at bottom plates
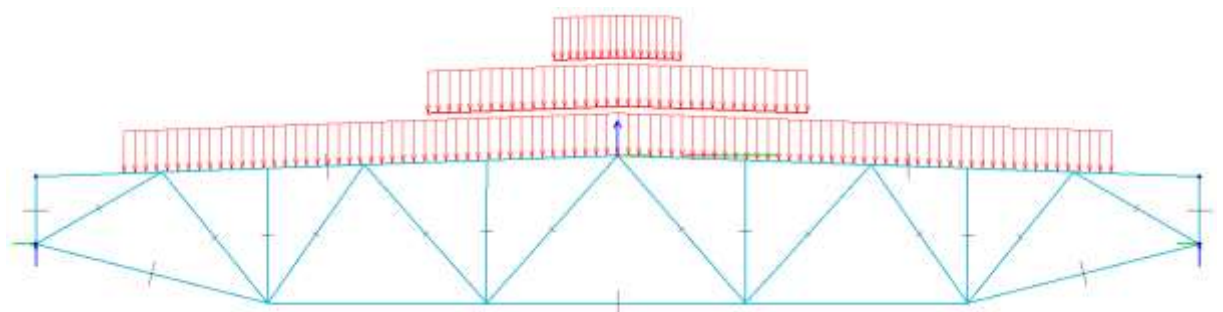
Traffic load q_1 = 10 kN/m between parapets q_2 = 11,6 kN/m in most loaded lane and axle loads as equivalent line loads q = 133,3 kN/m in 3 most loaded lanes.

Capacity is found sufficient for all considered load cases. See bridge girder design report for calculations [15].

11.3   Fatigue limit state (FLS)

See section 10 for summary of fatigue assessment results

11.4   Accidental limit state (ALS)

11.4.1   General

The design of column/girder connections are governed by ship impact. Reference is made to SBJ-33-C5-OON-22-RE-013 – 015 for documentation of ship impact. The following sections summarizes the assessment.

11.4.2   Results

The global response of the bridge due to ship impact has been studied. The main focus is impacts between ship deckhouse and girder and between ship bulb and pontoon. Girder impacts all along the bridge length have been considered, orthogonal to the bridge girder from both directions. Pontoon impacts have been considered on all three pontoon types, at selected characteristic locations along the bridge. Three impacts are considered; head on (0-degrees) and centric and eccentric side impacts (90-degrees). Pontoon impact from a sideway drifting ship and submarine impact has also been discussed. Post impact the bridge must withstand 100-years environmental conditions.

The global ship impact analysis shows that the bridge will survive both a ship impact as given in the design basis and the following 100-years conditions.

A performed screening of girder impacts gives a maximum girder strong axis bending moment of almost 3000 MNm in the bridge "span", while it is 3750 MNm at the south end (near the cable stayed bridge) and 6600 MNm in the north end.

The ship impact energy is expected to be reduced in the next phase. This will give lower global response and lower damage/indentation of pontoons and girder. It might still give large forces in the column and girder, so these are details that still needs to be addressed.

11.4.3   Resistance of cross section due to ship impact

The maximum estimated strong axis bending moment in the girder outside reinforced end spans are 3000 MNm.

From the cross-section properties we find that I = 114 m^3 in mid spans and the stress in outermost fiber is:

$\sigma = 3000 \cdot 13,8/114 = 363$ MPa

From the cross-section resistance we find that design compression stress in ALS is 376 Mpa > 363 MPa   OK

Maximum estimated strong axis bending moment at abutments are 6600 MNm.

From cross-section properties we find that $I = 329$ m^3 in mid spans and the stress in outermost fiber is:

$$\sigma = 6600 \cdot 14/329 = 280 \text{ MPa}$$

From cross-section resistance we find that design compression stress in ALS is 420 Mpa > 280 MPa   OK

11.4.4   Resistance of column/girder connection due to ship impact

The connection between girder and columns have been described in earlier sections. The design is governed by ship impact, and reference is made to report SBJ-33-C5-OON-22-RE-015-A   K12 - Ship impact, Bridge girder.

11.5   Summary of steel weights

Summary of the steel weights are given in the table below.

	Mass	Length - unit	[tons]
Girder type 1 – low floating bridge	13.506 t/m	4009 m	54146
Girder type 2 – high floating bridge	15.321 t/m	665 m	10188
Girder type 1 – cable stayed bridge	13.506 t/m	654 m	8833
Girder abutment connection south	19.300 t/m	56 m	1081
Girder abutment connection north	19.300 t/m	56 m	1081
Girder column connection axis 3 – 6	164 t	4 units	656
Girder column connection axis 7 – 41	112	35 units	3920
SUM STRUCT. STEEL			**79905**

12   PONTOONS AND COLUMNS

12.1   Finite element models

12.1.1   General

Linear and non-linear finite element models are developed. The linear finite element models in Sesam Sestra are used for structural dimensioning and fatigue evaluations, see report on design of pontoons and columns [16]. Non-linear finite element models in Abaqus are mostly used for structural verification, see the description in the following sections

12.1.2   Non-linear FE - Abaqus Models

Abaqus 2019 is used for non-linear finite element analyses. A finite element model for the pontoon at axis 3, which is closest to the navigation channel is used in the analyses. The finite element model consists of a 58 meter long and 16 meter wide pontoon. The height of the pontoon is 9 meters with a draught of 5 meters. Note that the pontoon width increased to 17 meters at the later stages of the project. The ULS analyses with different wave directions are updated to account for this, the ship impact ALS analyses are however not updated with the new pontoon width as it will have low impact on the results.

The columns are rectangular in nature with half circular short edges. The rectangular part is 8 meter long and 4 meter wide. The radius of the short edge circles is 2 meters making the total length of the column equal to 12 meters. The height of the column at axis 3 is 37.5 meters, while at the low bridge the height is 11 meters.

The pontoon and column are modelled as stiffened panels. In the pontoon, the outer walls, top- and bottom plate and internal bulkheads are stiffened with bulb-stiffeners in general, and additional T-girders for large panel spans (internal transverse bulkheads). In the column, the plates are stiffened with trapezoidal stiffeners, ring-frames and three internal bulkheads in the transverse direction. All plates and web of stiffeners are modelled as shells, while the flange of stiffeners and T-girders are modelled as "stringers" with proper flange characteristics (except for trapezoidal stiffeners, which is modelled in full).

The pontoon is modelled in several parts and tied at places sufficiently away from high stress areas. The interface between column and pontoon is modelled as single part to avoid tie-constraints in critical areas.

The pontoon and column are modelled with 8-node shell elements with reduced integration, with mesh size ranging from approx. 1.5m x 0.75 m (at pontoon outer surfaces) to TxT at column/pontoon interface (where T is the plate thickness).
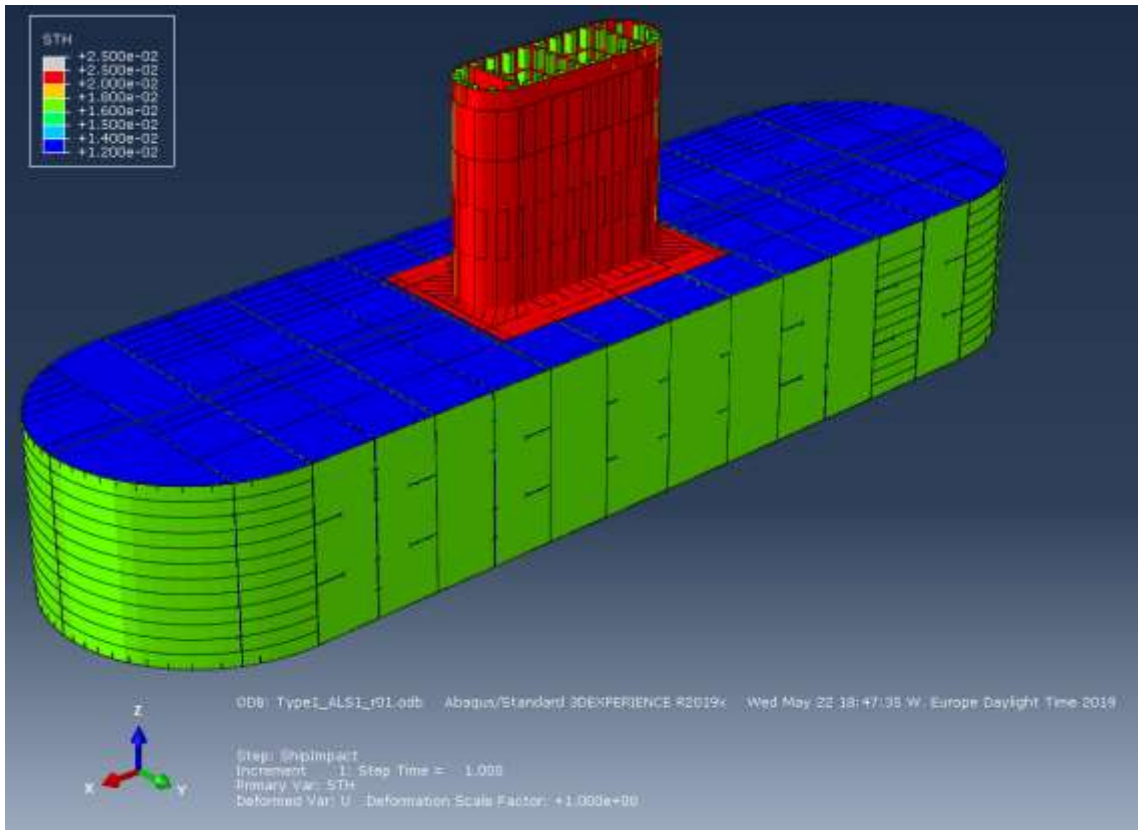
> *Figure 12-1 Thickness for pontoon and column*
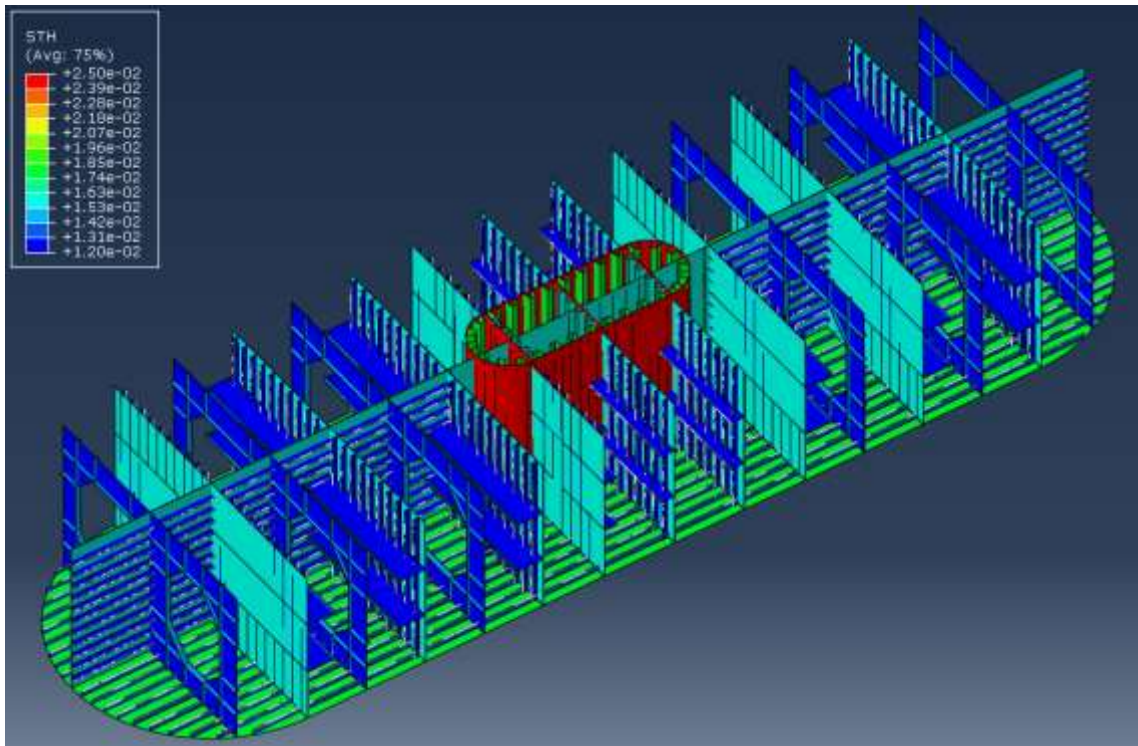
> *Figure 12-2 Thickness internal bulkheads and bottom plate*
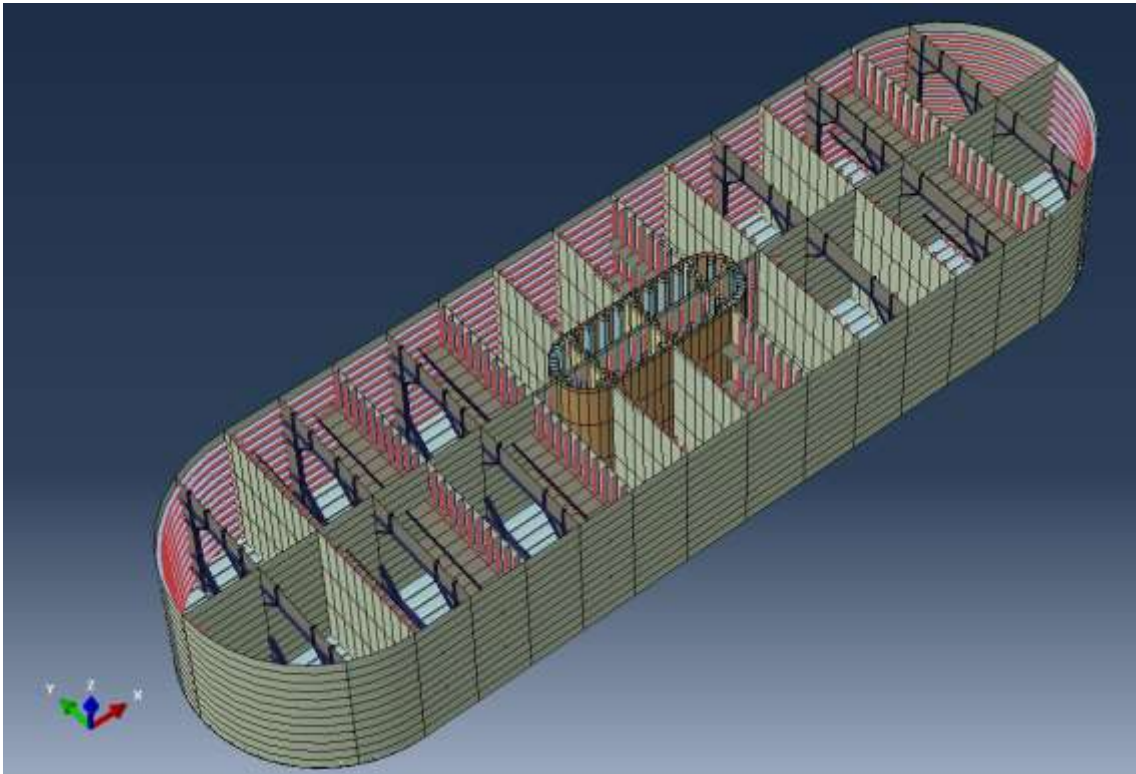
> *Figure 12-3 Internal compartments and bulkheads/frames*
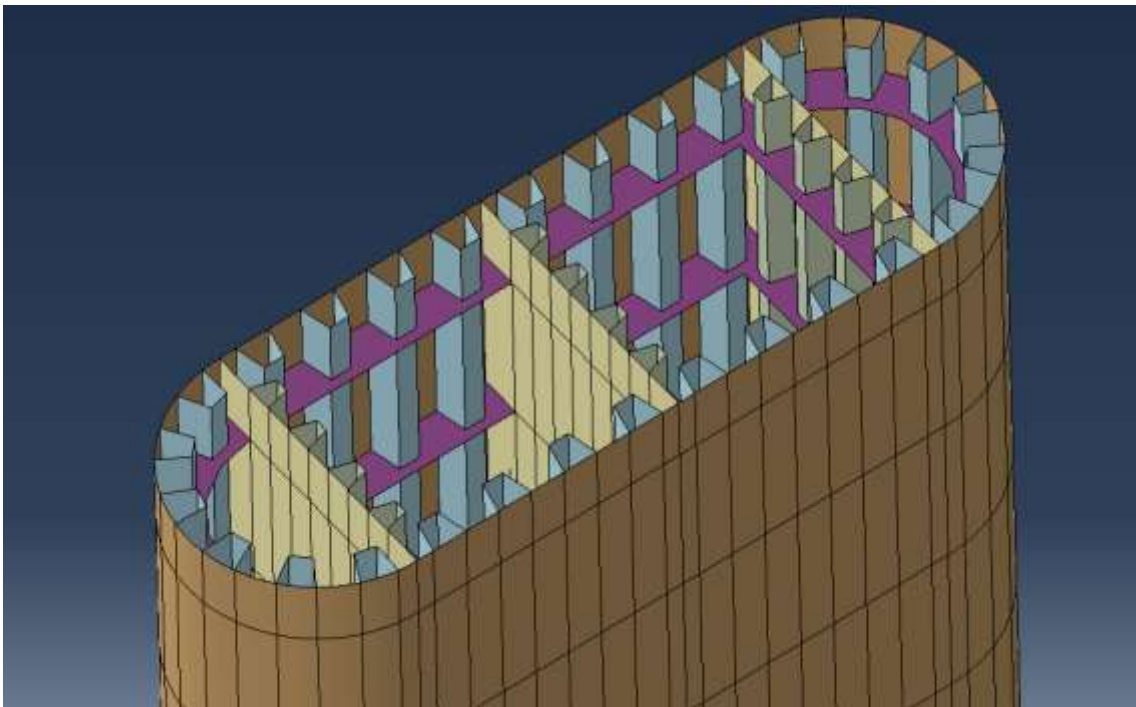
> *Figure 12-4 Column design, internal stiffeners and bulkheads*

12.2 Loading

12.2.1 General

The pontoon and columns will be designed for ULS, FLS and ALS. Most parts of the column and some parts of the pontoon have ship impact as the governing design load. For the pontoon, ship impact will be important in the interaction area between the pontoon and the lower part of the column.

Dynamic loading is applied as quasi-static loading without taking dynamic amplification (including effects from added mass) into account. As a first approach, column section forces from the analyses are compared with column sectional forces from the global model.

12.2.2 ULS

The following load cases are included in the analyses:
- Gravity
- Static water pressure
- Tank pressure
- Dynamic loading, wave directions with angles 0, 15, 30, 45, 60, 75 and 90 degrees to the pontoon longitudinal axis.

12.2.3 ALS

The following load cases are included in the analyses:
- Ship impact
- Gravity
- Static water pressure
- Tank pressure
- Compartment flooding

12.2.4 FLS

The fatigue evaluation consists of an evaluation of first principal stress ranges for the dynamic part of the loading. There are several levels possible for fatigue evaluation. Preliminary global model fatigue evaluations show low fatigue damage in the column-pontoon intersection area. Highest ULS-stresses are observed in this area and fatigue damage is believed to be highest in this area. Further fatigue damage evaluations will be carried out in a later project phase.

12.3 Results linear analysis

12.3.1 General

Linear analyses are used for dimensioning. The linear analyses indicate that the connection between the column and the pontoon will withstand the loading for both the ULS condition and the ALS condition.

For the long column the stresses at the top of the column become too high. Plastic collapse will probably take place before impact load becomes equal to the design value of 30 MN. The

short column will also have very high stresses, with highest values in the top region. Plastic utilization will be found in the non-linear analyses.

For the model with large pontoon and long column two knee-plates are introduced where the pontoon longitudinal bulkhead crosses the column skin. For the ALS and ULS condition non-linear analyses will most probably show that these knee-plates are not necessary. However, they will increase the fatigue life in this region. Later FLS evaluations will show if they are necessary.

The following sections show selected results for pontoon/columns towards the high bridge. Corresponding results for the low bridge can be found in [16].

12.3.2   ALS Results

The ship impact load is combined with static water pressure and gravity.
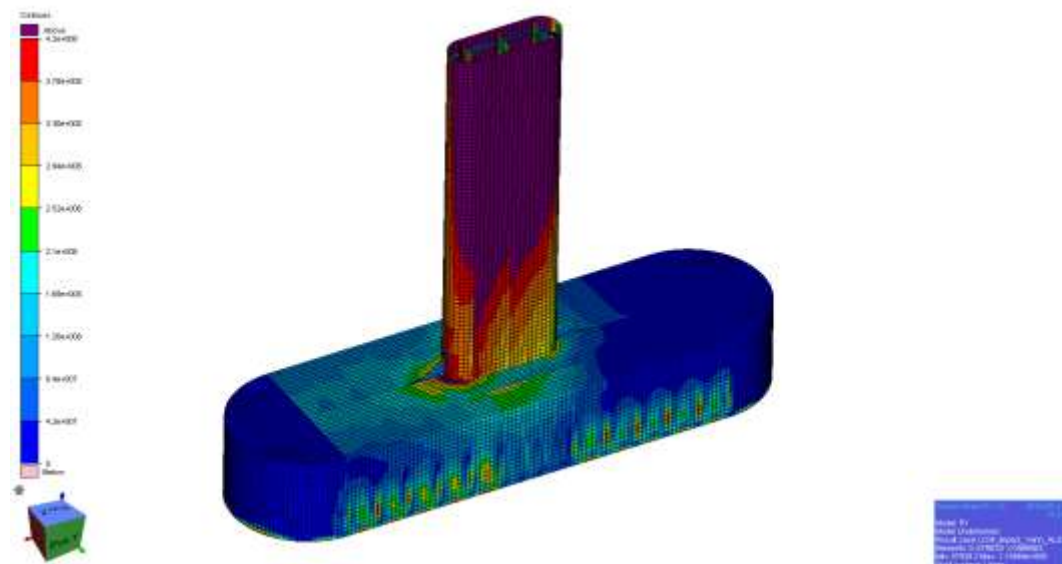
> *Figure 12-5   von Mises stress*
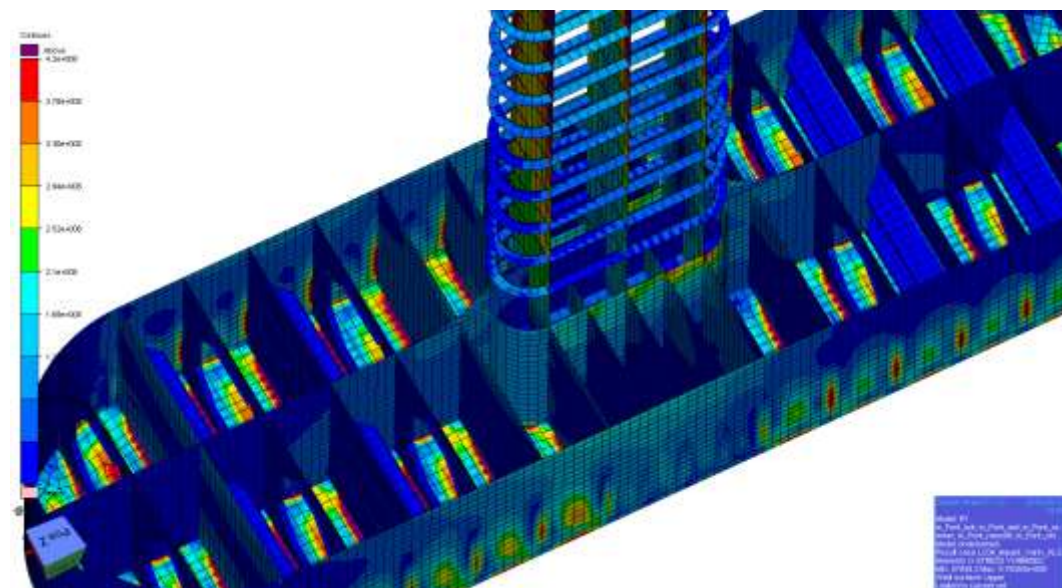
> *Figure 12-6*   *von Mises stress, column shell and pontoon top removed*

12.3.3 ULS Results, maximum Pontoon Moment

The load combination consists of static water pressure, dynamic water pressure and gravity.
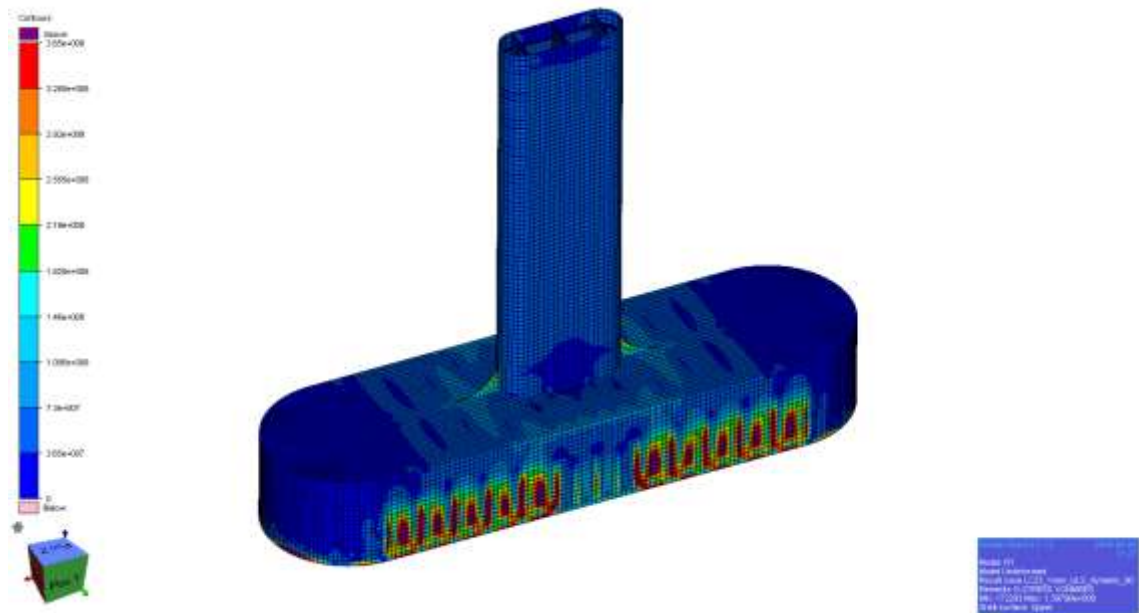
> *Figure 12-7*   *von Mises stress*
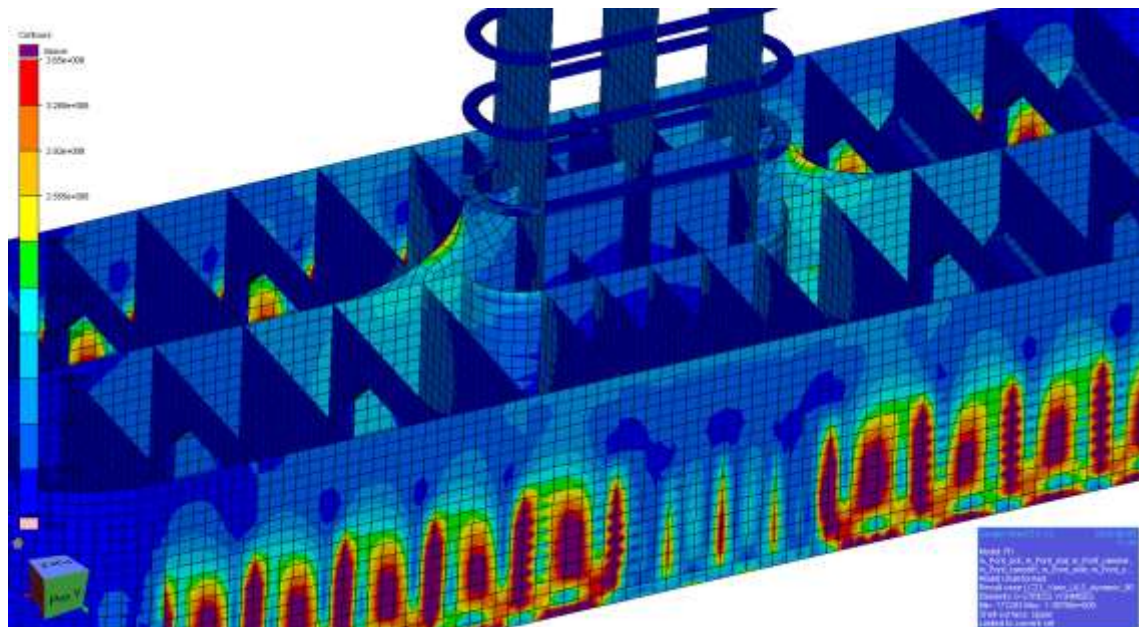
> *Figure 12-8*   *von Mises stress, column shell and pontoon top removed*

12.4 Results non-linear analysis

12.4.1 General

Same pontoon type (width 16 meters, length 58 meters) is used for both tall and short column non-linear analyses. As the major stresses from ship impact (except local stresses at impact zone) are in the interfacing part between the column and pontoon due to torsion, the width of the pontoon is of less importance and should not affect the results in any major way. It is considered acceptable to lose up to four compartments in flooding from ship impact, so the focus of these analyses is to verify the integrity of the overall strength of the pontoon-column interface and the column itself. Hence the ship impact load is treated as a uniform shear stress at the outermost bulkhead (situated 21 meters from the center of the column), equal to 0.2083 MPa which totals to 30 MN. The forces and moments in the column will thus be a shear force of 30 MN, together with a torsional moment of 630 MNm and weak axis bending moment with maximum value of 465 MNm for the short column and 1260 MNm for the tall column (in ship impact report, SBJ-33-C5-OON-22-RE-013, more accurate forces and moments are available).

Static water pressure and structural self-weight is applied with safety factor 1.0 for the ALS analyses. The FE analyses are checked without internal water pressure from ballast tanks.

ULS analyses for all wave directions are performed in Abaqus for largest pontoon (17 meter width) with refined mesh and bulkhead and plate stiffeners added. The analyses are run with linear-elastic material properties, but with non-linear geometry properties (i.e. 2nd order theory) to capture any local buckling behavior.

The following sections show selected results for pontoon/columns towards the high bridge. Corresponding results for the low bridge can be found in [16].

12.4.2 ULS Results

The ULS dynamic water pressure applied with wave bottom at ¼ of the pontoon length and wave crest at ¾ of the pontoon length, at an angle of 45 degrees to the pontoon longitudinal axis is shown to give the highest utilization.

All stresses are below the Mises yield criteria and no permanent deformation occur in ULS except for one local peak between pontoon longitudinal bulkhead and column intersection at top of pontoon. This peak stress will be reduced with added knee-plate mentioned in linear elastic analyses chapter. Elsewhere in the pontoon the stresses are far below yield limit. The knee-plate may also be necessary from fatigue life calculations.

In addition, the transversal bulkheads are checked with internal water pressure in a separate Stipla check with conservative stresses from the analyses (i.e. peak plate end stresses assumed uniformly over the plate length/height).

The maximum allowable yield stress for plates with steel grade S420 is 420 MPa / 1.15 = 365 MPa.

The maximum allowable yield stress for bulbflats with steel grade S355 is 355 MPa / 1.15 = 309 MPa.
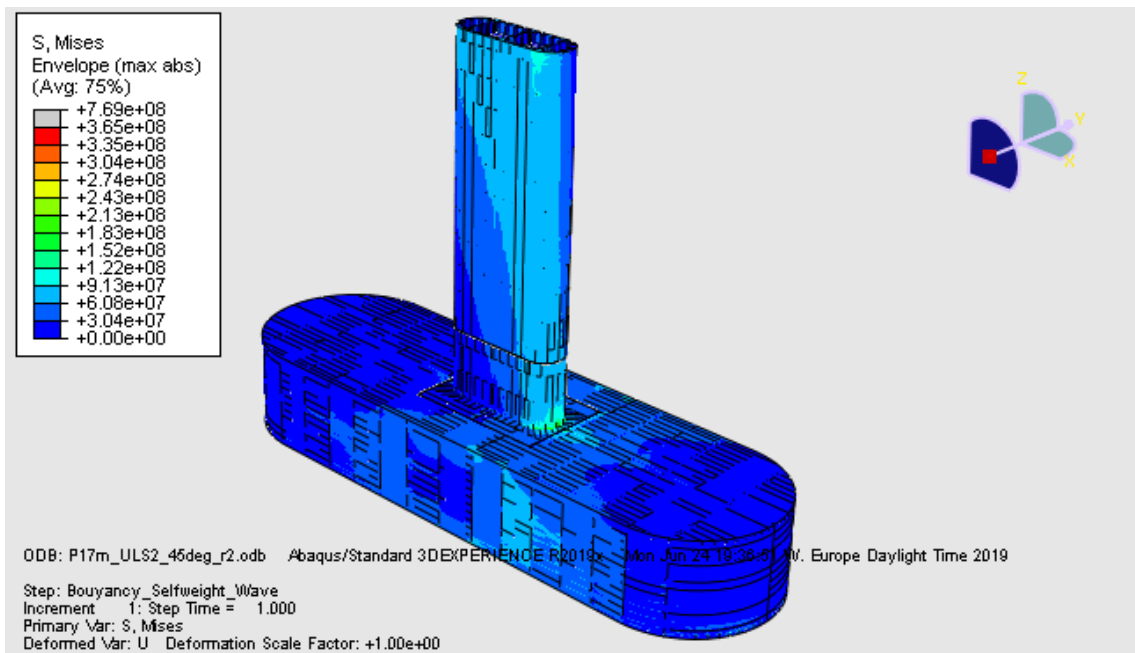
> *Figure 12-9 Mises stress at pontoon and column skin*

Overall Mises stress in pontoon and column for large pontoon (17 m width) is shown in Figure 12-9 to Figure 12-12 for the worst wave condition. Note that largest stress in legend is from tied mesh-constrain at the longitudinal bulkhead in the pontoon and not real stress. The mentioned peak stress in column pontoon intersection is shown in Figure 12-10 and Figure 12-12.
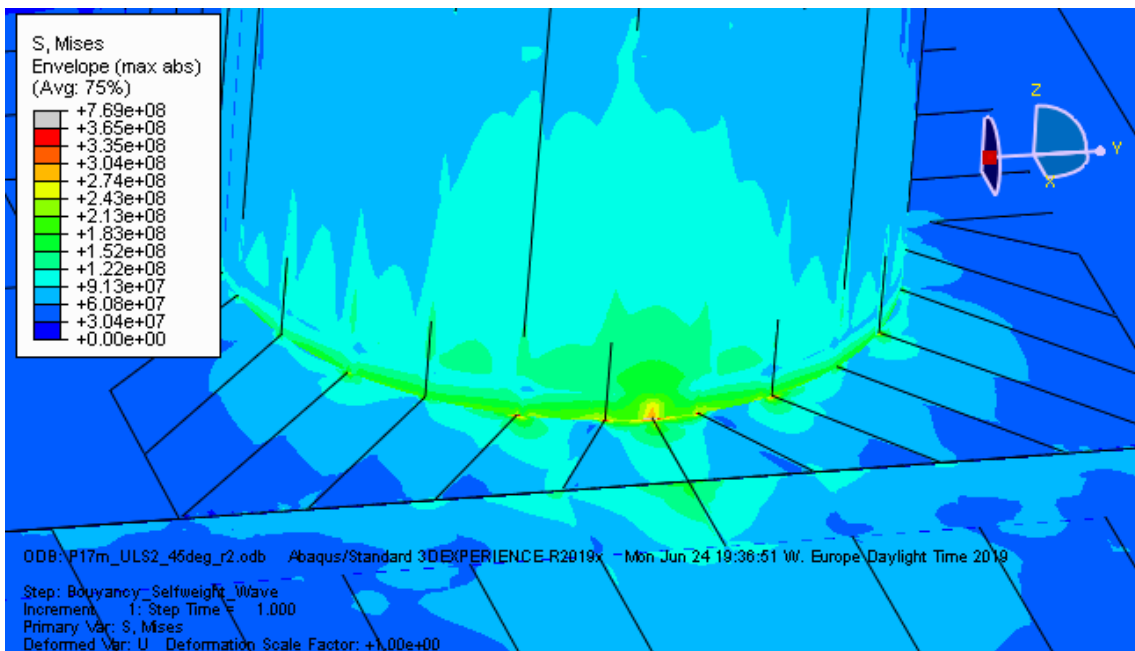
> *Figure 12-10 Mises stress at column-pontoon interface. Note that largest stress in legend is from tied mesh-constrain at the longitudinal bulkhead in the pontoon and not real stress.*
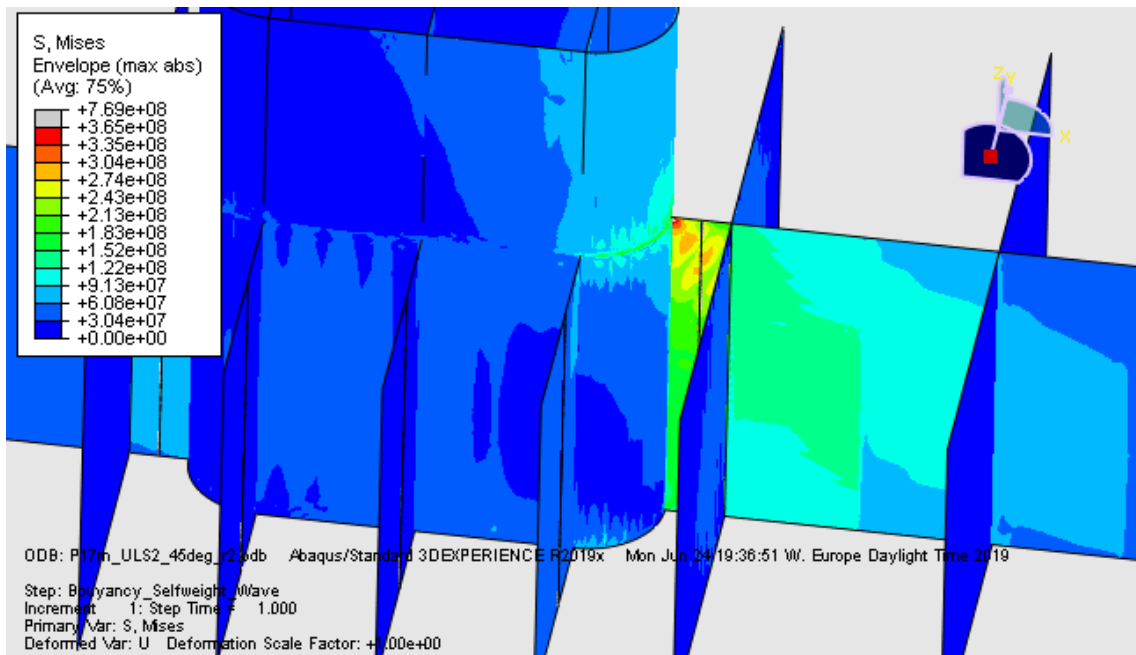
> *Figure 12-11 Mises stress at pontoon bulkheads*
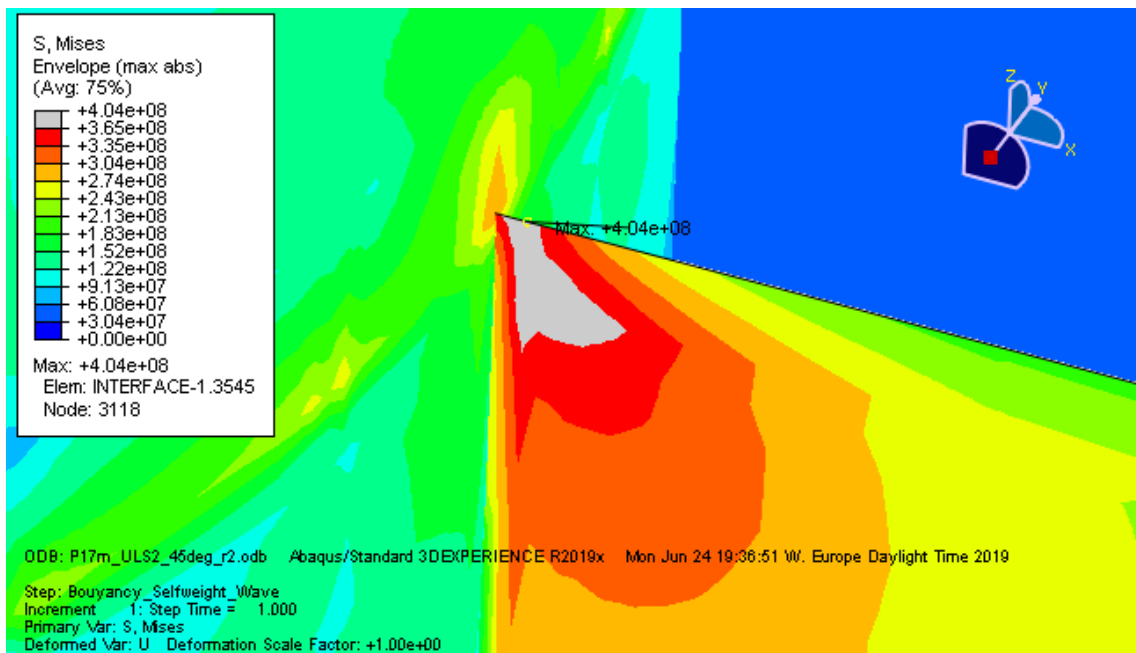
> *Figure 12-12 Maximum Mises stress at intersection between column and pontoon longitudinal bulkhead.*

> *Table 12-1 Largest reactions forces and moments taken from local ULS models compared with global analyses ULS response*

Reaction Force/Moment	Value	% of global analysis response*
Rx	+/- 4.5 MN	78 %
Ry	+/- 12.5 MN	124 %
Rz	- 37 MN	94 %
RMx	+/- 460 MNm	130 %
RMy	+/- 145 MNm	89 %
RMz	+/- 117 MNm	152 %

*) At column top; a percentage above 100% means that the response in local analyses is overestimated, a value below 100% indicates that the response in local analyses is underestimated with the applied ULS static loads.

The reactions forces and moments from the local ULS models are compared with the ULS response at top of column from the global analyses (for K12 model 27). The table above show the largest values compared with the envelope values from the global analyses. As seen from the table the applied static ULS load underestimates response in pontoon longitudinal direction by 11-22%, but overestimates the response in pontoon transversal direction by 24-30% and for column torsional moment by 52%.

Bending moment of the pontoon itself is the main contribution to the stresses in the pontoon column interface, so the difference in column shear force of 22% or 1.3 MN (from 5.8 MN to 4.5 MN) results only in additional sigma-X stress equal to less than 10 MPa at the top of the longitudinal bulkhead, if the bulkhead transfers this added load alone.

A Stipla check of transverse bulkhead for 17meter wide pontoon has also been performed with a maximum utilization ratio of 0,72.

12.4.3   ALS Results

Two analyses are performed for the large pontoon with tall column. First, a fully non-linear analysis was performed for the ship impact at the large pontoon with the tall column. At 75-80% of the ship impact load, extensive yielding and subsequent local buckling is seen at Figure 12-13 and Figure 12-14. Due to large rotations, the non-linear analysis performed with statically applied impact force solved implicitly, the analysis did not manage to complete any further. To avoid time-consuming dynamic analyses to solve the problem, the upper part of the column was treated as linear-elastic and local buckling prevented, so that the analyses was managed to run completely. As the plastic hinge is already verified in other dynamic ship-impact analyses, and the establishment of such a hinge is shown to occur here, it was deemed sufficient to model the column such that the analysis could complete as the focus is primarily on the interface between column and pontoon. Figure 12-15 and Figure 12-16 show the stresses and plastic strains in the lower part of the column modelled with non-linear material.
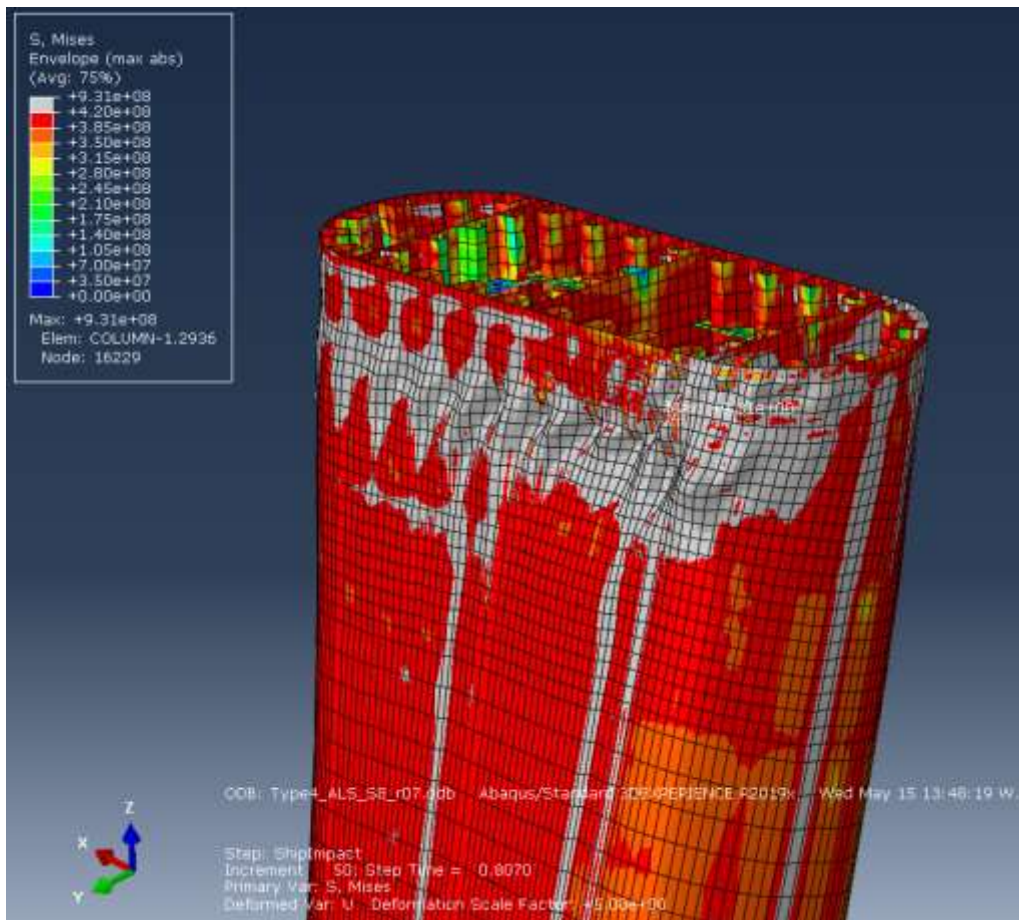
> *Figure 12-13 Yielding and local buckling at 80% ship impact load, which shows the establishment of a plastic moment hinge at the top of the column.*
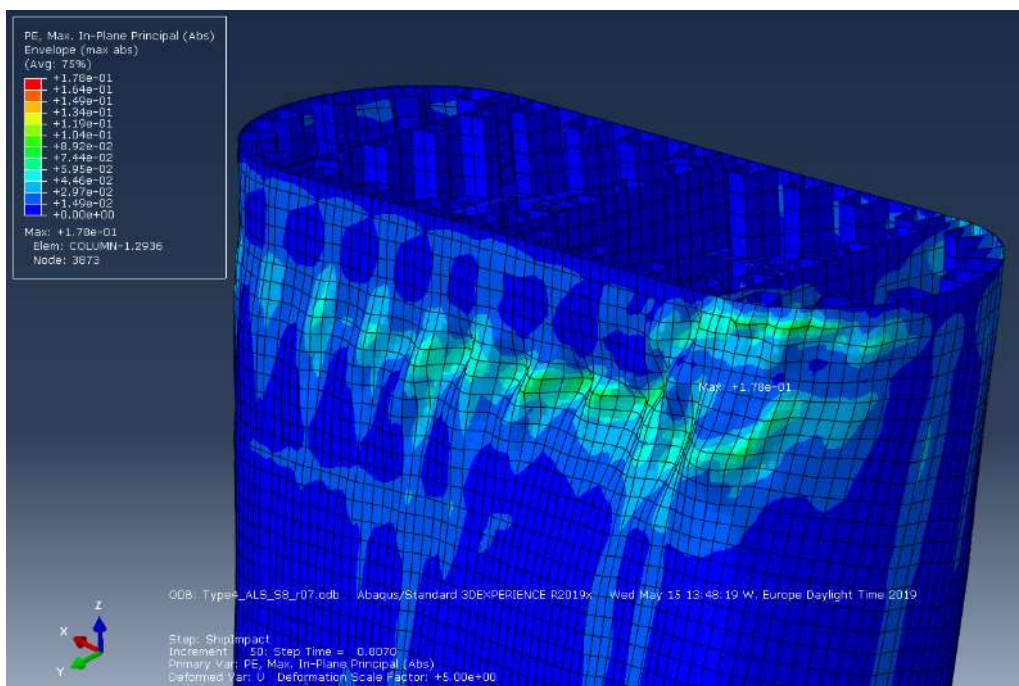
> *Figure 12-14 Plastic strain at column top at 80% of ship impact load.*
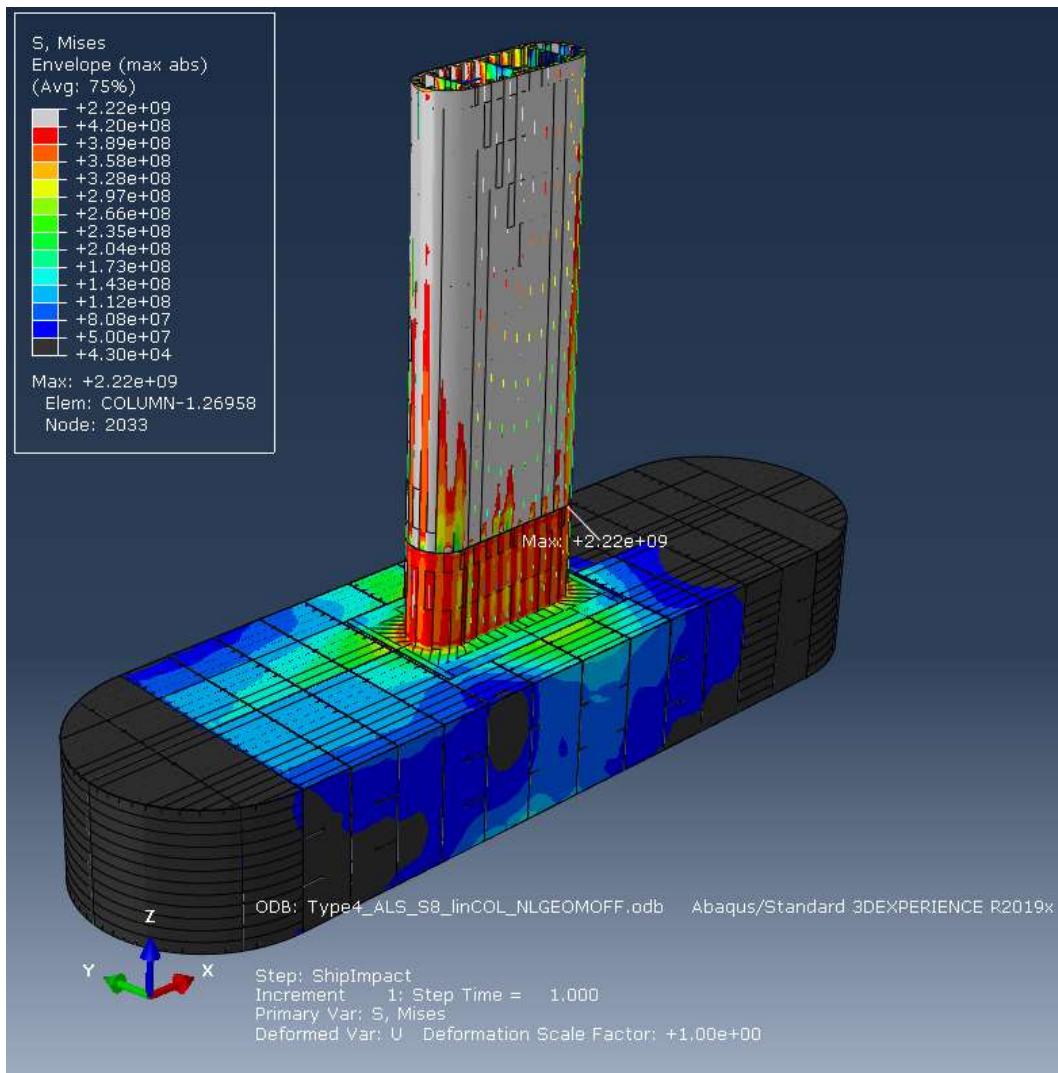
> *Figure 12-15 Mises stress at 100% impact load, with linear elastic material in column (except for 6.25 meters closest to pontoon) and NLGEOM turned off, i.e. no local buckling to occur.*
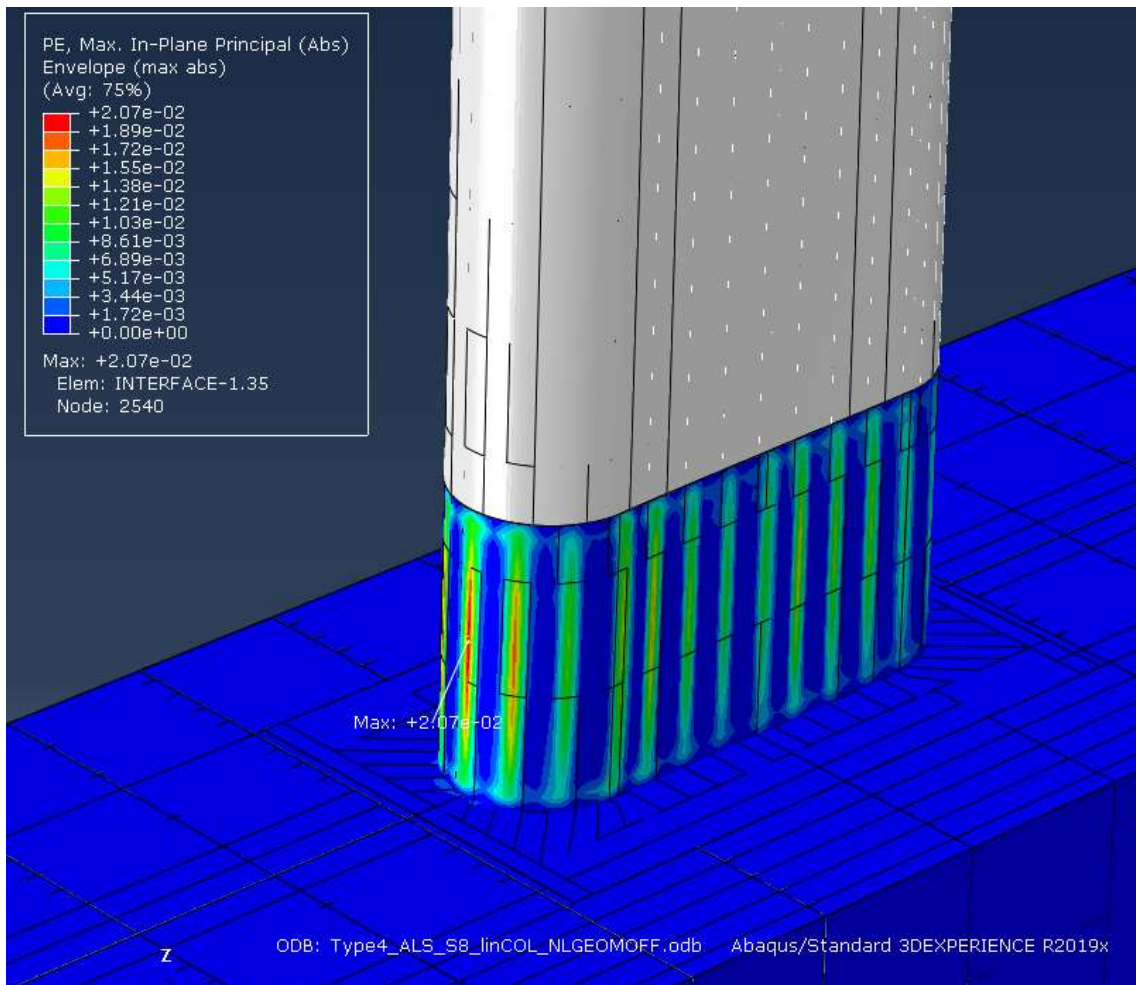
> *Figure 12-16 Plastic strain in column part with non-linear material at 100% impact load. Maximum 2.1% due to combined torsion and shear force from eccentric impact load.*

12.5   Fairlead

12.5.1   General

A moonpool area is established for the large pontoon linear finite element model. Based on drawing SBJ-33-C5-OON-22-DR-123, Pontoons and Columns, Type 2A Anchor – Structural Arrangement, a fairlead-like shell structure is modelled inside the moonpool area. The fairlead and a corresponding area at the pontoon top has been given loads corresponding to the MBL-load for the mooring line.

12.5.2   Loading and Boundary Conditions

The minimum breaking load for the mooring line is set to 10 MN (i.e. 9864 kN). With a load factor of 1.25 (DNVGL-RP-C103, Chapter 6.1.2 [39]), the dimensioning anchor line breaking load becomes:

$F_l = 1.25*10 \text{ MN} = 12.5 \text{ MN}$

The most unfavorable loading direction for the mooring chain is used, horizontal direction or zero degrees inclination. The inclination is expected to be between 5 degrees and 32 degrees.

The transverse loading is set to 5 percent of the dimensioning anchor line breaking load:

$F_t = 0.05*F_l = 0.05*12.5$ MN $=0.625$ MN
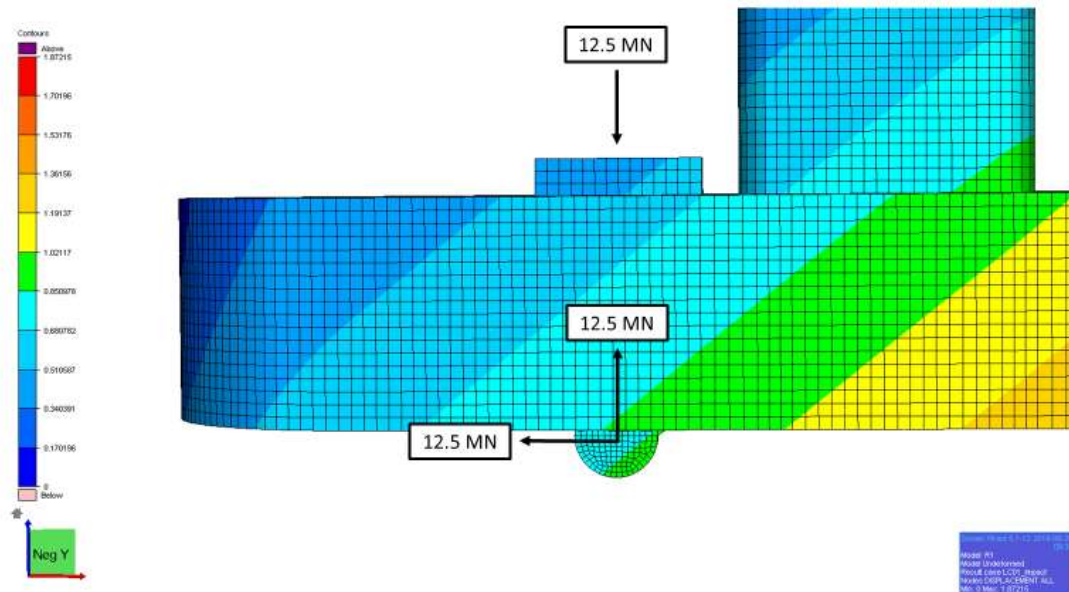
> *Figure 12-17 Load application, in-plane loading*

The boundary condition is the same as for the original analysis. The top of the column is kept completely fixed.

12.5.3   Fairlead Shell Thickness and Structural Reinforcement

A 30 mm support plate is inserted behind the upper transverse fairlead plate, and the thickness of the pontoon bottom plate is increased to 30 mm in a local area behind the lower transverse fairlead plate.

All fairlead plates have been given a thickness of 40mm.
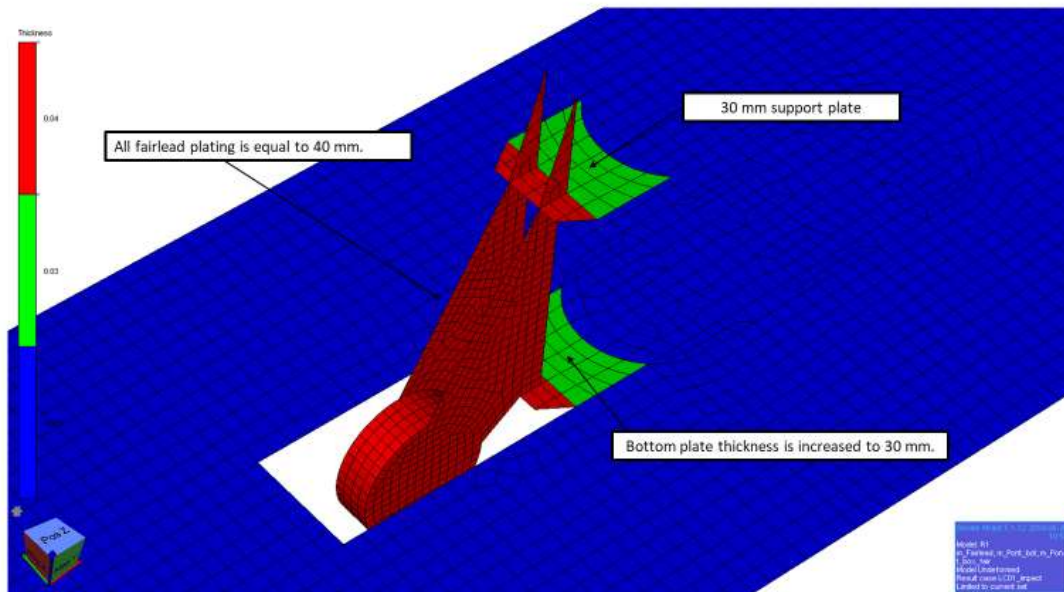
> *Figure 12-18 Thickness of fairlead plating and structural reinforcement in the fairlead intersection area*

12.5.4 Results

Both the fairlead itself and the surrounding pontoon structure have local linear stresses above the 365 MPa stress limit.
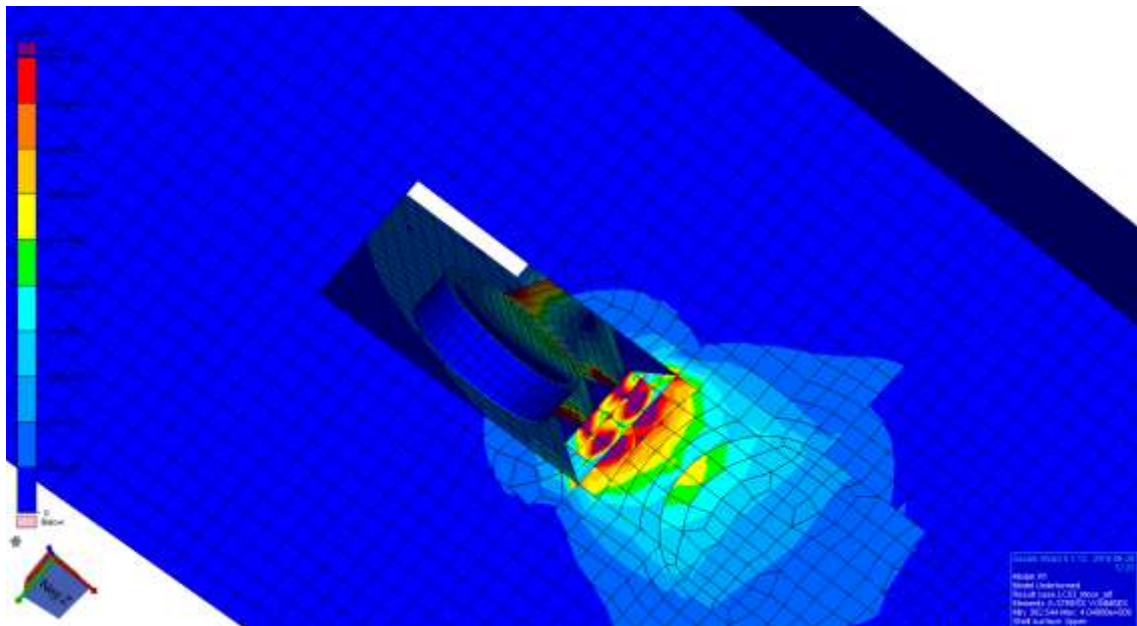
> *Figure 12-19 Finite element model shown with von Mises stresses, bottom view*
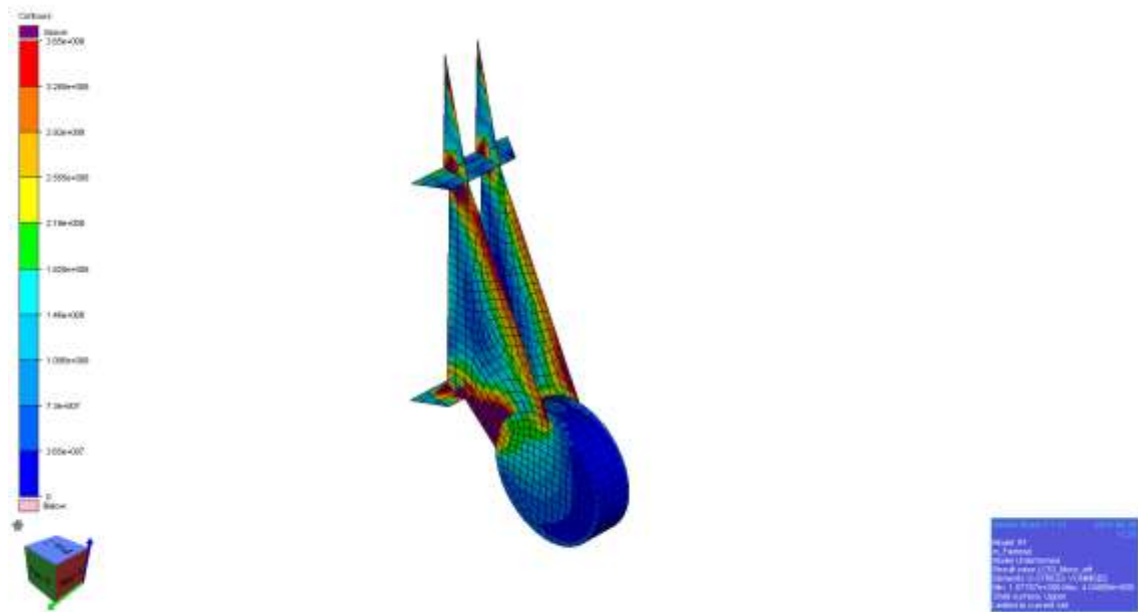
> *Figure 12-20 Fairlead, von Mises stresses*
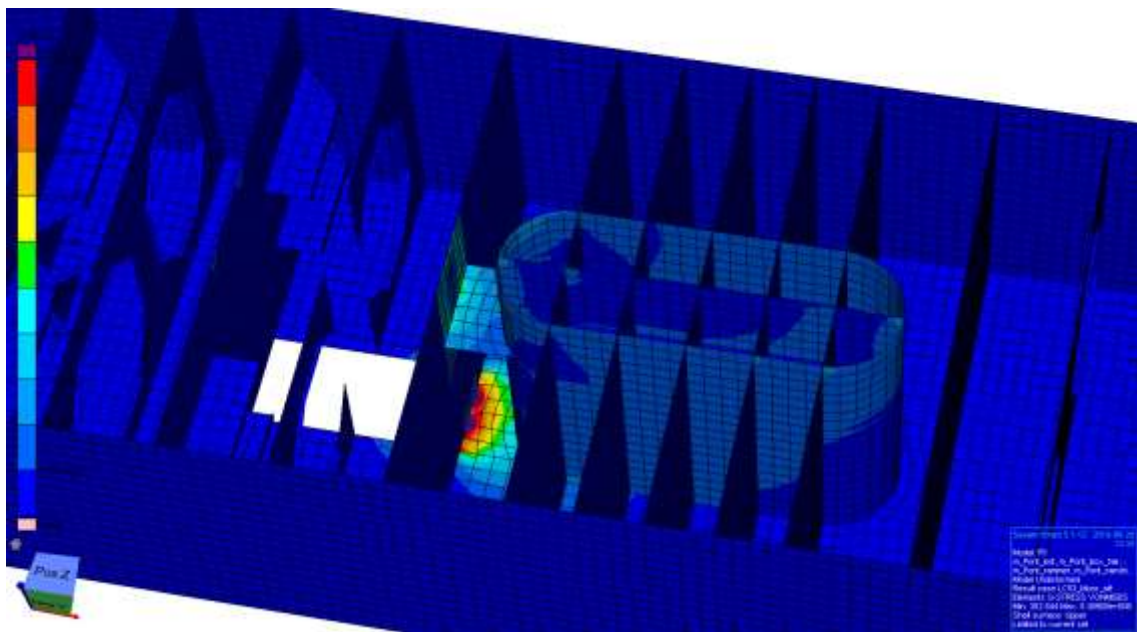
> *Figure 12-21 Critical parts of pontoon, von Mises stresses*

The fairlead is assumed to be designed for the anchor chain used by supplier or in detail design and is not further evaluated.

When it comes to the pontoon structure, local reinforcements will be necessary in the interaction areas with the fairlead. For the ULS condition these local reinforcements are considered feasible. Fatigue evaluations must be carried out in a later phase of the project.

13 MOORING

13.1 Influence on global structural behaviour

In the beginning of the project several principle mooring restoring stiffness levels were analysed with the global model to check the effect on response and modes of the entire bridge. It was decided that the mooring system should contribute at small amplitudes of transverse bridge displacement. It was also concluded that linear stiffness would be beneficial as this a predictable and reliable mooring response. The required stiffness to reduce the response of the bridge and alter the eigen modes was rather high and will thus limit the number of possible systems.

Based on the evaluation of ship impact and the risk of extreme events causing larger transverse motion of the bridge than expected in ULS it was considered beneficial to have a system with high elastic capacity ensuring that the system can provide restoring for significantly higher displacements than expected from extreme environmental loads.

13.2 Mooring system

Several mooring system configurations have been studied and evaluated in the project:
- Catenary system
- Taut system
- Taut system with intermediate buoyancy element connected to the pontoon to reduce transfer of vertical forces from the mooring system into the bridge
- Tension legs

A taut system consisting of fibre rope with sufficiently high flexibility and good elongation properties is considered to provide a rather linear restoring characteristic from the mooring. Due to practical aspects the fibre rope will typically be connected to chain at seabed/anchor and at the top of the mooring line to ease connection with the pontoon. These short chain segments will not alter the desired linear response of the mooring system as the stiffness of the system will be provided by the axial stiffness of the fibre rope. Taut systems are typically sensitive to creep as this might reduce the effective pre-tension and thus increase the risk of slack. The creep behaviour of known fibre ropes as polyester is well understood and documented from the oil&gas industry and can be accounted for during design and installation. Generally, it is important to ensure that the fibre rope is sufficiently bedded-in before installation to avoid creep due to the rope structure. It is also important to ensure that splices in the fibre rope is bedded-in to avoid elongation at these points during extreme loads. Bedding-in can be ensured by pulling the fibre rope during installation. It is expected that utilizing the installation vessel to pull the bottom chain and fibre rope before connection with the pontoon should provide sufficient bedding-in.

A taut line mooring system is proposed, consisting of polyester fibre rope as main component, with mooring chain towards the anchor and pontoon terminations. A principle sketch of the system is shown in Figure 5 3. A taut system based on polyester mooring will give a robust and reliable system with a practically linear restoring stiffness. The lines will generally also have additional capacity with respect to extreme offset beyond the expected ULS offset. The lines are prestressed to avoid "slack" during the expected range of pontoon motions. Slack in this context does not mean that the rope goes into compression, but that it loses its pretension and hence stiffness. As long as the bottom chain is lifted from the ground a minimum level of pre-tension is always ensured. The local analysis will be used to document the behaviour of the proposed configuration for expected extreme offsets.

The system will consist of proven components with a track record from the oil&gas industry and other marine industries. Polyester fibre rope has good fatigue properties possibly limiting the need for replacing the main mooring line during operation. The proposed system can rather easily be adapted to new anchor locations as the stiffness is given by the fibre rope geometry and can thus be adjusted based on changes in the design assumptions. The fibre rope dimension will typically be governed by the required stiffness of each mooring line providing significant additional capacity of the rope for extreme offsets in accidental conditions.

13.3   Mooring layout

13.3.1   Plan view

The mooring system consists of two groups of mooring lines, each group consisting of eight mooring lines. The lines in one group are connected to four pontoons, with one line to each side. The groups are to the extent possible equally spaced along the bridge length (Approximately at 1/3 and 2/3 of the length). The plan view of the mooring system is shown in Figure 13-1.
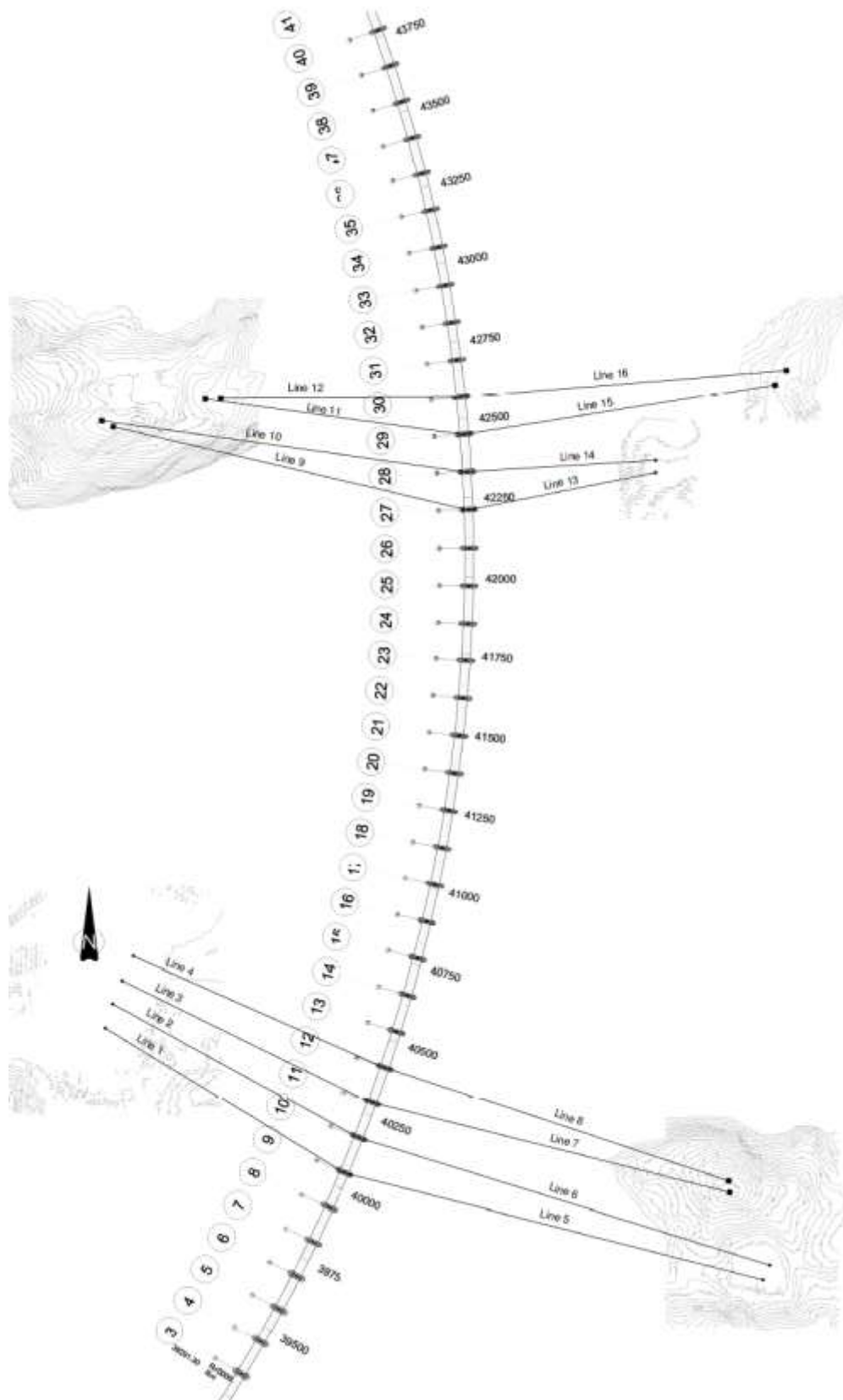
> *Figure 13-1: Mooring plan view*

13.3.2 Anchor positions, line lengths and depths

The geometric properties for the anchor lines is summarized in Table 13-1. Definition of the geometric values is shown in Figure 13-2.

> *Table 13-1 Anchor line geometric properties*

Line No	Horizontal length (m)	Anchor depth	Horizontal Angle (local)	Northing Pontoon	Easting Pontoon	Northing Anchor	Easting Anchor
1	913.5	-561.5	351.2	1 233 333.19	93 406.54	1 233 791.88	92 649.84
2	914.2	-561.2	352.3	1 233 444.16	93 452.09	1 233 868.78	92 673.69
3	905.8	-561.1	353.5	1 233 556.19	93 494.97	1 233 941.73	92 704.51
4	894.1	-561.2	354.3	1 233 669.21	93 535.15	1 234 019.10	92 739.73
5	1343.3	-359.3	188.7	1 233 333.19	93 406.54	1 232 996.20	94 734.33
6	1338.3	-359.2	184.4	1 233 444.16	93 452.09	1 233 042.63	94 756.02
7	1140.6	-291.7	186.1	1 233 556.19	93 494.97	1 233 271.95	94 625.02
8	1121.3	-296.5	180.5	1 233 669.21	93 535.15	1 233 308.72	94 622.53
9	1161.2	-123.2	344.1	1 235 438.93	93 801.78	1 235 699.97	92 679.12
10	1171.4	-123.5	347.9	1 235 558.78	93 796.68	1 235 720.03	92 643.06
11	829.5	-167.2	346.4	1 235 678.47	93 788.72	1 235 789.46	92 972.18
12	759.4	-158.1	353.0	1 235 797.93	93 777.88	1 235 793.91	93 021.29
13	598.6	-382.2	190.2	1 235 438.93	93 801.78	1 235 554.88	94 392.12
14	593.1	-380.5	181.1	1 235 558.78	93 796.68	1 235 594.93	94 392.40
15	992.0	-410.3	184.9	1 235 678.47	93 788.72	1 235 835.63	94 769.60
16	1030.0	-411.8	179.1	1 235 797.93	93 777.88	1 235 882.81	94 805.79
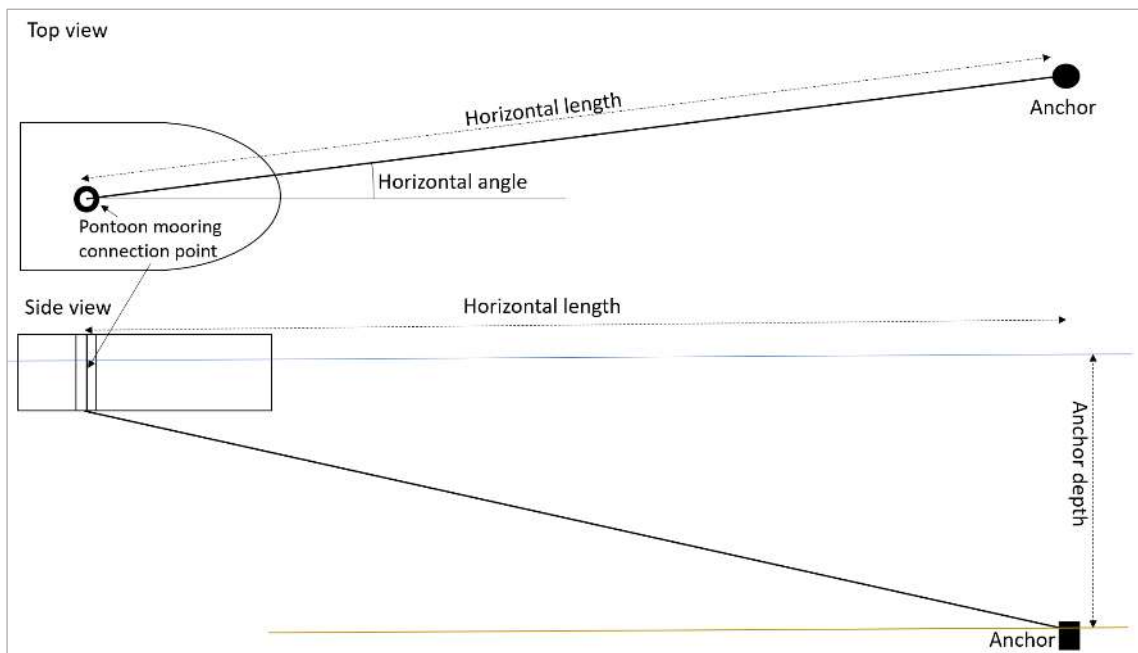
> *Figure 13-2 Definition of local system for angles and horizontal length/depth*

13.4 Mooring system components

A side view principle drawing is shown in the figure below. Then follows a summary of the main features of the different components.
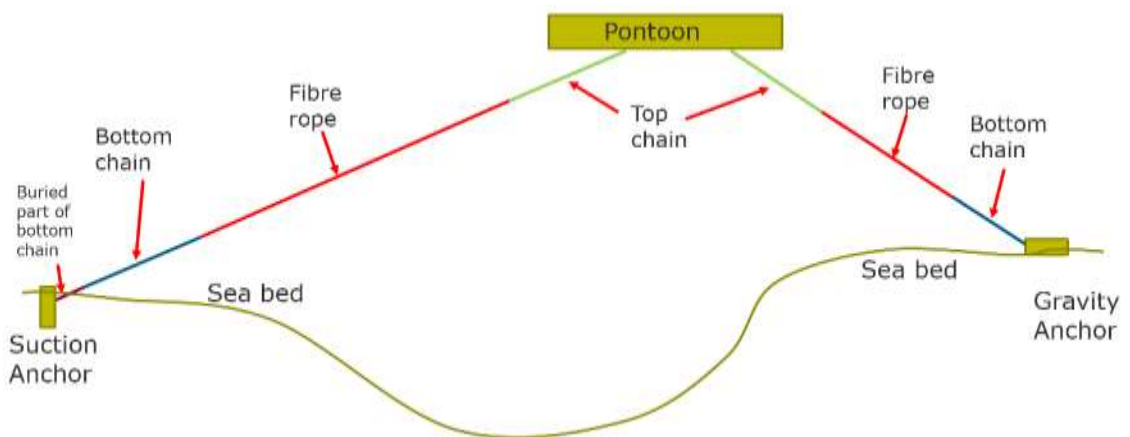
> *Figure 13-3 Principle drawing (side view) of one pair of mooring lines.*

Buried part of bottom chain (for lines to suction anchors only):

- Installed together with anchor
- Not inspectable, and hence more complicated to replace.
- Must be robust wrt. fatigue and corrosion

Bottom chain:

- Sufficient length to prevent contact between fibre rope and seabed.
- Easy connection to preinstalled anchor by ROV.
- Design lifetime may be an issue due to corrosion and fatigue.
- Proven for long term mooring in the oil and gas industry.

Fibre rope:

- Good elongation characteristics – gives nearly linear force-deformation curve.
- Easy to handle due to low weight
- Fatigue is not expected to be an issue
- Proven for offshore applications (i.e Aasta Hansteen spar platform and Goliat FPSO)

Top chain:

- Robust during installation and tensioning (wear and tear)
- Gives termination of fibre rope at reasonable depth, reducing risk of damage by ship propeller and degradation by marine growth and UV light.
- Gives tolerances for determining pre-constructed rope lengths and
- Easy to replace
- Corrosion and fatigue (tension-tension and OPB) may be an issue.
- Proven for long term mooring in the oil and gas industry

The main dimensions in the mooring line bodies is summarized in Table 13-2.

> *Table 13-2 Anchor line geometric properties*

Line No	Bottom Chain (R4 studless)		Polyester fibre rope		Top Chain (R3 studless)	
	Dim(mm)	Length(m)	Dim(mm)	Length(m)*	Dim(mm)	Length(m)
1	100	60	177	985	146	25
2	100	60	177	985	146	25
3	92	60	177	978	146	25
4	92	60	177	968	146	25
5	100	75	185	1279	146	35
6	100	75	185	1274	146	35
7	92	50	168	1091	146	35
8	92	50	168	1074	146	35
9	92	70	177	1047	146	50
10	92	175	168	952	146	50
11	92	70	145	725	146	50
12	92	50	145	675	146	50
13	92	50	145	633	146	25
14	92	50	145	627	146	25
15	92	150	168	897	146	25
16	92	100	177	982	146	25

Note: that the rope lengths are stretched lengths, adjustments due to bedding in and elastic elongation from permanent prestressing are not accounted for.

13.5   Global analyses

13.5.1   Model

In the global analyses model the mooring system is simplified by use of a single cable element oriented in the correct direction and with correct length. The single element acts as a spring, where the stiffness input is given in terms of a mooring line cross sectional area and corresponding elastic Young's modulus. The corresponding elastic stiffness is hence given as $k_{mooringline} = \frac{EA}{L}$.

The main functional requirement for the mooring line groups is to have sufficient horizontal stiffness to provide the same stiffness as estimated based on the global analyses. The global analysis indicated that a minimum required stiffness per group would be in the range of 0.6 MN/m. A minimum mooring group stiffness of 0.8 MN/m is thus set as a requirement for the mooring system design to account for uncertainty. This corresponding to 0.1 MN/m per line in horizontal direction and normal to the bridge.
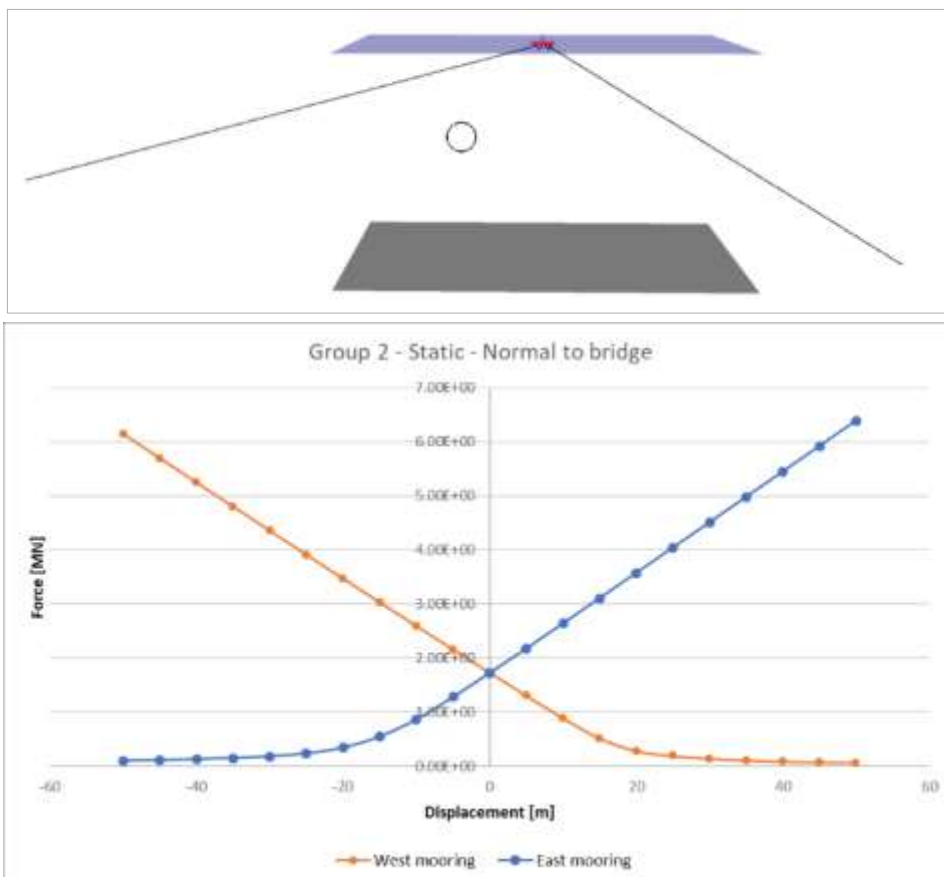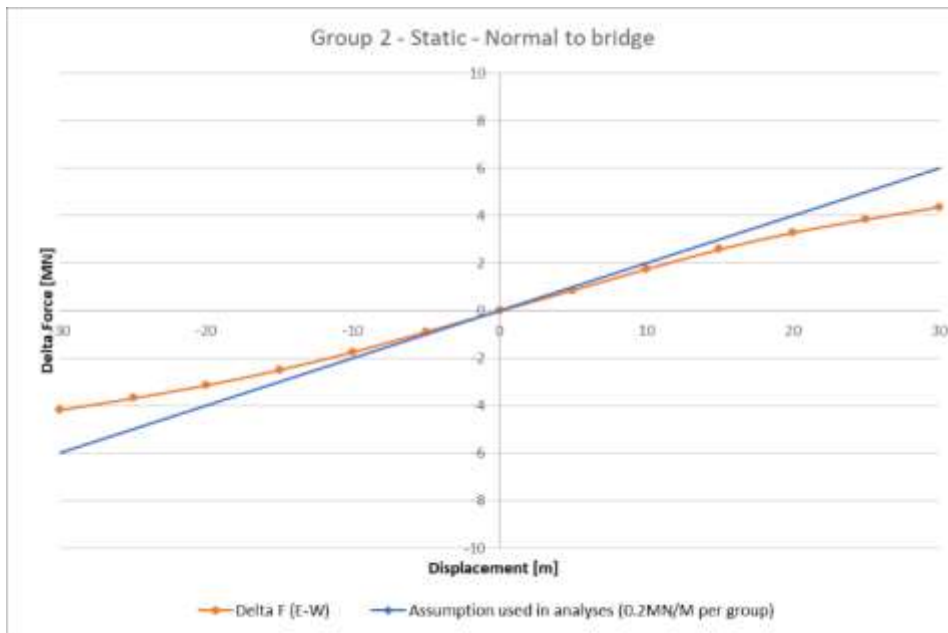
> *Figure 13-4: Example, static configuration, line behaviour and anchor group stiffness for group 2*

The mooring system in the global model is represented by linear springs with positive and negative tension values. The variation represents the dynamic variation in line force for different pontoon positions. The pre-tensioning level of the final configuration will be set to avoid slack in the mooring system. The mooring line forces are given in terms of local axial direction.

The pretension in each mooring line connected to the same pontoon is tuned to give equal load component normal to the bridge. This may result in different prestressing load in each line due to different line geometry. It will also result in different load components in the vertical direction as well as along the bridge. The line pretension varies from 1.6-2.3 MN.

13.5.2 Response in ULS operational condition

The operational loads mainly consist of:

1. Environmental loads
   a. Dynamic loads
      i. Wind sea
      ii. Swell
      iii. Dynamic component of wind forces
   b. Quasi-static loads
      i. Current
      ii. Tidal loads
      iii. Static components of wind force
      iv. Temperature
      v. Marine fouling on pontoons
2. Traffic loads

The load response component for each mooring line is summarized in Figure 13-5.

Figure 13-5 Load components in mooring line

The figure shows that approximately 50% of the load component is environmental dynamic loads, while the remaining is traffic and quasi-static environmental loads. Marine growth on the pontoons gives negligible loads in the moorings.

13.5.3 Ship impact

Reference is made to Ref. [11] for description of the response in the pontoons due to ship impact. The response of the bridge during ship impact is modelled by imposing time series of the displacements in the pontoons with mooring line attachment. Linear mooring behaviour is assumed in the ship impact analyses. A selection of time series showing total pontoon deflection is further shown in Figure 13-6.
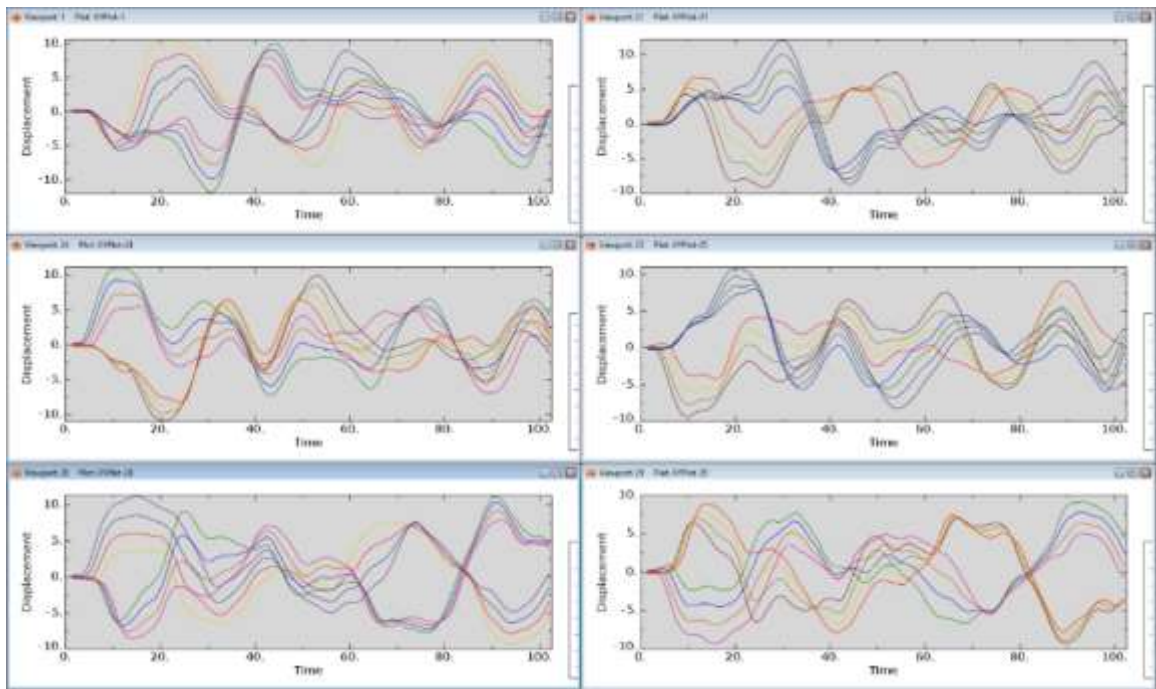
> *Figure 13-6 Ship impact time series for pontoon displacements.*

Compared to the ULS load combinations, the displacement and hence mooring line forces are of comparable magnitude. Given the reduced load factors in ALS, the mooring lines will show lower utilizations from ship impact than for the ULS condition.

13.5.4   Mooring line utilization

The following nominal and factored loads are shown in Figure *13-7*:

- Unfactored - Maximum load
    - Characteristic maximum loads from global model including pretension
- Unfactored – Minimum load
    - Characteristic minimum loads from global model including pretension
- Maximum factored:
    - ULS – DNV E-301 with ISO19901-7 B.2 factors.
    - Safety factor equal 2.2 on all load components
- Minimum factored:
    - ULS EQU – factorized Minimum loads
    - Factor 0.9 on pretension loads
    - Factor 1.6 on all other loads

As seen from the figure, the maximum dimensioning loads in ULS intact condition is 7.3 MN, and all lines above 0MN for ULS EQU.
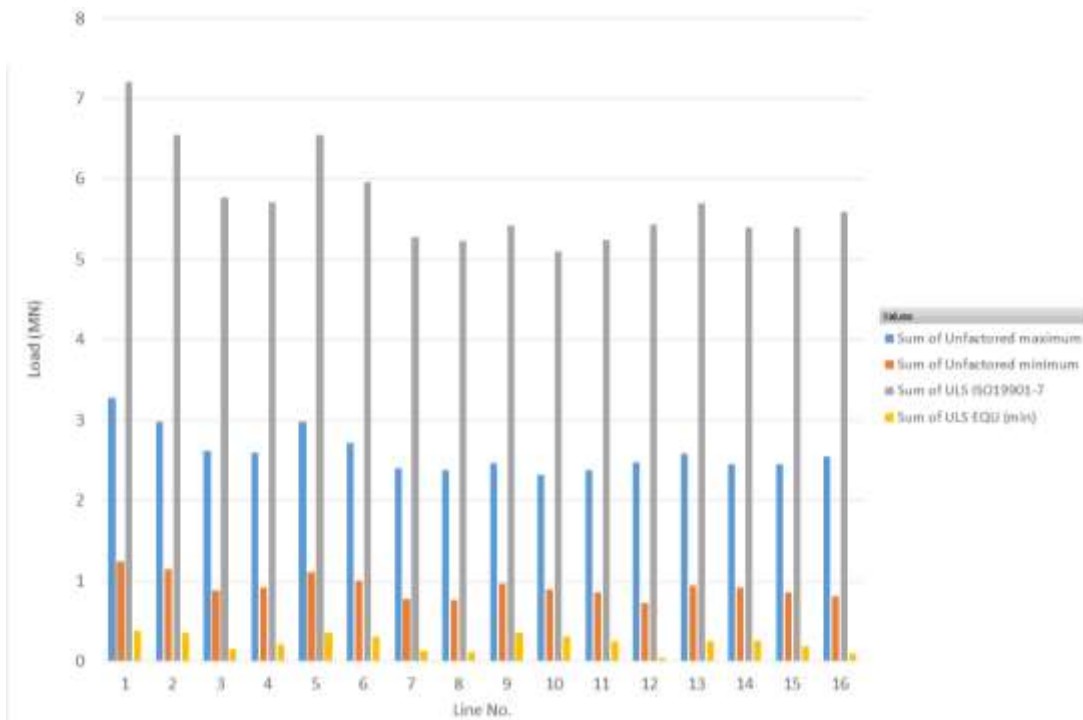
> Figure 13-7 Unfactored and factored loads

The utilization of the different mooring line segments is summarized in Table 13-3 below. All mooring line segments have sufficient capacity according to the design requirements.

> *Table 13-3 Utilizations*

Line No	Bottom Chain		Polyester fibre rope	Top Chain	
	Uncorroded	Corroded (50 year)		Uncorroded	Corroded (50 year)
1	0.77	0.95	0.77	0.40	0.76
2	0.68	0.84	0.62	0.36	0.68
3	0.70	0.86	0.70	0.37	0.69
4	0.62	0.77	0.57	0.33	0.62
5	0.72	0.90	0.62	0.32	0.61
6	0.65	0.82	0.62	0.29	0.55
7	0.71	0.89	0.61	0.32	0.60
8	0.64	0.81	0.62	0.29	0.55
9	0.67	0.84	0.58	0.30	0.57
10	0.69	0.87	0.86	0.31	0.59
11	0.63	0.80	0.61	0.28	0.54
12	0.68	0.86	0.84	0.31	0.58

13	0.65	0.82	0.80	0.29	0.55
14	0.66	0.83	0.63	0.30	0.56
15	0.67	0.85	0.83	0.30	0.57
16	0.69	0.86	0.59	0.31	0.59

13.5.5   Fatigue analyses

Fatigue analyses are carried out for the main mooring line components such as top chain, bottom chain and fibre rope. The following failure modes are investigated:

Tension-Tension (low cycle fatigue)	TT
In-plane Out-of-Plane Bending (low cycle fatigue)	IPB/OPB
Vortex induced vibrations (high cycle fatigue)	VIV

Table 13-4 and Figure 13-8 present the relevant and analysed failure mode for each component. VIV on top- and bottom chain is written in parentheses as VIV is not expected on chains itself. However, VIV on fibre rope will cause a stress range in the entire mooring line and hence also indirectly affect fatigue damage of the chains.

Component	Fatigue failure mode
Top chain – segment 1	Tension -Tension (VIV on fibre rope)
Top chain – segment 2	In-plane out-of-plane bending (at fairlead) (VIV on fibre rope)
Bottom chain	Tension -Tension (VIV on fibre rope)
Fibre rope	Tension -Tension Vortex induced vibrations

> *Table 13-4 Fatigue failure mode per component*
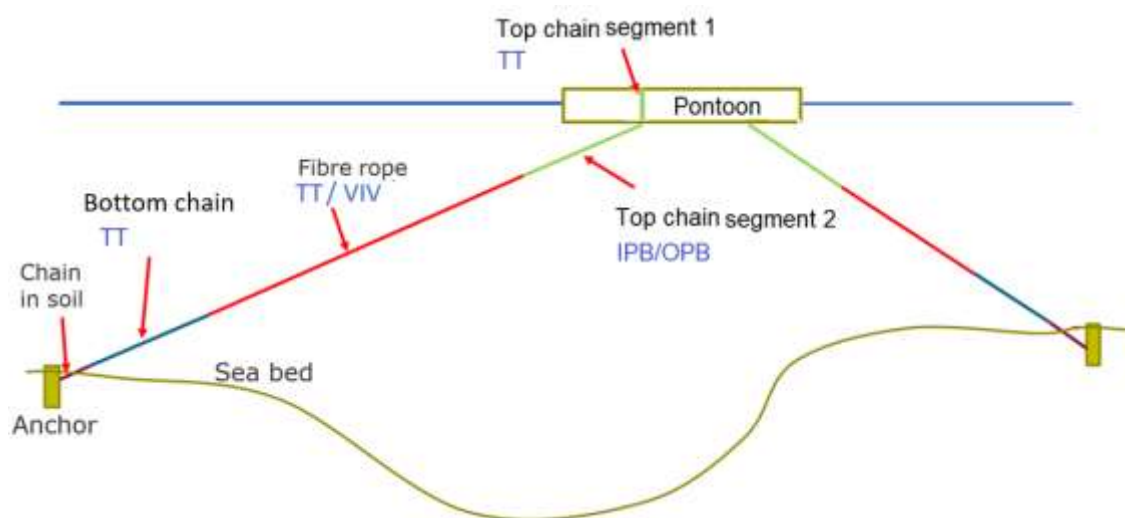
> *Figure 13-8 Fatigue failure mode per component*

13.5.6 Fatigue design life

The fatigue life is generally 100 years or more for all main mooring line components, except from the top chain at fairlead which has a fatigue life of 25 years. The fatigue damage for the top chain is caused by out-of-plane and in-plane bending of the chain at the fairlead. More refined analysis and design of the fairlead might reduce the damage. Corrosion allowance is accounted for when evaluating the capacity of the mooring lines.

Results for in-plane and out-plane fatigue combined with tension-tension fatigue are summarised in Table 13-5. Damage is presented for 25years and the four different SCF locations (see Figure 13-9). Damage is below 1.0 for all SCF locations for 25years of design life.

The maximum damage is found for SCF case C ref. Table 13-5. Figure 13-10 presents results for case C. The x axis in this figure presents the four locations of link 1 and 2 with link2 being 90deg rotated in regard to link 1 (see also Figure 13-9).

Line ID	Damage - 25year-(incl. DFF) Maximum of location 1-4 and link 1 and 2			
	SCF hotspot A	SCF hotspot B	SCF hotspot B'	SCF hotspot C
01	3.72E-02	0.68	0.85	0.91
02	2.88E-02	0.67	0.83	0.89
03	1.69E-02	0.43	0.53	0.57
04	2.41E-02	0.43	0.54	0.57
05	3.46E-02	0.55	0.68	0.73
06	2.75E-02	0.53	0.66	0.71
07	1.63E-02	0.35	0.44	0.47
08	2.61E-02	0.36	0.45	0.48
09	3.73E-02	0.34	0.42	0.45
10	2.34E-02	0.27	0.34	0.37
11	2.12E-02	0.27	0.34	0.36
12	3.34E-02	0.27	0.33	0.35
13	2.86E-02	0.47	0.58	0.63
14	1.83E-02	0.35	0.44	0.47
15	2.38E-02	0.31	0.39	0.42
16	3.21E-02	0.30	0.37	0.40
Max	0.04	0.68	0.85	0.91

> *Table 13-5 Fatigue damage, top chain IPB/OPB*
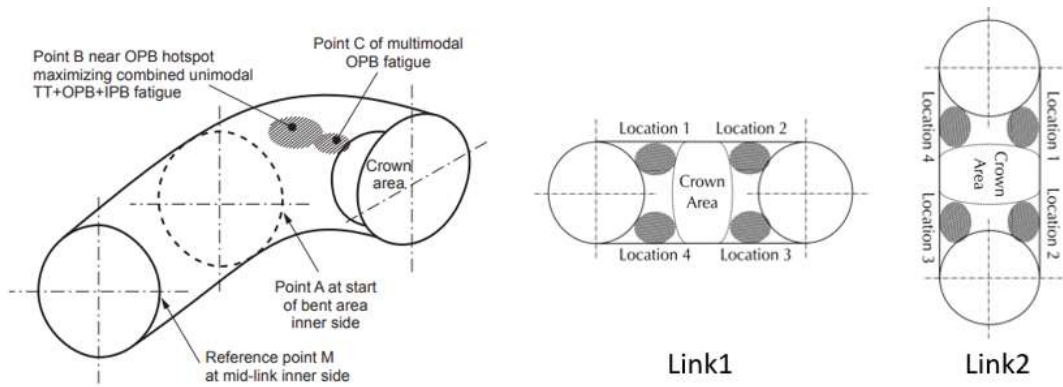
> *Figure 13-9 SCF and failure locations*
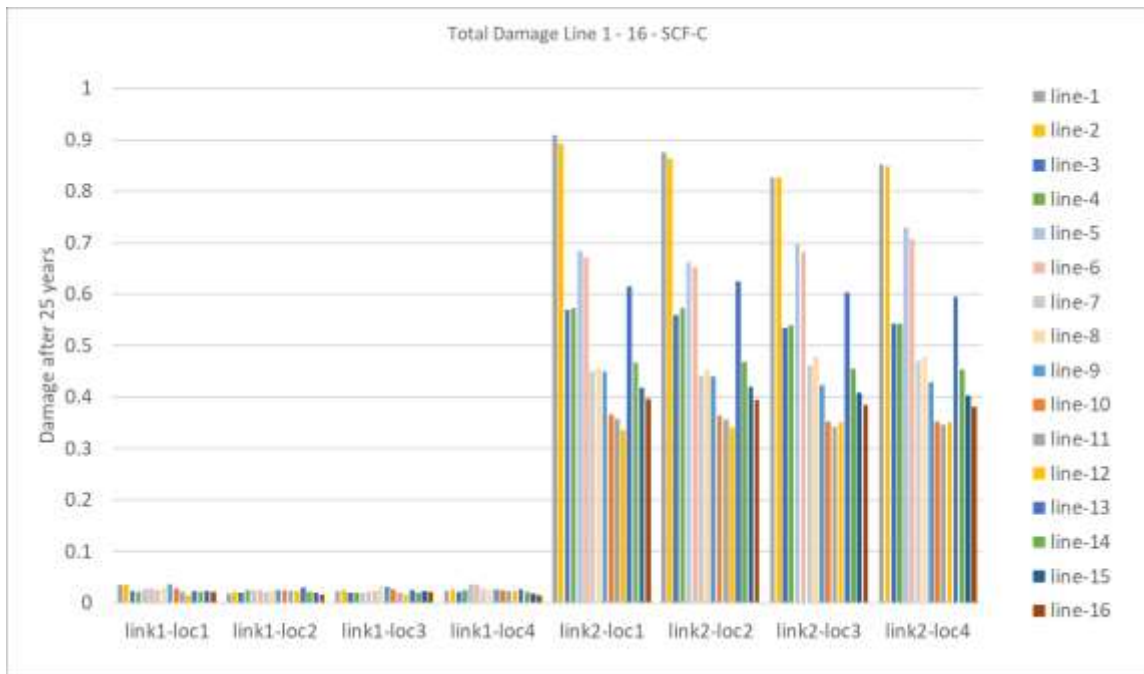
> *Figure 13-10 Fatigue damage, top chain IPB/OPB – SCF hotspot C*

14 ANCHORING

14.1 Bathymetry and isopach

The fjord is asymmetrical with undulating seabed. On the southern side there is a steep inclination down to the basin. The basin itself stretches out almost two thirds of the crossing distance and has a depth of about -550 m. The last part in the north, which is shallower from about -150 m to -50 m depth, consists mainly of exposed bedrock as shown in Figure 14-1. The map below shows the bathymetry, prepared by NGI. ref. [40], coast line from "Felles KartdataBase" in red and height contours on land from Hoydedata.no.
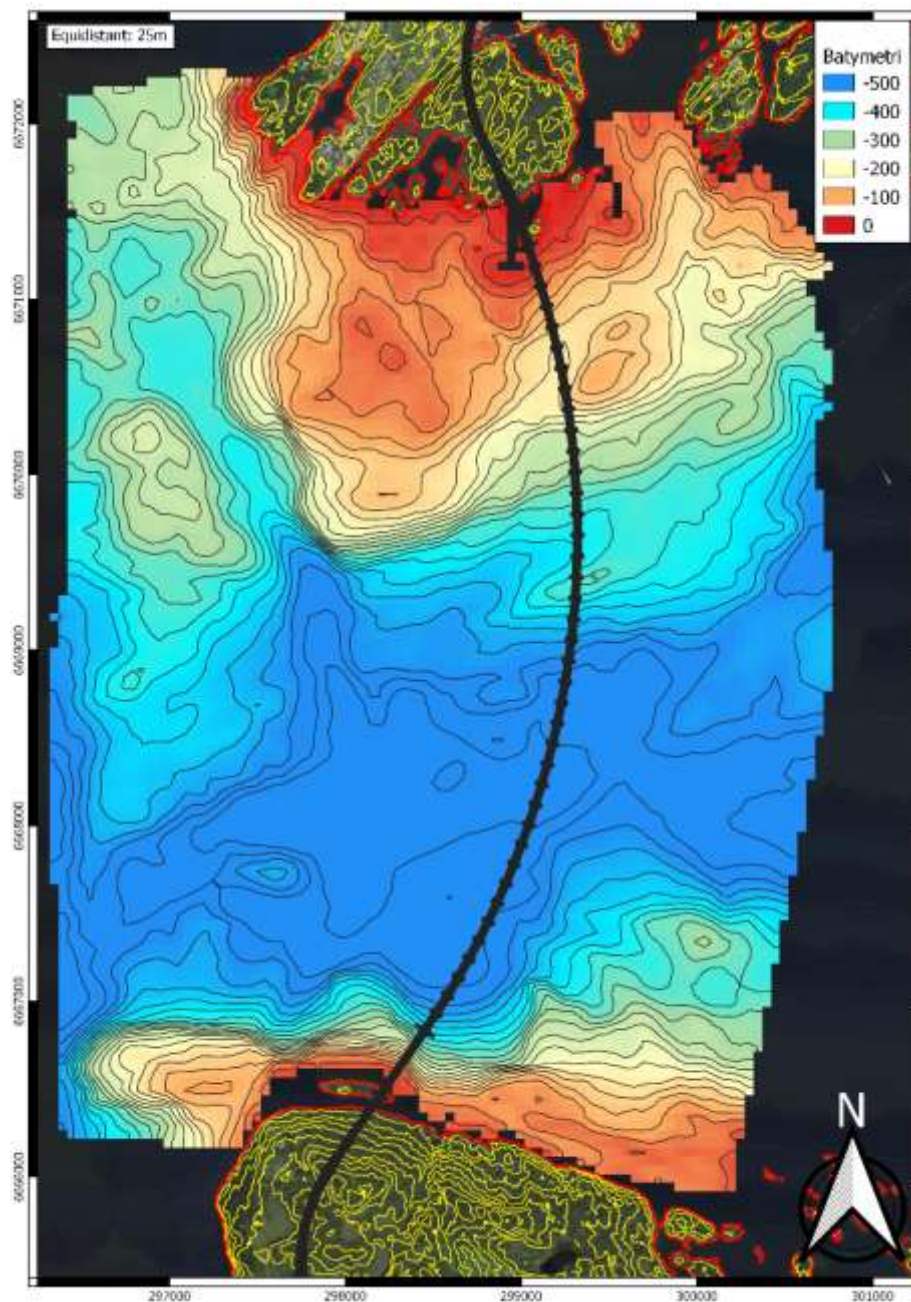
> *Figure 14-1: Bathymetry of Bjørnafjorden shown together with proposed anchor locations*

Acoustic measurements were done in 2016 and 2018 by DOF SubSea. Figure 14-2 presents the post-processed data done by OON which includes data from 2018. Although deviation in depth to bedrock is expected, in this phase the isopach is assumed to be exact. The bedrock can thereby be calculated by subtracting the bathymetry with the isopach map which is shown in Figure 14-3.

> *Figure 14-2 - Interpolated isopach from data provided by DOF 2016 and 2018 shown together with proposed anchor locations.*
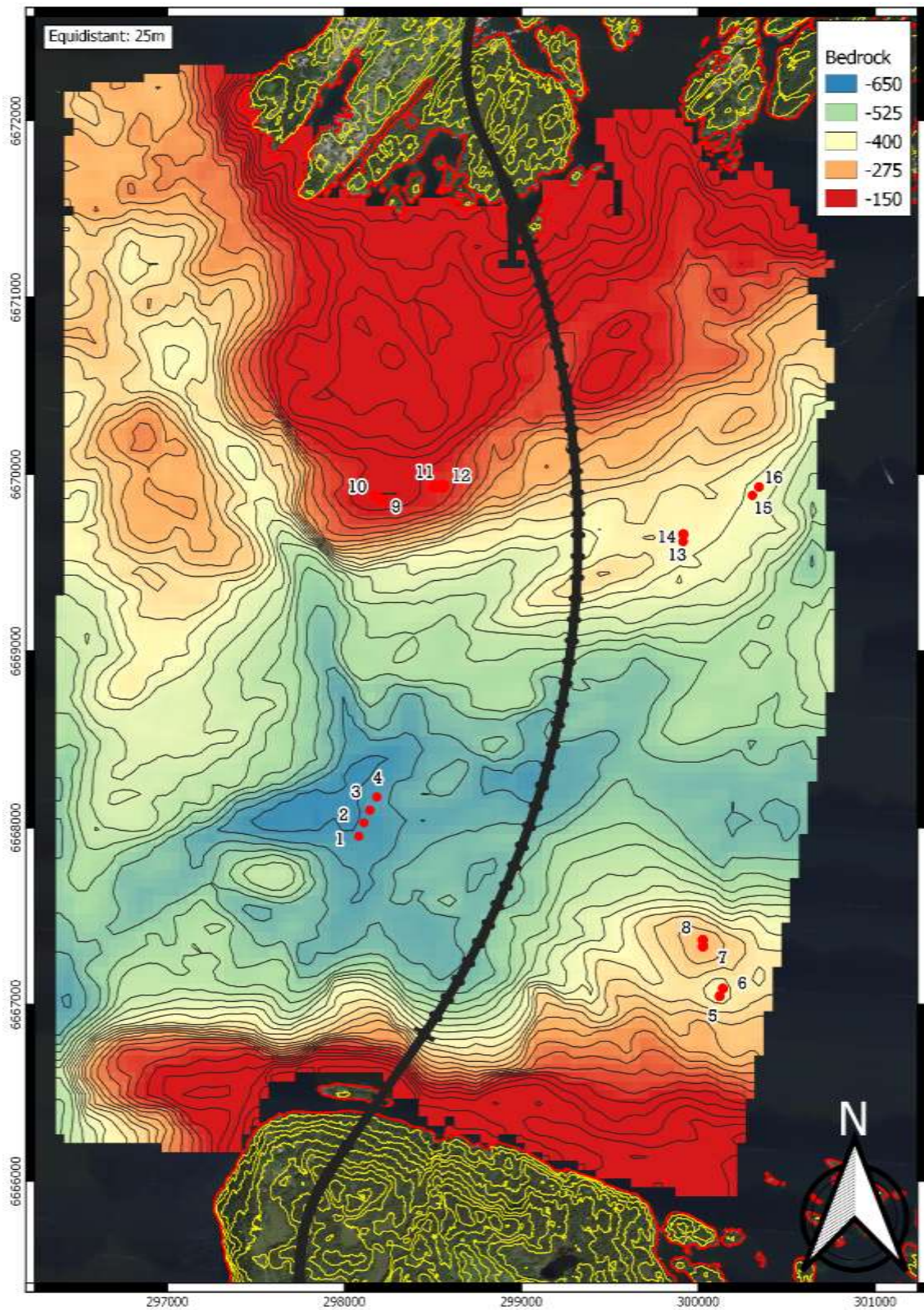
> *Figure 14-3 – Calculated bedrock based on measured bathymetry and isopach.*

14.2 Soil conditions

Where soil is present, slightly overconsolidated clay is assumed. This is based on measured and derived parameters, ref. [41]. In-situ geotechnical data and soil samples are only collected at 5 locations, all of them taken in the central flat seabed basin.

> *Table 14-1 Summary of representative soil parameters ref. [42].*

z (m)	w (%)	γ (kN/m³)	γ_s (kN/m³)	I_p (%)	FC (%)	CC (%)	OCR (-)	S_t (-)	S_{uD}/S_{uC} (-)	S_{uE}/S_{uC} (-)
0 - 46	70 - 41	15.7 - 18.0	27.3	35	96	50	3.6 - 1.2	4	0.75	0.60

Note that the soil density increases linearly with depth. As a simplification a constant value will be used in calculations. In most cases 16 kN/m³ will be used. In special cases with deep failure zones the value may be increased and vice versa for shallow failure zones.

14.3 Anchor locations

The anchors are placed at approximately 1/3 and 2/3 of the bridge length within the following main limitations:

- Maximum mooring line length 2000 m
- Inclination from seabed max. 45 °

The anchor clusters are placed such that the overall bridge response is reduced and thereby also reducing the mooring load. The anchor locations have been chosen based on a geohazard assessment, maximum attainable holding capacity and installation requirements. The last requirement involves keeping the lines as normal as possible to the arc of the bridge.

Gravity anchors are here considered to be the most reliable and predictable type and have therefor been prioritized when considering possible anchor locations. In total 8 locations have been found to be suitable for using gravity anchors.

For the rest of the anchors, the anchors are placed at areas where the soil thickness is the highest. The reasoning behind this is that the anchors can be embedded further down to achieve higher holding capacity if required. Based on previous experience and the surrounding terrain, it is proposed to use suction anchors for the 8 remaining anchors with varying skirt lengths. The anchor locations are shown in Figure 14-1 and Figure 14-2.

> *Table 14-2 Summary of proposed anchor locations in UTM32N and NN2000 coordinates.*

Group	ID	East	North	Elevation [m]	Isopach [m]	Seabed inclination [°]	Anchor type
1	1	298080.6	6667952.1	-561.5	58.6	1.2	Suction
	2	298108.5	6668027.6	-561.2	57.4	0.3	Suction
	3	298143.2	6668098.9	-561.1	54.2	0.4	Suction
	4	298182.4	6668174.3	-561.2	47.1	0.8	Suction

2	5	300120.3	6667047.1	-359.3	35.1	0.7	Suction
	6	300144.4	6667092.3	-359.2	30.0	1.0	Suction
	7*	300025.7	6667328.3	-291.7	5.6	1.6	Gravity
	8*	300025.2	6667365.1	-296.5	6.5	16.4	Gravity
3	9	298210.9	6669856.1	-123.2	0	2.5	Gravity
	10	298176.0	6669878.1	-123.5	0	2.4	Gravity
	11	298508.3	6669930.0	-167.2	1.9	3.2	Gravity
	12	298557.6	6669931.8	-158.1	1.8	3.0	Gravity
4	13	299914.0	6669620.5	-382.2	15.5	0.8	Suction
	14	299916.4	6669660.5	-380.5	13.7	3.1	Suction
	15	300305.9	6669880.9	-410.3	0.8	3.4	Gravity
	16	300344.5	6669926.1	-411.8	1.3	2.7	Gravity

* The values are measured at the seabed, and thus not representative since the soil will be dredged and partially exchanged with crushed rock prior to anchor installation.

14.4 Geohazard and slope stability

14.4.1 Screening of anchor locations

Several hazard maps have been developed by NGI in the previous phase, ref. [42]. These have been used for preliminary anchor site evaluation. Most of the geohazard calculations are based on an assumption of infinite slope with undrained shear failure with linearly increasing weight and shear strength. It is observed that the results are closely tied to the slope angle both for the calculated static FoS and the estimated maximum transient shear strain for an earthquake with an annual exceedance probability of 2750 years recurrence period. This is due to increasing shear strength and increasing in-situ stress with depth. Figure 14-4 and Figure 14-5 indicates that several areas are unstable.
A similar static FoS has been calculated by OON using SAGA GIS. Drained, infinite slope failure is assumed with a constant value of friction angle, saturation, density and cohesion. The isopach is also included in the calculations, however the software does not distinguish between soil and rock, i.e. showing poor slope stability at steep areas. Note that the friction angle has been scaled so that the FoS by OON matches the one calculated by NGI and is thus not representative for drained analysis. The purpose of the calculation was to extend the static FoS to the area that was measured by DOF SubSea in 2018.
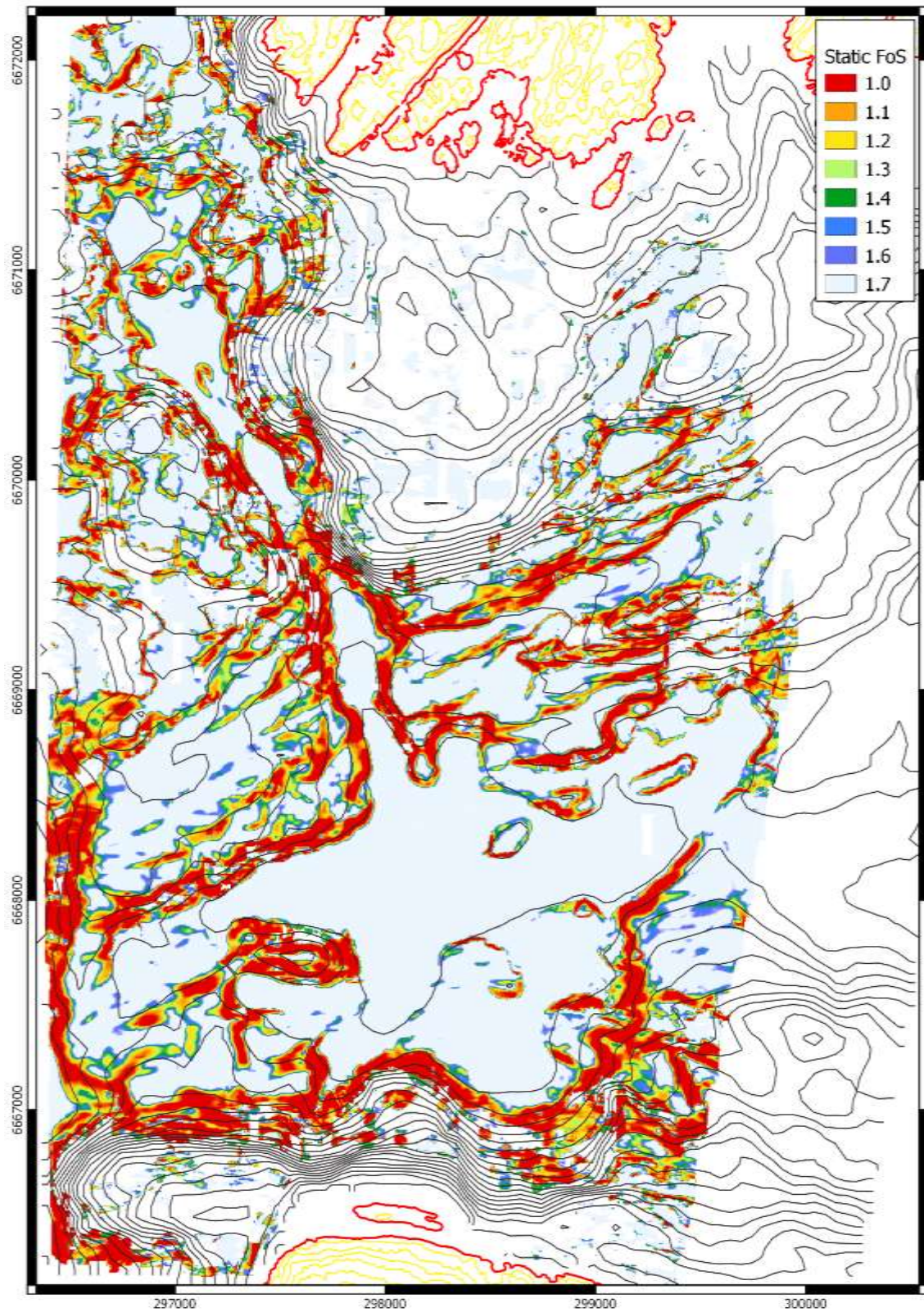
> *Figure 14-4 Static Factor of Safety calculated by NGI, ref. [42].*
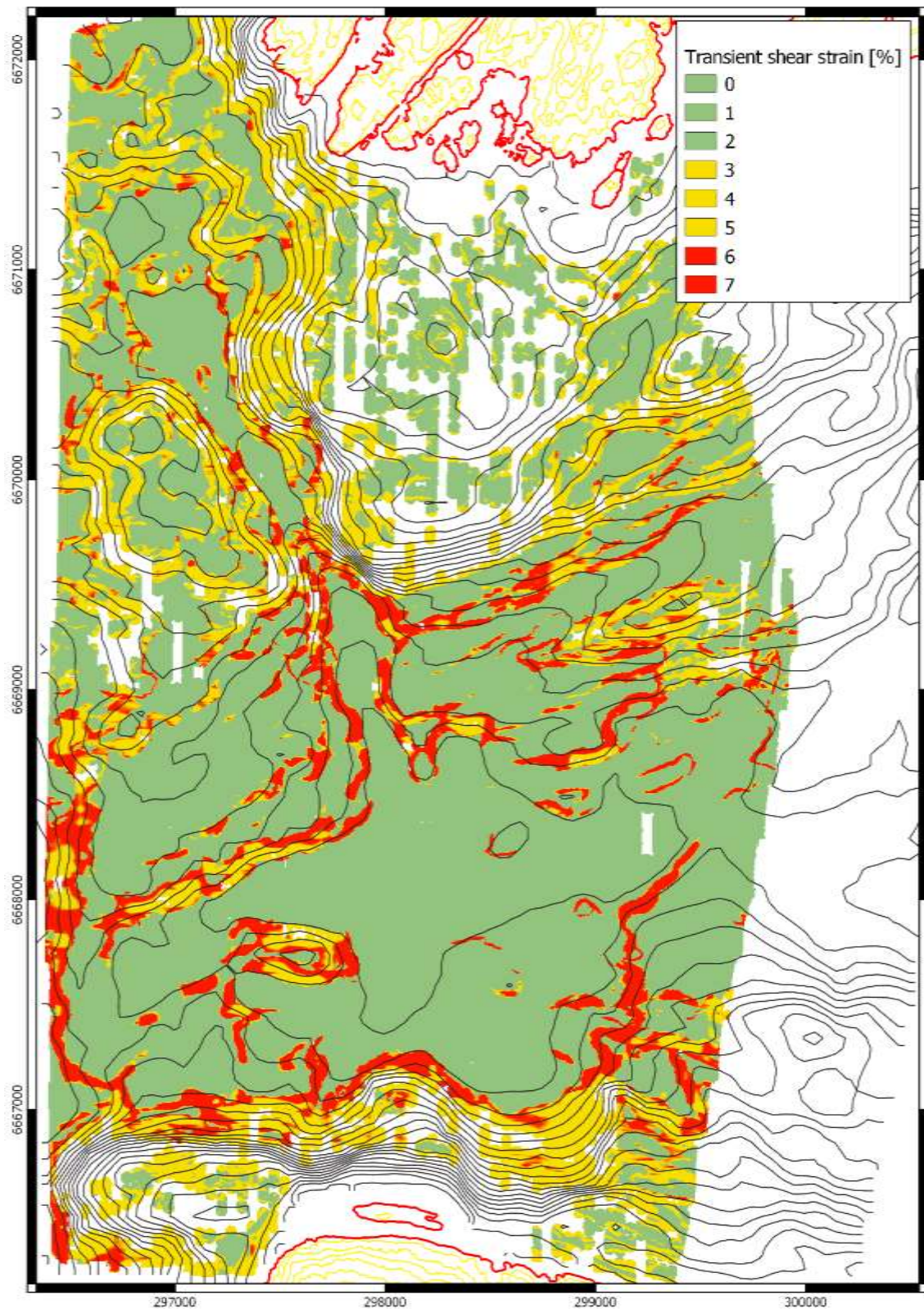
> *Figure 14-5 Maximum transient shear strain [RP=2750 years] calculated by NGI, ref. [42].*

Based on required holding capacity and installation requirements, certain criteria for anchor location has been defined. The proposed criteria given in the design basis for Mooring and anchor, ref. [25], has been used as a starting point. The maximum seabed slope is here restricted to 7.5° for suction and plate anchors and the maximum soil thickness for gravity anchors is restricted to 5 m. Furthermore, a distinction is made between areas with more than 15 m soil thickness, since here higher holding capacity can be achieved by embedding the anchor deeper.
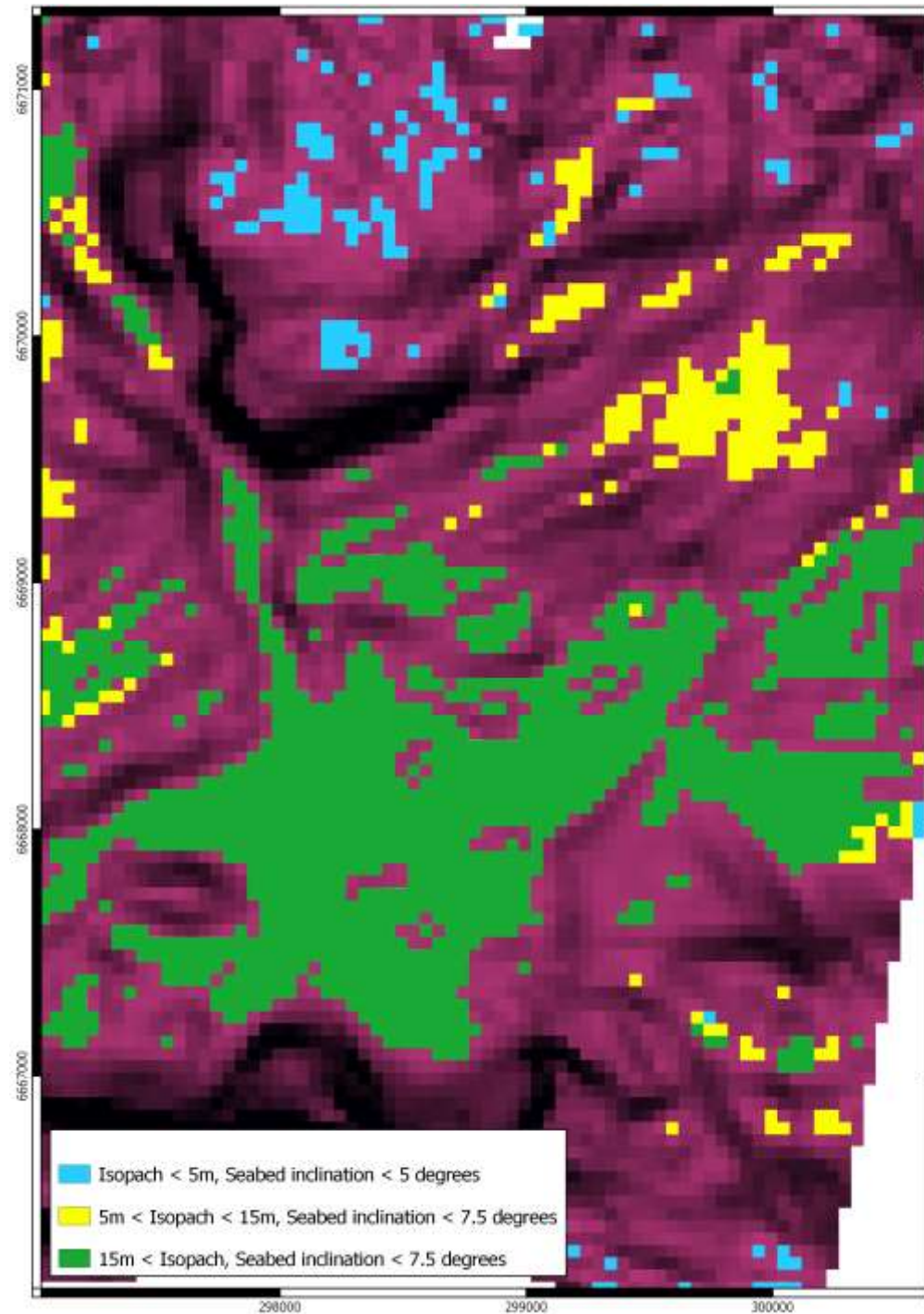
> *Figure 14-6 Anchor criteria used when selecting and evaluating anchor locations.*

14.4.2 Summary of slope stability results

The global slope stability is checked for what is regarded to be the most critical slopes near the anchor locations, as shown in Figure 14-7. For anchor locations 7 to 12 no critical slopes are considered to affect the anchors. Stability calculations are carried out for Profiles shown in the figure below. Calculations for Profile G4 A-A are valid for a preliminary position of anchor 13 and 14.
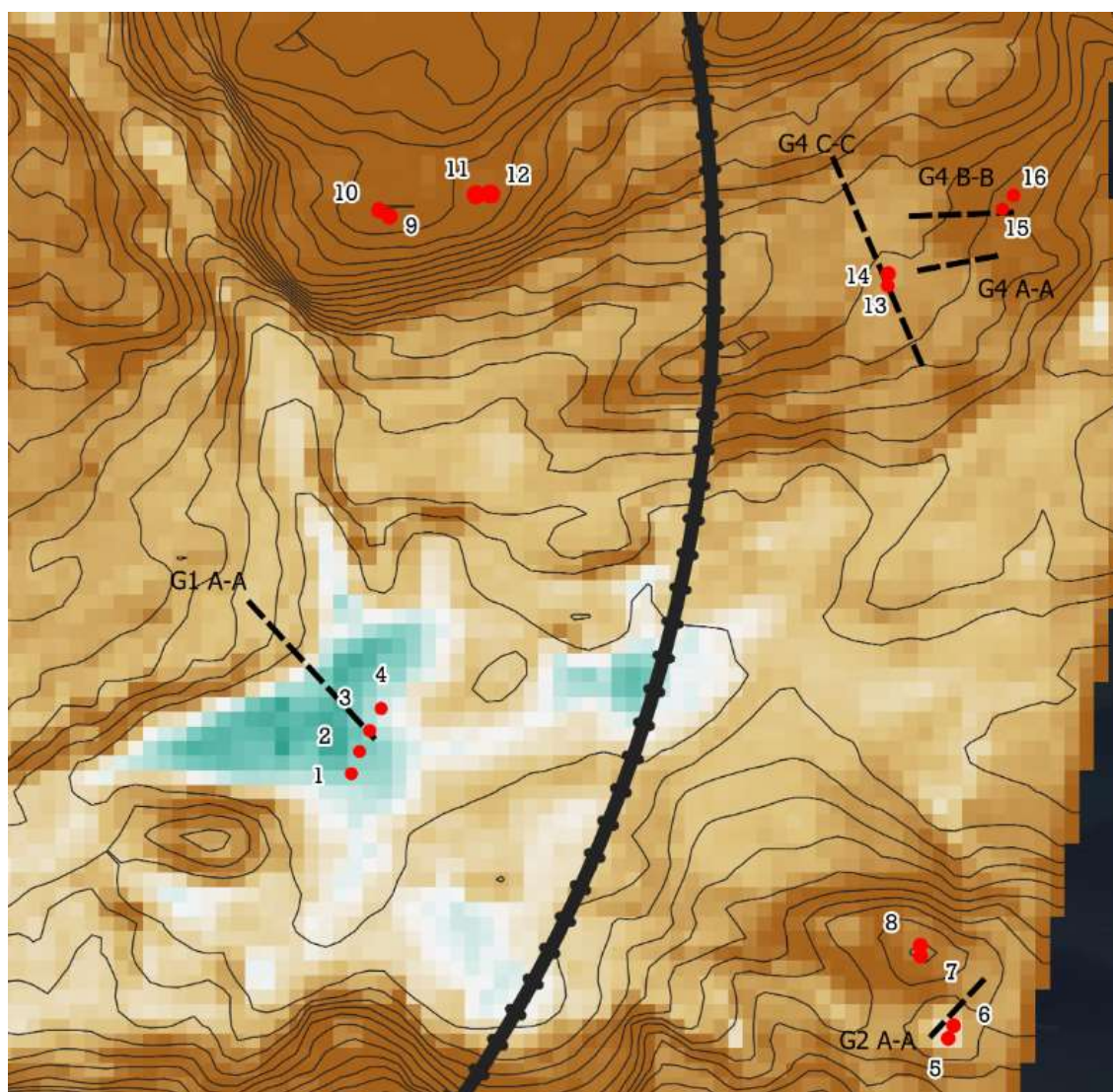
> *Figure 14-7: Anchor locations with profiles for Geosuite stability checks*

Table 14-3 shows the calculated factor of safety for undrained and drained static slope stability of failures that do not and do reach the anchors:

- F_c: Undrained static slope stability calculated safety factor for the most critical failures surfaces in the profile
- $F_{c,a}$: Undrained static slope stability lowest calculated safety factor for failure surfaces that reach the anchor locations
- $F_{c\varphi}$: Undrained static slope stability calculated safety factor for the most critical failures surfaces in the profile

- $F_{c\varphi,a}$: Undrained static slope stability lowest calculated safety factor for failure surfaces that reach the anchor locations
-

> *Table 14-3: Calculated factor of safety for undrained and drained static slope stability*

Profile	F_c	$F_{c,a}$	$F_{c\varphi}$	$F_{c\varphi,a}$
G1 A-A	1.23	2.32	1.76	4.73
G2 A-A	1.29	1.57	1.78	2.25
G4 A-A	1.72	-	2.18	-
G4 B-B	2.39	-	2.69	-
G4 C-C	1.14	2.24	2.22	6.27

In conjunction with dynamic slope performance, static slope stability has been calculated for 15 different profiles in Plaxis 2D. Thus, the same Plaxis models is used for dynamic and static analysis with different loading and boundary conditions. The profiles are shown in Figure 14-8.
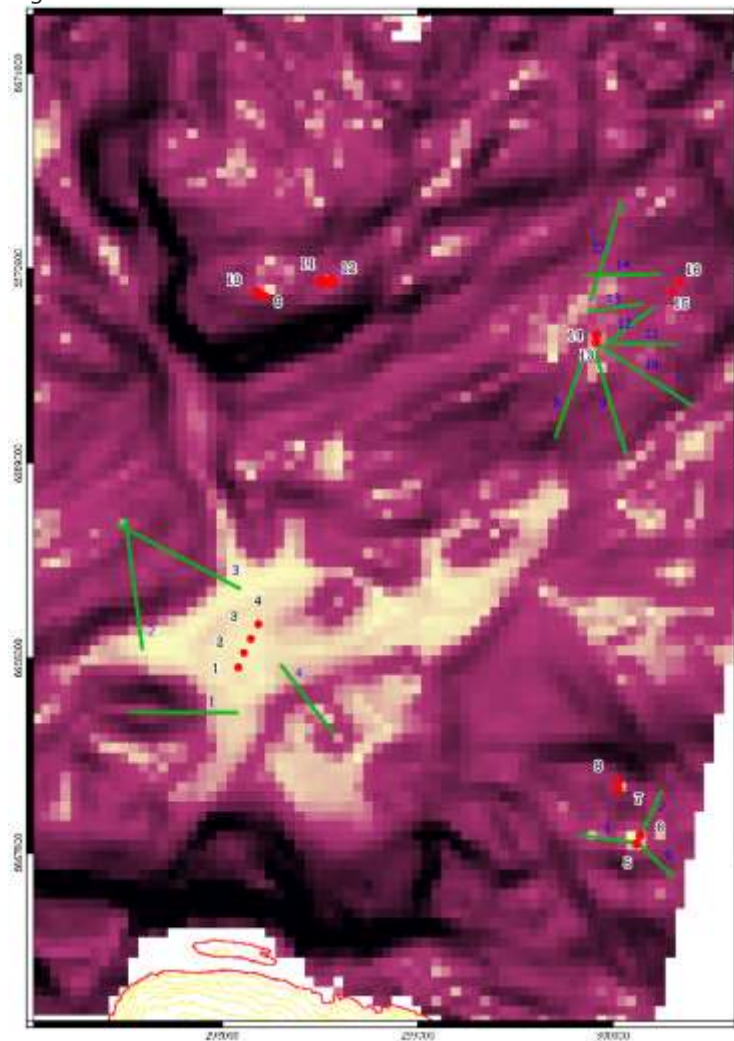
> *Figure 14-8 Profiles calculated in Plaxis 2D.*

> *Table 14-4 Plaxis results of drained and undrained slope failure.*

Profile	FoS of critical failure mode		FoS of second critical failure mode
	Drained	**Undrained**	**Undrained**
1	1.316	1.127	-
2	1.288	1.037	1.717
3	1.902	1.318	1.357
4	2.251	1.584	-
5	5.103	3.111	-
6	1.545	1.212	-
7	1.829	1.329	-
8	2.232	1.505	-
9	1.418	1.259	1.346
10	1.285	1.126	1.512
11	1.458	1.274	-
12	1.944	1.603	-
13	1.976	1.730	-
14	1.977	1.625	-
15	2.089	1.539	-

14.4.3   Seismic slope stability

Calculations for seismic conditions are carried out with pseudo-static analysis in GeoSuite Stability. Calculation are performed for the profiles shown in Figure 14-7. The calculations carried out in GeoSuite Stability shows that the required safety factor for pseudo-static stability is far from met. In fact, for all the slopes investigated the calculated factor of safety is below 1.0 for the pseudo-static calculations. In this regard it is important to remember that the calculations carried out are based on a simplified pseudo-static approach to a dynamic problem, and that the calculations are for an earthquake with a return period of 2750 years.

As the safety factor for the pseudo-static stability is not satisfactorily, dynamic analysis with Plaxis 2D has been performed. As one can see in Table 14-5, several of the slopes does not satisfy the criteria for all ground motions. The results correspond well with the profiles with low static safety factor in Table 14-4. The static and dynamic thus shows that there is a possibility for slope failure and should be considered in design of exposed anchors.

> *Table 14-5 Maximum permanent deviatoric shear strain in slope.*

Profile	Sierra Madre	Whittier Narrows main shock	Whittier aftershock
1	~ 6.4%	~ 5.2%	~ 3.2%
2	~ 9.1%	~ 8.2%	~ 4.6%
3	~ 2.0%	~ 1.3%	~ 1.0%
4	~ 2.0%	~ 1.0%	~ 0.58%
5	~ 0.5%	~ 0.3%	~ 0.2%
6	~ 6.4%	~ 3.6%	~ 1.9%
7	~ 3.8%	~ 2.9%	~ 2.0%
8	~ 2.3%	~ 1.2%	~ 1.0%
9	~ 8.1%	~ 6.3%	~ 4.3%
10	~ 5.7%	~ 3.7%	~ 2.5%
11	~ 5.8%	~5.0%	~ 3.0%
12	~ 2.0%	~ 1.2%	~ 0.72%
13	~ 1.9%	~ 1.0%	~ 0.95%
14	~ 2.1%	~ 1.1%	~ 0.98%
15	~ 2.1%	~ 1.2 %	~ 0.76%

14.4.1   Run-out

Based on stability calculations the critical failure surface is at the interface with bedrock. This is due to the assumptions of homogenous clay above bedrock. Other failure modes may be critical, but they are not identified in the stability calculations, and therefore not included in the Run-Out evaluations.

14.4.2   Group 1

The anchor group is located approximately in the centre of the basin. Since the anchors are placed at the lowest point, they are exposed for landslide debris in all directions. This is confirmed by the stream lines calculated by NGI and the flow accumulation calculated by OON.

14.4.3   Group 2

Anchors 5 and 6 are placed in a local pit with a large sediment thickness, while anchors 7 and 8 are placed on top of a hill. The soil thickness on the hill is roughly 5-7 m thick and it's assumed that the soil consists of clay which can be removed, thus avoiding any risk of landslides from above.

Anchors 5 and 6 is in a pit surrounded by a soil thickness of around 10 to 15 m with a differential height variation of about 20 m in the near vicinity. By examining the slope angle map and the high-quality 3D bathymetry one can observe bedrock in the north-west and south-west. Furthermore, the flow accumulation calculations indicate the possible run-out sources are fairly limited compared to anchor groups 1 and 4. Based on the above observations, it's believed that in case of a landslide, the volume and kinetic energy will be finite and manageable by embedding the anchors deeper.

14.4.4   Group 3

All the anchors in group 3 is placed directly on bedrock and the surrounding soil thickness is very limited. Based on this information run-out is evaluated to not be relevant in this area.

14.4.5   Group 4

It can be seen from the calculations that the static slope stability is poor for the slopes near anchor 13 and 14. Additionally, one can observe that the current anchor positions are located at the centre of a stream line. This suggests that if a retro progressive slide were to occur, the surrounding soil masses could disappear. In fact, it's assumed this have been the case for the area where anchor 15 and 16 is currently located. The static and dynamic slope stability up stream is deemed to be satisfactorily for anchors 13 and 14. Further description is given in the geotechnical design report [20].

Anchors 15 and 16 are placed in a previous landslide area. They are partially shielded from potential run-out debris in the north, and the slope calculations in the west indicate satisfactorily safety factors. Due to the limited amount of potential run-out debris and slope stability results the anchors are deemed to be well secured.

14.5   Risk assessment for anchor groups

14.5.1   Group 1

The anchors are exposed for possible landslide run-out sources in all directions. Even though calculations may show adequate FoS and performance to earthquake, the uncertainties tied to this are high. By doing additional soil investigation and advanced numerical analysis of run-out dynamics one might be able to predict the likelihood and impact from possible run-out sources. However, due to the nature of soil variability and behavior, this will be a challenging and demanding task. Another possibility could be to do similar calculation to a PSHA for earthquakes. By quantifying possible sources, doing flow calculations based on flooding and combining the FoS to a given probability of failure, one could perhaps estimate the impact force for a given probability.

As a simplified approach to the challenge with landslide run-outs for this phase of the project, it is proposed to assume remolded shear strength in the top meters, due to possible landslide ploughing. The additional load from debris flow forces is not accounted for, as they are assumed to be small due to energy dissipation over large distances. It is also assumed that global failures involving the anchors are highly unlikely. A 3 m deep zone with remolded clay is included in the holding capacity calculations.
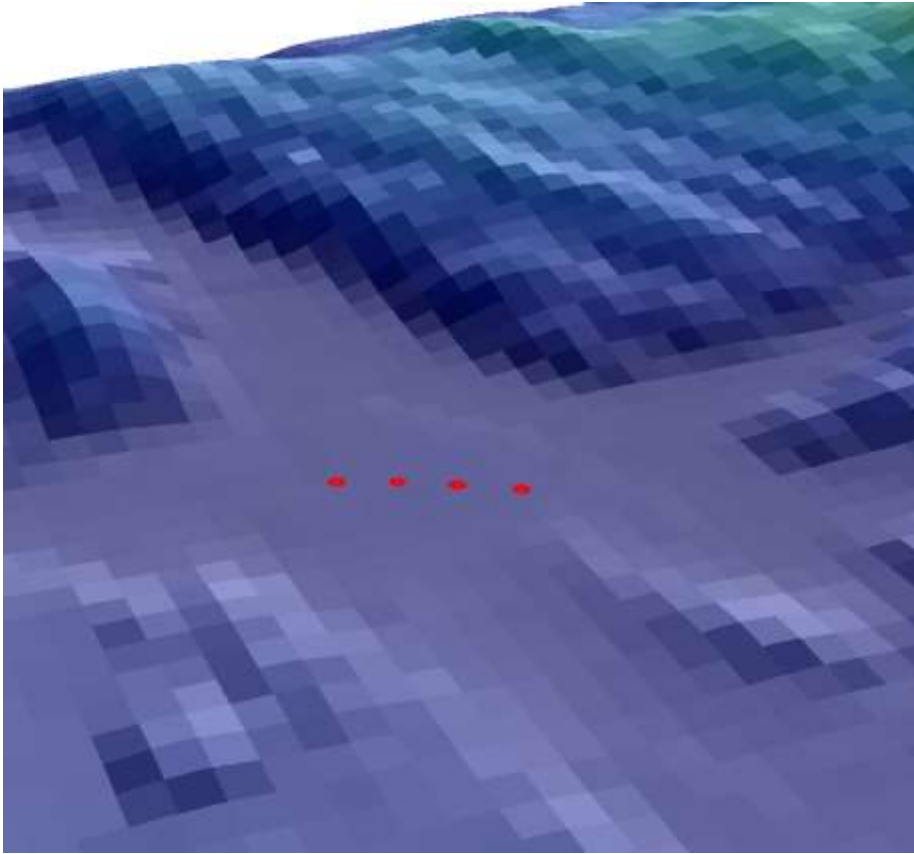
> *Figure 14-9 High-quality 3D bathymetry of anchor group 1.*

14.5.2   Group 2

Anchors 7 and 8 are placed on top of the hill and are therefore regarded as safe with respect to run-out debris. The only issue tied to this location is increased seismic acceleration due to topography layout.

The amount of possible run-out debris for anchor 5 and 6 is limited, as can be partially observed in Figure 14-10. One can therefor similarly to group 1 assume remolded shear strength in the meters to determine the required skirt length to achieve sufficient holding capacity.
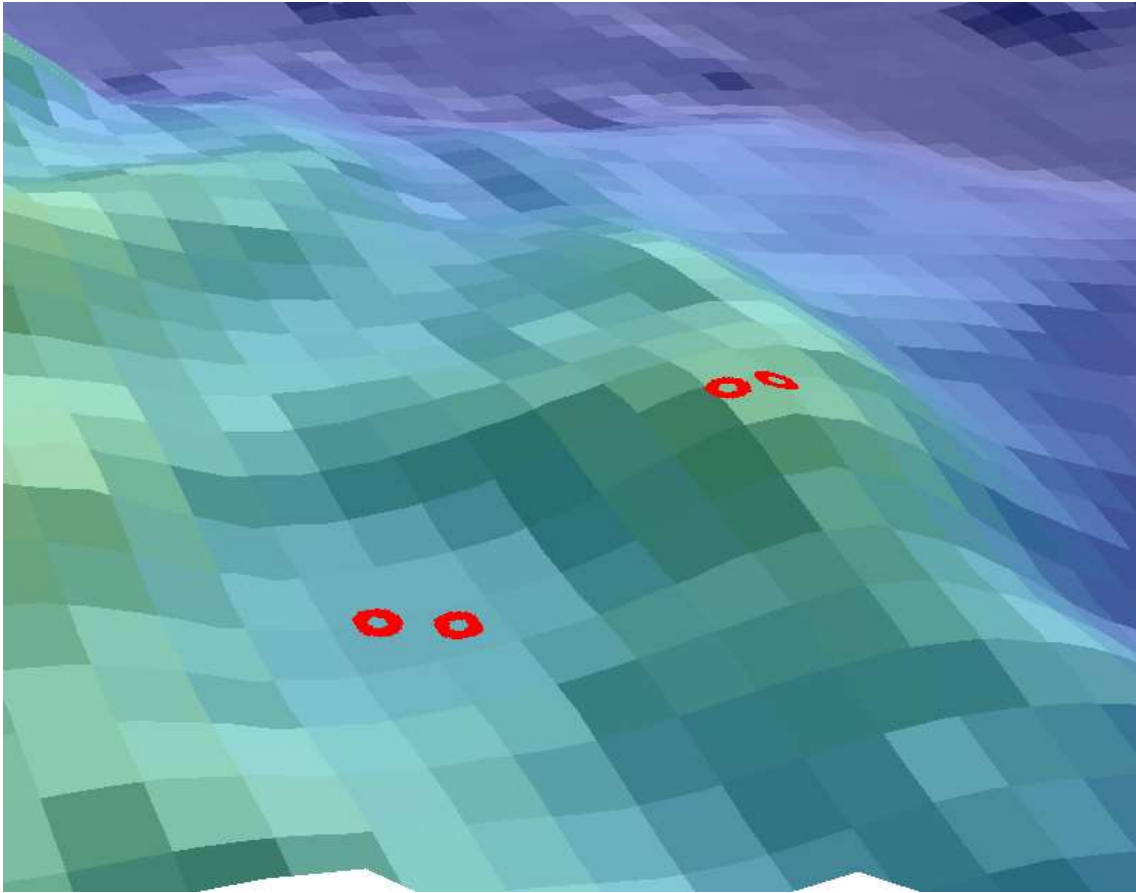
> *Figure 14-10 High-quality 3D bathymetry of anchor group 2.*

14.5.3 Group 3

No issues with respect to geohazard and anchor capacity are identified at this location. Ideally the anchors would be placed more normal on the bridge, but this is not possible due to the steep slope which can be seen in Figure 14-11.
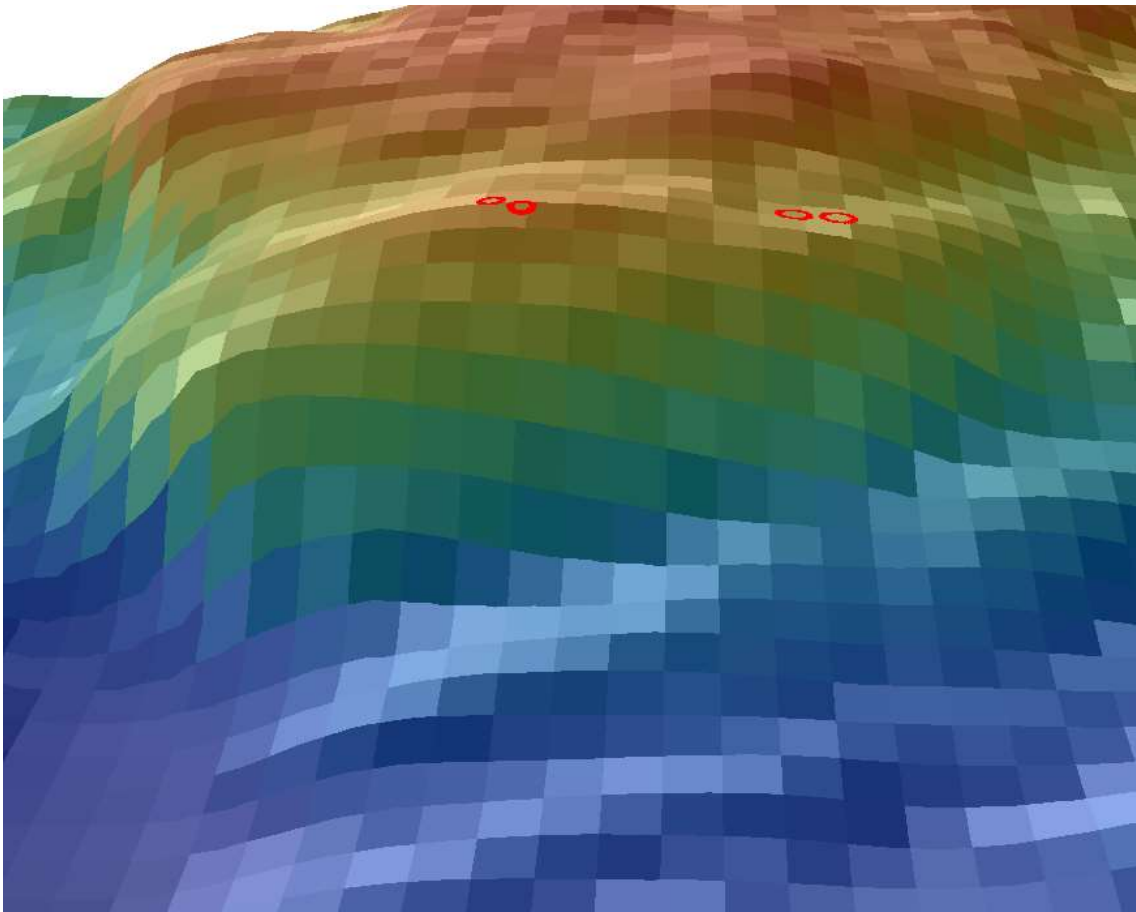
> *Figure 14-11 High-quality 3D bathymetry of anchor group 3.*

14.5.4   Group 4

Anchors 15 and 16 are placed firmly on bedrock and is partially shielded in the north from run-out debris. The slope stability towards west has been calculated to be adequate, ref. Table 14-4, and watershed maps indicates that the potential debris volume is fairly limited. It is thus concluded that these anchors have a safe position.

The slope stability calculations for anchor 13 and 14 indicates that the safety factors are inadequate with respect to the criteria given in design basis, ref. [24]. One can also observe scars from previous landslide in Figure 14-12.

The area for anchor 13 and 14 may thus be troublesome with regards to landslides, both from north and in the southern direction. Landslides towards south can lead to loss of soil, as the anchors are located at a streamline. It is not possible to design the anchors for a complete loss of the soil. At this stage the challenges caused by possible landslides, are solved by having spare capacity, assuming 3 m of remoulded soil in the top, taking slides from the north. For worst case scenario, with slide towards south, the anchors may be lost. As the bridge is designed to sustain this case, it is regarded to be acceptable. Additional soil investigations in this area is recommended to determine the optimal anchor position with respect to retro-progressive slides and possible run-out debris.
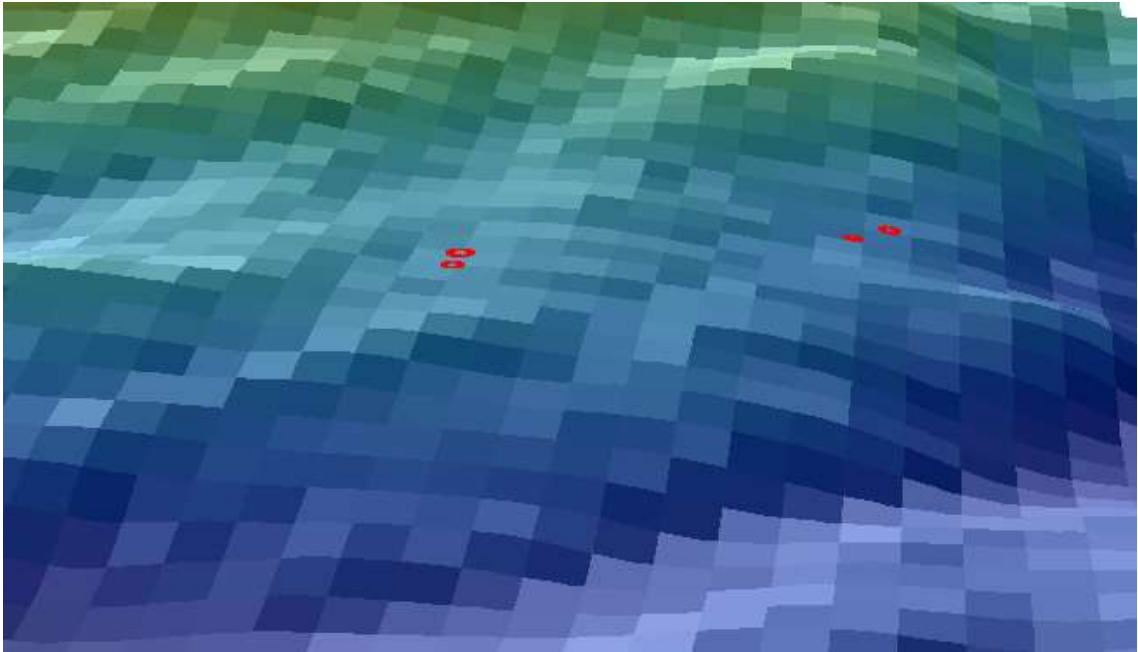
> *Figure 14-12 High-quality 3D bathymetry of anchor group 4.*

14.6   Anchor design

14.6.1   Gravity anchor

Simplified anchor design has been performed to verify sufficient structural capacity of the anchors.

The gravity anchor is proposed to be constructed of steel and afterwards filled with olivine after installation. The geometry is B x L = 15 x 15 m and the height is 5.3 m, where the skirts are 0.3 m long. Plates and diagonal stiffeners are introduced to ensure that the forces acting on the padlock is uniformly distributed across the anchor. Horizontal stiffeners are also included to take care of the bending moments caused by earth-pressure.

It's assumed that the gravity anchor is placed on prepared crushed rock or gravel. The ribs are v-shaped and consists of two plates welded. The ribs are oriented transversally to the mooring load for maximum efficiency and a c/c of 600 mm is proposed. It is also proposed for the current anchor design to paint and use galvanic anode to avoid corrosion and thereby ensuring 100 years of life service.
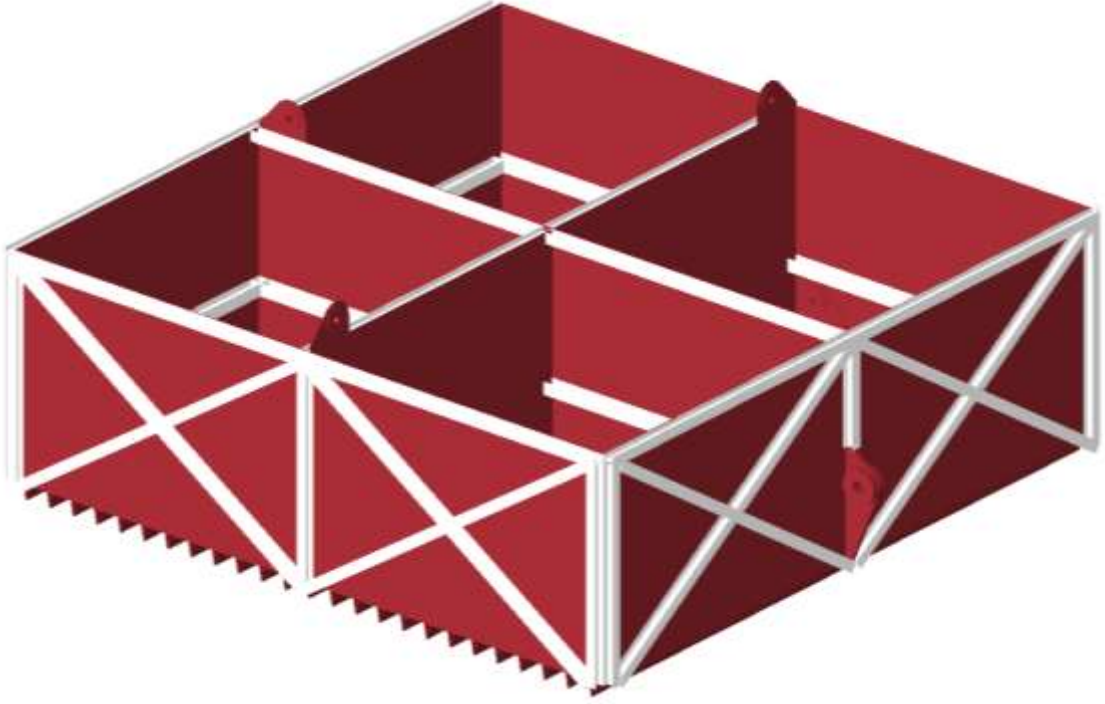
> *Figure 14-13 Illustration of gravity anchor*

14.6.2 Suction anchor

A single cylindrical shell with a flat top cap is considered in the current anchor configuration. The global dimensions are determined from marine geotechnical calculations and are summarized in Table 14-6. Reinforced plate with an inner stiffener is introduced to ensure evenly distribution of the load from padlock, as shown in Figure 14-14. The reinforced plate also acts as a ring stiffener and thereby reducing the risk of ovalization of the anchor.

> *Table 14-6 Summary of anchor dimensions used in marine geotechnical calculations.*

Anchors	Diameter	Length	Tolerance	Total skirt length	Assumed weight, W
[#]	[m]	[m]	[m]	[m]	[kN]
1, 2, 3, 4, 5, 6	9	11.5	1	12.5	2254
13, 14	9	10	1	11	2054

The plate thickness is determined from the weight necessity required in geotechnical calculations. However, this is recommended to be optimized at a later stage to ensure more cost-efficient design. A plate thickness of 50 mm is assumed in the calculations, with reinforced plate and inner stiffener with 70 mm thickness which 2.5 m high. It is also proposed for the current anchor design to paint and use galvanic anode to avoid corrosion and thereby ensuring 100 years of life service.

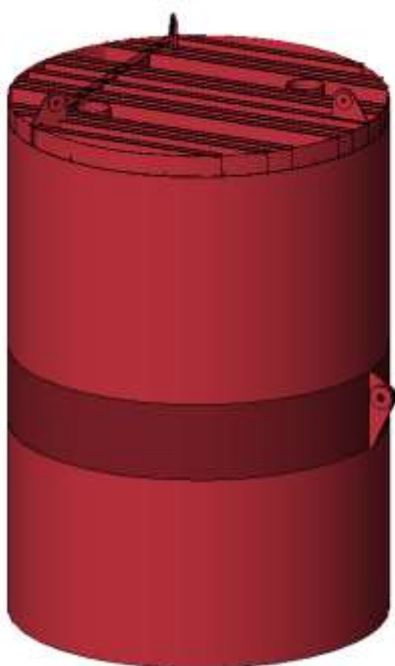> *Figure 14-14 Illustration of suction anchor*

15 DESIGN OF CABLE-STAYED BRIDGE

15.1 Structural analysis

15.1.1 Analysis overview

Short overview of the programs used, with a more detailed description of the programs given in ch. 2:

- 3DFloat – Time-domain analysis of environmental condition, used in ULS/SLS
- Sofistik – Static loads and load-combination in ULS/SLS
- PatranPre – Modelling of tower geometry and loading
- TenLoad – Application of tendon loads on FEM model
- ShellDesign – Local analysis and code design check of tower. Used in all analysis of the tower
- Abaqus – Used in ALS ship collision, together with DynNO for fatigue design, and construction phase analysis
- DynNo – Fatigue analysis and dynamic analysis of freestanding tower and freestanding cable stayed bridge

15.1.2 ULS/SLS

The operational phase ULS/SLS is analyzed with 3Dfloat for the dynamic loads and Sofistik for the static loads. Load-combination is done in Sofistik. The model is used for design-force extraction of cables, rock anchoring, sockets and girder.

The tower model is a volume-element model from Patran with post-tensioning forces from TenLoad. The design calculations are done in ShellDesign and accounts for the nonlinear behavior of reinforced concrete due to cracking etc. when establishing the response of the cross-section. ShellDesign has also the capability to include the non-linear material behavior of reinforced concrete into the structural FE analysis (nonlinear FE-analysis). The method is based on an iterative analysis/design process. The linear elastic analysis with nonlinear design calculation is used here, and nonlinear analysis is only partly used to show robustness. Load from self-weight, post-tensioning and wind on the tower are combined with the cable-loads from Sofistik and 3D-float in SLS/ULS.

To be able to attain the correct operational phase geometry of the bridge a form finding routine is applied on the bridge giving the correct initial lengths of the cables. The form finding is explained in [2]

15.1.3 ALS - Ship impact

The ALS-design is conducted in Abaqus. Reference is made to ship impact reports [11] [12] [13]. Note that the ship collision only hits the girder and the pontoons, not the tower. The tower distance from the shore is so large that the ship will stop on the rocks before hitting the tower.

Ship impact has been combined with $\psi_2=0,5$ for traffic load according to Design Basis [22]. The ALS forces for the cables including load factors are considerably smaller than the forces from ULS design.

A special check from ALS-design is that the girder should not get major dents from hitting the bridge tower. The critical distance between the top point of the girder and the tower leg

is 3.8 m, and the maximum horizontal deflection is 3.85m in collision 711_16. This is deemed sufficient. See ship impact report [11]

15.1.4   ALS - Sudden loss of stay cable

Sudden loss of stay cables is not calculated in this phase of the project. In traditional cable-bridges (due to a high safety factor) this analysis is not a design driver for the cables but could be design driver for girder/tower attachments, but usually not more than maximum 5-10% of added force. These connections are designed partly by practical steel size and is not utilized 100%. This means that a sudden loss of cables is probably not a design driver, and at least not adding any cost risk to the project.

The girder will have minimal additional load from the sudden loss of a cable. The grouping of the cables will make the force only redistribute to the other cables that are nearby and the girder will be almost unaffected. The girder will usually not get critical even for suspension bridges with 20m center distance between hangers.

15.1.5   FLS

The fatigue analysis is done with the same procedure as in the report [14], with stochastic dynamic loads from DynNo and traffic-loads from Sofistik. Cholesky-decomposition of the frequency domain data combined with traffic loads gives time-series that are rainflow-counted to get the correct stress-cycles.

Summary of findings from the fatigue analysis for the cable-stayed bridge:
Minimum fatigue life of cable is approximately 1000 years.
Minimum fatigue life of cable connection to tower and girder is approximately 800years.

Note that the fatigue analysis of the cables is according to Eurocode, and the rest according to DNV-GL. Furthermore, it is assumed that one stay cable can fail without the collapse of the bridge. This is a design case in ALS.

15.1.6   Construction phase

The following design-situations are checked for the stay-cable bridge:

1. **Freestanding tower in construction**
   Wind loading on in transverse and longitudinal direction, with added wind area for formwork, temporary beam between the tower legs, before the post-tensioning of stage 3 is finished. See figure below:

> *Figure 15-1 Tower in critical construction phase*

2. **Freestanding tower**

   Wind loading of the full free-standing tower in longitudinal and transversal direction. Added wind area from formwork.

3. **Freestanding cable-stayed bridge**
   Wind loading in transverse direction, without asphalt weight. Including formwork area at the end of the cantilever.

4. **Freestanding cable-stayed bridge with ballasting**
   Maximum forces from course adjustment of the elements.
   Separate model with ballast and 10-year summer storm.

15.1.7   Tower stiffness

The actual stiffness of the tower has contributions from different sources:

– Modulus of elasticity of concrete
– Reinforcement amount
– Degree of cracking of the section
– Creep and shrinkage
– Geometric stiffness

The inclination of the tower in longitudinal direction of the bridge makes the entire situation complicated. This inclination is not normal for stay cable bridges of this size. The transverse inclination of the tower legs is normal.

To have more control over the stiffness and displacement of the tower in all phases the towers are post-tensioned. This increases the effective stiffness of the tower forcing it to stay inside stadium I for an increased loading period. On top of that the displacement from the post-tensioning reduces the displacement from self-weight. Giving smaller 2.nd order effects.

On the other hand, the calculation procedure, with construction phases with and without post-tensioning, long term effects on both concrete and the reduction on post-tensioning gets more complicated.

The effects of the tower stiffness on the structure is different in the different phases of the bridge. A stiff tower in construction phase gives higher eigenfrequencies giving lower dynamic wind load, smaller displacements, and less 2nd order effects from geometric stiffness.

A stiffer tower in operational phase gives higher eigenfrequencies, but the dynamics of the full bridge is less sensitive for the tower stiffness. Displacement from the deformed freestanding tower needs to be straightened with the stay cables to get final geometry, giving different forces in the cables. The effects of creep in the full bridge is mostly countered with changes in cable forces. In general, the conservative for the bridge is to use the highest reduced stiffness plausible.

The concrete in the tower is B70. The Modulus of elasticity of the concrete from EC2 is 41GPa. In traditional Norwegian bridge design, the stiffness for B45 is reduced from 36GPa to 32GPa due to the softness of the concrete aggregate. This is conservatively done here also from 41 to 36GPA.

Effect of tower stiffness has been evaluated for the following conditions:
- Free standing tower stiffness
- Stiffness of the tower in full phase
- Effects of long-term effects on the full bridge
- Eccentricity due to building errors

15.1.8   Wind stability

The flutter wind speed of the stay-cable bridge is calculated in validation report [3]. The flutter wind speed is approximately 112m/s and is well within the criteria. Other instability phenomena are included in the same report. The wind stability is sufficient. But the ViV wind speed of the girder in construction phase estimated are in the lower bounds of what is acceptable. This should be investigated further in the next phase.

15.2   Bridge tower

15.2.1   Tower design

Minimum reinforcement according to NS-EN 1992-1 is 1900mm2/m (ø25c250) for walls with thickness 900mm and 4530mm2/m (ø32c175) for walls with thickness 2m. The north and south walls are 2m tick at the bottom and 0.9m where the legs meet. All other wall sections are 0.9m tick. The actual reinforcement is shown below and are well beyond the minimum required. In a later phase it could be investigated whether some of the reinforcement should be replaced by more post-tensioning and concrete to reduce the highest intensities. It is assumed that the reinforcement can be grouped together and put in different layers.

The maximum allowable crack width in temporary phases is 0.6mm in accordance with N400 [34]. For the operational phase the limit is set to 0.2 for both the infrequent and quasi permanent loads situation. The crack width is not dimensioning for the tower and the utilization is low for the entire tower both in temporary and operational phases. In the quasi permanent situation there should not be tension where there is post-tensioning cables present.

Further details on the analysis of the tower is given in the cable-stayed bridge design report [17].

Horizontal reinforcement, outside · Horizontal reinforcement, inside · Shear reinforcement
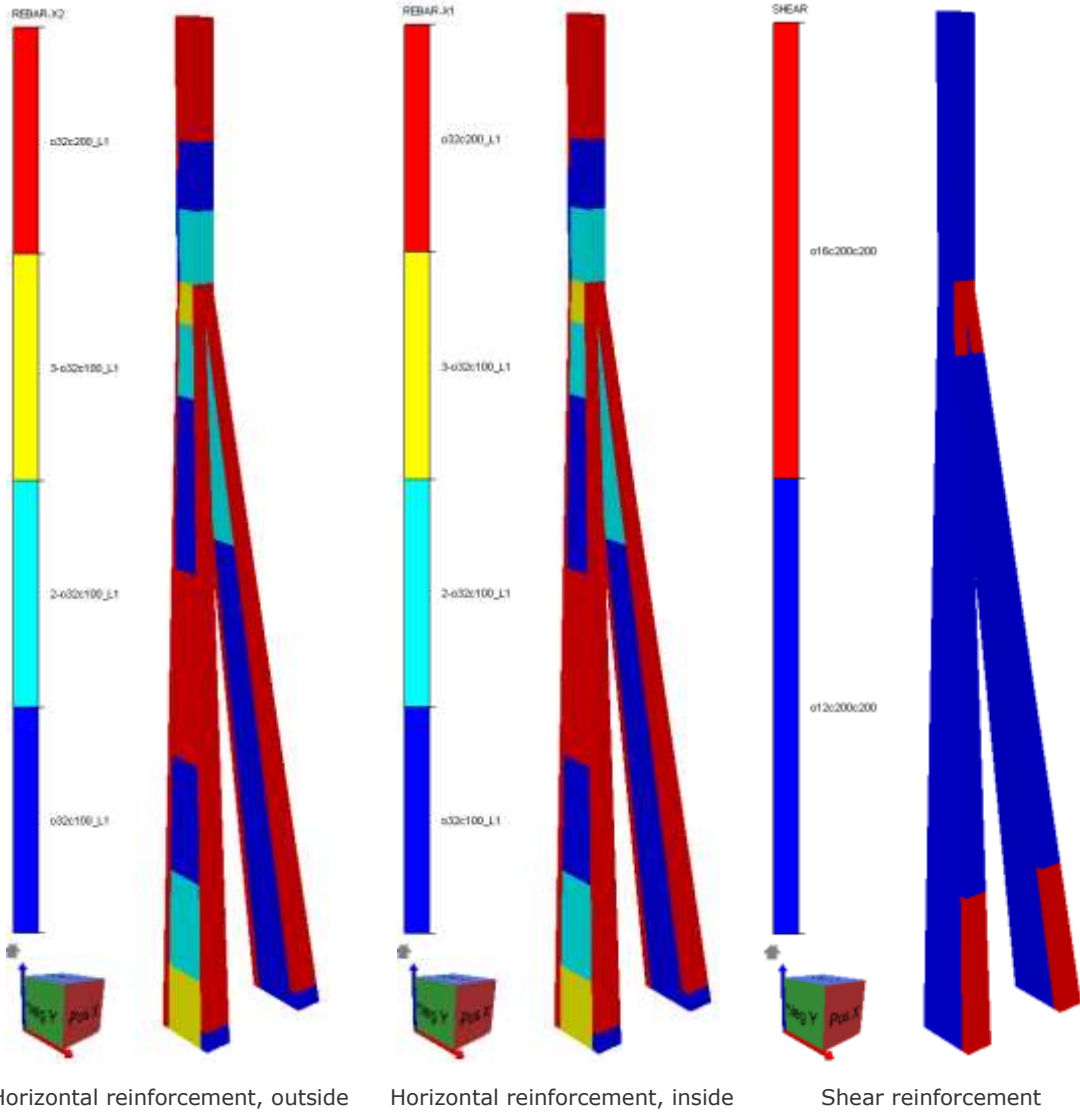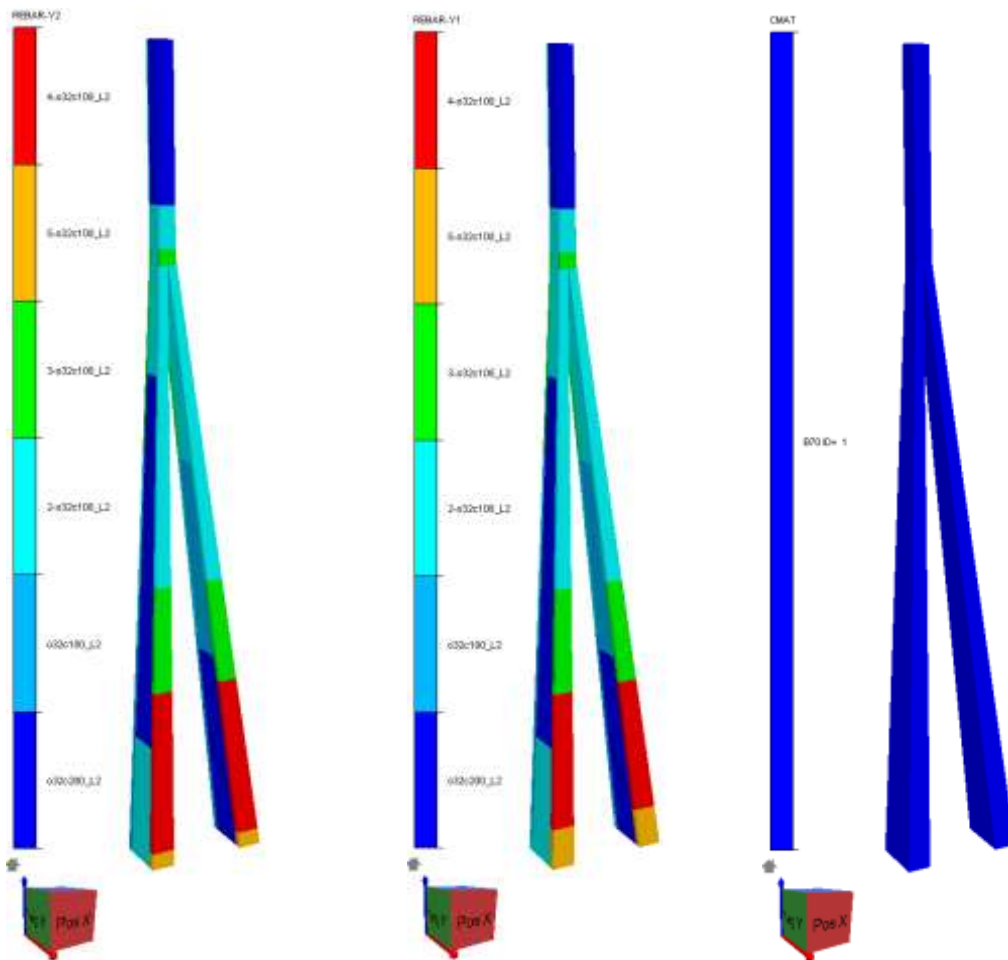
Vertical reinforcement, outside   Vertical reinforcement, inside   Concrete material

15.2.2   Construction phase

Free-standing tower is dimensioning for the vertical reinforcement in the south wall. All utilizations are well within limits and can be seen in [17] appendix F.

For free-standing stay-cable bridge, all utilizations are well within limits for this phase and can be seen in [17] appendix F. Only the resulting beam forces from the dynamic analysis is matched in the bottom part of each tower leg. For this reason, only the lower part of the model displays the correct results. The utilization levels are low and for this reason the rest of the sections are not controlled in this phase.

15.2.3   Local analysis of connection to tower

The temporary bracing between the girder and the tower is resulting in a force of about 16MN on the tower. In this elevation local strengthening is necessary. The added strength could be in the form of a concrete slab or a steel bracing inside the tower. The concrete slab will distribute the force to the entire cross section and could be used as a natural platform for access to the bridge girder.

15.2.4 Tower foundation

The following figures are used to calculate the bridge foundations:
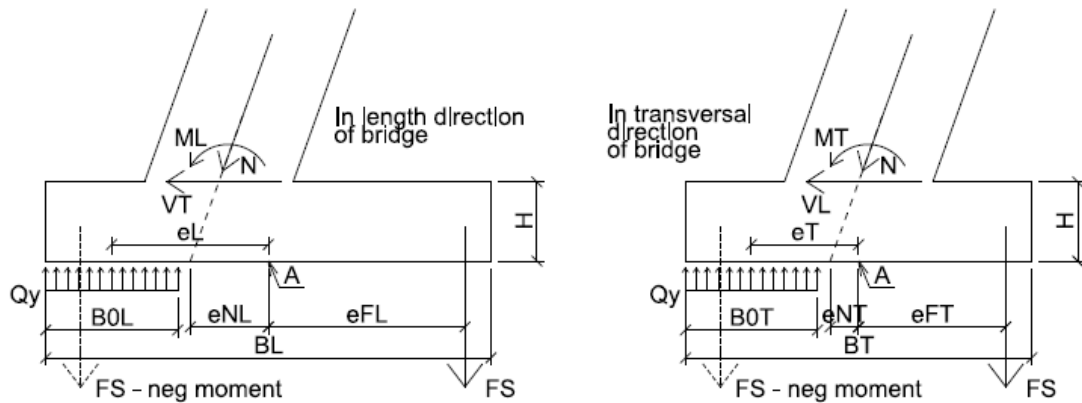
Explanation	Naming convention	Value	Unit
Width foundation, length direction	BL	22	m
Width foundation, transversal direction	BT	15	m
Height of foundation	H	8	m
Eccentricity of normal force	eNL	0.70	m
Eccentricity of normal force	eNT	1.28	m
Density of concrete	GammaBet	25	kN/m3
Number of rock anchors	n	6	
Eccentricity of rock anchor, in length	eFL	9.5	m
Eccentricity of rock anchor, in transversal	eFT	6	m
Force single rock anchor	FKar	5022	kN
Reduction coefficient for anchor	GammaStag	0.65	
Reduced force from rock anchor	FDim	3264.3	kN

Forces from the free-standing tower in construction phase is used as an example:

Load-Combination	N[kN]	VL[kN]	VT[kN]	ML[KNm]	MT[KNm]	YG
Free tower, wind from north	123443	-11192	-13612	-1249961	308081	0.9

Without rock anchors

	Without anchors		
Moment around A, in lenth dir	MLA=ML+VT*H+N*eNL	-1272787	kNm
Moment around A, in trans dir	MTA=MT+VL*H+N*eNT	377115	kNm
Weight of foundation	Nfund=BL*BT*H*yBet	66000	kN
Normal force at A	Na=N+Nfund*YG	182843.2	kN
Eccentricity of the reaction force	eL=MLA/NA	7.0	m
Effective width, length dir	B0L=BL-2*eL	8.1	m
Eccentricity of the reaction force	eT=MTA/NA	2.1	m
Effective width, transversal dir	B0T=B0T-2*eT	10.9	m
Ground pressure	qy=NA/(B0L*B0T)	2081.4	kN/m2

Rock anchors: Rock anchor type is 18 strands of 150mm^2 with f_{pk} of 1860MPa.
V220 chapter 10.5.2.1 gives reduction factor of 0,65.

With rock anchors

	With anchors		
Force from rock anchors	FS=n*FenkDim	19585.8	kN
Normal force at A	NA=NA+FS	202429.0	kN
Moment around A, in lenth dir	MLA=MLA-FS*eFL	1086721.7	kNm
Moment around A, in trans dir	MTA=MTA-FS*eFT	259600.4	kNm
Eccentricity of the reaction force	eL=MLA/NA	5.4	m
Effective width, length dir	B0L=BL-2*eL	11.3	m
Eccentricity of the reaction force	eT=MTA/NA	1.3	m
Effective width, transversal dir	B0T=B0T-2*eT	12.4	m
Ground pressure	qy=NA/(B0L*B0T)	1445.3	kN/m2

The goal of the analysis is to keep the Ground pressure(qy) below 10 000kN/m^2, this is according to the geology report.

The rest of the analysis can be found in [17] appendix G.
The maximum ground pressure is found to be 3600kN/m^2. The foundation size could be reduced in the detailed design phase, when exact allowed ground pressure is clarified.

15.3   Bridge Cables

15.3.1   Cable design

There are several different cable types available which can be used for cable stayed bridges.
1. Locked coil cables. This is prefabricated spiral strands, with round wires in the core and normally Z-shaped wires in the 2 or 3 outer layers to give a smooth and almost watertight surface. This is the most common cable type in Norwegian suspension and cable stayed bridges. Each cable is supplied with a steel socket in each end. The cable-end is spread out like a brush and fixed inside the socket in a conus casted with zinc.
2. Parallel wire cable. The cable is built up with several round wires laid up in hexagonal form using very long helix length and put into a close-fitting polyethylene tube which is filled with grease. Same type of sockets as for locked coil. Sometimes the cable end is fitted to the socket with an epoxy-compound instead of zinc which improve the fatigue properties (Hi-Am-socket). This is the most common cable type for cable stayed bridges abroad. Former, steel tubes injected with mortar were used instead of polyethylene. Consequently, these cables could not be pre-fabricated because the injection as well the steel tube erection had to be done after installing the cable.
3. Parallel strand cable. Like the parallel wire cable, but instead of single wires, the cable is built up with single strands. Normally the strands are locked to the socket with wedges like common post-tensioned reinforcement.

The different types have different properties. The parallel wire/strand cable has a higher E-modulus than the locked coil (ca. 200 GPa compered to ca. 160 GPa). The spinning of the locked coil reduces the stiffness compered to pure steel. These cables are normally cheaper than the locked coil.

Experience shows that the locked coil has better vibration characteristics due to wind than the other.

The parallel strand is easier to tension because you can tension every single strand separately with a small jack instead of jacking the socket. On the other hand, it is very complicated to slacken the cable if that is needed during the construction phase. You must inject the cable tube with grease after the cable is installed.

For the Bjørnafjorden Bridge, we have chosen locked coil cables for this phase. This is of course not an irreversible choice for the project, but it is sensible to reduce the variables as much as possible. Regardless, the impact on the analyses from the cable type is almost insignificant.

Because every cable pair in a cable stayed bridge has different angels, the ULS-tension will be different. Consequently, an optimal design gives different cross section of all cable pairs which will be iterated in our analysis. However, in the detailing design phase, from economic reasons, one would prefer to reduce the number of different cables and therefor divide the cable dimensions into 4 or 5 groups. Hence, some cables will be oversized.

In the analysis it is important to input a correct stiffness of the cables. Because of the cable sag, the stiffness of a cable is lower than EA, (E-modulus multiplied with cross sectional area). EN 1993-1-11 has the following formula in paragraph 5.4.2 to take this effect into account:

$$E_t = \frac{E}{1 + \frac{w^2 l^2 E}{12\sigma^3}}$$

E: E-modulus of cable
w: Cable weight
l: Horizontal span
σ: Cable stress

This reduced stiffness is calculated in our analysis for all cables, using the cable stress from eigen weight. That is normal procedure.

For detailed dimensioning, see [17] Appendix B.

15.3.2   Sockets

There are several available socket-types for cables. For the Bjørnafjorden Bridge, we have chosen alt. 1, plain cylindrical socket, for the passive end in the pylon and alt. 2, cylindrical socket with external thread, for the active end in the bridge deck. Two other types of sockets for heavy bridge-cables have also been considered; The block socket and the hammerhead socket.
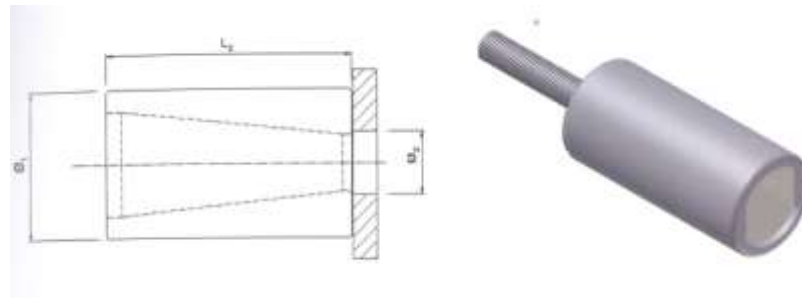
Figure 7.2-1   Plain cylindrical socket – alt. 1

The plain cylindrical socket, alt. 1, is the most common socket used for cable stayed bridges. It is cheap and simple, but the only way to regulate the cable length during installation is using shim plates between socket and supporting plate. It is most relevant for the passive end of the cable.
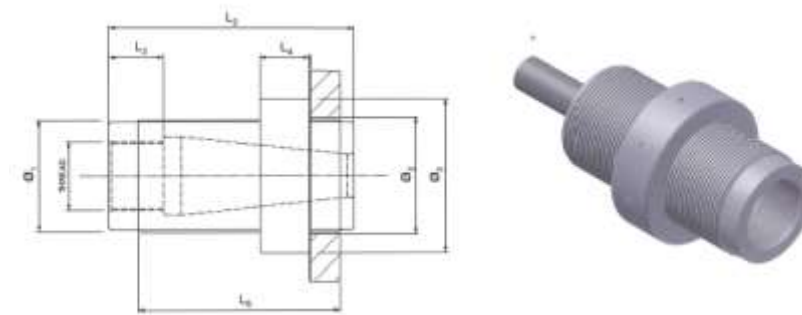

Figure 7.2-2   External thread cylindrical socket – alt. 2

The cylindrical socket with external thread, alt. 2, is a more sophisticated solution which is easy to adjust, but also more expensive. It is very suitable for the active end of the cable.

15.3.3   Attachment of cable to bridge deck girder

The cable is attached partly inside the bridge deck. The box girder has an extra plate parallel to the external vertical plate and with two load-bearing plates in between to support the socket. The socket will be located outside, under the box girder. The tube with neoprene damper and sealing will be located on the upper side of the bridge deck. The bulkhead close to the cable attachment must be locally strengthened. With this alternative, the position of the cable attachment has not to correspond exactly to the position of the bulkhead and gives more freedom. To give the bridge girder an aerodynamic shape, "noses" will be installed on both side of the girder. The chosen attachment of cables will not affect these "noses". Besides, the location of the attachments must not correspond to the bulkheads in this alternative.
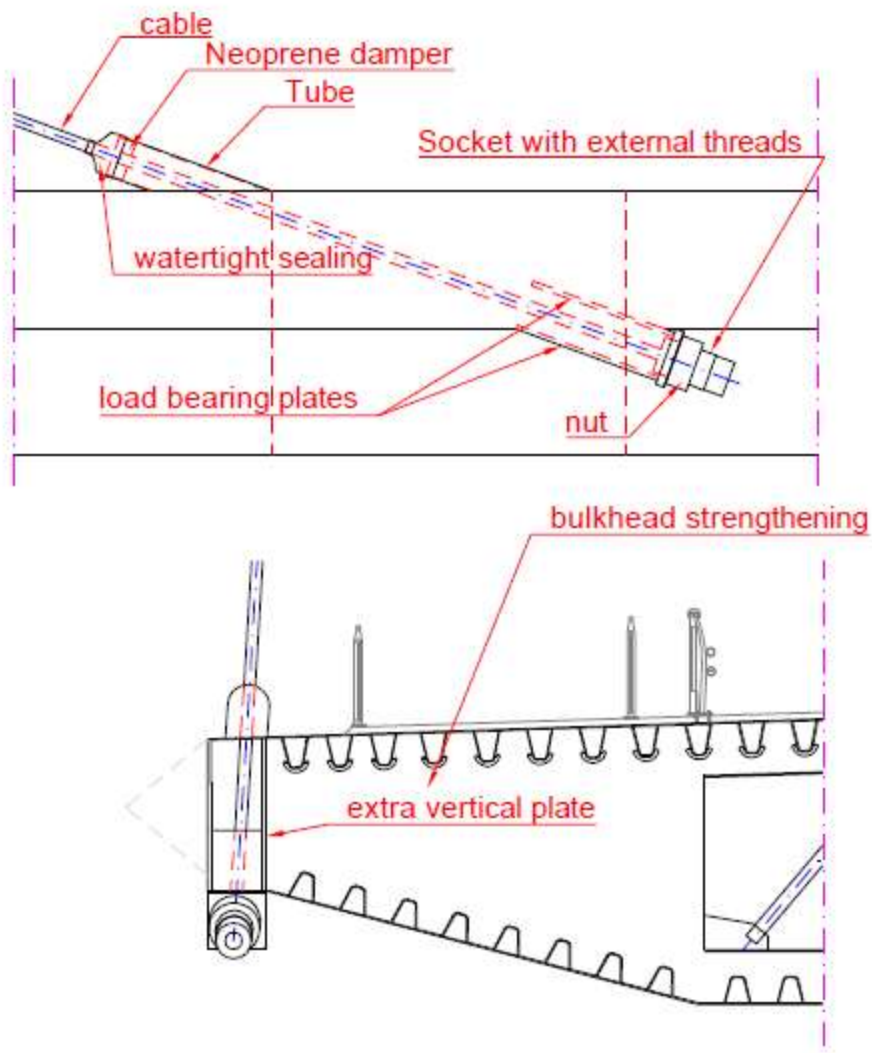
1.

Figure 7.3-2   Cable attachment to bridge deck – alt. 2

15.3.4   Attachment of cable to pylon

Traditionally two different ways of attaching cable and a concrete pylon have been used, see figure below:

1. The cable socket is supported by a steel plate embedded in the concrete wall. The vertical component of the cable tension is transferred directly to the concrete. To transfer the horizontal component from one side of the pylon to the other, loops of post tensioned tendons are used.
2. The cable is attached to a steel-box which also serve as inner formwork for the pylon and connected to the concrete by headed stud connectors. The horizontal force component is taken care of by the side walls of the box, and the vertical component is transferred to the concrete by studs.
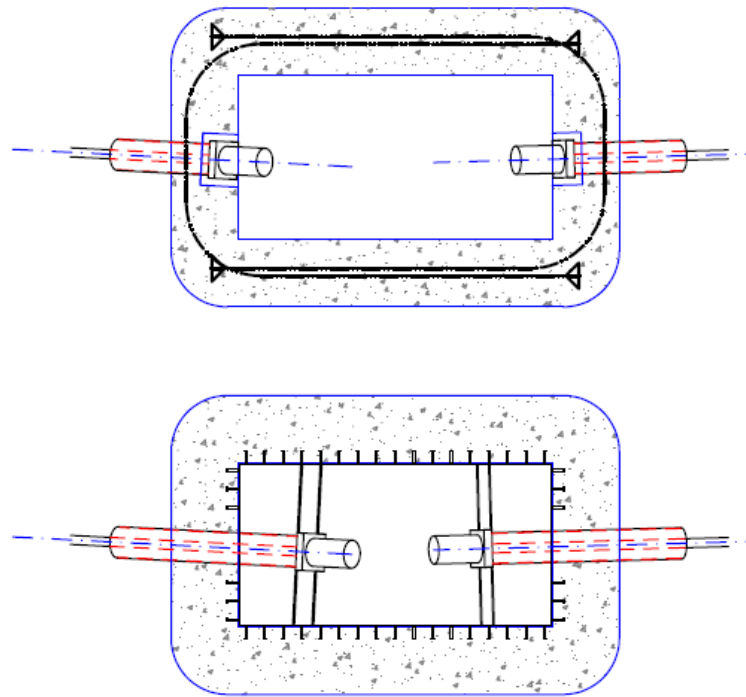
Figure 7.4-1   Cable attachment to pylon – alt. 1 and 2

If the forces are moderate and the number of cables limited, the first alternative is simple and economic. However, with a large number of heavy cables, the split-forces will be challenging, and the number and size of the tendons will complicate the construction process of the pylon.

For the Bjørnafjorden Bridge we recommend the latter alternative except for the lowermost cables which are very steep with low tension and small corresponding split-forces.

The general arrangement is shown in figure 7.4-2 and 7.4-3, and the he details are shown in figure 7.4-4.

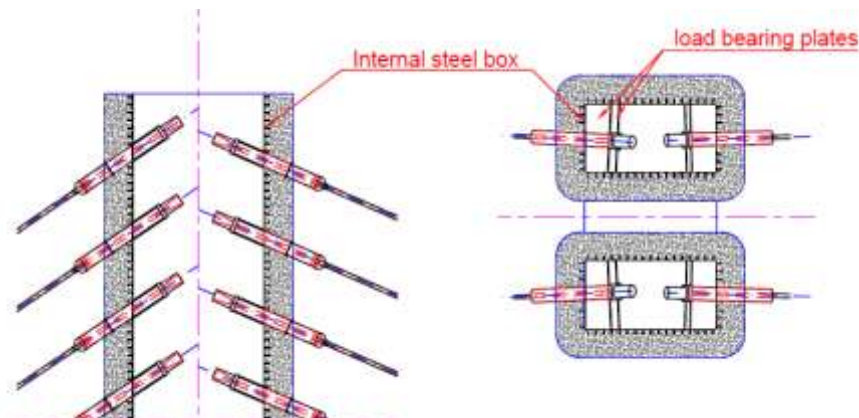*Figure 7.4-2   Cable attachment to pylon with inner steel box*
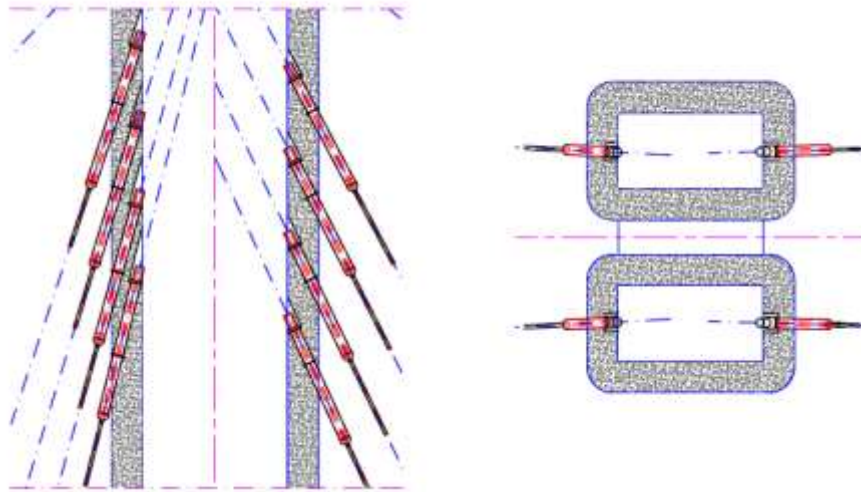
Figure 7.4-3   Cable attachment to pylon the lowermost cables
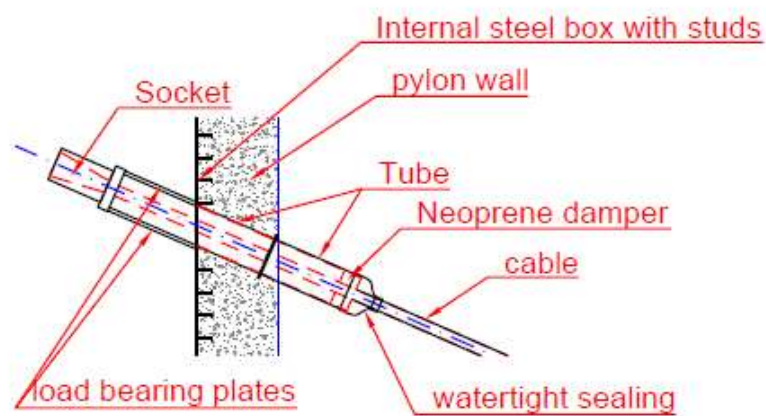

Figure 7.4-4   Cable attachment to pylon – details

For detailed design, see [17] Appendix B.

15.4   Rock anchoring

15.4.1   Design

Rock anchoring of bridge cables is used for several Norwegian suspension bridges and for one or two cable stayed bridges as well.
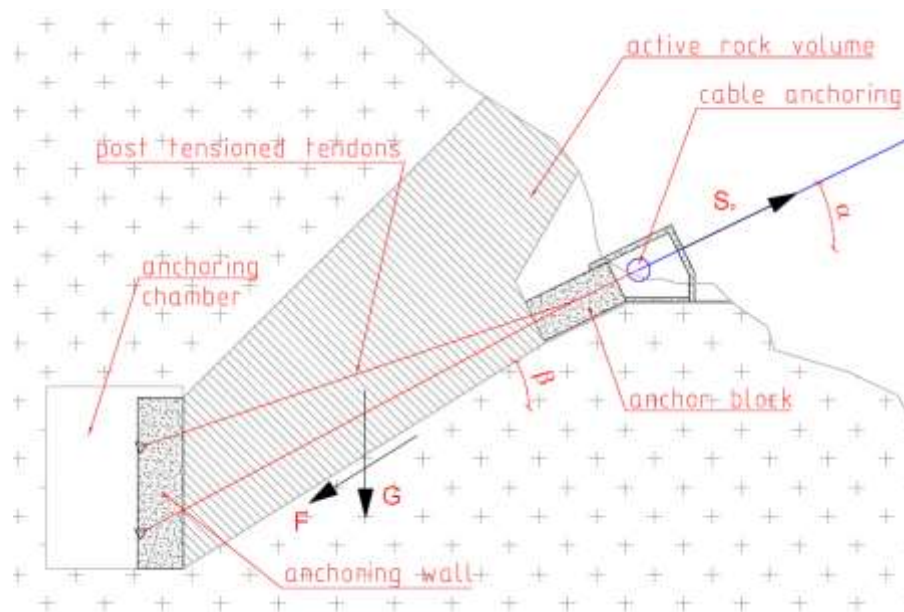
Figure 8.1-1   Rock anchoring - principle

The typical anchoring system includes a rock-chamber with an anchoring wall and an anchor block outside where the cables are attached. The anchor block and the anchoring wall are connected by post tensioned tendons through the rock, protected by polyurethane tubes, see fig. 8.1-1.

To calculate an exact capacity of a rock anchor like this is difficult and probably not possible. Therefore, simplified and conservative methods have been used. The system shown in the figure defines a rock volume which gives the capacity of the anchoring by its weight **G** and the friction force **F** only. Friction coefficient is set to 1,0. The material properties of the rock (shear and tensile strength) are not considered. In addition, the rock density is reduced because of the buoyancy from a presumed level of the groundwater.

15.4.2   Local cable-attachment

The easiest way to fasten the cable to the anchor block is using a block socket connected to two stays which are attached to the post tensioned tendons by a steel plate, see fig. 8.2-1. This is the traditional way which is used on a number of suspension bridges in Norway.
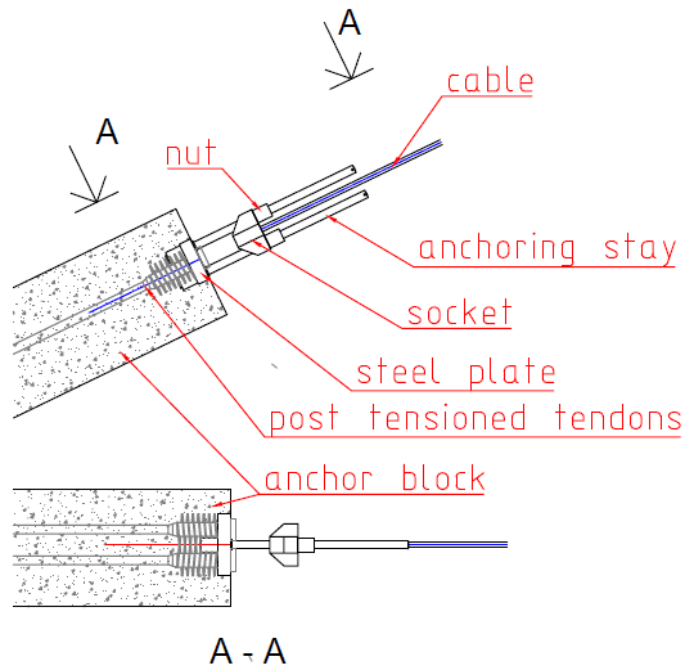
Figure 8.2-1   Attachment cable/anchor block

However, with a cable stayed bridge there is a need for jacking during the erection process which is unnecessary for a suspension bridge. A standard block socket is not suitable for jacking. Therefore, the sockets must be designed so that jacking is possible. Sockets for cables of this size will always be tailor-made, so a special solution will hardly give rise to the costs. A possible solution is showed in fig. 8.2-2.
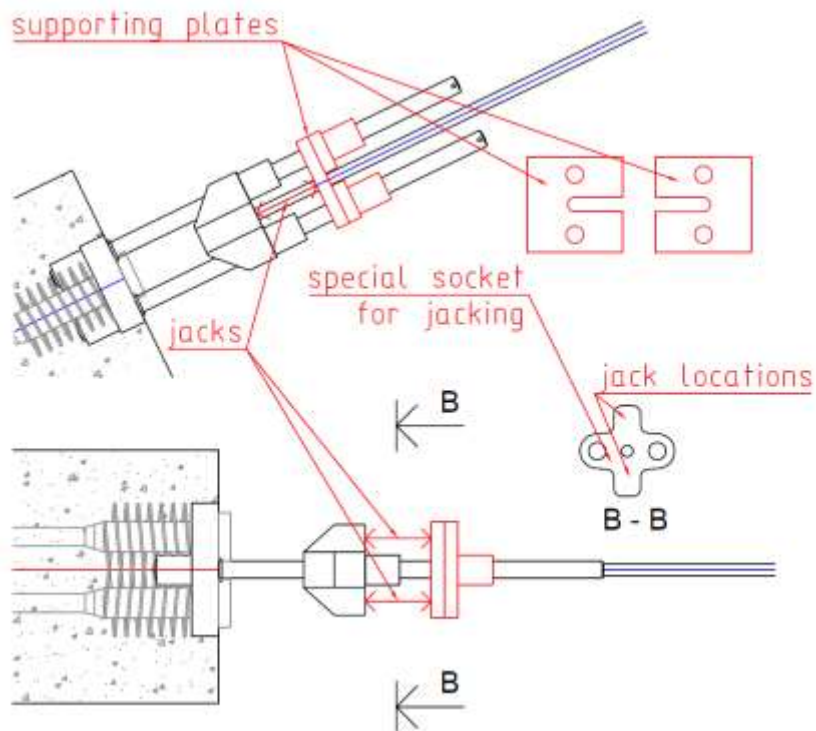
Figure 8.2-2   Possible solution for jacking

15.5   Equipment

15.5.1   Temporary bearing against tower

The temporary horizontal bearing between the girder and the tower, and the local strengthening of the box girder is calculated in appendix C

15.5.2   Damping on cables

Necessary dampers on stay-cables is a complicated topic. In the validation report [3] necessary added damping for galloping is found to be 0.9%, and 0.7% for parametric excitation. It is important to note that damping from parametric excitation should be mechanical dampers and not aerodynamical measures.

Additional dampers come in many shapes and forms and are used on most conventional long span cable stayed bridges. In the cable chapter, a neoprene damper is suggested, but also frictional and viscous dampers are regularly used.

The final damper properties are up to the manufacturer of the cable-system to decide, but we need to know that it is possible to produce the damper that we specify. The possible amount of damping is dependent on the placement of the damper from the support. [43] gives a good overview of some types of dampers and their properties. If the detailing phase suggest that the final additional damping amount is 0.9%, and we use a friction type damper from VLS international and place the damper 8,5m from the cable ends, we could get a damping amount of about 0.6% from a single damper. Each cable is usually fitted with dampers at both ends giving a damping of 1,2%. This shows that we can easily get dampers that satisfy our demand.

> *Figure 15-2 Example of damper, VSL - friction damper*
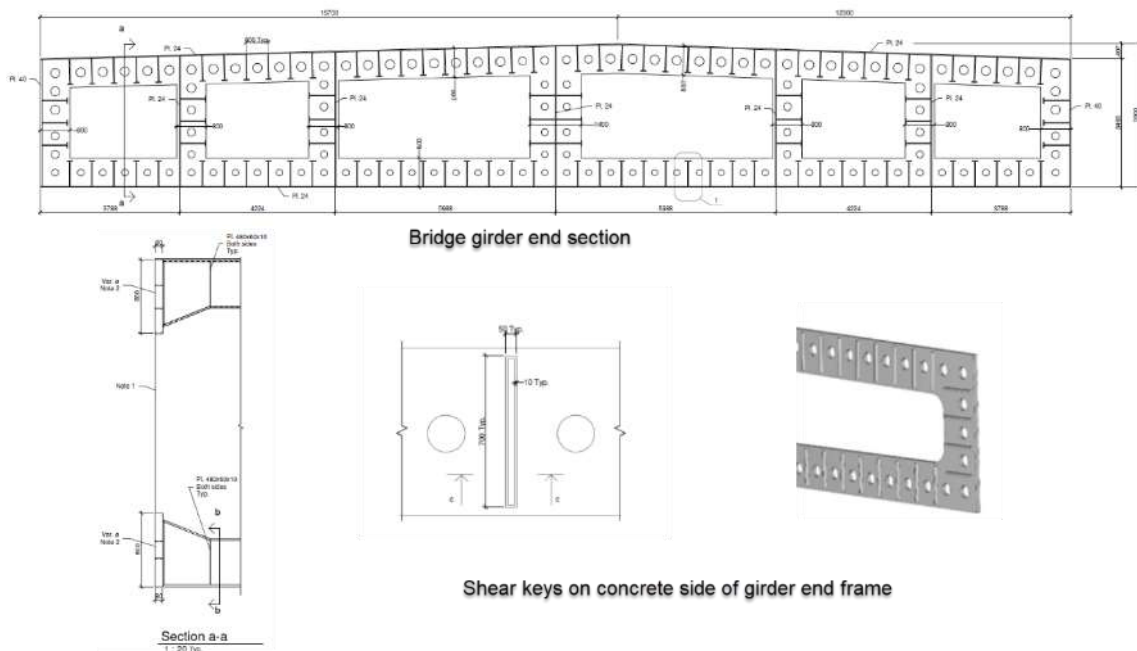
16 ABUTMENTS

16.1 General

Both abutments are founded on prepared bedrock base. The south location is on the island Reksteren and the north is located on the islet Gulholmane. The bridge box girder is monolithically connected to the abutments in both ends. The restraint of the superstructure is resolved by concrete gravity base structures with a box-shaped, cellular configuration. Solid ballast (olivine) and post-tensioned rock anchors are used to enhance the overturning and sliding resistance.

This report focuses on the design of the structural features deemed crucial for the feasibility and performance of the integral abutment concept:
— The direct, integral connection between bridge girder and abutment
— Abutment global stability

16.2 Bridge girder end section

The flexural response in the bridge girder increases substantially towards the abutments and is significantly higher than what can be resisted by the standard box girder cross section generally adopted for the Low Bridge. To strengthen the steel box girder at the ends, the trapezoidal section is transformed into a rectangular section by removing the chamfer and introducing longitudinal diaphragms as well as T-stiffeners for the arrangement of post-tensioning anchors at the joint. The rectangular box has a width of 28.0 m towards abutment north, and a width of 27.6 m towards abutment south. The deck height is 3.5 m as in rest of the bridge.

> Figure 16-1: Bridge girder end section towards abutment north. Front view and section.

The center distance between the trapeze stiffeners in the bridge girder end section matches the T-stiffeners in the general bridge girder section. Within the bridge end girder there is a transition from trapeze to T-stiffeners, ref. drw. SBJ-33C5-OON-22-DR144.

16.3   Bridge girder connection to abutment

The fixed end restrain of the bridge deck is obtained by means of post-tensioned tendons closely arranged along the periphery of box girder and anchored directly into the girder end frame. In order not to interfere with the assumptions for the dynamic behavior, the joint is designed to remain in compression in the ultimate limit state. The necessary post-tensioning level has been determined from the simplified assumption of plain strain distribution over the interface.

As can be seen from Figure 16-2 a high level of post-tensioning is required to compress the joint at abutment north under full loading at ultimate. The post-tensioning level is lower for the abutment south connection, see Figure S-3. For the north abutment, the assumption of a rigid end frame yields a total post-tensioning force of 1 173 MN (before losses), which is achieved by 124 post-tensioning tendons, varying from 6-53 tendons in the upper corner to 6-22 in the lower mid. For the south abutment a total of 84 post-tensioning tendons are needed to suppress tensile stresses over the joint, with a total post-tensioning force equal to approximately 410 MN (before losses). The tendon size varies from 6-31 in the upper corner to 0 in the lower mid.

The tendons and anchors are distributed with constant center distance 600 mm, arranged in between each stiffener.

The shear is transferred by means of multiple steel keys welded to the back of the end frame and arranged in the same pattern as the stiffeners. The shear capacity of the joint is a function of the net force normal to the joint and development of friction on the joint face. The shear resistance at the interface is predicted according to the construction joint provisions in EC2 6.2.5 [44] with the beveled shear keys configured in compliance with the indented surface specifications.

The end frame plate has a general width of 800 mm. The net contact area is 53.1 m^2 for abutment north when accounting for the holes for the PT trumpets (net-to-gross ratio ~0.92). A high strength concrete with a concrete grade of B85 (f_{cd} = 48 MPa) is required to resist the bearing stresses in the joint in ULS. The compressive stresses at service load level is well within the limits to avoid longitudinal cracks, micro-cracks and excessive creep.

> *Figure 16-2: Post-tensioning arrangement at the joint in abutment North (showing number of 0.6" strands per tendon). Center distances are 600 mm for PT as well as for stiffeners.*
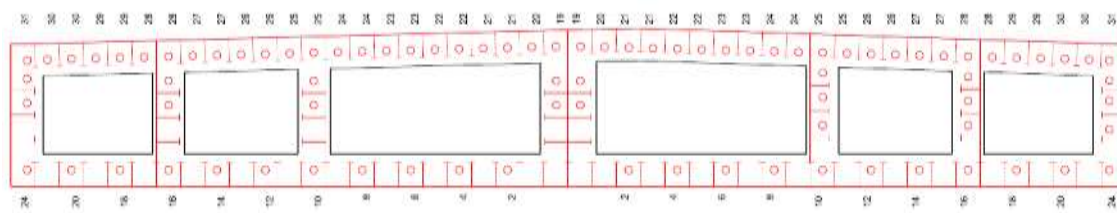
> *Figure 16-3: Post-tensioning arrangement at the joint in abutment South (showing number of 0.6" strands per tendon). Center distances are 600 mm (or multiples of) for PT as well as for stiffeners.*

The caisson is designed as a box composed of slabs and walls which are predominantly subjected to membrane action. In the front part the cells are concrete filled, to distribute the post-tensioning forces into the structure. The bonded PT tendons are anchored in the first open cell row as shown in Figure 16-5. A fraction of the PT-tendons continues over the entire abutment length (joint by couplers) in order to reduce the amount of reinforcement needed to cover up for the tension behind the PT-anchors.

16.4   Foundation

Both abutments follow the same design principle. However, with the current overall dimensions, rock anchors are not necessary for abutment south. The abutments are founded directly on the bedrock. A level base is established whereby weathered and fissured rock is removed/excavated by blasting. To assure a predictable transfer of base shear and normal pressure, only the walls in limited areas in the front and rear parts of the abutment are cast directly onto bedrock whereas the base slab is cast onto a sand/gravel layer. The sliding capacity is determined from base friction only.

As for the joint, to conform with the boundary conditions assumed for the global dynamic analysis, no uplift at any point within the foundation footprint is accepted for the ultimate limit state. The contribution from post-tensioned rock anchors to the base friction capacity and to the overturning resistance is well within the limits prescribed by N400 11.6.2.2 [34]. The rock anchors (north abutment only) are distributed in the front part of the abutment.
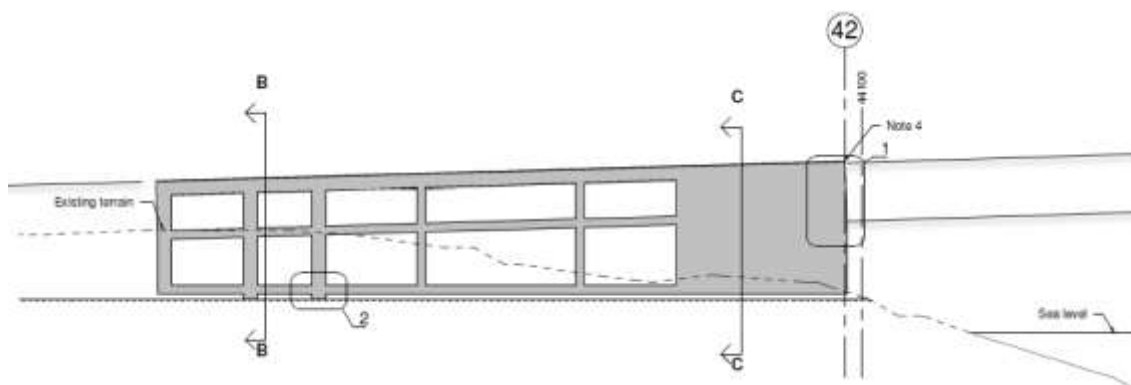
> *Figure 16-4: Elevation of north abutment.*

Norconsult   DR. TECHN. OLAV OLSEN
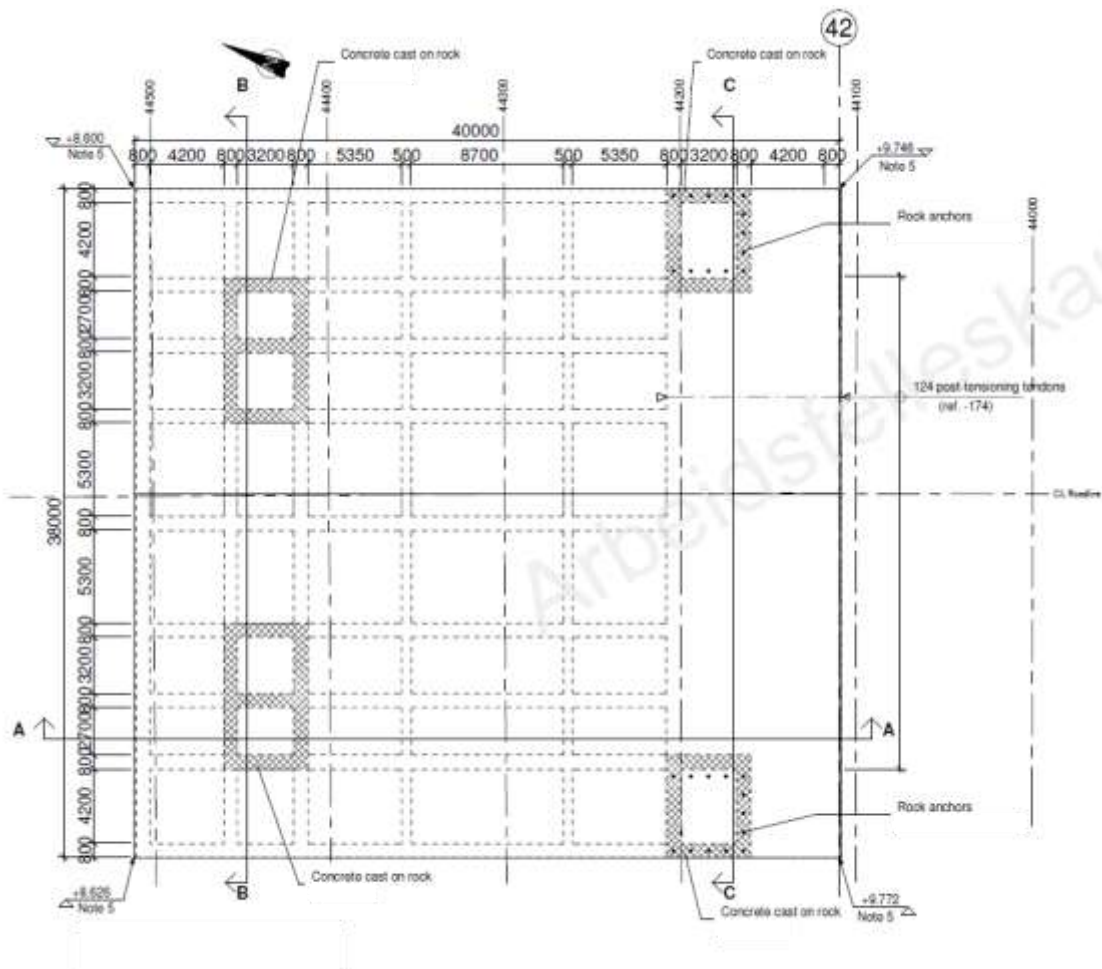
> *Figure 16-5: Plan of north abutment. The shaded areas show the foot print, i.e. concrete cast on rock. The principles are the same for abutment south.*

To get enough capacity for both sliding and overturning at the north abutment the size of the gravity base structure is 40 m x 38 (length x width) with an average height of approximately 7.5 m. Generally, the forces at abutment south is somewhat smaller than for abutment north, except for the axial force which is more than the double. The size of the gravity base structure is 35.5 m x 38 (length x width) with an average height of approximately 15 m. The large height is generated as a consequence of the abutment location in the terrain. Placing this abutment some 10 meters further south will reduced the height, as the ground forms a slope towards the sea. This is recommended to do in a later design phase and will be esthetically as well as economically beneficial.

Depending on the location of the abutment, there may also be an opportunity to provide anchorage by post-tensioning directly into the splay chamber for the cable-stayed bridge. It may then be possible to further reduce the abutment dimensions, since such arrangement may be higher utilized compared to rock anchors.

16.5   Stressing of tendons

The stressing anchors will be located within the walls and slabs and in special brackets, to achieve necessary space for the stressing anchors and jacks. The anchors within the girder end frame are passive, and the stressing anchors are located inside the first cells as shown in Figure 16-6. Stressing will be performed before casting the floor, intermediate walls and roof slab in this area.
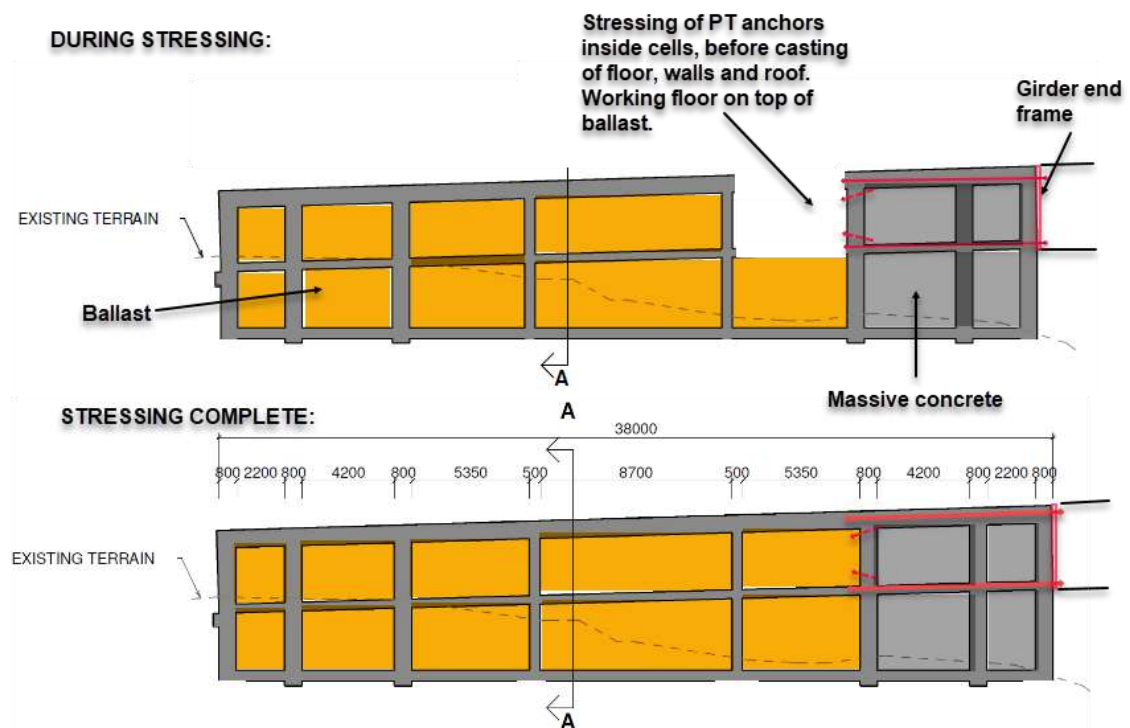
> *Figure 16-6: Stressing anchors inside the cells. Post-tensioning is performed before the floor, walls and roof is cast in the cells of concern. Tendons in walls not shown.*

17 CONSTRUCTION AND INSTALLATION WORKFLOW

17.1 General

Several possible strategies for fabrication and installation have been evaluated throughout this phase of the Bjørnafjorden crossing project, with the aim to improve robustness of the suggested strategy towards the end of the project. In order to highlight possible improvements from automated fabrication, two distinct methods and locations for fabrication of bridge girder elements are outlined in the following sections. The two methods represent two alternative workflows in the total fabrication and installation strategy workflow. For the first alternative, bridge girder elements, pontoons and columns are assumed fabricated at shipyards in Far East, while for the other alternative the bridge girder is assumed fabricated in an automated plant facility locally at site, being able to produce complete bridge girders in longer sections compared to limitations set by sea freight.
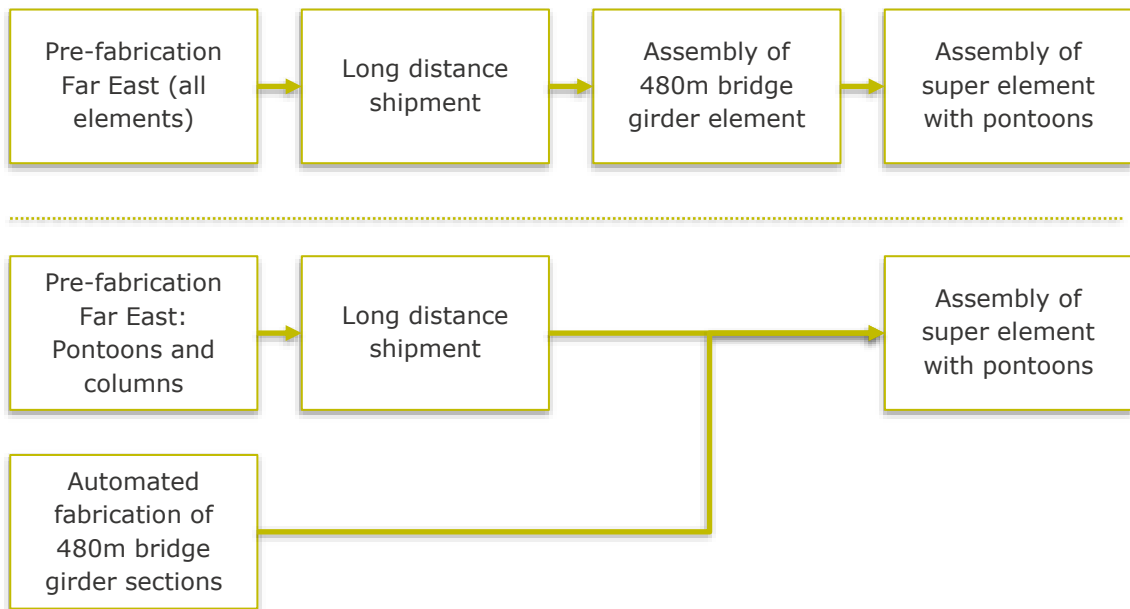
> Figure 17-1: Alternative construction workflows for floating bridge.

The complete fabrication and installation strategies presented are as follows:

— Fabrication of pontoons and columns at shipyards in Far East.
  o For the low bridge, these will be preassembled and shipped as one unit.
  o For the high bridge /ramp, the column will be divided into two and delivered separately to the pontoon with column due for stability reasons.Long distance shipment of pontoons with columns on vessels like «Boka Vanguard» or similar.

— Fabrication of bridge girder elements
  o At yards in Far East. Complete in lengths of 50 to 120 meter. These elements require proper handling both on contractor yard and on destination, by the use of Self-propelled modular transporters (SPMT), cranes and similar. Except for the cable stayed bridge, elements will be assembled and welded into sections up to 480 meters
  o At an automated plant facility locally at the assembly site (e.g. Hanøytangen). The elements will be fabricated into complete lengths up to 480 meters.

— Assembly of super elements in range of 290 meters for north abutment, and 360 and 480 meters for the remaining floating bridge. The pontoons with columns preinstalled will be positioned in dock afloat. The assembly process includes lifting and positioning of the bridge girder, for bolt-joining operations of columns, by the use of mobile gantry cranes.

— Abutments and tower with foundation will be completed in parallel to above described activities.

— Towing and installation of 10 m and 290 m floating bridge at north abutment

— Towing of super elements in lengths of 360 and 480 meter to suggested location for complete bridge assembly (e.g. Søreidsvika).

— Assembly of complete bridge, including high bridge/ramp sections, to a total of 4 430 meters. The elements will be secured by the use of temporary mooring system connected to the pontoons, and by a set of consoles welded to the bridge girder outer skin used to hold position during welding of elements. The operation will be supported by the use of a purpose-built semisubmersible rig during approach, positioning and mating of bridge girders.

— Installation and joining of bridge girder elements for the cable stayed bridge, including installation of cables will be performed in parallel to the complete inshore assembly.

— Installation of anchors and mooring lines will be completed in parallel to above described activities. The installation must be completed at least one year in advance of the final hook-up in Bjørnafjorden. Meanwhile, the mooring lines will be connected to buoys.

— Towing and positioning of complete floating bridge assembly, starting by positioning at the northern end towards already installed floating bridge section (300m).

— Installation and joining operations at both north and south end. The ends will be temporary secured by the use of consoles welded to the bridge girder outer skin. For the northern side, the semisubmersible rig will be used for final positioning. The southern side will use an arrangement of ISO ballast tanks that may be filled with water to adjust the cantilever and compensate for change of tides during installation.

— The mooring lines will be hooked up to the installed bridge, in groups of two for each pontoon through the already fabricated «moon pool», by the use of AHTS and a chain tensioner mechanism.

— Completion works.

17.2 Fabrication of pontoons and columns

The columns are standard stiffened steel plated structures and thus well suited for fabrication at a large range of shipyards and fabrication methods. A flange will be welded at the top of the column shell plating and bulkheads. A mobile machining tool will machine the horizontal surface plane and drill holes where bolts will be deployed for connections to the bridge girders. Dimensions and weight of the columns are listed in below table.

> *Table 17-1: Column dimensions and weights*

| Column types	L (m)	B (m)	H (m)	Weight (ton/m)	Qty
1. Low bridge - Axis 13 through 41	12	4	10.25	15.5	29
2. Ramp - Axis 7 through 12	12	4	17.34 (avg.)	13.2	6
3. High bridge – Axis 3 through 6	12	4	36.24 (avg.)	13.2	4
Total				~ 8 481 ton	39
Total surface area:	26 220 m²				

The pontoon design is standard ship type construction [45] with internal bulkheads and stiffeners suited for worldwide fabrication at a large range of qualified shipyards. It is vital to ensure that the shipyards adhere to the strict surface preparation and coating requirements and have the required welding procedures for welding the corrosion resistant splash zone.

The pontoons can be fabricated on land, on a slip way or in dock and can be transported on own keel (towed) or transported on a barge or transportation vessel. It is recommended that the pontoons fabricator is also liable for the fabrication of columns and that the columns are installed to the pontoons and joint painted before shipment to the assembly site in Norway. 8 of the pontoons will have chain fairleads attached to the bottom plating. These pontoons will need some 2.1 m keel block during fabrication and transportation (assuming dry transport and not wet tow). The chain fairleads could however be installed wet in a later stage. Dimensions and weight of the pontoons are listed in below table.

> *Table 17-2: Pontoon dimensions and weights*

Pontoon types	L (m)	B (m)	H (m)	Weight (ton)	Qty
1. Axis 13 through 26 and 31 through 41	58	12	9	898	29
2. Axis 7 through 12 and Axis 27 through 30	58	14.5	9	1 074	6
3. Axis 3 through 6	58	17	9	1 247	4
Total				~ 38 174 ton	39
Total surface area:	55 000 m²				

The flange on top of the column, machined with bolts installed are shown in below figure. A total of 740 bolts are needed based on a configuration of 2xM42 bolts for every 100 mm of the circumference.
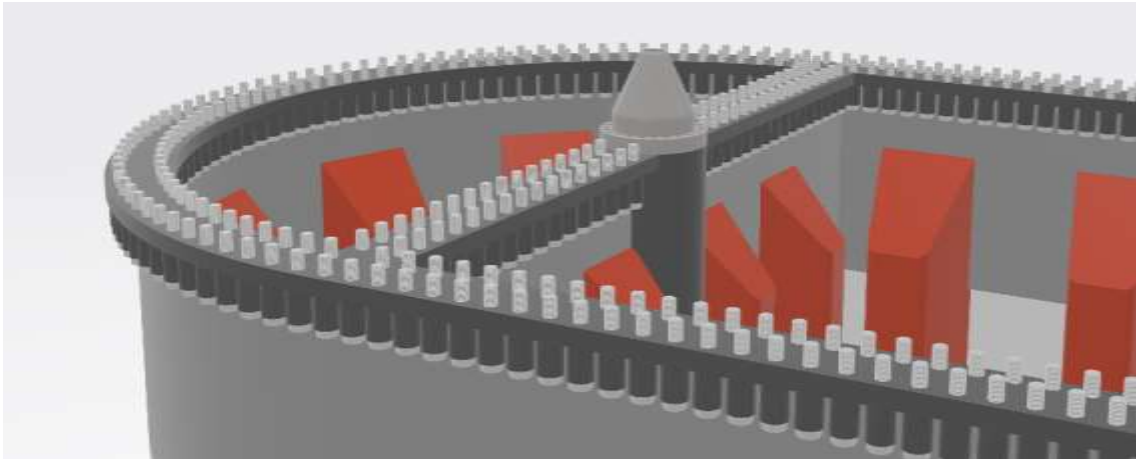
> *Figure 17-2: Top flange of columns showing bolts installed.*

17.3   Fabrication of bridge girder elements

The bridge girder is standard steel bridge structures suited for worldwide fabrication. However, in order to ensure proper tolerances for later joining operations without the use of infills, the elements must be fabricated to an adequate match. Two different methods have been considered to ensure perfect fit between adjoining girders segments: «diamond-wire» cut or by fabricating the end sections in matching jigs.

Depending of the method chosen for fabrication of bridge girders, the elements are either assumed produced at foreign yards (e.g. Far East) or fabricated locally at an automated plant facility. For the first alternative, bridge girders may be fabricated in lengths up to 120 meters, while the automated plant facility may produce into complete lengths up to 480 meters.

The bridge girder for the suspension bridge are in both cases fabricated in about 50 m long segments from the south abutment and to the temporary cantilever structure outside the pylon and 100 m lengths from the end of the bridge girder at the temporary cantilever until end of the suspension bridge.

Automated steel fabrication of the bridge girder requires an advanced factory including laser cutting tools, robot mounting, laser welding, and highly qualified personnel. The factory will require a total area between 10 000– 12 000 m², as detailed in below table. This includes plate storage and all prefabrication. The factory may very well be located at the assembly site for super elements (e.g. Hanøytangen). However, if it is difficult to find a suitable location of this size, much of the prefabrication may be done at other locations, reducing the space required for the main factory.

> *Table 17-3: Automated fabrication facility and size.*

Description	Length	Width	Area
Total workshop area incl. workshop			**10 600 m²**
Warehouse	45 m	40 m	1 800 m²
Prefabrication area	60 m	60 m	3600 m²
Main assembly cell	40 m	60 m	2 400 m²
Surface treatment	45 m	60 m	2 700 m²
Machining of pontoon support	20 m	50 m	1 000 m²
Outdoor assembly area	**500 m**	**200 m**	**100 000 m²**

Using advanced tools and welding processes the fabrication capacity can be increased, making the automated alternative particularly interesting as an alternative to the traditional methods used by most shipyards globally. Below is an example of welding speed for the bottom plates. For this operation, automated welding will give a welding time 12 – 15% of manual welding. By introducing laser welding, the welding time will be 1 – 2% of manual welding.

> *Table 17-4: Welding speed, bottom plate.*

| Plate 12 mm, butt weld (Bottom plate)	Manual MIG/MAG	Robot MIG/MAG	Laser hybrid	Pure laser
Number of welding beds	3	4	1	1
Welding speed	3 m/hour	0,5 m/min	2 m/min	3 m/min
Time for welding of 84 meter	84 hours	11,2 hours	42 min	28 min

An overview of the complete shop floor layout and process are shown in below figure. A more in depth summary of the automated fabrication alternative are outlined in section 18.3.
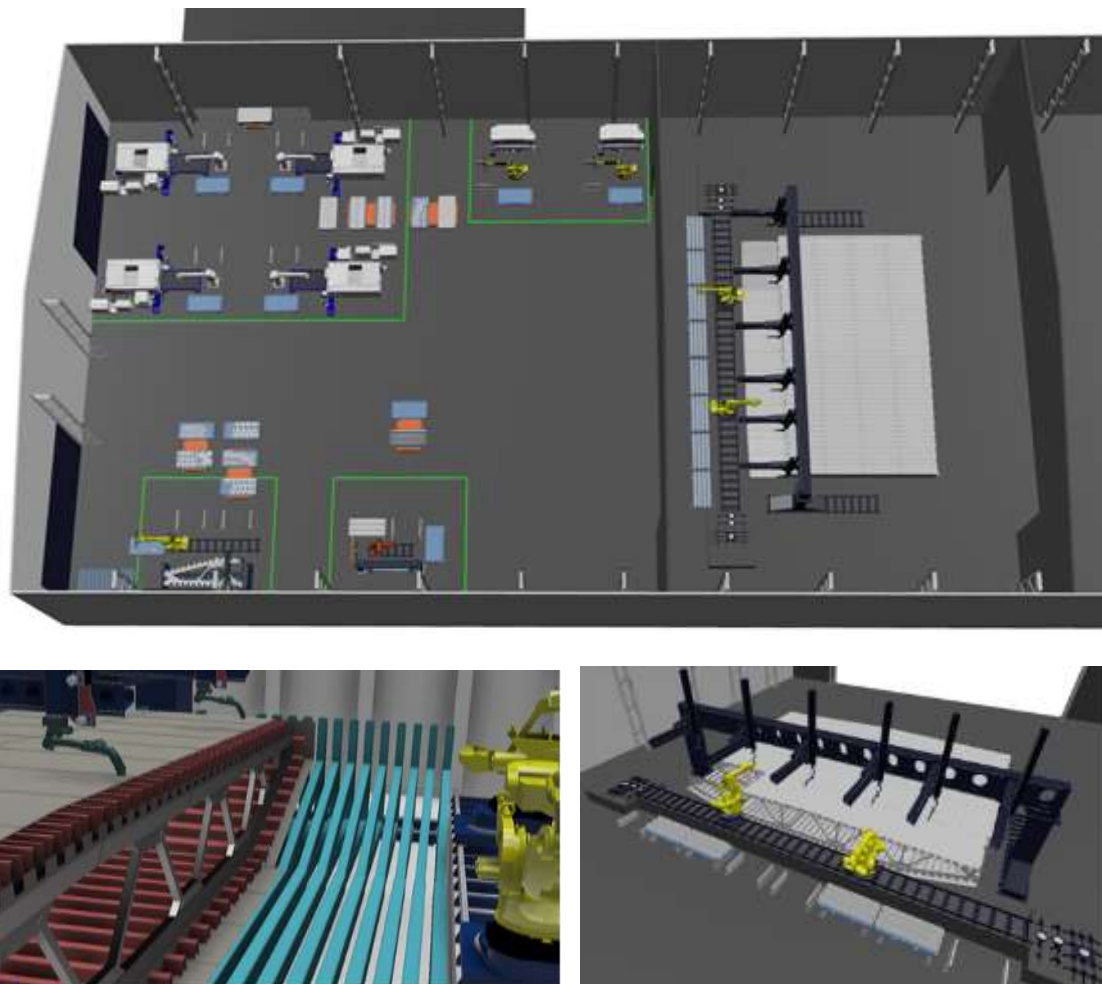
> *Figure 17-3: Shop floor layout, automated fabrication.*

17.4 Transportation of pontoons and columns (and bridge girders) from foreign shipyards

Below figure illustrates a possible deck configuration for pontoons with columns installed and bridge girder elements in lengths up to 120 meters on the vessel "Boka Vanguard". Smaller vessels may also be used for transportation, but estimates indicate this to be more costly when fabricating at yards in Far East. For the alternative with fabrication of all elements at foreign yards, a total of 4 shipments are needed, while for the alternative with local fabrication of bridge girders, number of shipments are reduced to a total of 2. SPMTs are assumed used for load-off of the girders and storage on land, whereas the pontoons are floated off and stored in the dock area.
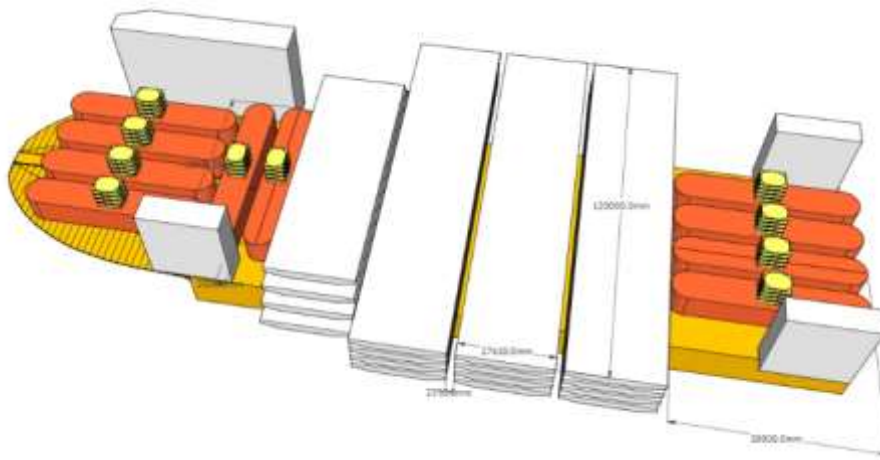

> *Figure 17-4: "Boka Vanguard" configuration example*

17.5 Cable-stayed bridge

The construction of the south abutment with anchoring structures and the tower will start first and independently of each other. The tower is supposed to be constructed utilizing slip-forming or climbing scaffolding techniques.

The following installation of bridge girder elements will be divided in two:

- Landside: 50 meter bridge girder elements will be lifted onto a temporarily built steel scaffolding structure from the vessel by a floating crane («Seaway Strashnov» or similar). The elements will be skidded towards the south abutment one by one and interconnected by welding. Before installing the seaside elements, temporary horizontal bearings must be installed at the pylon to give the girder sideways support during the construction phase.
- Seaside: The deck elements at the seaside will be lifted in position by a crane vessel ("Taklift 4" or similar) and two cranes rigged on the previous installed bridge girder, giving a 3-point suspension to control elevation and tilt longitudinal and transversal. The element will be connected to the existing deck-end by a temporary bolt connection and one pair of the cable-stays will be installed. In addition, installation of two rock anchored stays may be useful to control the movement of the pylon top. After adjustments, the welding of the element connection will be performed and finally the complete cable-stay group will be installed. After finishing welding and cable installation, the cranes are moved to the end of the element for the next lifting operation. These deck elements will be in length of 100 m. The final element (20 m) will be installed by the deck cranes alone.
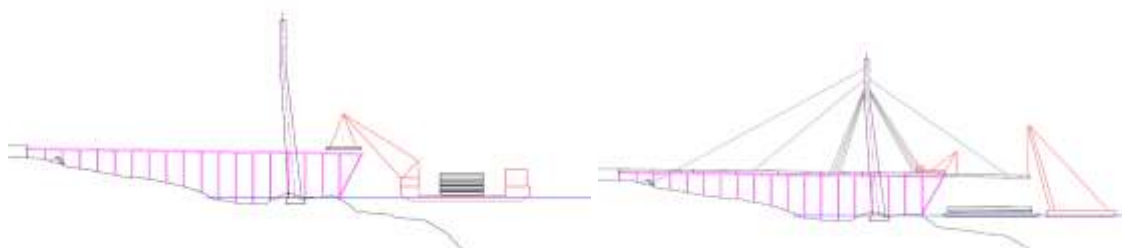
> *Figure 17-5: Installation of bridge elements (left: landside, right: seaside)*
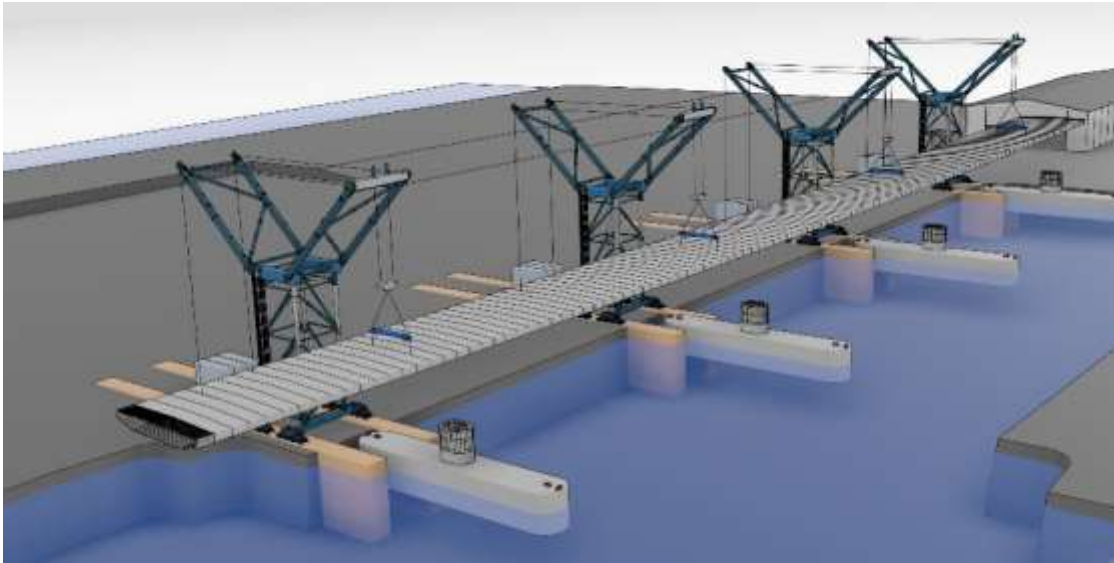
17.6 Assembly of super elements

For the alternative with bridge girders fabricated abroad, maximum length is naturally limited by freight options. Hence, an additional operation is needed to assemble 120 m elements into 360 and 480 m sections.

SPMT's will be used to perform transportation and handling, while the gantry cranes may be used for support to unstack the elements arriving by sea. The elements will be positioned onto cradles at joining area. An insulated tent heated at a constant temperature with circulated air, will be installed at each joint section. In order to avoid difficulties caused by temperature expansion effect, typically heat from the sun expanding the topside of the girder, making an arc, it is advised to start by joining the two middle sections as the first step. When the middle sections are joined the process of surface treatment may start, while the end sections are joined by same method as the middle sections, both in parallel. The joining operation will be performed by single v butt welding, without the process of infill, enabled by the «diamond-wire» method.

For the alternative with automated fabrication, bridge girders may be produced to final length (360 / 480m), avoiding the above described process.

The elements are further lifted into position above the floating pontoons with columns installed by the use of up to 4 gantry cranes, se figure below. The operation requires a location with proper dimensions and a quay area, e.g. Hanøytangen. To reduce time and cost related to transportation operations, it is advised to gather all operations related to super element assembly, and automated fabrication, at the same location.

> *Figure 17-6: 4 mobile gantry cranes for assembly of super elements*

When the bridge element is properly positioned towards the two guide pins at top of the column, two set of strand-jacks are connected and used for fine-positioning of the element during lowering by the cranes. When the element is lowered into position, pressing the pontoons downwards some 2 meters and transferring the deck element load from cranes to the pontoons, strand cables may be tensioned to secure the column towards the bridge element, as shown in below figure. The final bolting operation may now start.
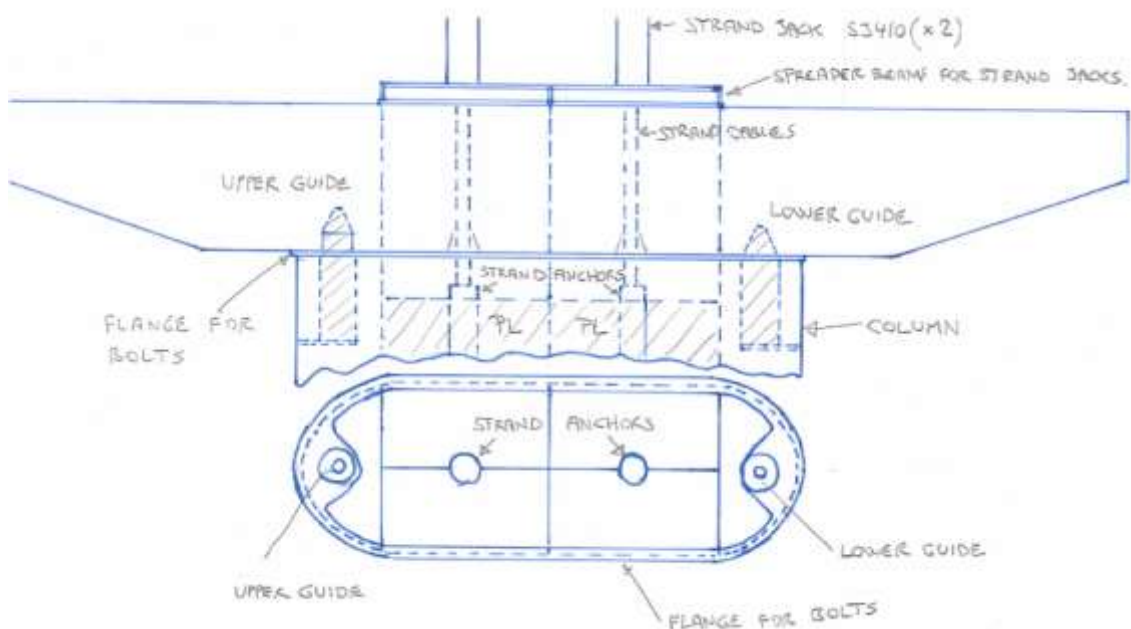
> *Figure 17-7: Guides and strand-jacks for securing columns towards bridge element*

The pontoons at the upper part of the ramp section doesn't have sufficient stability (negative GM) why out rigger has to be attached to 4 pontoons to secure stability prior to positioning for building of the upper ramp section.

The table below summarize number of super elements to be assembled.

> *Table 17-5: Total number of super elements assembled at assembly site 1*

Super elements	Qty	L (m)	Total length (m)	Location
High bridge/ramp	2	470+480	950	Axis 3 – 10
Low bridge	5	480	2 400	Axis 11 – 39
	3	360	1 080	
Abutment North Connection	1	300	300	Axis 40 – 41

17.7 Transportation to inshore assembly site

The towing distance for the entire floating bridge to installation site in Bjørnafjorden is shorter from Søreidsvika why this fjord is the frontrunner for now and assumed to be the assembly site in our method description. The super elements are transported on own keel supported by 5 tugs from Hanøytagen to the bridge assembly site in Søreidsvika along the inshore towing route shown in below figure. The figure also illustrates the most critical point of the towing rout, Vatlestraumen.
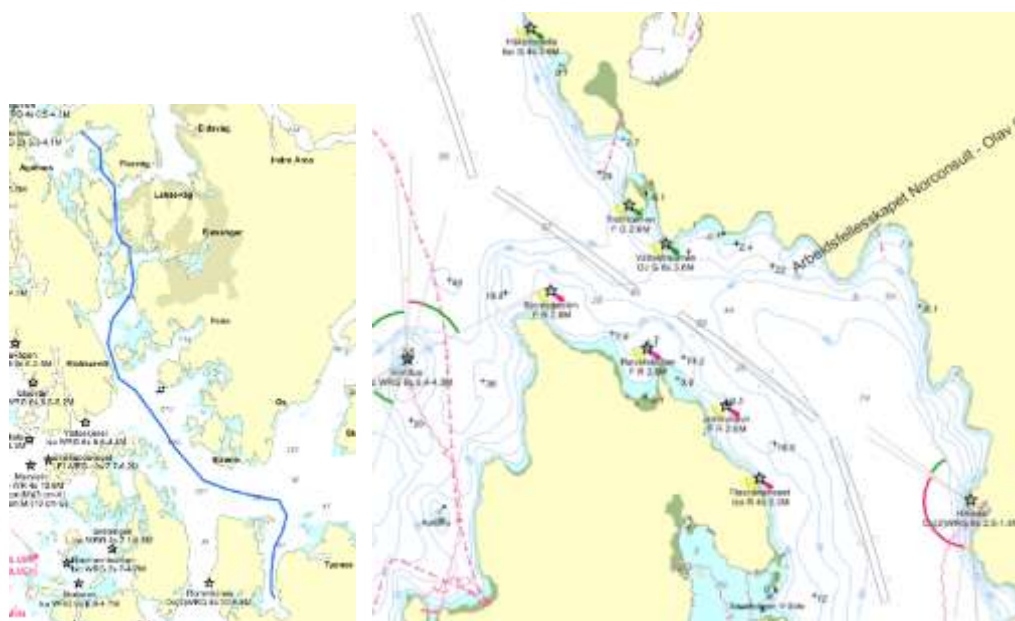
> *Figure 17-8: Towing route (left) and towing of super element through Vatlestraumen (right).*

Upon arrival Søreidvika the pontoons of the 480 m element will be moored to pre-installed mooring lines. The first element will be moored to 4 off mooring lines. The other bridge elements will be connected to the already moored bridge elements and two mooring lines at pontoon the pontoon at located to the North.

A total of 26 mooring lines are pre-installed. Six of the mooring lines are connected to strong point at shore while remaining 20 connections are to anchors. All lines are buoyed off with good clearance to bridge elements towing route.

17.8   Inshore assembly

The super elements of 480m arriving from Hanøytangen will be assembled to a complete bridge in Søreidsvika starting from the low bridge in south of the fjord and finishing with the ramp/high bridge in the north end of the fjord.
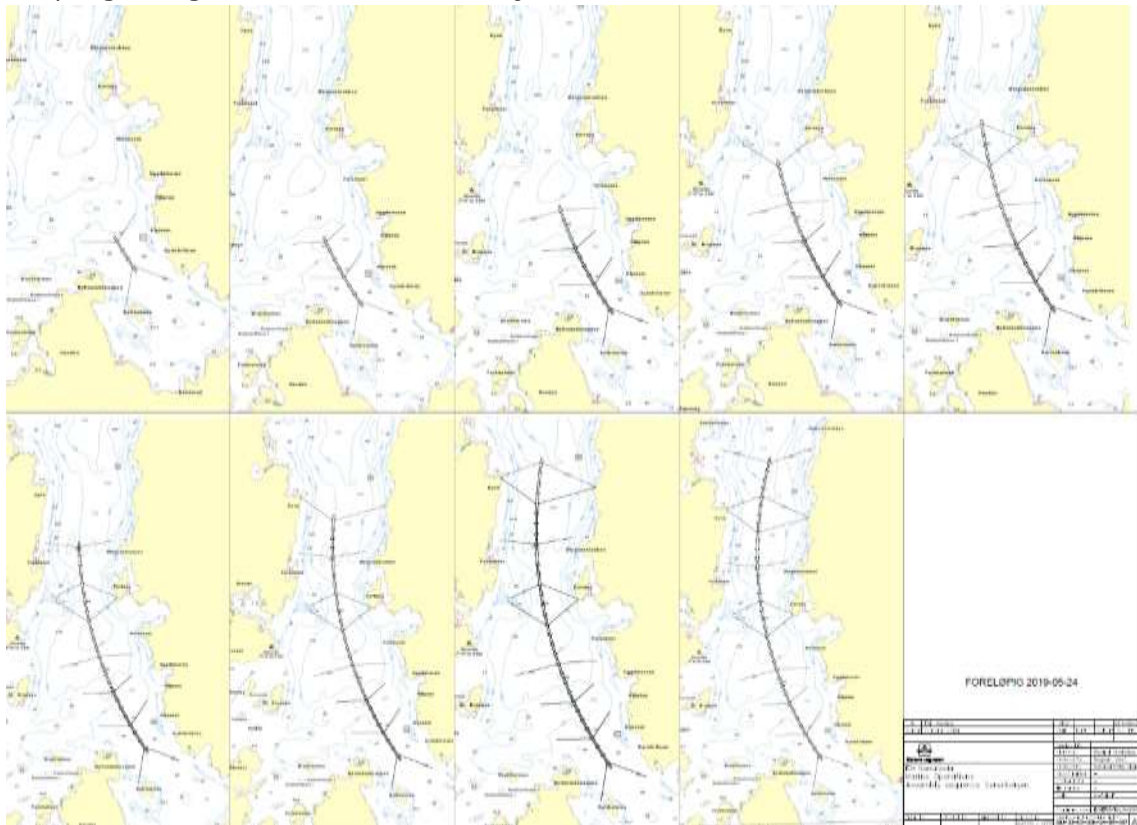
> *Figure 17-9: Inshore assembly Søreidsvika*

A purpose-built semisubmersible rig will be used to support all joining operations. The main purpose of the rig is to lift the cantilever ends of the bridge girders to keep them levelled at mating and to assist with the positioning of arrival new 480 m bridge sections, see figure below.
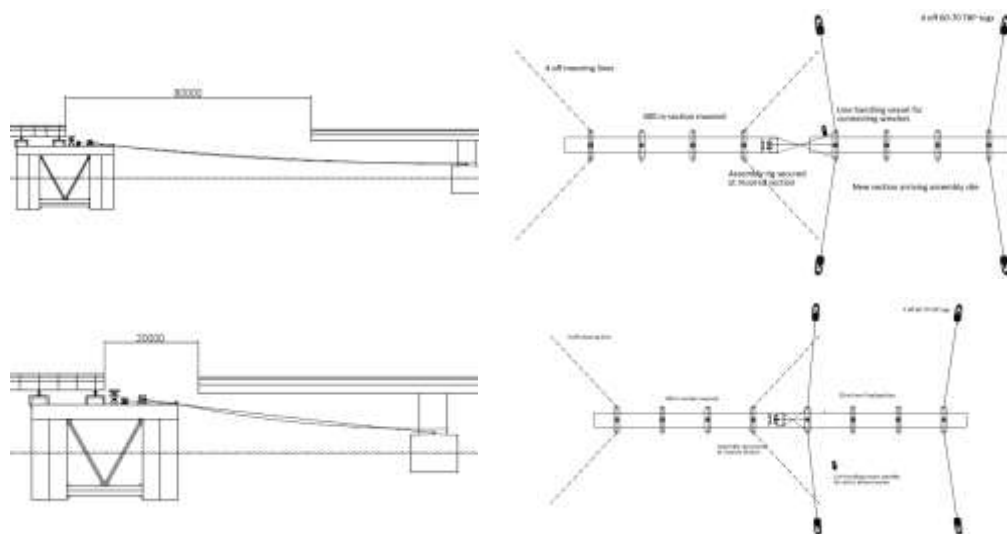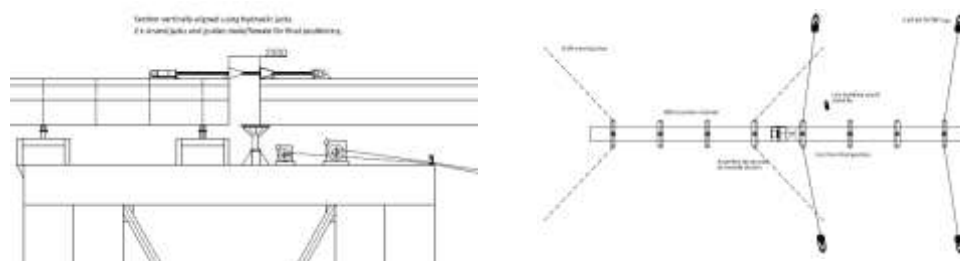
> *Figure 17-10: Inshore assembly method Søreidsvika*

17.9   Installation of north floating bridge segments

A preassembled bridge element consisting of two pontoons and **290m of** bridge girder, and a 10 m bridge girder section, totaling in 300m, will be installed at the North abutment well in advance prior to arrival of the floating bridge section.

The first bridge girder section will be transported on a barge to installation area and lifted in place by using a floating crane («Uglen» or similar). The bridge girder section will land on temporary supports and on a guiding system at the concrete anchor. Anchor cables will be rigged between the 10 m section and the concrete anchor.

The second bridge section will thereafter be towed from bridge section fabrication site by the use of 4 tugs and a barge to support the overhang. The barge will be equipped with 4 mooring winches of about 50 ton pulling capacity each. The mooring lines will be connected to 2 shore bollards. The winches will control the approach and positioning of the bridge girder end section towards the previous installed 10 m bridge girder section whilst the tugs hold back and control the orientation of the bridge section. Male/female connections and strand jack systems between the two bridge girders will secure the final position between the two girder ends. The barge is further equipped with hydraulic jacks to regulate height of bridge girder end for contact towards guides on the 10 m bridge girder and for regulating for tidal variation to ensure constant supporting force of the bridge girder when connecting the bridge girder ends, avoiding a hogging shape of the girder and keep the end of the girder in a horizontal plane.
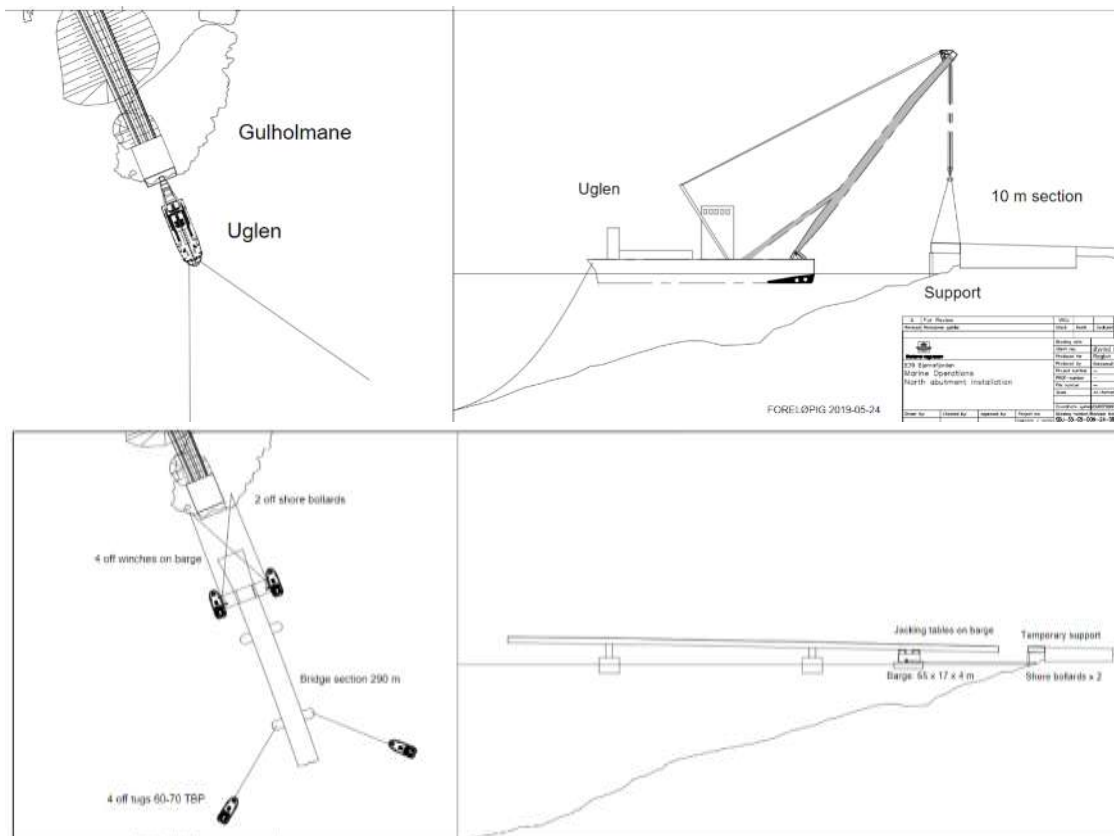
> *Figure 17-11: Installation floating bridge sections north abutment*

17.10 Towage and positioning of the floating bridge at Bjørnafjorden

The floating bridge of 4 430 m will be towed in one piece from Søreidsvika to installation site in Bjørnafjorden. The sailing distance is about 10 Nm, following the route in below figure. The bridge must be turned 180 degrees during the tow.
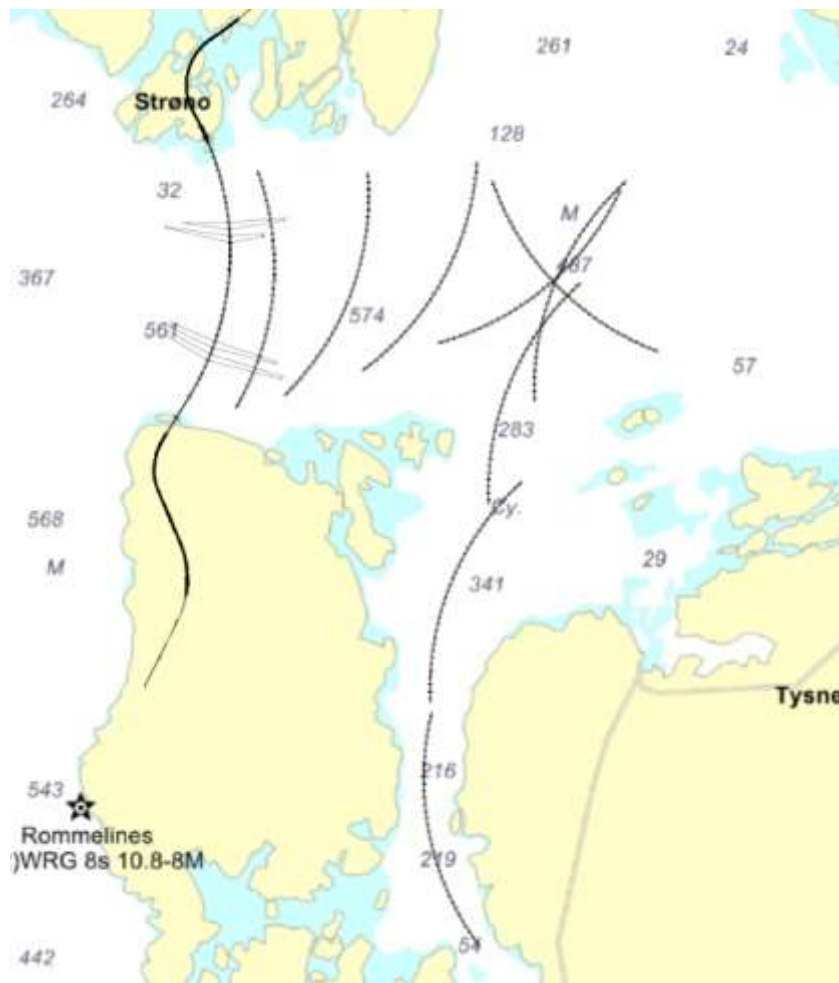
> *Figure 17-12: Towing route from Søreidsvika to Bjørnafjorden*

A total of 8 250 TBP AHTS and 10 60-70 TBP tugs will be used during the tow operation. The tractor tugs control sidewise positioning and rotation of the floating bridge, and the large AHTS give motive power for towage and breaking. The towing operation is expected to take approximately 8-10 hours which includes 3 hours for turning the bridge at arrival Bjørnafjorden. Normal towing speed is expected in the region 1.5 to 2 knots. Normal weather limitation for towing operations is maximum Beaufort 5 for the first 24 hours, which is equivalent to maximum wind of 10.7 m/s.

The fleet is designed to handle a 100 years summer storm if the final installation faces some issues and the bridge need to be kept in a holding position in Bjørnafjorden whilst the problem is being fixed [46].

Upon arrival Bjørnafjorden the bridge will stop the movement and stay in same position while turning the bridge to correct orientation before proceeding to installation location and starting positioning at North abutment.

The overall installation sequence may be summarized in:
   (1) Approach free floating controlled by tug fleet
   (2) Winching in and connecting to north abutment
   (3) Pull into temporary connecting/ guiding structures at north abutment, supported by special purpose semi rig

(4) Connect end of floating bridge and north abutment bridge section by 22 strand cables and pretension

(5) Swing in and pull into temporary connecting structures at Cable Stayed Bridge

(6) Make up permanent connections at north abutment supported by special purpose semi rig

(7) Make up permanent connections at Cable Stayed Brdige side, supported ballast tanks for adjustment to tidal change

Both the Cable stayed bridge side and the north abutment is erected and pre-equipped with arrangements and guiding structures for pulling in and making up the quick connection, prior to the arrival of the floating bridge. For the north abutment, such erection is done by support from the semi-submersible rig similar to the process in Søreidsvika, while the cable stayed bridge is erected using ballast tanks and a temporary cable arrangement.

Starting at the north end, two AHTS will be connected to shore bollard and the bridge will be winched into position, using the winches of the AHTS, until a predicted clearance between the ends of the girders of the floating bridge and the bridge section attached to the north abutment, as shown in below figure.
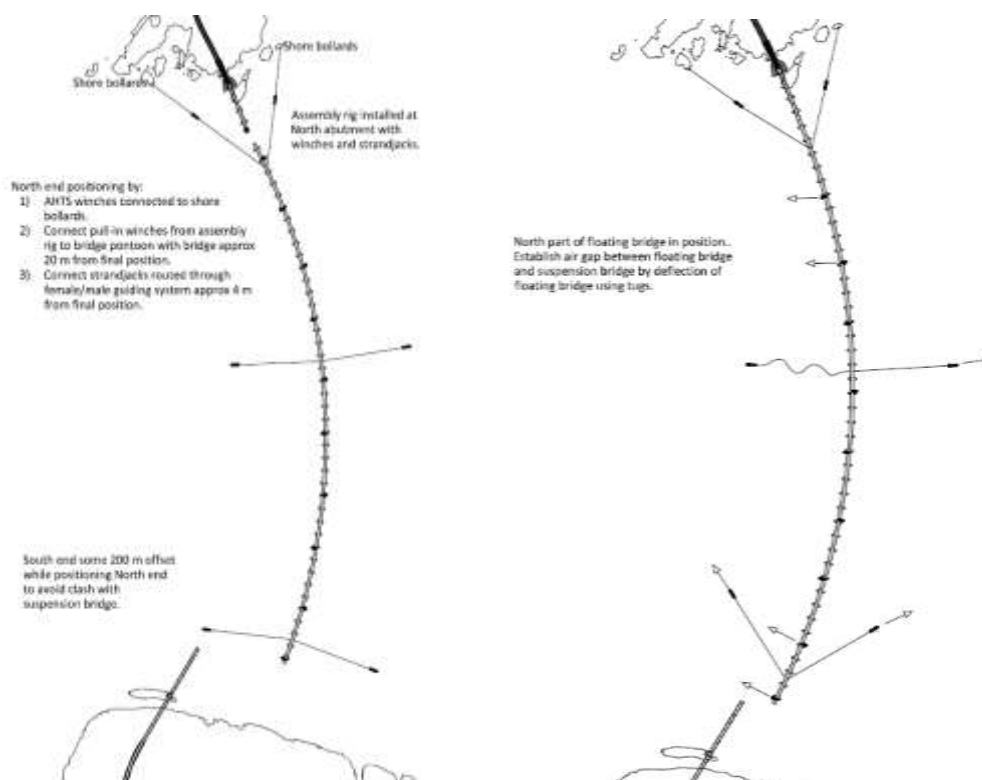
> *Figure 17-13: Installation sequence Bjørnafjorden*

Final approach toward mating will thereafter be controlled by linear winches with support from the tugs until contact with inflatable fenders and a guide securing transverse position of the floating bridge end. The sliding table of the rig underneath will adjust the height to ensure the ends of the bridge girders are levelled. The compressed air in the fenders will be released moving the bridge girder ends closer to each other until contact with temporary structure for the strand jacks, as illustrated in below figure.
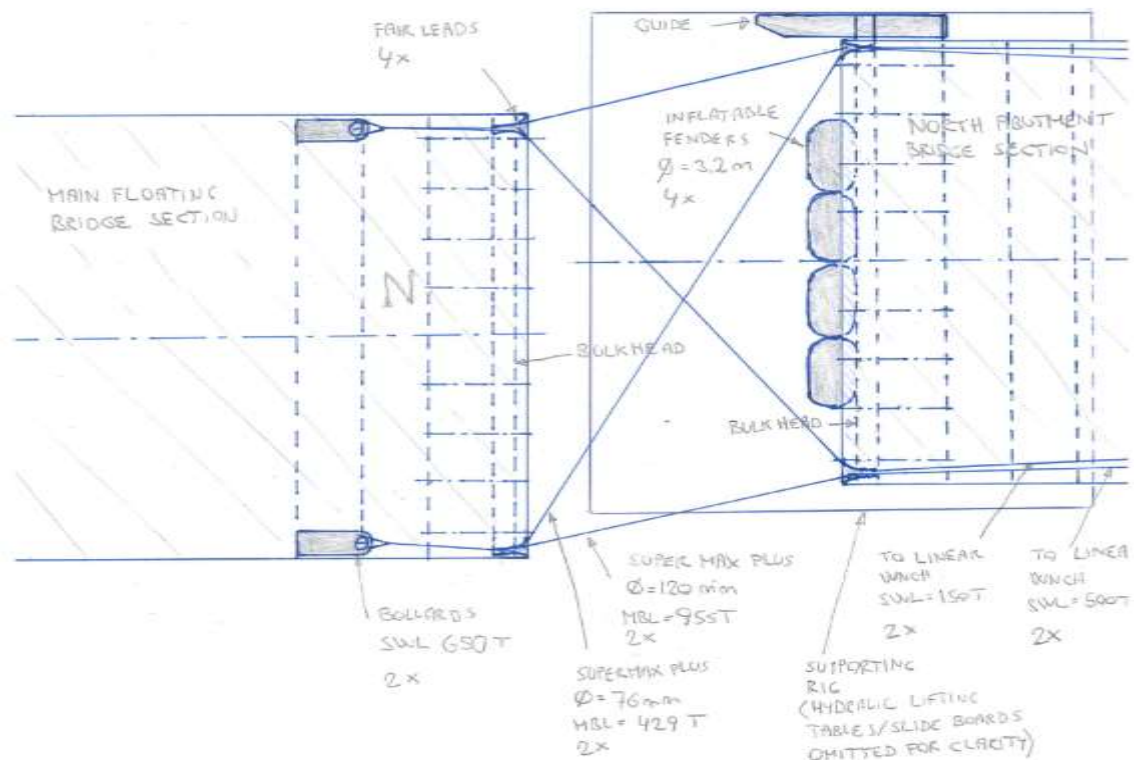
> *Figure 17-14: Final positioning Bjørnafjorden, north end*

The proposed solution for the temporary connections for the closure joints consists of a set of opposite tubular consoles with integrated post-tensioning tendons. The consoles are pre-welded to each of the bridge girders on the outside of the cross-section with shear plates. It is used a total of 9 consoles on the top deck and 9 consoles on the bottom plates. At the girder edges a larger console each accommodating 2 tendons is used. 3 consoles have a dowel (male/female) connector which will be stressed to full contact secure initial alignment. The remaining consoles are equipped with cones and endplates with a defined plate-to-plate gap allowing for shimming to full contact prior to post-tensioning.

When completed, the vertical and horizontal shear forces will be transferred as friction in the endplate connectors whereas the axial force and biaxial bending moments will be resisted by the PT tendons.
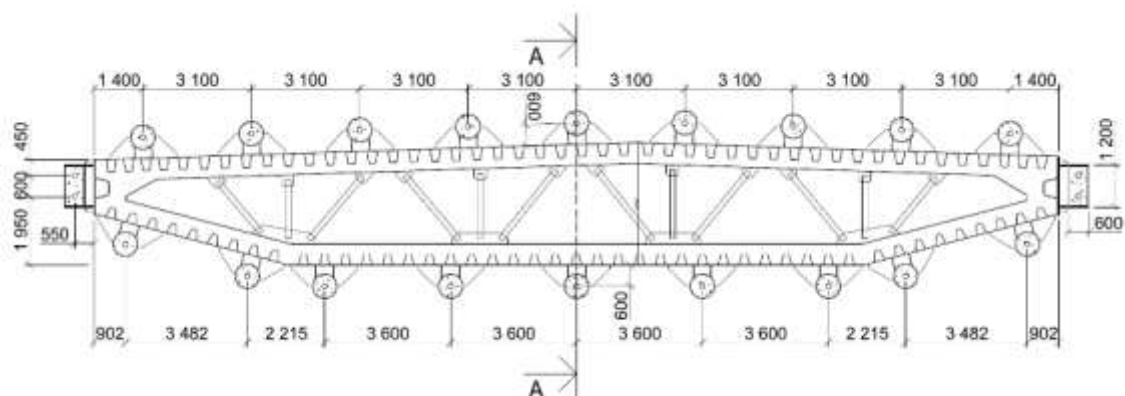
> *Figure 17-15: Temporary consoles at north and south end*

When the temporary connection is secured, adjustment and welding of infill plates may start at one side. This operation does not depend on the weather conditions. After the infill plates are adjusted and welded all around the cross-section, welding to the opposite side of the connection can be done. This operation depends on good weather conditions because heavy wind and waves will cause movements in the welding seam and possibly cause cracking in the weld if this occurs before a continuous weld is established all around the cross-section.

After the infill plates are installed and welded to both sides of the connection, the infill of the stiffeners can be adjusted, installed and welded. This operation does not depend on good weather conditions and are not time critical. After the stiffeners inside the bridge girder are installed, the temporary connection can safely be removed. The loads are transferred from the temporary connection to permanent joint without any significant stress concentrations.

17.11 Installation and hook-up of mooring system

As introduced earlier, the anchors will be installed well in advance of the floating bridge installation, minimum 1 year in advance. A total of 8 gravity anchors and 8 suction pile anchors (SPA) will be deployed and installed alongside 16 fiber ropes.

After the complete bridge is fully installed and secured in Bjørnafjorden, the mooring line hook-up process begins. The pontoons are pre-rigged with anchor chains through two «moon pools», as well as two chain tensioners with power pack and handling gear, se figure below.
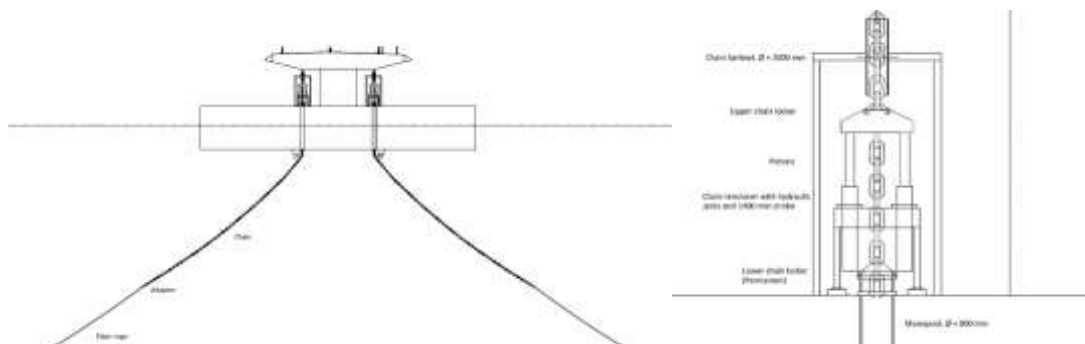
> *Figure 17-16: Tensioning the mooring lines*

The mooring lines must be connected to the pontoon symmetrically. Two AHTS will work in parallel with hook up of mooring lines from anchors, to chain from chain tensioner on deck of the pontoon, as shown in below figure.
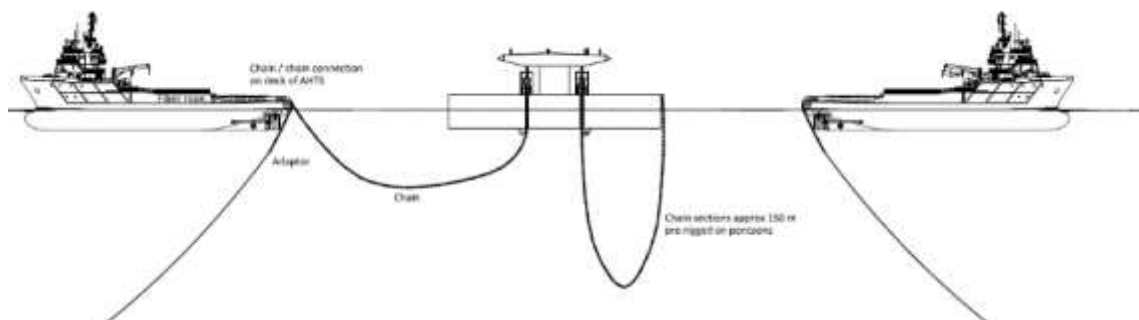
> *Figure 17-17: Hook-up of mooring lines*

17.12 Schematic overview - all processes

Below figures illustrate a schematic overview of the total workflow for above described fabrication and installation strategy, for the two alternative methods: bridge girder fabrication at yards in Far East and fabrication at an automated local plant.
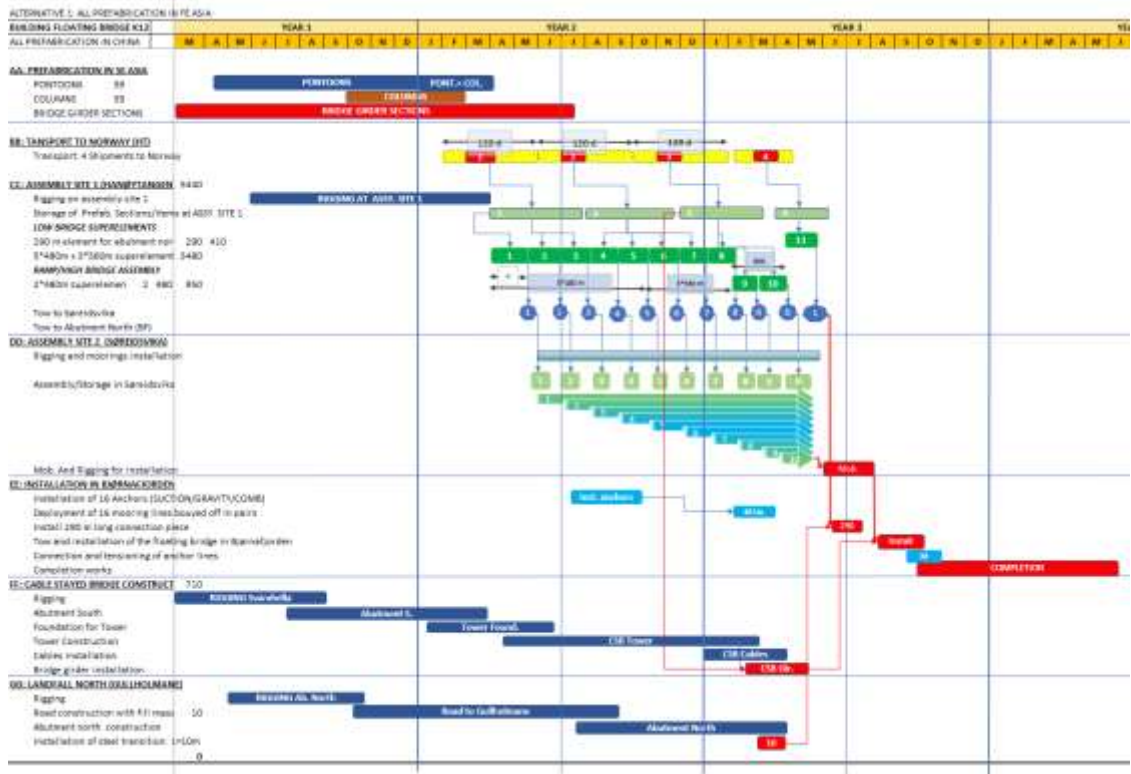
> *Figure 17-18: Schematic overview of activities and process for the alternative with fabrication at shipyards in Far East*
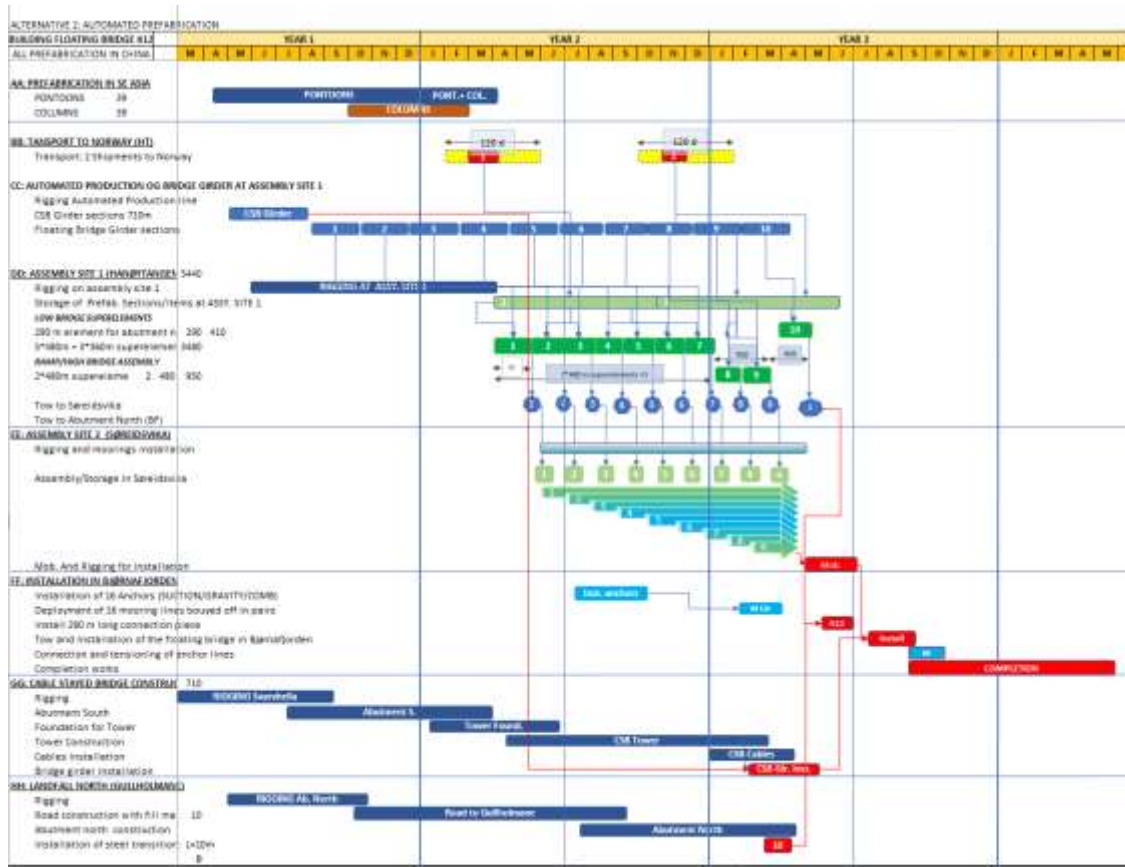
> *Figure 17-19: Schematic overview of activities and process for the alternative with fabrication at an automated local plant*

17.13 Simulation videos

Simulation videos are made to illustrate key operations of both the automated fabrication process, and subsequent processes of assembly and installation, as summarized in Table 17-6.

> *Table 17-6: Simulation videos, execution of construction*

Simulation video and link	Alternative
Plate Handling & Cutting	2
Profile Bending	2
Prefabrication of Top Panel	2
Prefabrication of Framework	2
Bridge Girder Assembly - Mount & Weld Bottom Plates	2
Bridge Girder Assembly - Mount & Weld Bottom Profiles	2
Bridge Girder Assembly - Mount & Weld Framework	2
Bridge Girder Assembly - Mount & Weld Top Panels	2
Bridge Girder Assembly - Assembly Move & Painting	2

Production Facility Overview - Fast Forward	2
Bridge Assembly Operation - 480m Bridge Girder On Pontoons	1 & 2
Bridge Towing Operation - Vatlestraumen	1 & 2
Bridge Assembly Operation - Søreidsvika	1 & 2
Bridge Towing Operation - Bjørnafjorden Overview	1 & 2
Bridge Installation Operation - Bjørnafjorden North Abutment	1 & 2
Bridge Installation Operation - Bjørnafjorden South Abutment	1 & 2
4D Planning Example	

18 AUTOMATED STEEL FABRICATION

18.1 Technology

18.1.1 Application of existing technology for use in bridge fabrication

Development of a brand-new bridge-building technology that increases quality and reduces cost significantly, requires automated mounting and welding operations. Automated mounting and welding operations require high precision as well as a design adapted to this building method. This technology will also give benefits such as significantly less building area, much higher building speed and removes a lot of dangerous manual operations.

All welding and prefabrication equipment, the cutting cell and storage facility are dimensioned to fabricate 12 meters each day. The output from the workshop will be continuous bridge modules with length up to 500 meters. The modules will be fully welded, and the surface treatment will be finished inside the manufacturing area. The length of bridge modules can be extended if required. After leaving the workshop, the bridge modules will be assembled onto the pontoons. There are several methods for the assembly operation, the chosen method is described in report SBJ-33-C5-OON-22-RE-023 K12 *Execution of construction* [21].

Technology
An automated fabrication using robot mounting requires higher accuracy than in traditional fabrication. To obtain higher accuracy, the fabrication includes many advanced tools. The main technology areas involved are:

- Robot welding
- Robot assembly
- Laser welding
- Laser hybrid welding
- Laser cutting
- Advanced automated fixtures
- Advanced press brakes for forming profiles
- Object-based 3D model for simulation, robot programming, work instructions and quality, and lifetime information
- 4D planning

The combination of smaller sheet sizes, high precision cutting and bending and laser welding makes it possible to produce the bridge deck module continuously in a fixture.

In addition to cost-saving, important beneficial effects will be introduced:

- Higher weld quality equals better fatigue properties
- Higher accuracy
- Easier logistics and planning
- Reduced number of fabrication errors

Material quality
For automated fabrication, the requirement for the material quality is higher than for traditional fabrication. Laser welding has a higher requirement for the chemical composition, and the bending machines have a higher requirement for the plate thickness. Because of the high requirement for material, an automatic fabrication may give a higher material cost than traditional fabrication.

The Design Basis [22] describes S420 as the highest material strength grade that can be used in the design of bridge steel structure. Available on the market are material quality with yield stress up to 1 100 MPa made for laser welding. In the future it should be evaluated if high strength material can give benefits in bridge design.

The fatigue properties will not be improved, so if the fatigue is the governing factor, a higher material quality will not give any benefit.

Steel structural design
Modern production methods will be most effective if the design is optimized to the production capacity and tools. New tools will also give the designers room for development and application of new solutions and structural details that can improve the production capacity or save weight.

The use of welding robots makes it easier to pre-heat the material before welding. Because of easier pre-heating, other material quality or thicker steel plates which require pre-heating will be easier to use when using robots compared to manual welding. Tools for induction heating can be mounted on robots, but pre-heating can also be done by defocusing the laser beam in the laser welding tool.

In traditional fabrication, welding is very time consuming and expensive. The design will therefore try to increase the plate size as much as possible. Another benefit using advanced tool and automated building process is higher speed and lower cost for welding, and it may be economically beneficial to weld together smaller parts. This gives possibility to design in a new way.

Using advanced cutting and bending with high precision, the plates and profiles can be designed in such a way that components go into each other and mounting the wrong way is not possible. Plates and profiles can be designed with a common interface, e.g. slots and notches, which will prevent incorrect assembly.

18.1.2   Potential benefits

Cost savings
Currently, the cost related to building the pontoons with columns and bridge deck girder in low salary countries represents less than 50% of the cost for the final assembled steel structure. The remaining expenses are related to the assembly on location, transport from Asia, cost of the supply chain, quality cost and cost of delays. By having an automated fabrication in Norway, the workforce cost is significantly lower compared to traditional production in Asia.

By using modern production tools, it will be revealed that cost savings for the steel constructions compared to the traditional way of producing can be significant; Potentially more than 30%. Savings will be a result of fabrication of the bridge, assembly of bridge sections to modules, assembly of the bridge girder to pontoons and lifting of parts onto the high bridge.

The following list presents some of the cost-saving areas:
- Same or lower salary expenses producing with robots in Norway compared to the Chinese workforce.
- Reduction in transportation cost from Asia
- Reduced number of hours spent in Norway connecting short bridge elements and connecting pontoons to girders.

- Lower cost for heavy lift and offshore operations.
- Better production planning.
- Reduced fabrication and assembly time

All the cost savings and comparison between traditional building and automated fabrication in Norway is reported in SBJ-33-C5-OON-22-RE-023 K12 *Execution of construction* [21]

Green(er) production
An automated steel fabrication close to the assembly site for the bridge is considered to give less environmental footprint.

Less energy consumption due to better welding method.
Less activity for assembly in open sea.
Less transport of personnel.
Less transport of fabricated steel.
Fewer marine operations

High focus on steel delivery is important, to buy the steel far away may give high environmental footprint also for an automated Norwegian fabrication.

HSE
Health, safety and environment are important aspects for the whole project. A strong focus on HSE is required from contract to production and throughout the bridge lifetime with maintenance.

Generally, it is assumed that a new production method will improve HSE quality compared to Asian production facilities, but for an Asian fabrication, there will be other issues than for an automated Norwegian fabrication.

For Asian fabrication, it will be issues regarding:

- Leadership attitudes for safety
- Personal health
- Welding fumes
- Crush injuries
- Codes of conduct and ethics….?

For automated Norwegian fabrication the main issues will be:

- Eye injuries from the laser light
- Crush injuries from robot operations

Laser welding tools are very dangerous for human eyes and there will be a high requirement for safety. The heavy handling robots are powerful and propose a high risk of serious injury.

Quality assurance by having data model with process data
A digital production plant with input from the 3D model makes it possible to gather data directly from machines and sensors. Welding information related to each weld is especially interesting and can be collected without manual time-consuming processes. Data can be stored in the 3D model if each weld is an object in the 3D model.

Collecting the production information is considered highly important. The difficult part when collecting large amounts of data is to extract the most valuable information.

One concept can be to make each weld unique. This means that when the design process is complete, and the product is ready for production preparation, each weld will be

automatically created in 3D, with its unique ID-number. If the user needs information about one specific weld, the user finds the ID-number and acquire the information required for the specific weld. Weld specification includes information such as throat thickness, welding parameters, etc.

When the robot initiates the welding procedure on one specific weld, it reports starting time, welding settings, continuous amp, voltage, gas parameters, welding position, and welding wire. This means all data available from the different equipment is stored in a database and can be visualized live in the 3D model as progress. This 3D model can also be stored in a cloud database that can be accessed by people with the right privileges. Same goes for assembly, cutting, press brake, even internal transportation.

NDT (Non-destructive testing) results can be reported in the same way directly on each weld number. The effect of this is that NDT results can be matched with the welding program to find the cause of what happened in the area where a weld does not meet the quality requirements.

18.1.3 Welding methods

This fabrication method is dependent on high welding speed and laser welding tool is evaluated as an alternative to the traditional MIG/MAG welding.

There are different benefits with each of them, the MIG/MAG welding head is small, and is the best solution for areas with limited access. Laser welding tools have higher welding speed and less heat input. A short summary of some welding methods below.

- Laser welding: Pure laser welding is a well-known method in various industries with a large amount of welding, or if high precision is necessary. For bridge steel structures it is considered to be a new technology. Pure laser can make a butt-weld between two plates with thickness up to 12 - 15 mm. In practical use for bridge building, this is difficult because the maximum gap between the plates is 0,1 mm when using pure laser. The plate edges must be machined and clamped together. Pure laser can be used for "gluing" two plates to each other. If the stiffener profiles are made with a flange, pure laser can be used to weld the stiffener profiles to the bottom plates.
- Laser hybrid welding: Laser hybrid welding combines laser welding with MIG/MAG welding. This gives a high welding quality with very high welding speed. For butt-welding, laser hybrid method is chosen to accept more gap between plates. Because laser hybrid adds material, the process can accept higher gap than a pure laser process. Welding speed up to 8 m/min for thin material. For plate thicknesses used in bridge building, welding speed up to 2,5 m/min may be possible. The laser hybrid technology has less heat input compared to MIG/MAG welding, and therefore less welding deformation.
- MIG/MAG welding: For some of the welding operations, it will be preferable to use traditional arc welding methods. The reason for this may be accessibility, tolerances or cost. The laser hybrid welding head is quite big and there may be challenges to get access for the equipment. For other operations, it may be challenging to obtain the required tolerances or gap required by the laser or laser hybrid welding technology. The MIG/MAG is a slow welding process that in many cases will increase building time significantly. If the welding length is short and welding time with traditional arc welding does not influence the building time it may be an economic benefit to use MIG/MAG welding.

18.2   Workshop and Processes

There are a lot of options for building methods and processes combining different designs, welding methods and fabrication sites. This chapter describes how automated manufacturing of bridge girder is planned according to the chosen fabrication method.

The use of robots to assemble and weld with laser/laser hybrid is a well-known technology. But information about this methodology in bridge constructions with plate thickness as in the Bjørnafjorden bridge is close to non-existing.

The workshop (**Error! Reference source not found.**) contains 4 compartments. Warehouse, prefabrication area, bridge girder assembly area and area for completion and surface treatment. The workshop must have a length of appr. 200 meters and a width of 45-50 meters between columns. Outside the workshop behind the main assembly of the bridge girder, there should be 500 meters of open space on a quay to store the bridge girders and this is the location for the final assembly where the bridge girder is mounted to pontoons.

> *Figure 18-1: Factory at Hanøytangen*

> *Table 18-1: Area requirements for automated bridge deck fabrication*

Description	Length	Width	Area
Total workshop area incl. workshop			**10 600 m²**
Warehouse	45 m	40 m	1 800 m²
Prefabrication area	60 m	60 m	3600 m²
Main assembly cell	40 m	60 m	2 400 m²
Surface treatment	45 m	60 m	2 700 m²
Machining of pontoon support	20 m	50 m	1 000 m²
Outdoor assembly area	**500 m**	**200 m**	**100 000 m²**

18.2.1   Warehouse

Material storage and handling are important parts of the fabrication area. The steel plates going into fabrication need to have high quality without any corrosion or other damages. The logistics are also very important, due to the use of various plate thicknesses and material qualities. The steel plates must be stored in an area with controlled temperature and air humidity to prevent corrosion during storage. The storage capacity for steel plates must be about 6-8 000 tons. In the sketch below there is enough space for 100 pallets with about 70 tons each, which means totally 7 000 tons of steel.

A normal production rate is planned to be 12 meters each day. In this production rate, the flow of steel through the workshop will be roughly 180 tons (including scrap). The storage area must have the capacity to process a shipment of 3 000 tons after 16-18 days. There must also be a minimum material stock for 2 weeks of production at all time, in case of delays in the supply chain.

The pallets with steel plates will be stored in special racks with height about 1,25 meters adapted to transport the pallets by multi-wheelers.
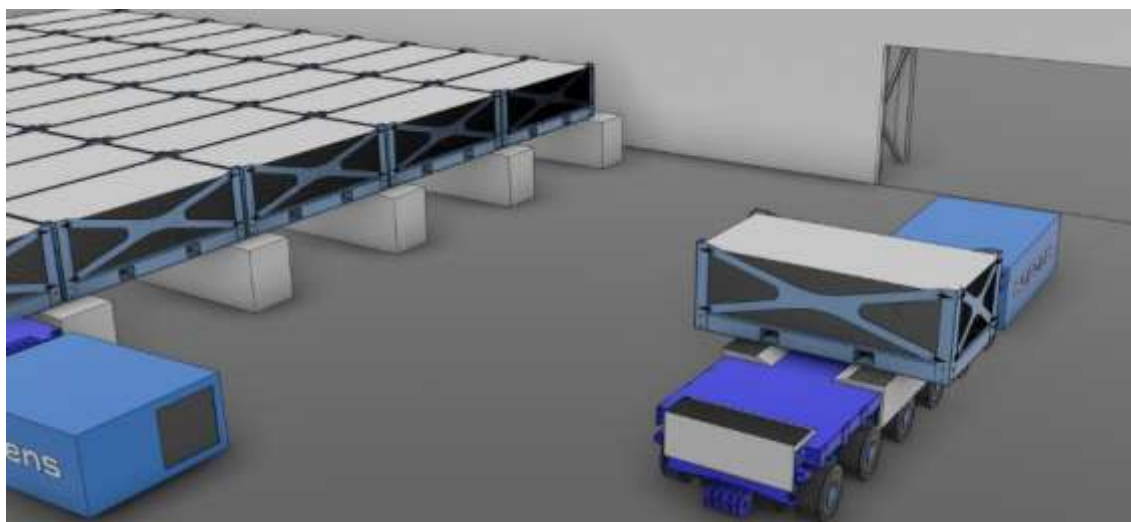
> *Figure 18-2: Storage and transport of plates in the factory*

18.2.2   Prefabrication

The automatic fabrication of the bridge girder is a complex composition of advanced process equipment. By dividing the factory into several small prefabrication areas, the factory becomes more lucid and streamlined, and it makes it possible to pre-fabricate some components at other sites if necessary.

To do the automated fabrication it is necessary to increase the tolerances requirement compared to a traditional fabrication and other types of process equipment are necessary. The most important process equipment is described below.

– Control station for plates. To ensure the correct quality of the plates, it is planned to have a control station before cutting. This control station will verify the quality, weight, outer dimension and thickness on several points on the plates. If a plate is disapproved by the automatic control, it will be manually checked.

- Material cutting. All plates with dimensions less than 20 mm to be cut with Laser cutting machine. Other plate thickness to be considered for each case. TRUMPF is a market leader for laser cutting tools and it is planned to use laser cutters type TruLaser 3040. This laser cutter has high cutting capacity and precision. The laser cutter has two cutting tables, one inside the machine for cutting operations and the other outside for removing cut parts and reloading with a new plate. This laser cutting machine can handle plate formats up to 2 x 4 meter. Link to simulation video file: Plate Handling & Cutting
- Welding groove preparation. The laser cutters from TRUMPF do not have the possibility to angle cut and it will be necessary to use machining tools to prepare welding grooves. The type of tool for this is not evaluated, but it will be necessary to have a fully automated cell for machining the welding grooves.
- Bending of plates. There is a need for different types of bent parts in the bridge design. Most of the parts are longitudinal stiffener profiles and parts for the transverse girder. All bent parts must be made with maximum quality due to the tolerances needed in the laser welding. To achieve the necessary tolerances and gap for laser welding it is necessary to have high accuracy on the cold forming of profiles. It is therefore proposed to use marked leader machines from TRUMPF for these operations as well. These machines have a very high accuracy that is achieved by pre-bending about 98% of the angle, then measure the angle and then bend the last 2%. Link to simulation video file: Profile bending
- Prefabrication cell for transverse girder. To reduce the welding in the main assembly line, it will be preferable to weld together components in a prefabrication cell where it is possible. This will increase the building speed. In order to get manageable component weights it is proposed to divide the transverse girder into four smaller parts and assemble these four parts into the bridge girder. The dimensions of these four parts are small enough to be handled by a robot of type Fanuc M-2000iA/1700L. Link to simulation video file: Prefabrication of Framework
- Prefabrication cell – top plate elements. There are a few different solutions for how to build the steel structure at the top of the bridge girder. For this project it is chosen a solution were the stiffener profiles are welded to the top plate before mounting on the bridge girder. This reduces welding in the assembly cell but requires full welding of the stiffener profile before the next element is positioned. It is recommended to use laser hybrid welding for this prefabrication cell for increased speed and capacity and reduced heat input. Link to simulation video file: Prefabrication of Top Panel
- Prefabrication of side plate elements. The stiffener profile will be welded to the side plates before it is assembled to the bridge girder. There will be only one stiffener profile on each side plate. Due to the large weight and dimensions, it has to be performed in a semi-automatic prefabrication cell. All lifting operations must be done manually by crane. It is also proposed to perform the welding operation using MIG/MAG.
- Prefabrication of column support. There will be an area above each column subjected to higher loads where thicker steel plates are necessary. There are two alternatives, the first one is to include this in the automated fabrication. Because of thicker plates, the plate size must be reduced to a weight that can be handled by a robot. Reducing plate sizes increases the welding, and because the plate thickness is higher than what can be welded by laser tools, it is proposed to build using traditional methods. It is therefore proposed that the bridge girder area over each column will be made the traditional way and lifted into the welding jig by crane. That will be a component with dimensions approx. 12 x 18 meter, with a weight of 80 – 120 ton.
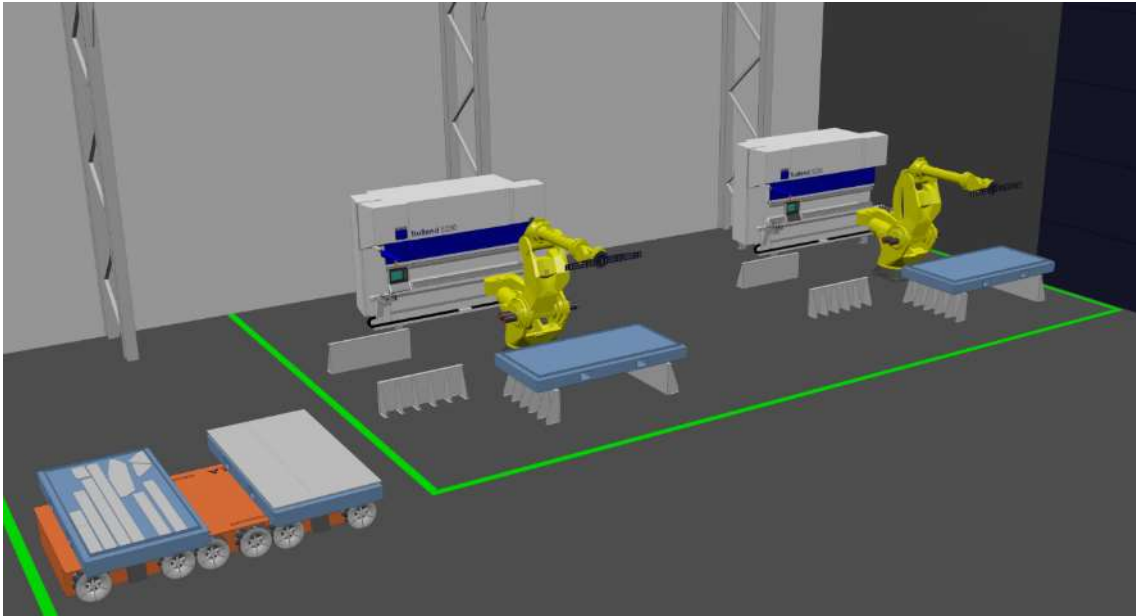
> Figure 18-3: Bending cell with two bending machines and handling robots
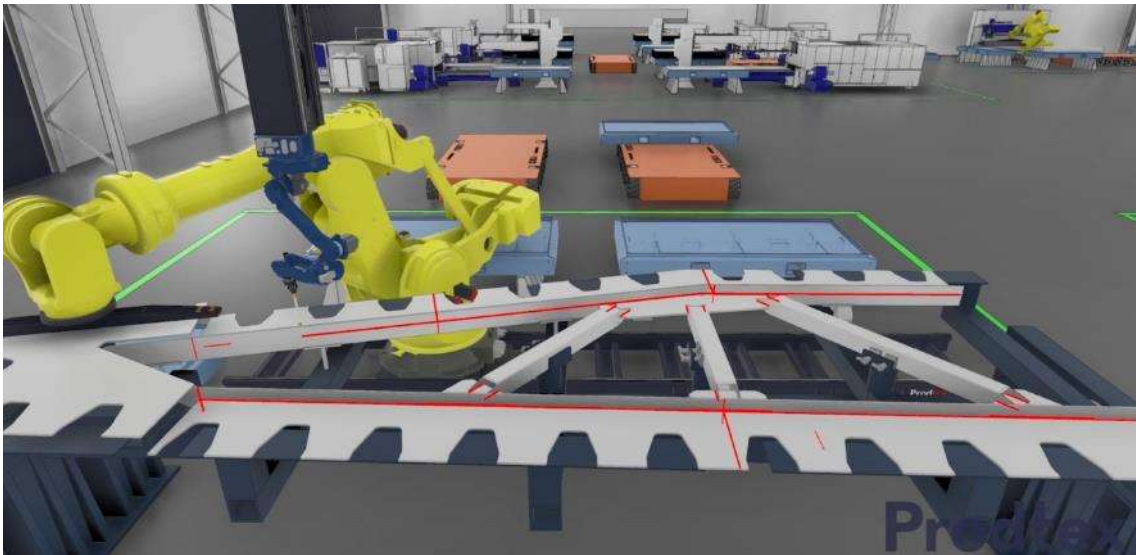
> Figure 18-4: Prefabrication cell transverse girder
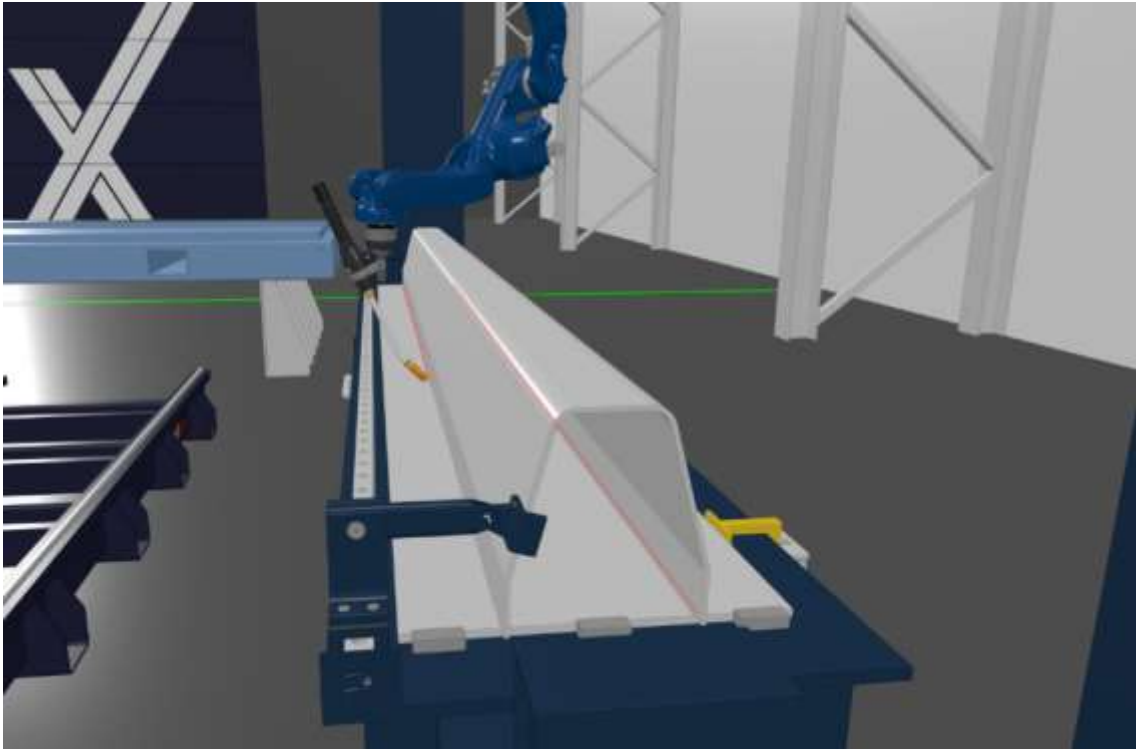
> *Figure 18-5: Prefabrication cell top plate elements*

18.2.3   Main assembly cell

The main assembly cell is the heart in this new technology and is developed for bridge girder assembly. The technology may also be used for other types of steel structures.

The method is building a bridge section with 4 meters length fully automated, move the girder 4 meters and perform the same operations again. Fabrication of 12 meters each day requires 3 launchings each day. To reach this fabrication rate, mounting and welding must be done within 6-7 hours and launching the bridge girder about 1 hour.
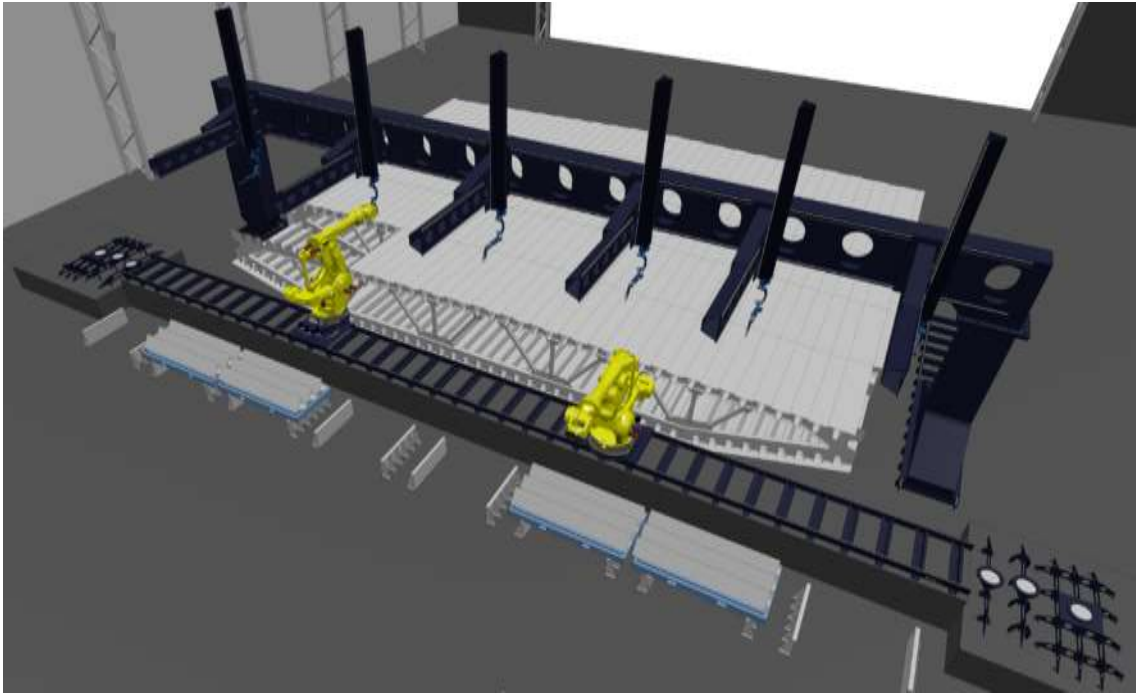
> *Figure 18-6: Main assembly cell*

The assembly cell includes a welding jig, 2-4 heavy lift handling robots mounted on rails and a gantry beam equipped with 6 -8 welding robots. On the gantry beam, it is proposed that 4 of the robots are equipped with MIG/MAG welding technology and two robots with laser hybrid technology.

An advanced logistics system is also required, especially for the curved bridge girder. For the curved bridge, all plate and stiffener elements will be different. This will be handled automatically through software from material cutting to bending and mounting.

The welding jig must be adapted to the bridge girder design with high accuracy. In the bottom of the jig, there will be grooves for backing under each butt weld. The jig also needs to release the side edges to do the movement of the bridge girder every 4 meters section fabricated.

After launching the bridge girder, it is necessary to place and lock the bridge girder with high accuracy before the assembly of the next section is initiated. The jig will include advanced measuring equipment, hydraulic and/or electrical positioning and locking devices.

The handling robots shall handle and position many different components. It will be necessary to develop lifting tools for all components.

It will also be necessary to develop different specialised lifting tools adapted to the components, as for example mounting of the stiffener profiles. This tool must have the strength to press the profile with high force to the bottom plate without deformation of the stiffener profile. In the prefabrication cells, there will also be necessary to develop tools for handling plates and profiles.
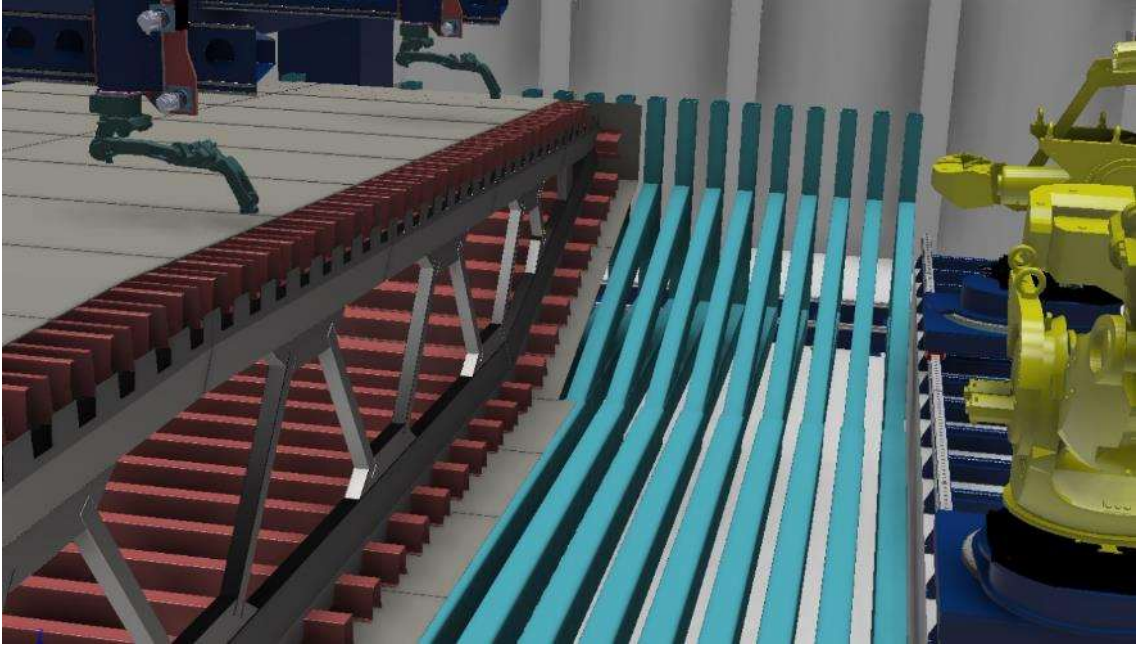
> *Figure 18-7: Jig - main assembly cell*
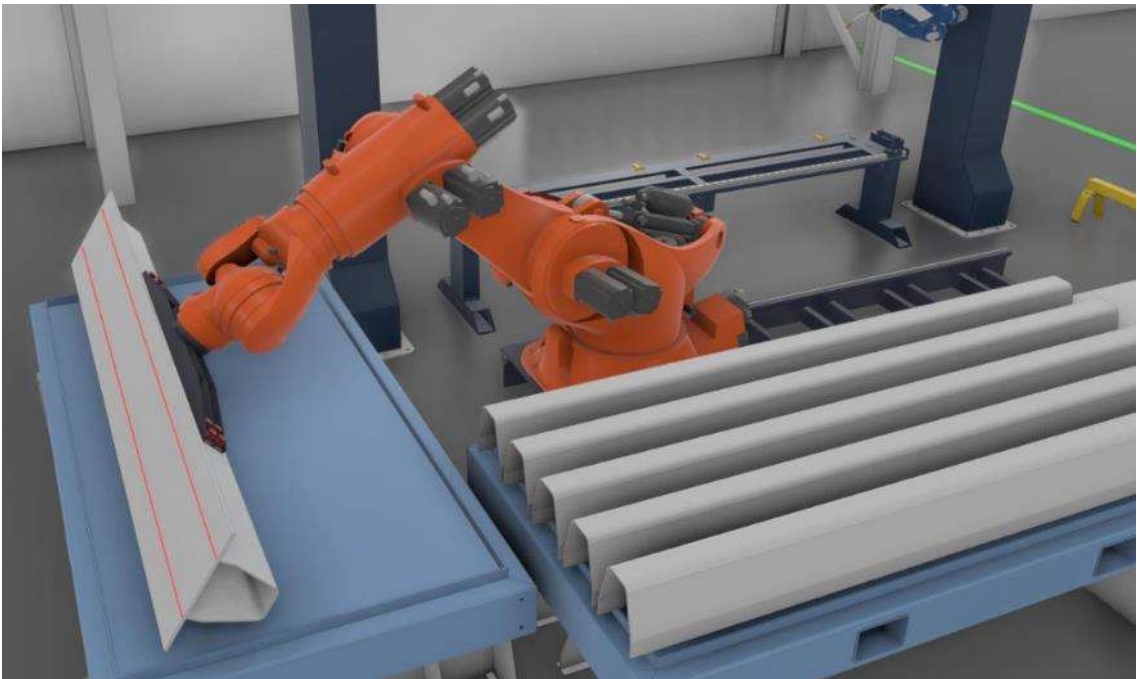
> *Figure 18-8: Lifting tool for top plate elements*

In order to weld the bridge girder, it is necessary to have a 30-meter wide gantry beam with several robots attached to reach across the bridge structure. The robots are connected to an XYZ-axis railway system, which makes it possible to set the positions of the robots in every horizontal and vertical position within reach restricted by the gantry.

To increase the building speed, it may be built another gantry approximately 12 meters from the first one to perform the welding of the top plate and side plates. The second gantry will also be used for attaching supports for rails, lights and welding of manholes on top of bridge deck girder.

The gantries will run on a railway with necessary motion length. Each robot can be operated separately and can weld all welds from the bottom plate to the top plate.
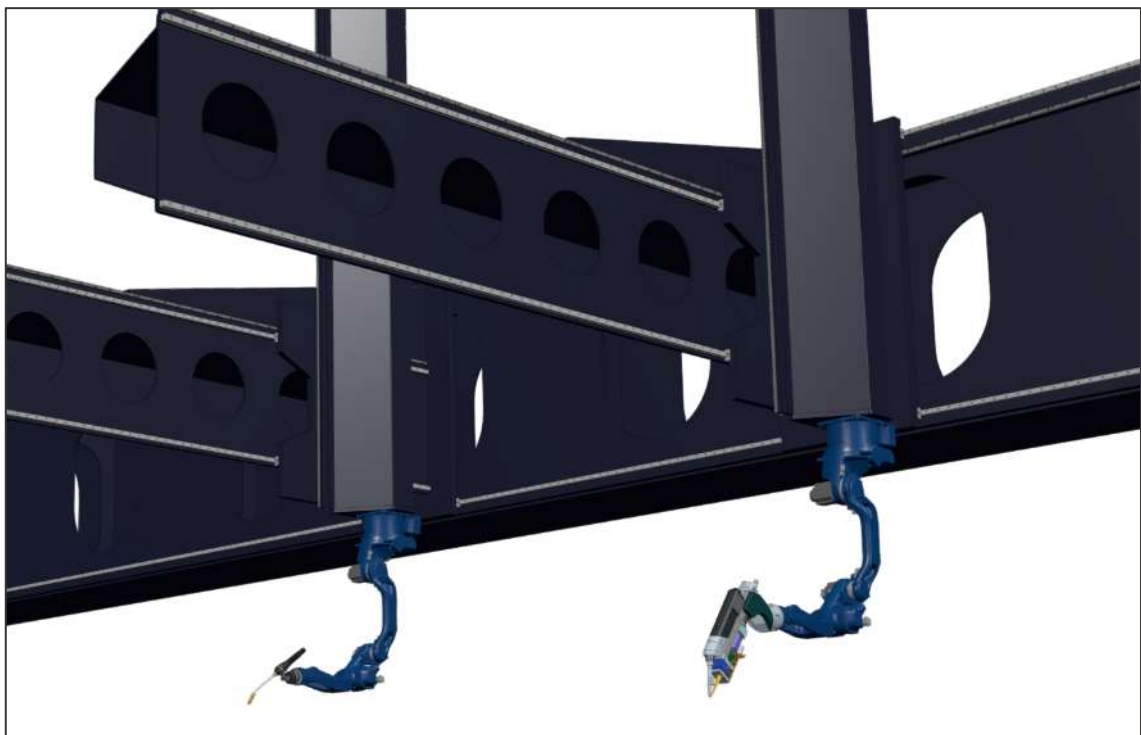
> *Figure 18-9: Welding robots on gantry. One mounted with MIG/MAG welding head and the other one with a laser hybrid welding head.*

18.2.4   Surface treatment

The surface treatment is a very important part of the bridge building process. The quality of the surface treatment will be significantly higher if done indoor with controlled temperature and environmental conditions.

Experience from Statens Vegvesen shows that surfaces that have been treated at an onsite workshop will give a much lower lifetime cost due to less wear and tear before final assembly.

The area to assemble outfitting and perform surface treatment requires at least a length of 100 meters right after the main assembly cell. Launching 12 meters every day, it will take 8 days to travel through the surface treatment cell.

The surface treatment:

- Blast cleaning
- Thermal sprayed
- Tie-coat
- Intermediate coat 1
- Intermediate coat 2
- Topcoat

Automated surface protection on the outside of the bridge girder is considered. This may be done using a robot gantry similar to the welding gantry. The robots must be adapted to surface protection and all the rails and toothed racks to be covered to protect from dust and coating spray.

Link to simulation video file: Bridge Girder Assembly - Assembly Move & Painting

18.2.5   Machining of pontoon support

The method used to connect the pontoons to the bridge girder requires the surface of the pontoon support on the bridge girder and the threaded holes to be machined before mounting. This operation needs to take place after the welding process.

This will be done using fixed or mobile machining equipment after the bridge girder is moved out of the welding jig. It will be preferable not to move the bridge girder during this operation. To prevent delay in the fabrication process, this machining shall be done 120 meters behind the welding of support for the next column.

18.2.6   Launching bridge girder 4 meter

The bridge girder will be mounted and welded automated in 4 meters sections in a jig. For each section fabricated, the bridge girder must be launched 4 meters with very high accuracy. When mounting the next section with robots it is necessary to know exactly the end position of the bridge girder element.

It will be different challenges with the moving and positioning from the first section to the last section. The first section will be 4 meters and have a weight of about 50 ton. To move for the last section, the bridge girder will be almost 480 meters long and have a weight about 6 500 ton.

The bridge girder may be moved by a skidding system or by multi-wheelers. The proposed system is a hydraulic skidding system that will have the best accuracy. This will make it possible to do a positioning in the welding jig within 0,5 mm.

The details regarding the skidding of the bridge girder are not evaluated. This has to be planned and designed together with the design of the welding jig. There must be an integrated positioning and measuring system in the welding jig.

The system for launching and positioning the bridge girder will be a complex and quite expensive system.

18.3 Proposed method

Using automated steel fabrication, the tolerance requirements will be stricter. To achieve greater accuracy, it is important to reduce heat impact from welding and it is recommended to use other welding methods than for manual welding.

Laser welding tools have significantly lower heat impact and welding deformation than MIG/MAG welding. It is therefore recommended to use laser welding tools whenever possible. The use of MIG/MAG welding is mainly because the MIG/MAG weld gun gives better access to the product and is therefore used in positions where the laser welding tool cannot reach. There will also be challenges with the use of laser tools for vertical welding.

Laser welding tools will also increase the welding speed. To fabricate 12 meters every day, it is necessary to increase the welding speed. All the welding equipment is designed to have this fabrication speed.

> *Table 18-2: Welding types in bridge girder*

Description	Plate thickness	Weld type
Butt weld bottom plate	10-12 mm	Laser hybrid
Longitudinal stiffeners to bottom plates	6-8 mm	Laser hybrid
Connection longitudinal stiffener profiles	6-8 mm	MIG/MAG
Welding of transverse girder	6-10 mm	MIG/MAG
Stiffener profile top to transverse girder	6-10 mm	MIG/MAG
Connection longitudinal stiffener profiles top	6-8 mm	MIG/MAG
Welding of longitudinal stiffener to the top plate (Prefab cell)	6-8 mm	Laser hybrid
Longitudinal welding between top plate elements	14 mm	Laser hybrid
Transverse welding of top plate	14 mm	Laser hybrid
Side plates	40 mm	MIG/MAG

In the next subchapters, each weld in the bridge girder is described. For many of the connections, there will be several solutions and welding methods. Only the method considered to be the best one is presented, but welding tests will be necessary to do verifications.

For all plates in the bridge structure, the plates should be mounted with an offset from the plates in front. It may be challenging to weld a groove where 4 welds meet into one point. To avoid this and improve the weld it is recommended to offset the plates 20-30 mm. This will give a point were 3 welds meet.

Below is an example for the top plate, the plates are offset 25 mm in the longitudinal direction. The offset may also be in the transverse direction.

> *Figure 18-10: Offset top plates*

18.3.1 Mounting of bottom plates

The production of the bridge girder begins with mounting the bottom plates to the jig. The plates will be mounted by robots, starting from the centre and continue out on both sides simultaneously with two mounting robots' side by side. When the mounting robot has mounted the bottom plate into the correct position, the welding robots will spot weld each plate to the bridge girder and the other bottom plates, while the mounting robot keeps it in the correct position.

For the butt weld of the bottom plates, laser hybrid will be the best welding method. Laser welding tool is necessary for the welding speed and laser welding will also give less heat impact and less welding deformation than a traditional MIG/MAG welding.

The table below shows the comparison between welding time for different welding methods on the bottom plates. Pure laser is the fastest but require machined surfaces and maximum 0,1 mm gap between plates. The use of pure laser will increase the cost of preparation significantly. The mounting tool will also be more advanced.

> *Table 18-3: Comparison of welding techniques for bottom plates.*

Plate 12 mm, butt weld (Bottom plate)	Manual MIG/MAG	Robot MIG/MAG	Laser hybrid	Pure laser
Number of welding beds	3	4	1	1
Welding speed	3 m/hour	0,5 m/min	2 m/min	3 m/min
Time for welding of 84 meter	84 hours	11,2 hours	42 min	28 min

To avoid welding from the underside it is necessary to use backing. There are two options for the backing. The first one, that most probably will be used is a water-cooled metal backing. The other option is to use a ceramic backing that must be changed after each welding. Laser hybrid welding requires a welding groove with a small angle, 2 x 3,5 degree is proposed by Swerim. Welding tests are necessary to find the best angle and other welding parameters.

The bottom plate has in many cases high fatigue load and the requirement for the welding between the plates are high according to standard fatigue rules. This welding is accessible from the underside after the bridge girder is moved out of the welding jig, and if necessary, the welding may be treated by grinding or other known methods.
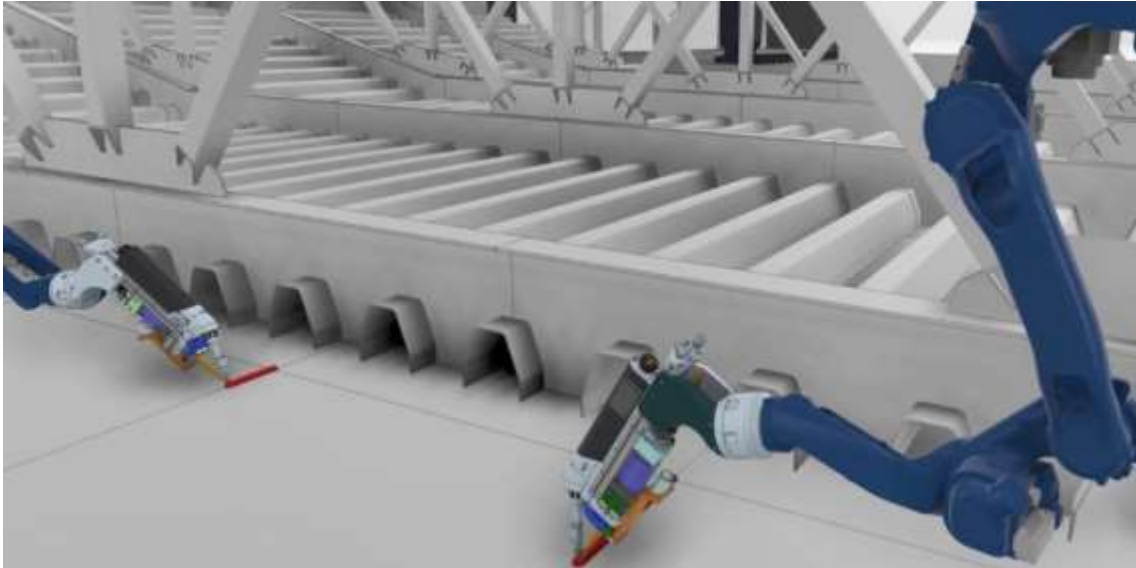

> *Figure 18-11: Welding of bottom plates*

Link to simulation video file: Bridge Girder Assembly - Mount & Weld Bottom Plates

18.3.2   Mounting of longitudinal stiffeners to the bottom plate

Next step is mounting and welding of longitudinal stiffeners. Before mounting of longitudinal stiffeners, a thorough of the bottom plates are necessary. The bottom plate must be smooth and no obstacles preventing good contact between the bottom plate and longitudinal stiffener profiles. If an irregularity occurs, reduce it by grinding or machining the plates to make a smooth surface. As for the plates, each stiffener has a different length to make the curvature on the bridge girder.

Welding of longitudinal stiffener to bottom plate represents a significant part of the welding operation in the bridge girder. It is therefore important to use pure laser or laser-hybrid welding to obtain the necessary welding speed. For increased tolerances laser-hybrid is the preferred welding method, which adds filling material to the welding seam. Welding of the stiffener profiles may also be welded using traditional MIG/MAG welding, but this will give a significant reduction in the fabrication speed. The heat input and the welding deformations will also be higher.
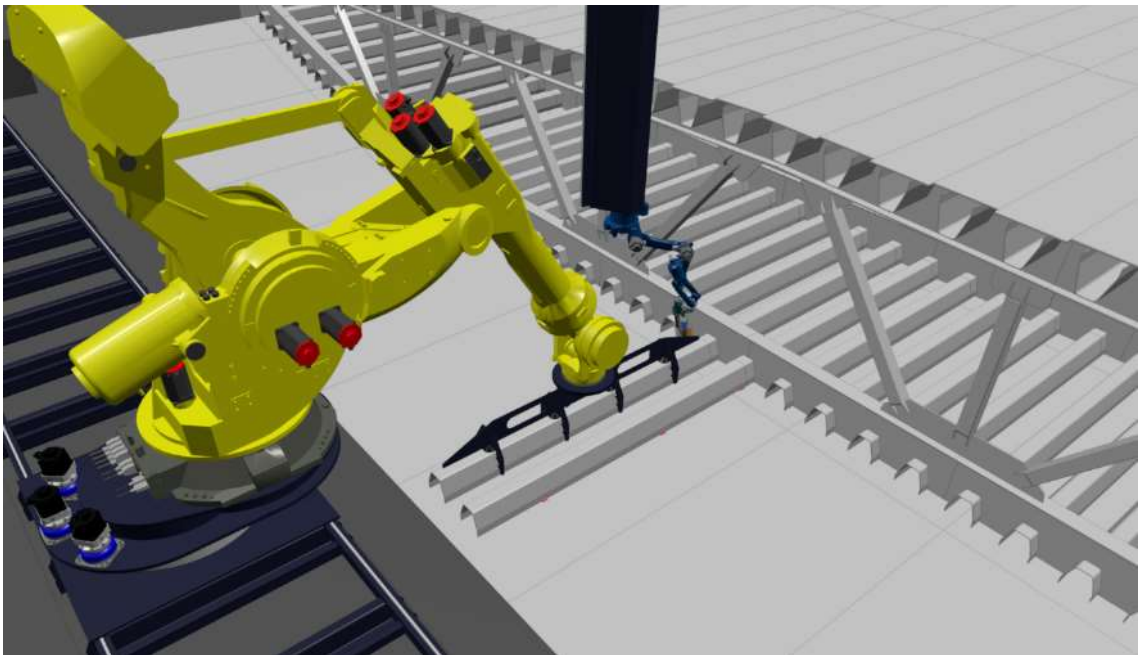
> *Figure 18-12: Mounting and spot welding of longitudinal stiffeners*
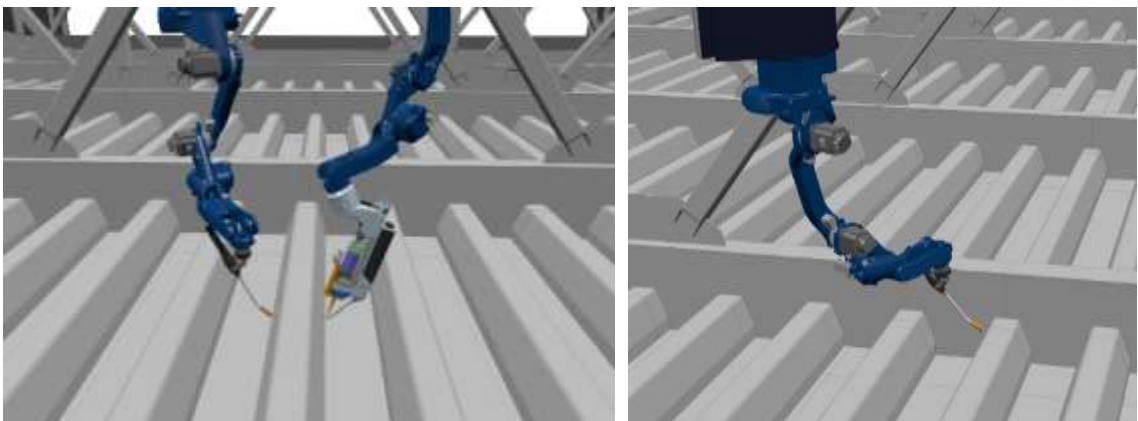
> *Figure 18-13: Welding of longitudinal stiffeners with laser hybrid welding at one side and MIG/MAG on the other side to show that both welding methods are possible (left) Welding of longitudinal stiffeners with MIG/MAG (right)*

The table below presents the welding time for different welding methods.

> *Table 18-4: Comparison of welding techniques for stiffeners on bottom plate.*

Stiffener 7 mm to bottom plate	Manual MIG/MAG	Robot MIG/MAG	Laser hybrid	Pure laser
Number of welding beds	2	2	1	2
Welding speed	3 m/hour	0,5 m/min	2 m/min	3 m/min
Time for welding of 368 meter	245 hours	24,4 hours	3,1 hours	4,1 hours
Time with 4 welding heads		6,1 hours	47 min	62 min

Link to simulation video file:Bridge Girder Assembly - Mount & Weld Bottom Profiles

The longitudinal stiffener includes a critical welding connection. This weld is exposed to high fatigue load and high-quality welding is required. There will be no access from inside of the stiffener profile, and a steel backing will be mounted. It may be challenging to do vertical welding using laser or laser hybrid. The process requires more testing and development of procedures than for horizontal welding. To be on the safe side, it is chosen MIG/MAG welding in the simulations and time schedule.

This welding operation will be done almost in parallel with welding to the bottom plate. This welding operation is also started in the centre of bridge girder and working towards the sides using one welding robot each side.

The welding length is 0,9 - 1 meter depending on the shape of the stiffener profiles. There are about 45 stiffeners at the bottom of the bridge girder. The table below presents the welding time for connection between the longitudinal stiffener profiles.

> *Table 18-5: Comparison of welding techniques for jointing longitudinal stiffeners.*

Plate 7 mm butt weld (connection stiffener)	Manual MIG/MAG	Robot MIG/MAG	Laser hybrid	Pure laser
Number of welding beds	2	2	1	1
Welding speed	3 m/hour	0,5 m/min	2 m/min	3 m/min
Time for welding of one stiffener profile (1 meter)	40 min	4 min	30 sec	20 sec
Time for welding of 45 profiles (two welding heads)	30 hours	1,5 hours	12 min	8 min

18.3.3   Mounting of transverse girder

The transverse girder will be pre-fabricated in four pieces to make them possible to lift and mount by robots. There are made a lot of different suggestions for the transverse girder but decided to go for a more traditional solution. This solution has one web plate and is welded to both the bottom plate and the longitudinal stiffeners.

A special tool for gripping and positioning the framework must be developed.

> *Figure 18-14: Robot mounting of transverse girder*
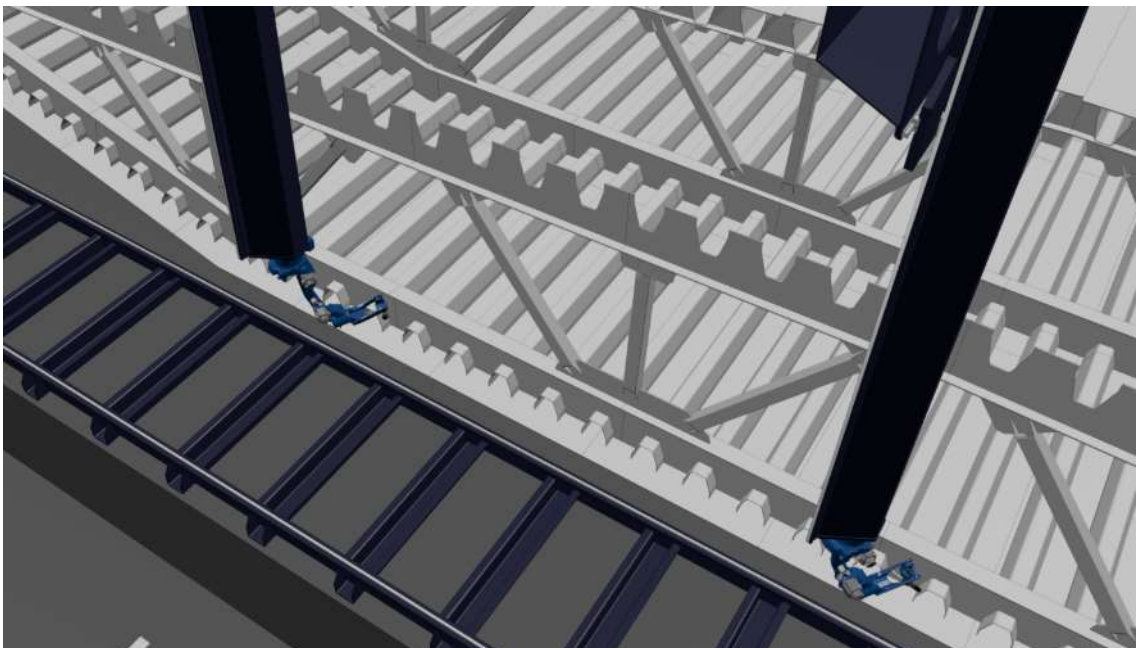
> *Figure 18-15: Welding of transverse girder*

It is considered to work further on with a traditional MIG/MAG welding. This is because a MIG/MAG welding has less requirement for the gap. It is considered difficult to make a perfect match between the transverse girder and the stiffener profiles at the bottom of the bridge girder.

The transverse girder will be mounted in four elements. To split the transverse girder into four elements, give a weight below 1400 kg and it will be possible to mount by a robot.

> *Table 18-6: Comparison of welding techniques for transverse girder.*

Transverse girder to bottom	Manual MIG/MAG	Robot MIG/MAG	Laser hybrid
Number of welding beds	2	2	1
Welding speed	3 m/hour	0,5 m/min	2 m/min
Time for welding bottom section (about 60 meters)	40 hours	4 hours	30 min

Because the transverse girder is split into 4 parts, it will also be some welding in the connections. This is not evaluated in detail and will most probably be done manually. Can be done after launching the bridge girder and will not influence building time.

Link to simulation video file: Bridge Girder Assembly - Mount & Weld Framework

18.3.4   Mounting of top plate element

The next step is mounting the top plate elements. The top plate elements are 0,6 x 4 meters and the stiffener profiles are welded to the top plate in a prefabrication cell.

> *Figure 18-16: Mounting of top plate elements*

The top plate element will be mounted using a robot and an advanced lifting tool with positioning and measuring equipment to secure the top plate element is placed within a tolerance requirement before welding. The top plate will be spot welded to the previous mounted element and the transverse frame while the mounting robot is holding the elements in the correct position. After spot welding, the mounting robot will be released and due to access full welding of all welds under the top plate must be performed before the next element is mounted. The welding speed under the top plate will have a direct influence on the building time and to find solutions for laser welding is necessary to reduce building time.

The welding between the top plate elements is done from the top side and can be done after the next element is mounted. The connection welding between the top plate elements will be done in parallel with mounting of the next element and will not increase building time.

Connection longitudinal stiffener profiles
The access for this weld is about the same as for bottom stiffener. Because of vertical welding, this weld will be done using traditional MIG/MAG. The welding time will be about the same as for the bottom stiffeners. Because this weld must be finished before the next element can be placed, the welding time will influence the building time for the bridge girder.

> *Figure 18-17: Welding of longitudinal stiffeners*

The static and fatigue load is high on this connection as well, which again requires a high-quality weld seam. To increase the welding root quality, it will be mounted a steel backing inside the stiffener.

Stiffener profile to transverse girder
The stiffener profile will be welded to the transverse girder. Much of the same challenges as for the connection of the stiffener profiles. Because of limited access underneath the top plate, the mounted top plate element must finish all of its weldings before mounting a new element. These operations are time-consuming and will influence the total production speed drastically for the bridge girder.

> *Figure 18-18: Welding to transverse girder*

Longitudinal welding between top plates
The longitudinal welding of the top plate is a large amount of welding and laser welding tools is necessary to increase welding speed. The prefabricated top plate elements with stiffener profile are lifted on place using robot and a spot welding is done.

The laser hybrid welding robot will fully weld all the longitudinal welds. All connection welding between the top plates is done from topside and can be done in parallel with mounting and welding of the top plate elements.
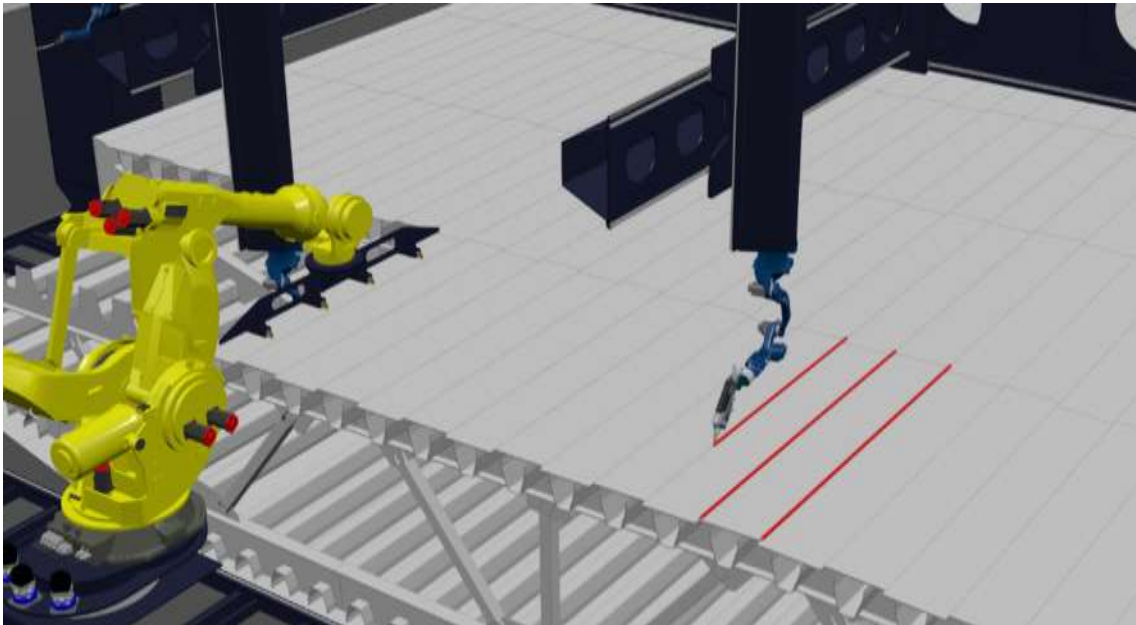
> *Figure 18-19: Longitudinal welding of top plates*

> *Table 18-7: Comparison of welding techniques for longitudinal welding between top plates.*

Plate 14 mm, butt weld (Top plate)	Manual MIG/MAG	Robot MIG/MAG	Laser hybrid	Pure laser
Number of welding beds	3	4	1	1
Welding speed	3 m/hour	0,5 m/min	1,5 m/min	2 m/min
Welding time for one profile 4 meter	4 hours	32 min	2,7 min	2 min
Time for welding of 45 elements (two welding heads)		12 hours	60 minutes	45 min

The table includes pure laser, but this welding method is not considered to be an actual method for this welding. Pure laser will require machined edges with very high precision that will be a difficult and expensive solution.

Transverse welding between top plates
This is one of the most important welds in the bridge girder with fatigue load from wheels and environmental loads. The weld will cross the longitudinal stiffener profiles that may give an increased risk for welding fault.

> *Table 18-8: Comparison of welding techniques for transverse welding between top plates.*

Plate 14 mm, butt weld (Top plate)	Manual MIG/MAG	Robot MIG/MAG	Laser hybrid	Pure laser
Number of welding beds	3	4	1	1
Welding speed	3 m/hour	0,5 m/min	1,5 m/min	2 m/min
Welding time for one profile 0,6 meter	36 min	5 min	14 sec	18 sec
Time for welding of 27 meter	27 hours	3,6 hours	18 min	1,5 hours

Link to simulation video file: Bridge Girder Assembly - Mount & Weld Top Panels

18.3.5 Mounting of side plates

Most of the bridge girder has side plates with thickness 40 mm. These plates will be more than 1900 kg and are too heavy to be mounted by robot and manual handling is necessary. To split the plates into smaller parts will make the plates possible to handle by a robot but will also increase the welding. Since it is only two plates each 4-meter section, it is considered to be the best solution with manual mounting of the side plates. Mounting and welding of the side plates can be done after the bridge girder is moved to avoid longer building time in the main assembly cell.
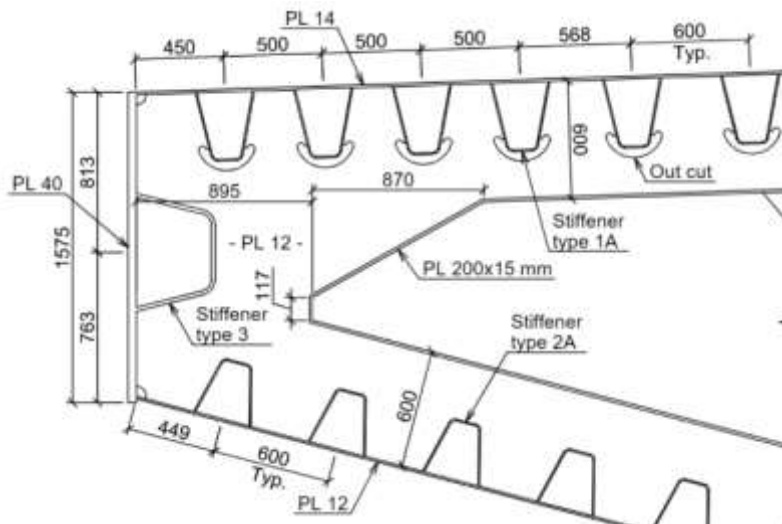
> *Figure 18-20: Side section of the bridge girder*

Because of the vertical welding and the plate thickness, it is proposed to do the welding of the side plates by traditional MIG/MAG welding. This is a much slower process, but the mounting and welding of the side plates may be done after leaving the welding jig and will not influence the building speed of the bridge girder.

> *Table 18-9: Comparison of welding techniques for side plates.*

Butt weld plate 40 mm, (Side plate)	Manual MIG/MAG	Robot MIG/MAG	Laser hybrid	Pure laser
Number of welding beds	15	20	3	-
Welding speed	3 m/hour	0,5 m/min	1,5 m/min	-
Welding time for one weld bed 1,5 m	30 min	3 min	1 min	-
Time for welding of one 40 mm plate	7,5 hours	1 hour	3 min	-

The butt welding can be robot welded from outside with a ceramic backing. Alternative from both sides, all inside welding must be done manually. The table shows the time for butt welding of side plates assuming manual or robot welding. This welding will most probably be a combination of manual and robot welding.

There will also be welding to the top plate and bottom plate. For all welding of the side plates, there is access from both sides, and it is easier to make good welding than for some

other welding in the bridge girder. Because the side plates will be mounted after the top plate, the welding inside will be a manual operation, and the outside welding may be done using robots. The welding grooves will be designed with less amount of welding inside to reduce manual welding.

The following welds must be evaluated for the side plates:
- Butt weld of side plates
- Welding to the top plate
- Welding to the bottom plate
- Connection of inside stiffener profile

The side plates have a high fatigue load and the welding must have very good quality. The details around these welds are not evaluated in detail because traditional methods will be used.

18.3.6   Manholes, foundations and brackets

This project has not evaluated automated mounting and welding of smaller foundations, ladders, manholes etc.

It is possible to do an automated mounting and welding of these parts also. Outside of the bridge girder it will be done after leaving the jig and will not influence the building time. All parts inside must be mounted and welded before the top plate is mounted and will thereby influence the total building time.

19   ARCHICTURAL STUDY

19.1   Generally

This chapter summarizes the architectural design of the floating bridge. Heyerdahl Architects AS has been engaged also in earlier phases of the project "E39 Stord - Os" with a proposal for an end anchored floating bridge. Experiences and assessments from previous work on the floating bridge have been utilized during this phase of the project. This applies in particular to the assessment of the bridge seen against the landscape, the design of the cable-stayed bridge and the landing in the north towards Røtinga and Os.
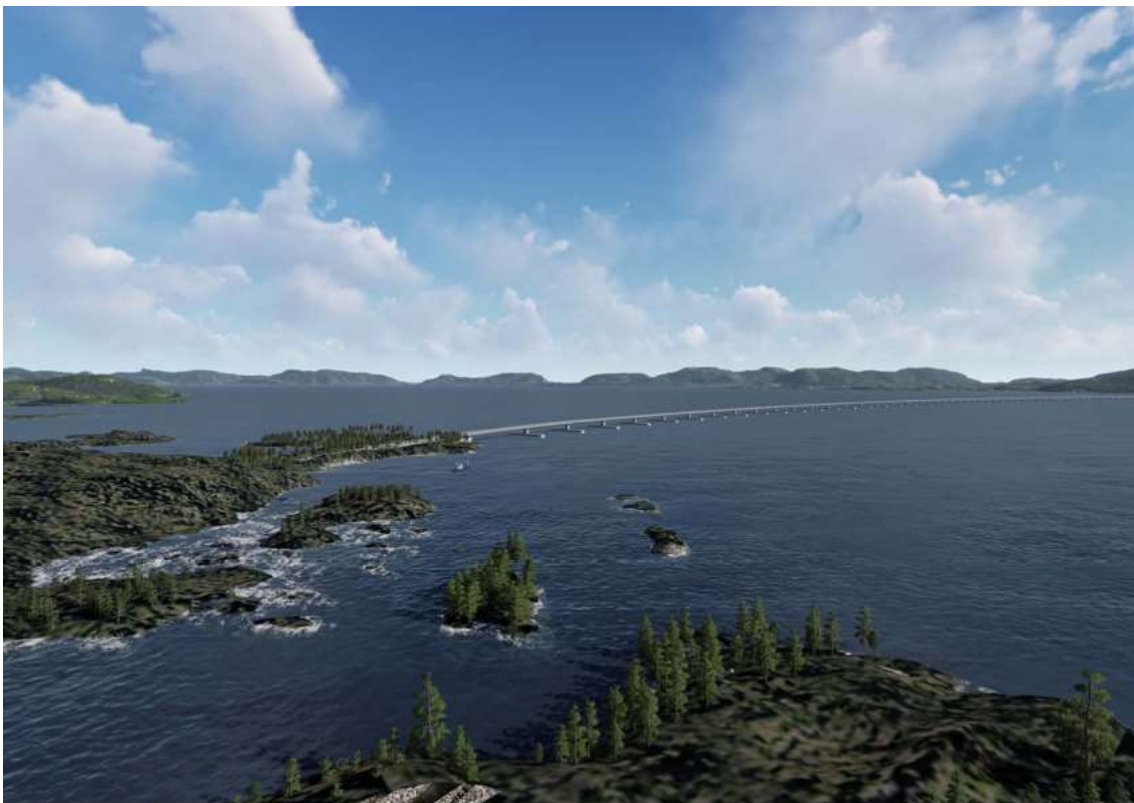
The north landfall. View from archipelago at Kobbavågen.

The work of the architects, besides seeking the best answer to the architectural challenges, has been to illustrate the consequences of the different construction principles. It was important to visualize, also for the whole team, the aesthetic and visual consequences of the different proposals.
Based on this work, 3 different proposals have been crystallized for the design of column and pontoon. In the final design proposal, we are using the same type of column and pontoon where it is not proposed submerged. For the cable-stayed bridge and bridge girder, only one design has been proposed. The same goes for the landfalls of the bridge.

19.2   Bridge and landscape

The crossing is 5 km. This is a long distance and by a curved bridge one gets a varied view along the curve and thus given varying perspectives of the bridge and the landscape. You will also, from the road, be able to experience the cable-stayed bridge seen from the side.

This will increase the visual experience of the floating bridge. By a straight line this would not be possible. This is, together with the "natural" shape, is one of the main reason why the architects prefer the K12 concept

E39, the crossing of Bjørnafjord. Seen towards the north and the archipelago at Kobbavågen. Night vision

The architects have proposed an asymmetrically constructed cable-stayed bridge. The cables will then point towards the sailing route and the bridge's position in the landscape will be better expressed. In addition, the architects suggest that the pylon is tilted backwards. This will increase the asymmetric effect. The construction in this way visually spans the floating arch and lifts the bridge on land.
The vertical curvature has been adjusted in this phase of the project. The curve has been smoothed to achieve a better visual effect and to improve the driving experience.

19.3   The landfalls

The landfall of the bridge in the north, at Gulholmane has been shown previously with a large filling between the islet and Røtinga. At the same time, the neighboring area at Kobbavågen is an important recreation area.
The architects have therefore, on an earlier stage of the project, recommended the filling reduced in order to form a canal between Gulholmen and Røtinga. This for the sailing of smaller boats. In this way you will still be able to sail protected behind Gulholmen to Kobbavågen. This design of the landfall has been continued in this phase.

In the south, it is set as a premise from SVV that the landfall should be high in the terrain to avoid tunnels. For K12 this means that there will be a cut in the Skarvhella hill, which is visually exposed to Langenuen and Bjørnafjorden.
By the concept of K12 the cutting or intersection in the hill is not to be avoided. On the other hand, given the current situation, the road gives access to an amazing viewpoint at the top of Skarvhella. One can be proactive by adding a visitor center to this area. In this way, the center will become visible from both road and fjord and be a part of the landmark.

The bridge seen from the visitor center

19.4   The architectural design of the floating bridge

It has been quite a task for the architects, as well for the team, to learn how to design for the forces that affect the bridge girder, columns and the pontoons. This has, during the process, resulted in three different proposal for pontoon, columns and transition to the bridge girder. All the proposals have been architecturally designed to the same level of presentation. The bridge girder is visually equal on all proposals.

Option 1 has a submerged pontoon, completely covered by the sea. Up of the sea, rise a center column and the the sides two large "floats". They are all firmly connected to the submerged pontoon. The option is currently set aside due to a possibility of "climbing" on to the pontoon at ships impact.

Option 2 is a traditional pontoon - column construction. The pontoon floats on the sea and is carrying the column. This option has, by the engineers, been given the most attention and is quality assured for use.

Option 3 is identical to option 2 except the top of the columns, where it is placed a rig of closed steel profiles. The principle is considered very interesting aesthetic and possible to produce effectively with modern production methods. The concept is briefly calculated and assumed feasible. It is recommended that this alternative is further investigated in the next phase of the project.

Columns and pontoons
The columns in option 2 is slightly cone-shaped against the top and a fracture bracket. At the top of the column there is an opposite cone-like shape that transmits the forces to the bridge girder. The steel rig in option 3 gives the possibility to increase the span and thus reduce the costs.

The pontoon is given a shape that meets the sea in a soft way. The pontoon is arching it´s back to visually carry the column. The pontoons are mostly welded up by single-curved steel plates. Only a small part has double curved surfaces

The bridge seen towards the south, option 2

The bridge seen towards the south, combination of option 1 and 3

20   REFERENCES

[1]   SBJ-32-C5-OON-22-RE-002, "Concept selection and risk management," Arbeidsfellesskapet Norconsult - Olav Olsen, 2019.

[2]   SBJ-32-C5-OON-22-RE-003, "Analysis method," Arbeidsfellesskapet Norconsult - Olav Olsen, 2019.

[3]   SBJ-32-C5-OON-22-RE-004, "Validation," Arbeidsfellesskapet Norconsult - Olav Olsen, 2019.

[4]   SBJ-32-C5-OON-22-RE-005, "Sensitivity studies".

[5]   SBJ-32-C5-OON-22-RE-006, "Parametric resonance".

[6]   SBJ-32-C5-OON-22-RE-007, "Wind loads and aerodynamic optimization".

[7]   SBJ-32-C5-OON-22-RE-008, "Hydrodynamic optimization," Arbeidsfellesskapet Norconsult - Olav Olsen, 2019.

[8]   SBJ-32-C5-OON-22-RE-009, "Automated steel fabrication," Arbeidsfellesskapet Norconsult - Olav Olsen, 2019.

[9]   SBJ-33-C5-OON-22-RE-011, "K12 - Architectural design," Arbeidsfellesskapet Norconsult - Olav Olsen, 2019.

[10] SBJ-33-C5-OON-22-RE-012, K12 - Structural response analyses.

[11] SBJ-33-C5-OON-22-RE-013, K12 - Ship impact, Global assessment, Arbeidsfellesskapet Norconsult - Olav Olsen, 2019.

[12] SBJ-33-C5-OON-22-RE-014, "K12 - Ship impact, Pontoons and columns," Arbeidsfellesskapet Norconsult - Olav Olsen, 2019.

[13] SBJ-33-C5-OON-22-RE-015, "K12 - Ship impact, Bridge girder," Arbeidsfellesskapet Norconsult - Olav Olsen, 2019.

[14] SBJ-33-C5-OON-22-RE-016, "Fatigue assessment," Arbeidsfellesskapet Norconsult - Olav Olsen, 2019.

[15] SBJ-33-C5-OON-22-RE-017, "K12 - Design of bridge girder," Arbeidsfellesskapet Norconsult - Olav Olsen, 2019.

[16] SBJ-33-C5-OON-22-RE-018, "K12 - Design of pontoons and columns," Arbeidsfellesskapet Norconsult - Olav Olsen, 2019.

[17] SBJ-33-C5-OON-22-RE-019, "K12 - Design of cable stayed bridge," Arbeidsfellesskapet Norconsult - Olav Olsen, 2019.

[18] SBJ-33-C5-OON-22-RE-020, "K12 - Design of abutments," Arbeidsfellesskapet Norconsult - Olav Olsen, 2019.

[19] SBJ-33-C5-OON-22-RE-021, "K12 - Design of mooring and anchoring," Arbeidsfellesskapet Norconsult - Olav Olsen, 2019.

[20] SBJ-33-C5-OON-22-RE-022, "K12 - Marine geotechnical design," Arbeidsfellesskapet Norconsult - Olav Olsen, 2019.

[21] SBJ-33-C5-OON-22-RE-023, "K12 - Execution of construction," Arbeidsfellesskapet Norconsult - Olav Olsen, 2019.

[22] SBJ-32-C4-SVV-90-BA-001, "Design Basis Bjørnafjorden floating bridges," Statens Vegvesen, 2018.

[23] SBJ-01-C4-SVV-01-BA-001, "Design basis MetOcean," Statens Vegvesen, 2018.

[24] SBJ-02 C4-SVV-02-RE-002, "Design Basis – Geotechnical design," Statens Vegvesen, 2018.

[25] SBJ-32 C4-SVV-26-BA-001, "Design Basis – Mooring and anchor," Statens Vegvesen, 2018.

[26] Nygaard, T. A., De Vaal, J., Pierella, F., Oggiano, L. and Stenbro, Development, Verification and Validation of 3DFloat; Aero-Servo-Hydro-Elastic Computations of Offshore Structures, Energy procedia 2016, Vol. 94, pg. 425-433, 2016.

[27] DNV, WADAM User Manual, 2010.

[28] Borgman, "Random Hydrodynamic Forces on Objects," *The Annals of Mathematical Statistics,* vol. 38, 1967.

[29] Sofistik, Sofistik Basics, 2016.

[30] Daussault Systemes, "Abaqus 2018," SIMULIA, Johnston, RI, USA, 2017.

[31] Svend Ole Hansen ApS, "SBJ-32-C4-SOH-20-RE-001 Wind model-tests Floating Bridge step 1 small scale testing," 2018.

[32] NS-EN 1991-1-4:2005+NA:2009, "Eurokode 1: Laster på konstruksjoner, Del 1.4: Allmenne laster, Vindlaster," Standard Norge.

[33] WAMIT Inc., "WAMIT," 2019. [Online]. Available: https://www.wamit.com/. [Accessed 14 08 2019].

[34] Håndbok N400 , "Bruprosjektering," Statens vegvesen Vegdirektoratet, 2015.

[35] DNV GL, "DNVGL OS C101 - Design of offshore steel structures, general - LRFD method," 2016.

[36] Arbeidsfellesskapet Norconsult - Olav Olsen, "https://interactive.olavolsen.no/index.php," [Online].

[37] NS-EN 1993-1-9:2005+NA:2010, "Eurocode 3: Design of steel structures - Part 1-9: Fatigue design of steel structures," Standard Norge, 2005.

[38] SBJ-31-C3-DNV-62-RE-020, "Fatigue design methodology for BJF floating bridges," DNV GL, 2018.

[39] DNV-RP-C103, Recommended Practice, Column-Stabilised Units, April 2012.

[40] NGI, "SBJ-31-C3-MUL-02-RE-100 Bjørnafjorden, straight floating bridge phase 3. Geohazard (Base Case)," 2017-06-02.

[41] NGI, "Bjørnafjorden 2016 Soil Investigations. Measured and Derived Geotechnical Parameters and Final Results. Doc.no. 20150804-04-R rev.0," 2016.

[42] Multiconsult/NGI/Aker AS. , "Bjørnafjorden, straight floating bridge phase 3 - Geohazard (Base Case). Doc.no. SBJ-31-C3-MUL-02-RE-100," rev. O. 2017.

[43] N. X. X. H. L. S. Haijun Zhou, "Full-scale test of dampers for stay cable vibration," *Structural Monitoring and maintanance,* vol. 5, no. 4, pp. 489-506, 2018.

[44] NS-EN 1992-1-1:2004+A1:2014+NA:2018, Eurocode 2: Design of concrete structures - Part 1-1: General rules and rules for buildings, Standard Norge, 2004.

[45] SBJ-33-C5-OON-22-RE-018, "K12 - Design of pontoons and columns".

[46] SBJ-33-C5-OON-22-RE-023, "K12 - Execution of construction".

[47] SBJ-30-C3-NOR-90-RE-105, "K7 Bjørnafjorden End-anchored floating bridgeAppendix E–Pontoon and column structural sizing and design," Dr.techn. Olav Olsen, Norconsult, Aker Solutions, 2017.

[48] SBJ-32-C5-OON-22-RE-003, " Analysis method," Dr.techn. Olav Olsen, Norconsult, 2019.

[49] SBJ-33-C5-OON-22-RE-001, " Alternative K12 - Consolidated technical report," Dr.techn. Olav Olsen, Norconsult, et. al, 2019.

[50] DNV GL, "RP C205 - Environmental conditions and environmental loads," DNV GL, 2017.

[51] RE-001-K11, "SBJ-33-C5-OON-22-RE-001 Alternative K11 – Consolidated Technical Report".

[52] RE-001-K12, "SBJ-33-C5-OON-22-RE-001 Alternative K12 – Consolidated Technical Report".

[53] RE-001-K13, "SBJ-33-C5-OON-22-RE-001 Alternative K13 – Consolidated Technical Report".

[54] RE-001-K14, "SBJ-33-C5-OON-22-RE-001 Alternative K12 – Consolidated Technical Report".

[55] NPRA, "Design Basis – Geotechnical design Doc.no. SBJ-02 C4-SVV-02-RE-002," 2018-11-12.